A novel additive manufacturing process for the production of metal parts

Anglia Ruskin University

Cambridge Chelmsford Peterborough

Javaid Butt, BSc (Hons), MSc

Department of Engineering and Built Environment

Anglia Ruskin University

This dissertation is submitted for the degree of

Doctor of Philosophy

Faculty of Science and Technology Jan 2016

Dedication

I would like to dedicate this dissertation to my loving parents Muhammad Azhar Ilyas Butt and Fozia Butt for their constant love, encouragement, support and blessings. Also, my siblings Jonaid Butt and Saniya Butt for strengthening my morale during the toughest of times and standing by me every step of the way.

Declaration

I hereby declare that except where specific reference is made to the work of others, the contents of this dissertation are original and have not been submitted in whole or in part for consideration for any other degree or qualification in this, or any other University. This dissertation is a result of my own original work and does not include work done in collaboration, except where clearly stated in the text.

Javaid Butt

Jan 2016

Acknowledgements

First and foremost, I would like to express my sincere gratitude to my supervisory team, Dr Habtom Mebrahtu, Prof Hassan Shirvani and Dr Mehrdad Asadi, for their enlightening guidance, meticulous suggestions, astute criticism and words of encouragement throughout my PhD journey. I am grateful that I had the honour and privilege to be working under the supervision of such brilliant and innovative minds. I can only hope to be a shadow of your fervour as I start my professional career.

I would like to give a very special thanks to Dr Ahad Ramezanpour, Dr Sathish Nammi and Mr Mashood Ahmed for sharing their knowledge in CFD and mechanical testing with me, as well as kind encouragement and comments in this study.

I am also thankful to my friends and colleagues at Anglia Ruskin University, the ones that are here and the ones that have left, not only for their support and comments that made my research work better but also for an enjoyable and pleasant time at the University. I am extremely grateful for your friendship.

I would not have been able to do this if it were not for the prayers and support of my parents. They have encouraged me, stood by my decisions and for that I am eternally grateful. I also want to express my heartfelt gratitude to my siblings who listened to my research endeavours and gave insightful comments. Your support has been a blessing.

Abstract

The majority of additive manufacturing methods use different materials for the production of parts. The current methods employing powder metals have their limitations and are very expensive. This research presents a novel additive manufacturing process for the generation of modest and high quality metal parts. The procedure, referred to as Composite Metal Foil Manufacturing, is a blend of Laminated Object Manufacturing and soldering/brazing strategies. A calculated model of a machine in view of the new process has been outlined and its parts accepted for usefulness either by experimentation or recreations.

The viability of the new process is accepted with lap-shear testing, peel testing, microstructural examination and tensile testing. Distinctive metals, such as copper and aluminium, with shifting thicknesses were used to demonstrate the adaptability of the procedure. Composites of aluminium and copper were additionally delivered and tried for their mechanical properties to show the flexibility of the process. The outcomes of the research attained have been promising and show that the new process is not just fit for delivering astounding metal parts efficiently but can create more grounded parts contrasted with customary subtractive techniques.

The comparative tensile testing demonstrated that the parts created by the new process had force values that were 11%, 8% and 11% higher than the parent copper, aluminium and composite examples individually. This shows that the procedure has the capability to be a solid competitor in the field of metal prototyping. It has been demonstrated that the proposed procedure can have a gigantic effect as it has lessened the confinements, for example, cost, pace, material determinations and beyond.

The additive manufacturing identified with the generation of metal parts using the new process can work with an extensive variety of metals under typical conditions regardless of their joining capacities. The feedback that parts delivered by added substance fabrication techniques are not sufficiently strong for genuine applications can without much of a stretch is hushed with the obtained trial results. Applications can extend from little bespoke parts to large scale functional products that can be utilized with minimal post handling.

Table of Contents

List of Figures

List of Tables

Nomenclature

Q_{int} = Internal heat generation rate (W m^{-3})

A = heat transfer area of the surface (m^2)

c(T) = Specific heat as a function of temperature (J kg^{-1} K^{-1})

E = Modulus of elasticity (GPa)

h_c= convective heat transfer of the process (W/ (m^2K)) or (W/ (m^2 °C))

k(T) = Thermal conductivity as a function of temperature (W m^{-1} K^{-1})

L = Length (m)

q = heat transferred per unit time (W)

T = Temperature (°C)

T = Thickness (m)

α = co-efficient of thermal expansion (µm/m. K)

ρ = Material density (kg m−3)

dT = temperature difference between the surface and the bulk fluid (K or °C)

Abbreviations

3D	Three Dimensional
3DP	Three Dimensional Printing
AF	Additive Fabrication
ALM	Additive Layer Manufacturing
AM	Additive Manufacturing
ASTM	American Society for Testing and Materials
CAD	Computer Aided Design
CFD	Computational Fluid Dynamics
CMFM	Composite Metal Foil Manufacturing
CNC	Computer Numerical Control
DED	Direct Energy Deposition
DMLS	Direct Metal Laser Sintering
EBAM	Electron Beam Additive Manufacturing
EBM	Electron Beam Melting
FDM	Fused Deposition Modelling
FFF	Free Form Fabrication
GMAW	Gas Metal Arc Welding
GTAW	Gas Tungsten Arc Welding
HAZ	Heat Affected Zone
HCF	High Cycle Fatigue
LC	Laser Cladding
LCF	Low Cycle Fatigue
LENS	Laser Engineered Net Shaping
LM	Layer Manufacturing

LMD	Laser Metal Deposition
LOM	Laminated Object Manufacturing
MMCs	Metal Matrix Composites
NPMS	Nip Pressure Measurement System
PTAS FFF	Plasma Transferred Arc Selected Free Form Fabrication
SFF	Solid Free Form Fabrication
SGC	Solid Ground Curing
SLA	Stereolithography
SLM	Selective Laser Melting
SLS	Selective Laser Sintering
S-N	Stress vs. Number of cycles
UC	Ultrasonic Consolidation
USS	Ultimate Shear Strength
UTS	Ultimate Tensile Strength

CHAPTER 1

1 Introduction to Additive Manufacturing

1.1 Problem Statement

Additive Manufacturing (AM) is an umbrella term referred to a group of technologies that produce three dimensional objects from computer aided design (CAD) data by laying down successive layers of material. A large number of AM processes are commercially available that use plastics, polymers, photopolymers, ceramics etc. to produce parts (Gomez et al., 2016; Fumo and Noorani, 2015; He et al., 2015; Zhang, et al., 2001; Pham and Gault, 1998; Himmer, Nakagawa and Noguchi, 1997; Dickens, 1995; Kai, 1994). These parts mainly serve as prototypes and do not give any insight into the design parameters. There has always been an emphasis on the production of metal parts using AM because it provides an environment for direct testing. A couple of commercially available AM processes capable of producing metal parts are Direct Metal Laser Sintering (DMLS) and Electron Beam Melting (EBM). They use powder metals and have been widely researched over the years (Marchese et al., 2016; Calignano, et al., 2012; Cormier, Harrysson and West, 2004; Mitchell, 1999; Park, Tari and Hahn, 2000; Simchi, 2006; Simchi, Petsoldt and Pohl, 2003). Although these technologies are capable of producing good quality parts, they still do not ease the pressure when it comes to the production of metal parts because of the very high cost of their machines and inability to cope with the material requirements (Lapcevic et al., 2016; Ponader, et al., 2007; Sonmez and Han, 1998). They have a number of limitations like materials, particular grain size of powder metal to achieve certain degree of mechanical integrity, size of parts being made, build speed, surface finish etc. Also, after production, the powder removal process requires more time and thus reduces the efficiency of the process (Yasa et al., 2016; Murr, et al., 2010; Khaing, Fuh and Lu, 2001).

The limitations greatly affect the efficiency of the methods, therefore, efforts were made to overcome them by pursuing other AM technologies. This idea led to the modification of Laminated Object Manufacturing (LOM). The LOM method originally made use of paper sheets with adhesives on one side but since the setup was inexpensive, further materials including plastic and metal laminates were experimented with, to enhance the capabilities of this technology (Prechtl, Otto and Geiger, 2005a; 2005b; Wiesensel, et al., 2004; Mueller and Kochan, 1999). Epoxy adhesives and glues have also been used to join metals sheets together using LOM but the produced parts are far from perfect in terms of their material properties and in some cases serious failures have occurred (Armstrong, 1997; Kinloch, 2003). Ultrasonic Consolidation (UC) is another AM technique that has made quite an impact in recent years. UC requires optimization of its parameters and requires the use of milling to machine the part after joining which results in waste of material (Kong, Soar and Dickens, 2003; 2004). All of these processes have been researched upon and parts have been produced using them but they are limited in what they can do and achieve in terms of producing metal parts.

In addition to making metal parts by alternative and low-cost methods, the production of composite materials has been receiving unprecedented attention from the academia, mainstream media, investment community and national governments around the world. Metal composites or metal matrix composites (MMCs) are gaining popularity because a number of industries rely on them to provide cost effective, lighter, and stronger alternatives. AM processes are not far behind in this endeavour either and a number of them have produced MMCs including Selective Laser Melting/Sintering (SLM/ SLS), Laser Engineered Net Shaping (LENS), Three Dimensional Printing (3DP), LOM and UC. However, it required a great degree of additional equipment and time to produce a metal composite using AM

processes and their mechanical integrity in some cases is far from ideal (Facchini, et al., 2010; Kumar and Kruth, 2010; Vandenbroucke and Kruth, 2007).

This study clearly indicates that there is a gap that needs to be filled when it comes to the production of affordable and high quality metal parts. Therefore, the aim of this research is to propose a novel additive manufacturing process that could produce metal parts at a lower cost and of such high quality that they could compete with existing technologies. The focus of the research would be on the fundamental problem which is the strength of the materials produced by the proposed process. Metals exhibit varying behaviour when joined together using industrial adhesives and glues which is not suitable for high temperature applications. One way of overcoming this shortfall is to consider metallurgical joining of the sheets. The new process will involve integrating of a cutting and stacking system with an appropriate metal joining process to produce metal parts from metal foils. The process should be able to work with a range of metals and should minimise the limitations of existing metal prototyping processes so that it could become a strong candidate in the field of AM.

1.2 Proposed Solution

The present study presents a solution to the problems related to metal prototyping by introducing a novel additive manufacturing process capable of producing low cost and high quality parts. The aim is to propose and design a new process as well as produce parts using its principles. The proposed process should reduce the limitations related to commercial metal AM methods such as range of materials, ease of operation and processing time. The parts made by the process need to be tested for their mechanical integrity and should be better in terms of affordability and strength if the proposed process is to compete with the existing AM processes. The proposed process, termed as Composite Metal Foil Manufacturing (CMFM), is a combination of LOM and soldering/brazing techniques. These two

technologies have been around for decades but never integrated together for the production of metal parts. The process combines the simplicity of LOM with the flexibility of soldering/brazing that makes it very efficient. Metal foils are bonded together using soldering/brazing paste to produce metal parts. Some significant advantages of the process include better processing times, material flexibility and low feedstock costs. Shirvani (2000) filed a patent in which honeycomb structures were made using the process of brazing and thin aluminium foils. A special brazing paste (80% zinc and 20% aluminium by weight) was utilized to remove the tenacious oxide layer on the surface of the metal and join the thin strips of aluminium together to produce the honeycomb structures. The final products showed better mechanical properties and corrosion resistance compared to the ones made by resin bonding. The results highlighted the advantages of brazing as a joining process and its effect on the thin strips of metal. A number of different pastes and fluxes from various manufacturers were tested before finalizing the same paste used by Shirvani. The reason is that the other pastes were unable to join the aluminium metal foils and owing to the popularity of this metal in the manufacturing industry, it was crucial to make and test parts made by aluminium.

The process of CMFM has been explained in detail in Chapter 3. Chapter 5 deals with the practices used for making sample parts for testing and Chapter 6 gives the experimental results that prove the tensile strength of the parts made by CMFM is higher than those produced by conventional machining/subtractive methods.

The structure of the thesis is illustrated in Fig. 1.1.

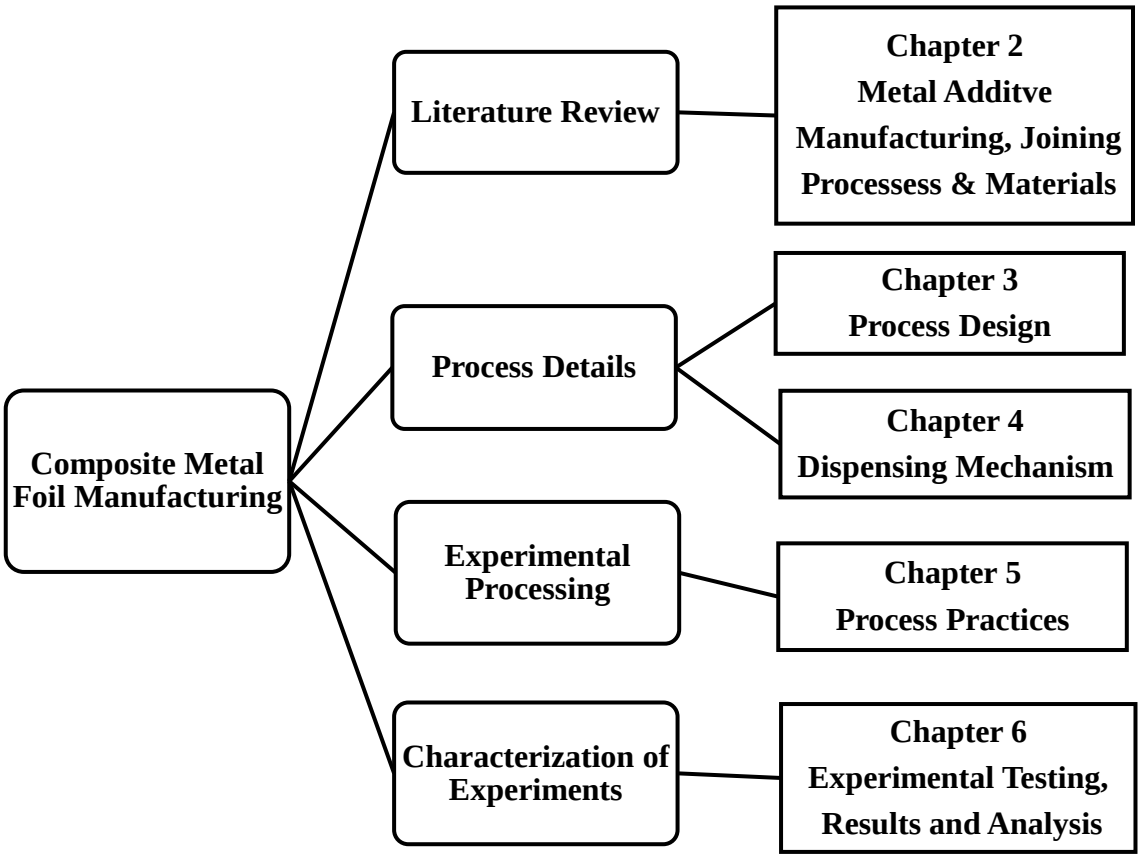

Figure 1.1: Structure of the thesis

1.3 Gap in Knowledge

Despite rapid advances in the field of AM, there exists a clear gap in knowledge when it comes to material properties of additively manufactured parts. They are often criticised for not being strong enough for real world applications. The new proposed process (CMFM) fills that gap in knowledge by analysing the strength of materials using composite metal foils. The process exploits the capability of LOM combined with a suitable metal joining method i.e., soldering/brazing especially with aluminium that is known for its poor soldering capability. CMFM can produce a range of parts with complex geometries. Hollow parts, like moulds including cavities, can only be made using additive processes as subtractive processes are unable to create such parts. There are huge commercial implications for the production of

large moulds for engines as shown in Fig. 1.2. Such moulds take weeks and CMFM is fully capable of achieving this goal with ease in a relatively less period of time.

Figure 1.2: Sand moulding of a Musket V-twin engine for motorbikes (TheKneeslider.com, 2012)

The proposed process can also produce parts from different materials (composites) without the use of additional machinery or equipment. This is an added advantage as the production of composite parts add versatility to the system. Composites have gained wide interest owing to their capabilities and the alternatives that they could offer. The process can produce composites using inexpensive, light-weight metal in the middle and then bonding layers of a stronger metal on the outside to create a light-weight and strong composite; such a composite product can have numerous applications in academia as well as in manufacturing industries.

1.4 Research Questions

The following research questions form the basis for this work and they will be answered in Chapter 7 after all the evidences have been presented in support of this research:

- Can LOM effectively work with metal joining methods such as brazing and soldering?
- How will the proposed process be automated?
- What type of geometries can be made using the proposed process?
- How much post-processing will be involved?
- Will the produced parts be of satisfactory quality for comparison with other processes?
- Will produced parts be free from cracks, voids and cavities as a result of thermal stresses?
- How fast will the proposed process be able to produce parts?
- How will the material properties be affected in the proposed process?
- To what extent can the proposed process reduce cost of production?
- Does the proposed process have the capability to compete with rival metal prototyping technologies?

1.5 Aim and Objectives

The aim of this research is to introduce a new additive manufacturing process for the production of high quality and low cost metal parts. Parts are to be produced using the principles of the proposed process and they will be tested following the British and International Standards. The process of making the parts has to be more affordable and it should have a comparable or better material integrity compared to conventional methods to be implemented in industries and to have any advantage to the consumers. The process

should minimise the limitations of commercial metal prototyping processes such as in material types, speed, cost etc., so that it can be considered as a strong candidate in the field of metal prototyping. The following is a list of objectives that had to be met for the successful completion of this research work:

- Review and analyse current metal prototyping processes
- Identify and understand the problems related to the production of metal parts
- Review Laminated Object manufacturing (LOM) in the context of the proposed process
- Investigate and propose a suitable metal joining process
- Design, develop and test the proposed process for the production of metal parts
- Create a three dimensional model using ANSYS and carry out transient thermal analysis for the metal parts
- Produce parts using the proposed method and design experiments for their mechanical testing
- Compare and discuss the test results with other methods

1.6 Methodology

There are three major approaches for research namely; qualitative, quantitative and mixed methods. Research methods should follow research questions in a way that offers the best chance to obtain useful answers (Connelly, 2009). This current research follows mixed method approach as it involves the analysis of both quantitative (numerical/measurable data) and qualitative (understanding of underlying reasons) data. The data is collected sequentially starting from theoretical knowledge (laws, principles, models, concepts, etc.) and then moving towards empirical knowledge (acquiring data through experiments, observations, facts etc.). The collected data is then integrated so as to make a complete model of research

that could either be inductive or deductive. This research first formulated a theory and then tested it, therefore, it falls under the deductive approach as like other engineering related researches. Inductive approach is the opposite of deductive and is more suitable to social sciences and humanities.

The aim and objectives of the research (Section 1.5) were formulated first so as to develop a road map for the research (Fig. 1.3). The next step is reviewing the literature and gathering the appropriate data for moving the research forward. Since additive manufacturing is making strides every single day, it is important to have up-to-date information about metal AM and joining methods so as to provide solutions tailored to the current market (Chapter 2). The literature (journal and conference papers, books, engineering articles etc.) helped in understanding the pitfalls of the work done and the next step is putting forward a conceptual model of a machine based on the principles of LOM and soldering/brazing techniques as a new additive process known as Composite Metal Foil Manufacturing (Chapter 3). The major components of the machine are then justified for their fitness of purpose through computer simulations (Chapter 3 and 4). The process of CMFM is then broken down into simple independent steps so as to produce parts and establish the effectiveness of the new process. A 3D model is also presented that can aid in the production of parts in the future and removes guess work regarding the heating time (Chapter 5). The parts including single lap joints, T-peel specimens and tensile specimens were produced and tested according to British and International standards. Aluminium 1050 with a H14 ½ hard temper and pure copper foils of varying thicknesses were used to make parts. Copper parts were made using Direct Soldering Paste (AL27-103-75) which is a product of Superior Flux & Manufacturing Company. A special brazing paste (ASN-892B-600) from Fusion Incorporated was used for joining foils of aluminium to make similar material parts as well as aluminium and copper foils to make composite parts. The results from lap-shear testing, peel testing and tensile testing were

compared to other metal AM as well as subtractive/machining methods to show the capabilities of the new process (Chapter 6). The final step is concluding the work and answering the research questions based on the data collected through literature and experimentation followed by some future work that will help enhance the scope of the work done in this project (Chapter 7).

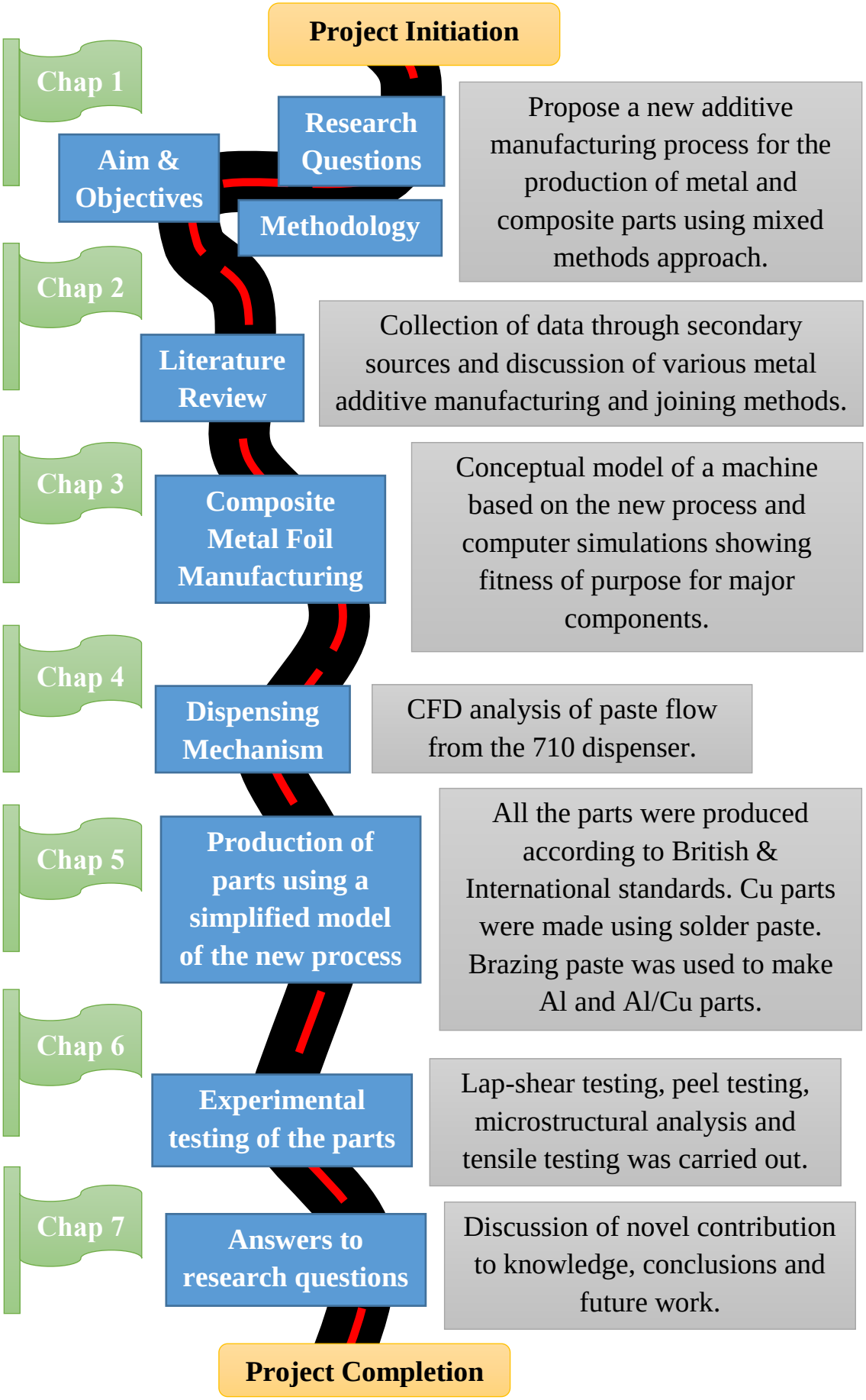

Figure 1.3: Road map of the PhD project

1.7 Thesis Structure

The thesis is divided into seven chapters. A brief summary of the contents of each chapter is given below:

Chapter 1 provides an introduction to the problem, methodology for the solution to the problem, the research aim and objectives.

Chapter 2 presents the background material on a number of topics. It starts with the overview of current commercial metal prototyping methods followed by metal prototyping techniques that have found success in academic research. It also justifies the choice of soldering/brazing as a metal joining method and gives an overview of the challenges faced with the metallurgical joining of different metals. This chapter also analyses the difficulty and importance of working with aluminium and producing composites as both of these topics are of great interest to the manufacturing industries.

Chapter 3 provides a detailed description of the proposed process termed as Composite Metal Foil Manufacturing (CMFM). It presents a conceptual model of an automated machine based on the principles of the proposed process followed by a flow chart of operation. The major components of the machine are discussed in detail and their functional capabilities are validated by numerical analyses.

Chapter 4 discusses one of the most important mechanisms of the machine; the dispenser. It gives an overview of 710 dispenser's working followed by computational fluid dynamics (CFD) analysis to show its capabilities along with the electrical circuitry and C++ code for establishing communication between the dispenser and the main machine.

Chapter 5 presents the experimental setup that was created to demonstrate the capability of the proposed process for the production of parts and testing specimens. The chapter gives a detailed description of every step involved in the production of parts and also presents a three dimensional model that can be used for making parts in the future without any guess work.

The model has been used to validate the experimental work by comparing the time taken to make a dissimilar aluminium/copper single lap joint with transient thermal analysis carried out in ANSYS.

Chapter 6 includes the experimental test results that include tensile lap-shear testing, peel testing, corrosion testing, microstructural analysis and comparative tensile testing. In some instances, the results have been compared with similar research work to analyse and validate the effectiveness of the proposed process.

Chapter 7 provides conclusions for the obtained results in the research and their commercial implications. It also discusses future work that could be done to further cement CMFM as a strong candidate in the field of metal additive manufacturing.

1.8 Related Publications

The following is a list of publications (published and unpublished) that are available at the time of thesis defence.

Published Peer-Reviewed Journal Papers

Butt, J., Mebrahtu, H. and Shirvani, H., 2016. Microstructure and mechanical properties of dissimilar 1050 aluminium/pure copper foil composites made with a new additive manufacturing process. *Journal of Materials Processing Technology*, 238, pp.96-107.

Butt, J., Mebrahtu, H. and Shirvani, H., 2016. Strength analysis of aluminium foil parts made by composite metal foil manufacturing. *Progress in Additive Manufacturing*, 1(1), pp.93-103.

Butt, J., Mebrahtu, H. and Shirvani, H., 2015. Thermo-Mechanical Analysis of Dissimilar Al/Cu Foil Single Lap Joints Made by Composite Metal Foil Manufacturing. *World Academy of Science, Engineering and Technology, International Journal of Mechanical, Aerospace, Industrial, Mechatronic and Manufacturing Engineering*, 10(1), pp.41-46.

Butt, J., Mebrahtu, H. and Shirvani, H., 2015. Peel and tensile test investigation of aluminium 1050 foil parts made with a new additive manufacturing process. *International Journal of Rapid Manufacturing*, 5(1), pp.95-115.

Butt, J., Mebrahtu, H. and Shirvani, H., 2015. Rapid prototyping by heat diffusion of metal foil and related mechanical testing. *The International Journal of Advanced Manufacturing Technology*, pp.1-10.

Butt, J., Mebrahtu, H. and Shirvani, H., 2015. A novel rapid prototyping process for the production of metal parts. *International Journal of Advancements in Mechanical and Aeronautical Engineering – IJAMAE*, 2(1), pp.15-18.

Book Chapter (Accepted: June 2016)

Butt, J., Mebrahtu, H. and Shirvani, H., In Press. Metal Rapid Prototyping Technologies. In: V. M. Petrova, ed. 2016. *Advances in Engineering Research. Volume 14.* New York, USA: Nova Science Publishers, Inc. Ch.2.

CHAPTER 2

2 Metal Additive Manufacturing, Joining Processes and Materials

2.1 Introduction

There has been a lengthy debate over the use of the terms additive manufacturing, rapid prototyping and 3D printing. This goes back to the late 1980s when the very first of these processes, stereolithography (SLA), came into existence. During that time, the process was only producing prototypes but it was doing it rapidly and thus the term rapid prototyping was used as it distinguished both its key advantage and primary application. But with the passage of time, the term became very limited and was often misused (Balzer, Goldman and Wile, 1982). The early 1990s saw the technologies move to the production of tools and other such parts. The industries coined the terms rapid manufacturing and rapid tooling to show that the technologies have moved past their days of producing prototypes. However, the term was still alluring to companies that were doing prototyping, tooling and manufacturing quickly and hence it stayed. This adoption created some serious confusion as it became very difficult to distinguish additive manufacturing processes from all others especially subtractive methods like machining and forming (Tripp and Bichelmeyer, 1990). Towards the mid-1990s, industries tried to coin terms such as freeform fabrication (FFF), solid freeform fabrication (SFF) but they did not stick. In the late 1990s and early 2000s, the manufacturing of parts became mainstream and garnered a great deal of attention from academia and industries alike. Therefore, another attempt was made to distinguish additive processes by promoting terms such as layer manufacturing (LM), additive layer manufacturing (ALM), additive fabrication (AF) etc., Some of them are still used today but everyone is not familiar with them (Lu, et al., 2009).

A few years ago, a standards body within ASTM (American Society for Testing and Materials) took it upon itself to standardize the term additive manufacturing and define the technologies that fall under this category. They defined **''additive manufacturing''** as a process of producing three dimensional objects additively in a layer-by-layer manner (ASTM F2792-10, 2010). Therefore, majority of the processes that were widely called rapid prototyping processes became additive manufacturing processes because they were producing parts by laying down successive layers on top of each other. This made sense as rapidly producing a part is a characteristic of the process and not the actual process itself. Unlike application based names such as rapid prototyping, rapid tooling, 3D printing etc., the term AM represents the fundamental principle. In this context, it became clear that an additive manufacturing process can also be a rapid prototyping process but all rapid prototyping processes cannot be additive manufacturing processes, for example inkjet printing of strain gauges is clearly additive manufacturing but it is not a rapid prototyping process. The term 3D printing, on the other hand, was invented at the Massachusetts Institute of Technology (MIT) in 1995 but it was used to an inkjet printing based approach (Grimm, 2004). Over time, the term spread because it was so descriptive and easy to understand by almost everyone. Additive manufacturing and 3D printing are synonyms of each other but for the sake of clarity the thesis will make use of the term additive manufacturing and not 3D printing or rapid prototyping. AM defines the process and rapid prototyping (prototypes for visualization, form/fit testing and functional testing), rapid tooling (moulds and dies), and rapid manufacturing (medium-to-high volume production of parts) are its applications.

This chapter presents an overview of the commercial metal prototyping processes along with their strengths and weaknesses. A number of processes that have been widely researched upon in academia will also be presented along with their advantages and disadvantages. Laminated Object Manufacturing will be discussed in context of the proposed process for

cutting and stacking of the metal foils. Several metal joining methods will be briefly discussed before justifying the use of soldering/brazing as an appropriate and suitable solution.

2.2 Additive Manufacturing Processes

These processes are different from subtractive and consolidation processes as they build parts by adding layers of material on top of each other. Subtractive processes such as milling, drilling or turning work by cutting/machining the material from the workpiece by using carefully planned tool movements to build the desired part. This results in high waste which increases the cost of production. Consolidation processes like casting or moulding, solidify the material into desired shape by using custom designed tooling and apparatus. In a sharp contrast to these, additive manufacturing does not require the use of specialized tooling or machinery. It works by taking a 3D CAD file and slicing it into thin layers which are used by the machine to build each layer sequentially until the required dimension of the part are achieved. There are a number of AM processes that are commercially available and each has its own market based on the materials used and the applications provided. Table 2.1 lists these processes with the different materials they use, their applications and the timeline when they became exceedingly important to manufacturing industries.

Table 2.1: Additive manufacturing processes, materials and their applications

Processes	Year	Materials	Applications
Stereolithography (SLA)	1986	Photopolymer, thermoplastics	Form/fit testing, functional testing, rapid tooling patterns, snap fits, presentation models
Solid Ground Curing (SGC)	1986	Photopolymer, thermoplastics	
Fused Deposition Modelling (FDM)	1990	ABS, elastomers, polycarbonate,	
Laminated Object Manufacturing (LOM)	1991	Paper sheets	
Ink-jet Printing	1995	Powder and ink	
Selective Laser Sintering/Melting (SLS/SLM)	1997	Nylon, polyamide, polystyrene	
Direct Metal Laser Sintering (DMLS)	1994	Powder metal	High heat applications, medical implants, aerospace parts
Electron Beam Melting (EBM)	1994		
Laser Engineered Net Shaping (LENS)	1997		
3D Ceramic Printing	2007	Ceramics	
3D Printing	Current trends	Plastics, metals, ceramics	Widely researched upon technologies
Jetting (Photo-curable polymer)		Photopolymer, thermoplastics	

The AM processes kept evolving with time and started using other materials than the ones initially intended for their use. These advancements have opened new research opportunities and the manufacturing industries have capitalized on them by continuing the work and proposing new ways to use different materials. The next section describes commercially available metal prototyping processes that have made a name for themselves by delivering high quality parts over the years. These were originally designed to produce metal parts from different metallic powders. The choices in terms of materials are limited but the research is ongoing and will keep providing more solutions as time goes by. The next section gives a more in-depth analysis of the methods capable of producing metal parts.

2.3 Metal Additive Manufacturing Processes

There are a number of AM processes capable of producing metal parts. They can be classified based on the energy source they use, the way feedstock is joined, the component used to join feedstock and the type of feedstock (powder, wire or sheet). Table 2.2 (Ding, et al., 2015) shows four broad classifications of the metal AM processes. They include

i. Powder bed systems, Section 2.3.1
ii. Powder feed systems, Section 2.3.2
iii. Wire feed systems, Section 2.3.3
iv. Sheet laminates, Section 2.4-2.6.

Table 2.2: Metal AM processes and types of materials they use

PROCESS	MATERIALS
POWDER BED	
Electron Beam Melting (EBM)	Metal powder
Direct Metal Laser Sintering (DMLS)	
Selective Laser Melting (SLM)	
Selective Laser Sintering (SLS)	
POWDER FEED	
Laser Engineered Net Shaping (LENS)	Metal powder
Laser Consolidation (LC)	
WIRE FEED	
Electron Beam Additive Manufacturing (EBAM)	Metal wire
Plasma transferred arc selected free form fabrication (PTAS FFF)	
SHEET LAMINATES	
Laminated Object Manufacturing (LOM)	Metal laminate, metal foil
Ultrasonic Consolidation (UC)	

2.3.1 Powder Bed Systems

They can only use one type of metal powder at any given time and work by sintering powder using a fibre laser or in case of EBM an electron beam. A powder bed is created by spreading metal powder across the working envelope of the machine. Layers of powder are added repeatedly following sintering or melting with laser until the required shape is achieved. The

powder bed system shown in Fig. 2.1 has a number of notable advantages including high resolution and dimensional accuracy of the parts produced. These systems are also known as laser melting processes because of using lasers to melt the metallic powder and are commercially available under different trade names manufactured by various companies from around the world as shown in Table 2.3 (Frazier, 2014). The variety of materials available for metal AM systems is continuously expanding. Common materials used are stainless steel, aluminium, nickel, cobalt-chrome and titanium alloys, with a number of machine manufacturers offering their own materials. The common specifications of metal powders suitable for AM are the spherical geometry of the particles resulting from the gas atomisation and a particle size distribution according to the layer thickness, usually between 10-50 µm.

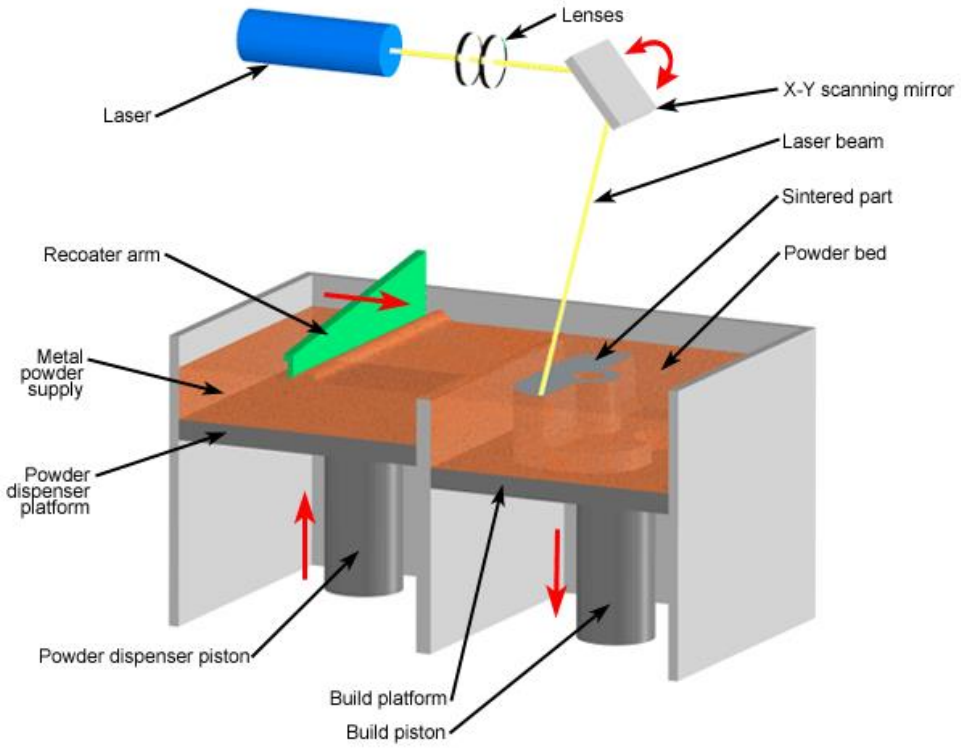

Figure 2.1: Powder bed system (Custom Part, 2009)

Table 2.3: AM equipment power sources and specifications

System	Process	Build Volume (mm)	Energy Source
Powder Bed			
ARCAM (A2)(a)	EBM	200 x 200 x 350	7 kW electron beam
EOS (M280)(b)	DMLS	250 x 250 x 325	200-400 W Yb-fibre laser
Renishaw (AM250)(c)	SLM	245 x 245 x 360	200 or 400 W laser
Powder Feed			
Optomec (LENS 850-R)(d)	LENS	900 x 1500 x 900	1 or 2 kW IPG fibre laser
Accufusion laser consolidation(e)	LC	1000 x 1000 x 1000	Nd: YAG laser
Wire Feed			
Sciaky (NG1) EBFFF(d)	EBAM	762 x 483 x 508	>40 kW @ 60 kV welder
MER plasma transferred arc selected FFF(d)	PTAS FFF	610 x 610 x 5182	Plasma transferred arc using two 350A DC power supplies
Country of Manufacturer: (a) Sweden, (b) Germany, (c) United Kingdom, (d) United States, and (e) Canada			

As parts produced by DMLS usually have a grainy surface finish due to powder particle size, layer-by-layer building and spreading of the metal powder prior to sintering by the powder distribution method, some post-processing is required to improve the surface quality of the parts. The un-sintered or loose metallic powder is removed and recycled for future use, making the process both economical and environmentally friendly.

2.3.2 Powder Feed Systems

These systems use metal powders, same as powder bed systems, but the way layers are built differs significantly. The powder flows through a nozzle being melted from a beam right on the surface of the treated part. Laser Cladding (LC), Directed Energy Deposition (DED) and Laser Metal Deposition (LMD) are some names that powder feed systems are also known by. A powder feed system is shown in Fig. 2.2.

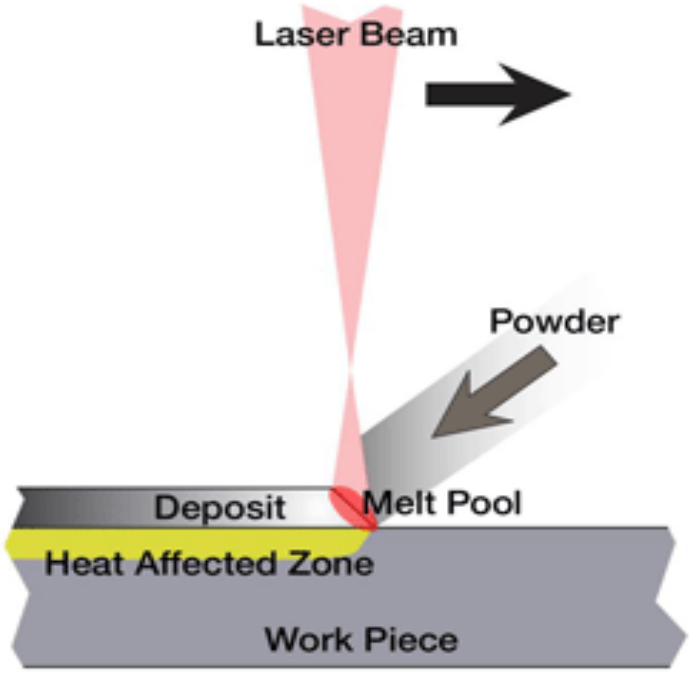

Figure 2.2: Powder feed system (Metal AM, 2010)

The process is highly precise and based on an automated deposition of a layer of material with a thickness varying between 0.1mm and several centimetres. The metallurgical bonding of the cladding material with the base material and the absence of undercutting are some features of this process. The process is dissimilar to other welding techniques in that a low heat input penetrates the substrate. LENS powder delivery system used by Optmec is a prime example of this technology which can easily add new materials to an existing part. This feature allows repair work to be done easily and makes the process flexible for users.

2.3.3 Wire Feed Systems

Wire feed AM is a promising technology and has come into existence majorly due to the high cost of metal powders that are used for powder bed and powder feed systems. The cost of wire feed-stock is much less than metallic powder (Ding, et al., 2015) but the process is not without flaws. Residual stress and distortion from excessive heat input, poor accuracy of the part due to stair stepping effect and relatively poor surface finish of the final parts are notable. These systems require careful monitoring of process parameters such as such as deposition width, layer thicknesses, wire diameter, wire feed rate and welding speed to achieve correct part dimensions and surface finish.

In addition, the residual stress-induced deformations are a major cause of loss in tolerances in wire-feed AM of large components. Depending on the energy source used for metal deposition, wire-feed AM can be classified into three groups, namely: laser based, arc welding-based and electron beam-based. Fig. 2.3 shows the wire feed process.

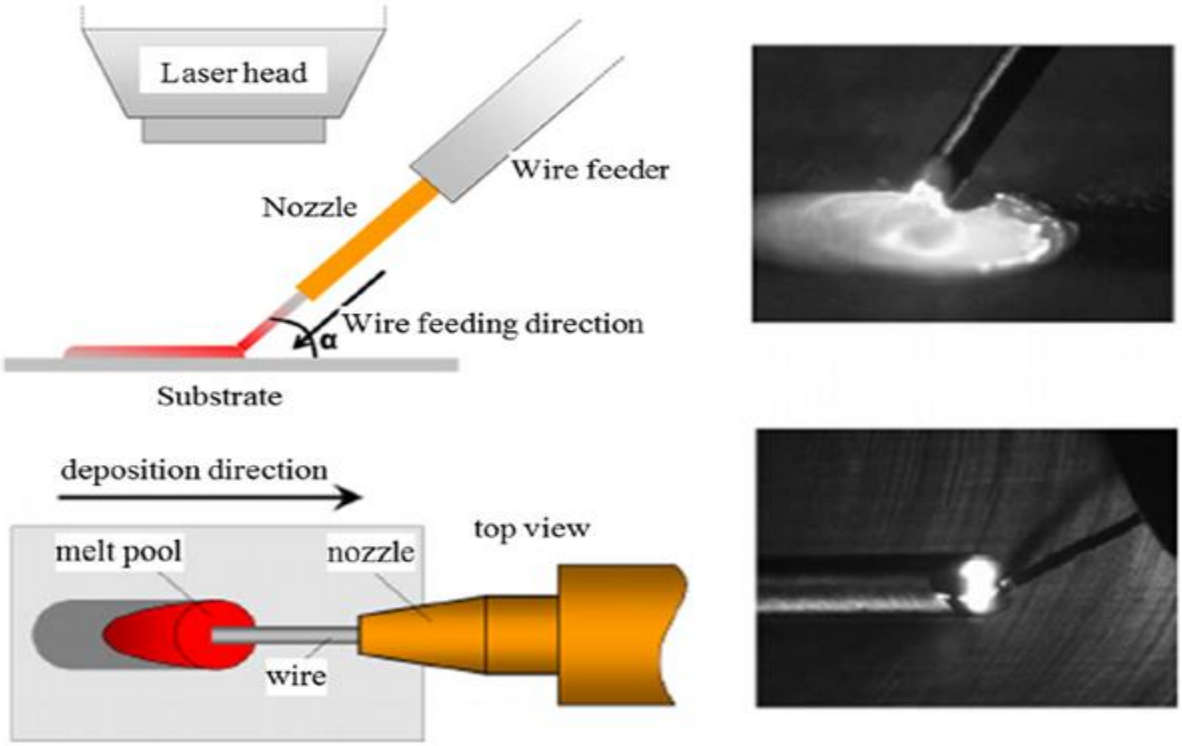

Figure 2.3: Schematic drawing on the left and real wire feed process on the right (Ding, et al., 2015)

According to Unocic and DuPont (2004), laser is precise but suffers due to poor energy efficiency (2–5%). The work done by Rännar, Glad and Gustafson (2007) shows that electron beam requires a high vacuum working environment and has a slightly higher energy efficiency (15–20 %). In comparison, the energy efficiency of arc welding processes such as gas metal arc welding (GMAW) or gas tungsten arc welding (GTAW) processes can be efficient as high as 90 % in some circumstances (DuPont and Marder, 1995; Stenbacka, Choquet and Hurtig, 2012). Additionally, the cost of the traditional arc welding equipment is relatively low when compared to the laser or electron beam equipment. The list of metal alloys used by wire feed systems keep on increasing with time but at the moment they can effectively utilize Fe-based (Moures, et al., 2005), Ti-based (Baufeld, Brandl, and Biest, 2011; Mok, et al., 2008) and Al-based (Xiao, 2002) materials, among which Ti- based material (Ti-6Al-4V) gets most wide attention due to its popularity in the aerospace industry. The diameter of the wire for the AM process normally ranges from 0.2 to 1.2 mm and is readily available from a number of vendors so procuring the feed-stock is relatively easy as compared to metal powder. EBM is an exception as it is available both as a powder bed system and as a wire feed system.

2.3.3.1 Secondary Finishing Processes

AM technologies that produce metal parts do not rely only on the main process but a few secondary processes as well to achieve better surface quality, geometrical accuracy and mechanical properties. These secondary processes improve the properties but at the same time consume time and money making the system more costly. The metal parts produced are not always the final products and some support material is usually kept in place for complex shapes. Since the support material is the same as the build material, the post-processing is done by machining the extra material off that could be time consuming. Milling, drilling, polishing are some of the usual operations that are generally performed on parts produced by

AM processes. Polishing of internal surfaces such as internal channels is done by abrasive flow machining. Heat treatment and shot peening are two of the most common processes adopted to improve mechanical and tactile properties of the surface of AM parts. Electro polishing is also a popular post-process and this electro-mechanical treatment significantly improves the surface finish. It minimises micro-roughness which reduces the risk of dirt or residues affecting the surface. Since this process does not involve mechanical, thermal or chemical impact, small and mechanically fragile parts can also be treated with ease (Metal AM, 2010).

2.4 Laminated Object Manufacturing

In the year 1991, Helisys, based in United States commercialized the manufacturing technology termed as Laminated Object Manufacturing (LOM). The raw material was inexpensive copier paper coated with thermally activated adhesive on one side that was then cut into the desired shape using a CO2 laser. The sheets of paper were stacked on top of each other and then joined by a heated roller that melts a plastic coating on the bottom side of the paper to create the bond as shown in Fig. 2.4. The entire process was automated but it created considerable smoke and localized flame during operation, therefore, a chimney was often built into the system. Even though the operation is quick and the raw material is affordable, the technology did not fare well over the years as a solution to additive manufacturing problems owing to the limitations related to detail and accuracy (Mueller and Kochan, 1999; Wiesensel, et al., 2004). Since paper parts were hardly used as functional products, other material laminates were introduced to work with LOM including ceramics, plastics and metals (Prechtl, Otto and Geiger, 2005a; 2005b; Gomes, et al., 2009; Zhang, et al., 1999). The LOM parts showed a comparatively higher accuracy but stair-stepping on the edges and lack of detail remained as significant problems.

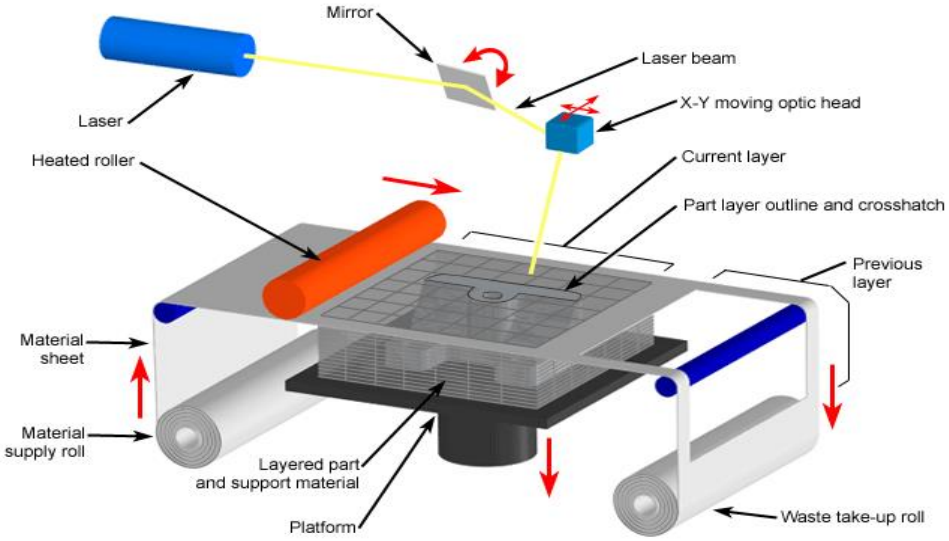

Figure 2.4: Laminated object manufacturing (Custom Part, 2009)

This process was chosen to be integrated with an appropriate metal joining method owing to its simplicity and capability to use laminated sheets. These factors make it an excellent candidate to work with metal foils. The reason for choosing metal foils for operation was because they are low-cost and readily available. A number of modifications were needed to the original LOM process which will be discussed in detail in Chapter 3.

2.5 Metal Foil LOM

The method works in the same way as paper LOM and makes use of metal foils to make metal parts. The work done by Prechtl, Otto and Geiger (2005a), showed that Metal Foil LOM is a two-step procedure where the foils are stacked and contours are made with the help of a solid state laser, Nd: YAG (neodymium-doped yttrium aluminium garnet), and then joined in a furnace. During the part building process, the very first layer is attached to a metallic base plate and the extra material is also left in place to be removed afterwards by hatching. This increases the post-processing after the part has been made. The layers are fixed by weld spots at defined intervals. Since welding is involved, the laser beam is used at short

pulses so as to have a smaller melt pool which will allow for better joining of the foils together. The metal stack that has been made after the layers have been fixed is not stable enough for any technical applications. It is then pressed at high temperature in combination with an inert atmosphere for a set period of time. The major application for metal foil LOM is in the production of large moulds but the setup is expensive and poses operating issues. The process cannot work with metal foils having thicknesses less than 0.5mm as anything less than that results in staircase effect. The process also requires the generation of contours that require a sufficient self-stiffness of the sheets and anything less than 0.5mm results in failure of the contour generation. The surface quality is not good and the products require post processing such as milling, build-up welding or shot peening where necessary (Prechtl, Otto and Geiger, 2005b).

2.6 Ultrasonic Consolidation

This technology has been making quite a name for itself in the academic sector and has proven to be an interesting prospect as it has shown great promise in working with difficult metals like aluminium and stainless steel. It combines ultrasonic seam welding of metals and layered manufacturing techniques to build up a solid freeform object (Ram, Yang and Stucker, 2006). The basic principle of UC and ultrasonic seam welding is similar. The difference lies in the fact that UC makes use of an ultrasonic transducer followed by a milling operation to achieve the desired shape of the part whereas ultrasonic seam welding is used to join two overlapped sheets. It can produce metal parts and tooling but it is also being developed further so that it could be able to produce metal matrix composites as a number of issues arise in trying to join different metals together. It is also referred to as a hybrid form of manufacture because it utilizes ultrasonic metal welding to sequentially bonds metal foils together using and then makes use of Computer Numerical Control (CNC) machining to

remove material to create the desired geometry. The term hybrid is used as it incorporates both additive and subtractive means to build parts.

The process of UC starts with attaching a base plate to the machine anvil and then metal foil is placed on the base plate. A sonotrode connected to a transducer is used to apply pressure and ultrasonic oscillations to the foil to bond it to the base plate. The process is repeated until the required height is achieved and then a CNC mill is used to trim the excess foil from the component and achieve the required geometry. Another finishing mill is brought into action to create the required tolerance and surface finish. After the trimming and finishing, the finished part is removed from the anvil (Ram, Robinson and Yang, 2007). The biggest challenge of this process is optimization of the process for bond density and plastic flow to have a better contact between the foils (Kong and Soar, 2005). The sonotrode contact with the metal surface (performed under pressure and with an oscillatory motion at ultrasonic frequency), creates a highly deformed surface that could lead to levels of porosity between the foil layers of an Ultrasonically Consolidated component. Yang, Ram and Stucker (2007) showed that inter-laminar porosity in UC could also result in reduced mechanical performance when compared to monolithic structures of the same material. The schematic diagram of the UC process is shown in Fig. 2.5.

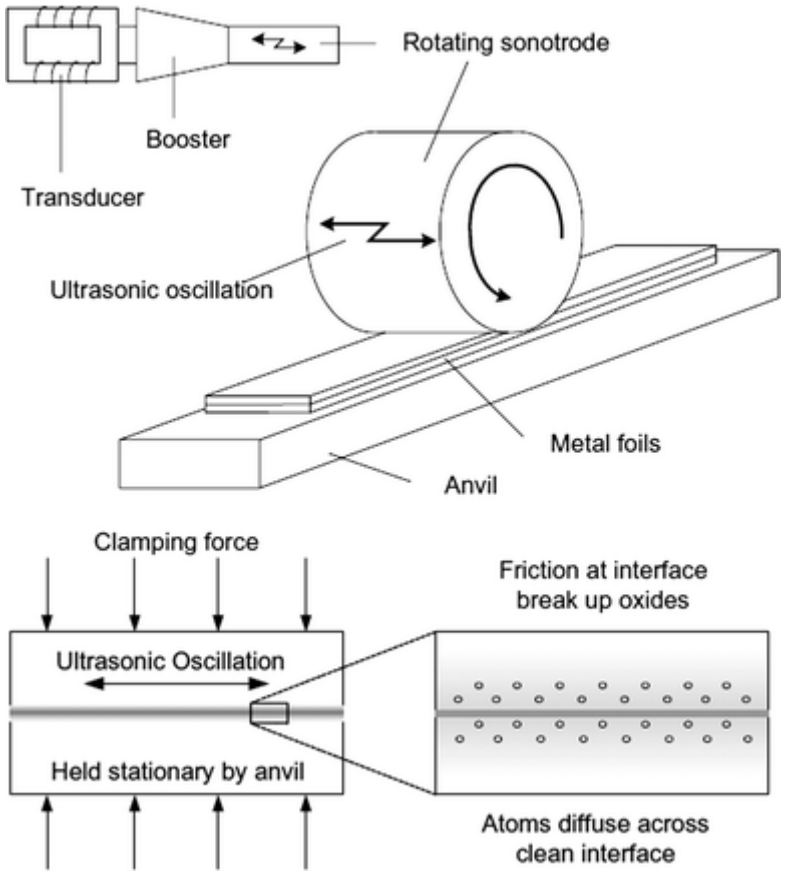

Figure 2.5: Ultrasonic consolidation process (Kong, Soar and Dickens, 2005)

2.7 Metal Joining Processes

There are a number of processes available for the joining of metal parts including:

- Riveting
- Bolting
- Adhesive Joining
- Welding
- Soldering/Brazing

Riveting and bolting are not very good options. They are permanent mechanical fasteners and are mostly used to make joints and hold metals parts together in construction. They are not suitable to integrate with LOM for the production of layered metal parts due to drilling holes

for installation as well as introducing an additional fastener for joining. Adhesive joining, on the other hand, is a very feasible approach and it can be easily integrated with the LOM process. Adhesives can join a number of metals with ease and do not require complex equipment for application. But they are not without their issues including their inactivity at high temperatures, long curing times, surface preparation and environmental effects (Kearns, 1980; Piva, et al., 2015). To fully compliment the LOM process, the joining process needs to be flexible and efficient so as to make a better AM process.

Welding is also a very popular metal joining method and has a number of options to choose from including oxyacetylene welding, shield metal arc welding, gas tungsten arc welding, plasma arc welding, gas-metal arc welding, submerged arc welding electro-slag welding etc. Most of these methods have low welding speed and cannot work with aluminium and titanium which is a big disadvantage (Gietzelt, et al., 2013). The equipment for welding is usually very expensive compared to other methods but the biggest disadvantage is that it requires very high temperatures that create large heat affected zones, which is why they are not well suited to work with thin metal foils (Wei, et al., 2014).

Soldering and brazing are liquid-solid phase bonding processes. They are quick, easy to use and operate at relatively low temperatures compared to welding. Soldering and brazing are similar to each other but the main difference lies in the operating temperatures as joining operations that are under 450 °C are considered to be soldering and those above 450 °C lie under brazing. Since the base metals are not being melted to create the bond, a low temperature heat source can be used which minimizes distortion and creates a much smaller heat affected zone (HAZ) compared to welding. This process also gives the freedom to disassemble the part by reapplying heat. The base metal is not damaged and can be reused which makes this process extremely cost-effective. Any metal can be joined using this process as long as the appropriate paste is available. This solves the problem of using

different metals that restricts a number of other metal AM processes. Joining dissimilar metals is done in the same way as similar metals without any additional tooling or equipment which makes this metal joining operation very versatile (Gao, et al., 2013). The process of soldering is used extensively in electronics industries because solder is metal; it conducts electricity (Suganuma, 2003). This feature makes the parts produced by this process all the more attractive to consumers. The biggest advantage of soldering is that parts of varying thickness can be easily joined without burning or overheating and because the proposed process makes use of metal foils, it is a merit point. Based on the reasons provided, it is evident that soldering and brazing are perfect choices for metal joining operation and could be integrated with the LOM process. The paste will be deposited by an applicator and heating will be provided by heated plates. The integration of the LOM process with soldering/brazing is explained in Chapter 3.

2.8 Solderability

The solderability of a substrate is a measure of the ease with which a soldered joint can be made to that material (Wang, et al., 2009). Good solderability requires good wetting so that a uniform, smooth, unbroken, adherent coat of solder can be formed on the base metal. Therefore, wetting is an essential prerequisite for soldering. Wetting means that molten solder diffuses into the solid surface of the metal to be soldered. It is only possible when the solder can come into immediate contact with the metallic surface of the solid metal part. Any barrier like oxides, oils on the surface to be soldered will prevent wetting and prove to be a hurdle in the formation of an intermetallic bond (Vianco, 1999).

Poor solderability leads to non-wetting and de-wetting where the solder does not adhere to the surface to be soldered and there is no bond formation. This condition is caused by a physical barrier (intermetallic or oxide) between the solder and the base metal. It is a good

practice to pre-tin the metals to be soldered using an active flux to achieve good solderability but that will require more time consumption and extra material purchase. It is advisable to find a solder paste with the right medium of flux that can solder a particular type of metal without any pre-treatment. It is kind of a trial and error approach but for difficult metals like aluminium, buying any solder paste is just not an option. The contents of the paste need to be researched along with the flux that is being utilized in its preparation. De-wetting is a serious problem in metal joining as it leaves irregular shaped mounds of solder separated by areas covered with a thin solder film. In this scenario, the molten solder has coated a surface and then receded as it was unable to diffuse in the metal surface because of the oxide layer or any other barrier (Law, et al., 2006). Copper, silver, and gold are easy to braze because they have good braze-ability. Iron, mild steel and nickel are next in difficulty. Because of their thin, strong oxide films, stainless steel and aluminium are even more difficult to braze.

2.9 Properties of Metal Foils Used

Two different types of metal foils were chosen to carry out the research work, one being pure copper and the second aluminium 1050 with a H14 ½ hard temper. The reason for choosing copper and aluminium is because of their extensive use in manufacturing industries. Making parts from them would help establish CMFM as a strong candidate in the field of metal AM processes. Joining copper is fairly simple and it can be done using basic solder pastes. Aluminium, on the other hand, is one of the toughest metals to join but because it is very popular in industries due to its light weight and high strength, it was imperative to make parts from it and test them to show the flexibility and efficiency of the new proposed process. Various aluminium alloys have different braze-ability: the 1xxx, 2xxx, 3xxx, 4xxx, and 7xxx series are easier to braze than the 6xxx series alloys. Magnesium content in the 5xxx series alloys makes them the most difficult to join. This is because, in addition to the oxide layer of aluminium, the oxide layer of magnesium needs to be removed to perform the joining

process. Additionally, on contact with air, a magnesium oxide layer is formed, thus there are two layers to remove when joining aluminium alloys containing magnesium (Davis, 1993). As the removal of the oxide layer is the key to the joining process, a special flux is used when brazing aluminium alloys. Although traditional tin/lead solders can be used to braze aluminium, the large difference in the electro potentials of the aluminium substrate and the tin/lead solder present a galvanic couple that can lead to accelerated corrosion. This problem can be avoided with the use of either tin/zinc eutectic solder or higher temperature zinc/aluminium solder as the bonding alloys for brazing aluminium. The removal of copper oxide is relatively easy and can be done with 'normal' soldering methods using mild fluxes whereas aluminium oxide requires stronger fluxes that can go up to temperatures of 550 °C (Byrnes, 1971). Other methods such as mechanical rubbing, ultrasonic, thermal spray, pre-coating etc., can also be employed to remove the oxide layer if no flux could be used. Tin/zinc soft solders are more commonly used with normal fluxes since their melting point is under 330°C and the zinc portion helps in preventing galvanic corrosion. The solders based on zinc are termed as hard solders because they use fluxes that offer higher melting temperatures to activate. Zinc is an element made up of hard, sharp-edged crystals that aid in abrading (scrubbing) through the tough aluminium oxide layer, thus permitting the metallurgical reaction between the filler and base metals to occur. This research deals with very thin aluminium foils so special attention should be given while brazing as there is a danger of pitting that will leave the specimens useless for testing.

2.10 Solder Paste

The solder paste used is called Direct Soldering Paste (AL27-103-75) and is a product of Superior Flux & Manufacturing Company. This paste was used to solder copper foils together as it was proving to be ineffective in case of aluminium. A different brazing paste (Section 2.11) was utilized to work with aluminium and aluminium/copper composites.

The solder paste is made from Type 3 Powder (-325/+500 Mesh Powder) with a unique flux binding system to keep the very active aluminium flux portion of the flux form degrading the solder powder. The paste utilizes a water-soluble chemistry so cleaning involves simply rinsing in hot water. The material should be refrigerated before use and when in storage. The temperature for printing and dispensing the paste is 20 – 23°C with 35-55% of relative humidity (Avery, 2011). The paste is 96.5/3.5 tin-silver consisting of a special flux medium and lead-free solder alloy. The alloy melting point is 227 °C. It has a soldering range of 280-380 °C. However, it should not be kept at the maximum temperature for more than 8 minutes as after this time the paste stops working.

2.11 Brazing Paste

The choice of a paste for aluminium was a difficult endeavour. A number of samples were tested from companies like Indium, MBO UK etc., but they did not work very well with aluminium. As discussed earlier zinc alloy pastes work well with aluminium, therefore, a special paste was ordered from Fusion Incorporated and tested with the foil samples. The paste proved to be a success and was wetting the aluminium surface very well. It is known as Aluminium Zinc Brazing Paste. The paste has a very high metal content consisting of 80% zinc, 20% aluminium by weight and a strong flux suspended in a binder. Just like any other brazing paste, its resistance to flow is not constant and it exhibits shear thinning. Most pastes are also thixotropic and their viscosity depends not just on the shear rate but also on the shear history of the paste. After stirring, the paste becomes less viscous but it is not the case with this paste. It was applied on the foils both after stirring and without stirring but the results were consistent showing that the paste is not thixotropic in nature. In addition to the dependence of viscosity on history, it also depends on temperature. Viscosity of a paste decreases at high temperatures owing to the change of state of one of the materials in the composition. The melting point of the solder paste in use ranges between 410 - 470 °C and it

becomes liquid in this range. However, it should not be kept at these temperatures for longer periods of time as the flux would burn off and the paste would not be able to penetrate the tenacious oxide layer on the surface of the aluminium foil. Its part number is ASN-892B-600 where the 'B' in the paste code refers to the micron size of the alloy powder which in this case is -150 microns to dust (Fusion-inc.com, 2013).

2.12 Composites

The production of metal composites from AM methods has been gaining popularity as they can provide better alternatives to engineering applications. SLM/SLS can produce composites by using three methods: (i) using various powders, (ii) in situ reactions, and (iii) furnace treatment. Fe-Graphite, WC-Co, Fe, Ni, Cu and TiC MMCs have been produced using the first method (Laoui, Froyen and Kruth, 1999; Maeda and Childs, 2004; Gu, et al., 2007). For the second method, Kumar and Kruth (2010) created in-situ particles during laser sintering by using laser-induced chemical reactions. Examples include formation of TiC-Al_2O_3 composite from TiO_2, Al and C (Slocombe and Li, 2001); Al_2O_3-Cu composite from CuO and Al (Kamitani, Yamada and Marutani, 2000). The third method involved post-processing of laser sintered materials for the production of composites. Aluminium infiltration of Al_2O_3 and SiC (Deckard and Claar, 1993); Mo-Cu composite (Liu, Bai and Chend, 2008) are a couple of examples of the third method. LENS is similar to SLS but the main difference as with all other AM methods lie in the way the powder is deposited to produce composites. Materials like WC-Co and Ti, TiB have been successfully utilized to produce MMCs (Xiong, Smugeresky and Schoenung, 2009; Banerjee, et al., 2004). 3DP is a powder based process that has the unique capability to control material composition by depositing powder from different nozzles to produce a rather innovative composite. It has utilized C, Ti-Cu alloy to successfully produce TiC/Ti-Cu composite (Zhang, et al, 2001). LOM uses sheets of metals and has successfully produced TiC/Ni composite using combustion synthesis but it is not a

very feasible operation. FDM utilizes different nozzles just like 3DP and is very effective when producing overhanging sections as a removable support structure is created using another nozzle. It has been able to utilize Al, Alumina to produce composites of Al/Alumina (Rambo, et al., 2005). Just like LOM, UC also makes use of metal foils and has been widely researched based on its innovative design (Kong and Soar, 2005). It combines ultrasonic seam welding of metals and layered manufacturing techniques to build up a solid freeform object. It has successfully bonded SiC fibre and shape memory alloy fibre along with an alumina fibre embedded over Al foil (Janaki Ram, et al., 2007).

This research will also produce and test composites of aluminium and copper. Producing a metal composite is a difficult process as each metal has its own unique set of properties. When a composite is made, different metals are used in such a way that every material can contribute to the structural integrity of the product. This is not an easy task when dissimilar metals are joined because two unique sets of properties are joined together to form something that is different from both parent metals. A number of industries rely on multiple material metal products to provide cost-effective, lighter, and stronger alternatives. It is because of the ever increasing demand of innovation that a composite of aluminium and copper makes a good substitute to traditional products. Copper has a number of prominent qualities that make it a very good candidate for industrial use including corrosion resistance, high thermal and electrical conductivity, strength and excellent solderability (Davis, 2001). Aluminium is one of the most difficult metals in terms of joining but has a number of important properties including low weight, high strength, superior malleability, easy machining, excellent corrosion resistance and good thermal and electrical conductivity (Hatch, 1984).

2.13 Mechanical Testing

The mechanical testing is explained in detail in Chapter 6 of the thesis. The testing starts off with the most basic of joints i.e., single lap joint where two foils are joined together with a very small overlap length. This test will allow the calculation of shear strength of the bond which should be kept in mind while designing parts for industrial applications. The next test is peel test and it also joins two single foils but over a much larger length. This test is important to analyse effects of peeling upon application of force. This test helps in calculating the peel strength for the parts. Microstructural analysis helps in establishing the proportion of bonded to unbounded area in a specimen as the more the bonded area, the better the joint. Tensile test analyses the performance of a specimen on the application of tensile forces, up to the point of yield or breaking, whether sharp or gradual. This test measures the strength of a material which is very important in the context of this research. Tensile test helps in measuring full tensile properties including ultimate tensile strength, yield strength, fracture strength and young's modulus.

Lap joints form the first step in analysing the strength of the joints formed by the proposed process. The primary function of a joint is to transfer load from one structural member to another. Therefore, it is important to know the value of load that could be transferred before producing a functional component. This requires testing of the lap joints produced by the proposed process at different speeds to assess the integrity of the bond between the two aluminium foils. For lap joints loaded in tension (Fig. 2.6), the load is transferred predominantly by shear stresses in the adhesive layer. However, because the substrates are deformed in tension, the shear stresses are concentrated at the ends of the overlap (Adams, Comyn and Wake, 1997).

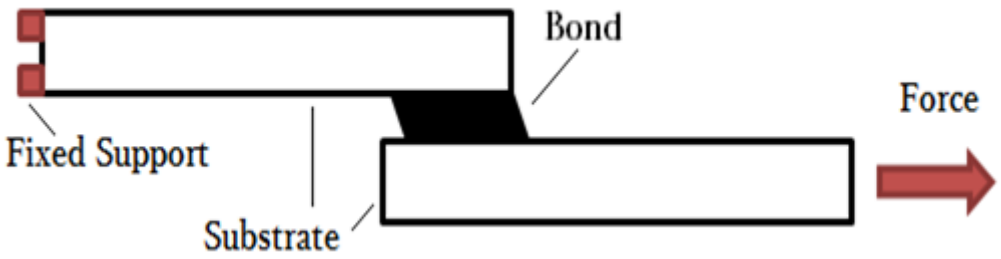

Figure 2.6: Schematic of a bonded assembly

Although the focus of this work is on joining metal foils using brazing paste, the lap-shear technique is frequently used to examine the strength of adhesives and/or interface strength bonded by adhesives. While there is no specific lap-shear test standard documented for parts made by additive manufacturing, British and International Standards for testing adhesive bonds do exist (e.g., BS EN 1465: 2009, BS ISO 4587: 2003). The test results will form the basis on which further work will be done to prove the effectiveness and flexibility of the proposed process. It should be noted that the results observed in the adhesives literature may not apply to the behaviour of lap joints produced by this process. The main reason is that most adhesives exhibit limited plasticity, while the brazing paste utilized for this research is highly plastic. The ultimate bond strength of the standard single-lap joint depends not only on the paste used but on many other factors as well. Some of these additional factors include thickness of the bond and that of the substrate, surface preparation of the substrate, modulus of elasticity and yield strength of the substrate. In addition, slight modifications to the joint configuration can have significant effects on lap joint performance (Her, 1999).

Peel testing is one way to characterise peel strength between two bonded surfaces. This peel strength may be referred to as the "stickiness" of a material as it is a measure of the specimen's resistance to separation from one another after a bond has been made. This measured value may then be used to determine if the bond is strong enough for the application and whether a different bonding process is needed. Peel strength can change as

the peel angle changes so careful consideration should be given while testing the specimens (Kim, Kim and Kim, 1989). These peel tests are usually conducted at a constant rate but at various angles. The most common types of peel tests for the measuring of peel strength are the T-peel, 90 degree peel, and the 180 degree peel. The T-peel test is a type of tensile test performed upon two flexible substrates that have been bonded together and placed into peel test grips such that one substrate sticks up and the other sticks down while the bonded area sticks out horizontally so that the entire setup forms a "T" shape (Choi and Oh, 2001). Tensile test is a fundamental materials test that is done majorly to determine young's modulus and yield strength. It is also known as tension test and show how a material will react to forces being applied in tension. This test shows how much force is required to permanently deform a material which is a direct measure of the material's strength. These tests are standardised and fairly simple needing only the right clamps to perform the testing. Flat parts (dog-bone specimens) should be tested using serrated wedges that should properly hold the part as shown in Fig. 2.7.

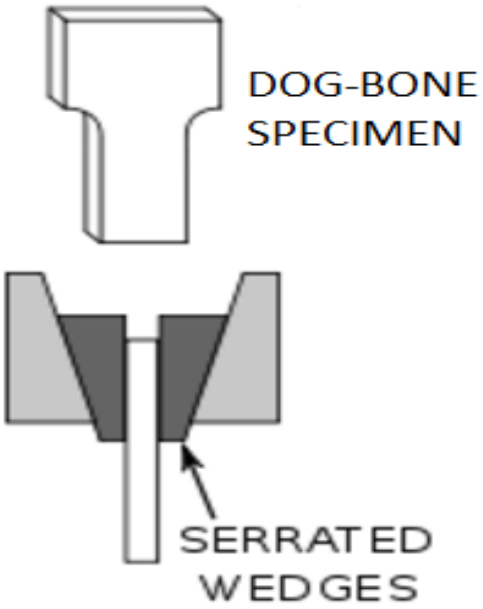

Figure 2.7: Wedges for tensile testing of flat parts (Davis, 2004)

2.14 Summary

This chapter provides the background knowledge needed for the research. It gives a brief introduction to AM technologies and in particular metal AM processes (powder bed, powder feed, wire and metal laminates/foils). The process of LOM has been explained as a potential stacking and cutting system for the CMFM process combined with a suitable metal joining method. Some techniques that make use of metal foils for the production of metal parts have also been described. A number of metal joining methods were analysed and then soldering and brazing were chosen as the best option for integration with LOM to realise the CMFM process. The properties of the metal foils, solder and brazing paste to be used for the process have been explained. Composites have garnered great interest from both academia and industries because of their properties and their importance has been highlighted in this chapter along with the AM processes capable of producing metal composites. A short description of the different types of mechanical tests has been given to highlight their importance with respect to the tests conducted in Chapter 6.

CHAPTER 3

3 Composite Metal Foil Manufacturing

3.1 Introduction

The proposed process is termed as Composite Metal Foil Manufacturing (CMFM) and works with a combination of LOM and soldering/brazing technologies. These two methods have been around for decades but they have not been integrated together as a process that is 'additive' in nature for the production of metal parts. The two processes have been explained in detail in Chapter 2. CMFM is a novel additive manufacturing process for the production of high quality metal parts. In general, quality can be assigned to a number of attributes but the ones investigated in this research are surface finish, time and cost for single build, pre and post processing as well as strength of the final products. A conceptual model of a machine has been designed based on the principles of these processes. This chapter describes the proposed process both in theory and in application. Firstly, the process objectives and the process flow are explained. They are followed by the explanation of the main components involved in the production of parts. As there are a number of open source and licensed software options for the AM processes, the software aspect for processing of the machine has not been explained. All of these software options serve the basic purpose of creating layer data from the 3D CAD model, stacking and cutting of the material. The addition to be made would be controlling the heated plates and then moving the part from the build platform to the heated plates for final joining. There are two options to choose from: Magics from Materialise (licensed) and Slic3r (open source). Both have their own market and have the capability to be developed further to accommodate larger operations such as controlling the CMFM machine.

In addition to the description of the machine components, a three dimensional transient thermal analysis has been carried out on a single lap joint of aluminium (grade 1050 with a H14 ½ hard temper and a thickness of 0.1mm) and pure copper foils (0.1mm thick) to serve as a reference model for future parts. It is to be noted that building a machine is a huge undertaking and would generally require a large company with all of its resources and manpower to get the job done. The conceptual model of the machine can easily be branched into a number of different research areas including mechanical, electrical, programming, integration etc., which would involve years of rigorous research work. Every component of the machine is a research area in its own and this chapter gives the best options available that can be bought straight from the vendors supported by validation of the functional capabilities of the selected components. The description covers their working principles and their role in the process.

3.2 Process Objectives

The process was designed while keeping in mind the aims and objectives of this research. They are related to the quality of the products to be produced. There are two sets of objectives; one for the process and the other for the products made by the process.

3.2.1 Process

- To successfully integrate LOM with soldering/brazing.
- To develop a low-cost, reliable, and effective process.
- To make high quality parts.
- To have the capability to manufacture multiple material parts.
- To be able to use a variety of metals for production of parts without the use of additional equipment.
- To reduce lead time.

- To achieve high speed and accuracy.
- To perform minimum post-processing.

3.2.2 Products

- To achieve a workable strength for direct testing.
- To have a good surface finish.
- To be free from cracks, voids, cavities, heat distortion etc.

3.2.3 Process Details

A conceptual model for a machine based on the process of CMFM is shown in Fig. 3.1. The main components of the machine are a feed mechanism that advances a metal sheet over a build platform, a laser to cut the outline of the part in each sheet layer, a dispenser that dispenses brazing paste on the metal sheets, a roller that smoothens the paste into a uniform layer, two laser sensors for measuring the thickness of the part at all times, a heated plate to apply pressure and heat to bond the brazing paste coated sheets together to produce the final product. The process can be divided into two stages with the first involving cutting and stacking while the second stage is the joining operation to produce the final product. The build envelope is 600mm wide, 1000mm long and 1000mm in height.

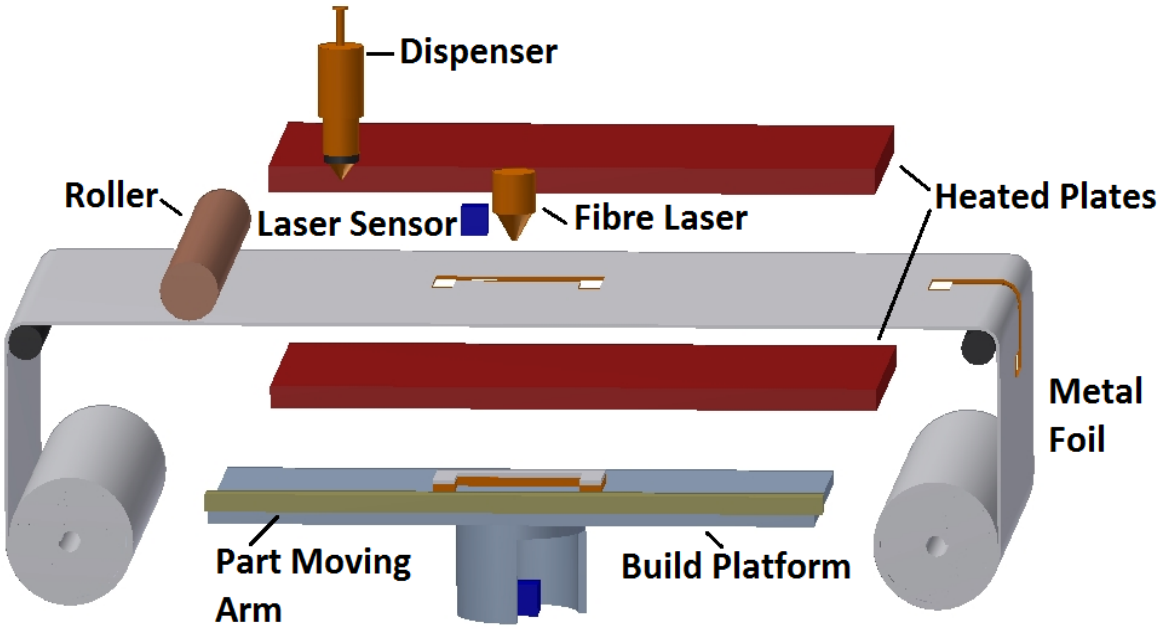

Figure 3.1: Composite metal foil manufacturing process

Like any other additive manufacturing process, CMFM also starts with the 3D CAD model of the part being transferred, by the use of 3D Slicer software, to a set of layer data according to the geometry of the part. The software creates layer data that is fed into the main program which then controls the flow of sheets from the material supply roll. The sheet metal comes in through the feed mechanism and the laser cuts the outline of the part in the first layer. A 300W fibre laser from MIYACHI is selected for this process as it has the capability of cutting metal sheets as thin as 50µm with high dimensional accuracy. Another advantage of using fibre laser is that it offers minimal thermal input, with fine control over how hot the work area gets. This is important because small parts heat up quickly and might otherwise overheat or deform. Fibre lasers are highly focusable to about 15µm. This makes it feasible to remove the minimum amount of material to make the cut, resulting in extremely high precision and accuracy. The laser starts cutting the outline profile on receiving the layer data from the CAD model. Fig. 3.2 shows a flow chart of the composite metal foil manufacturing process.

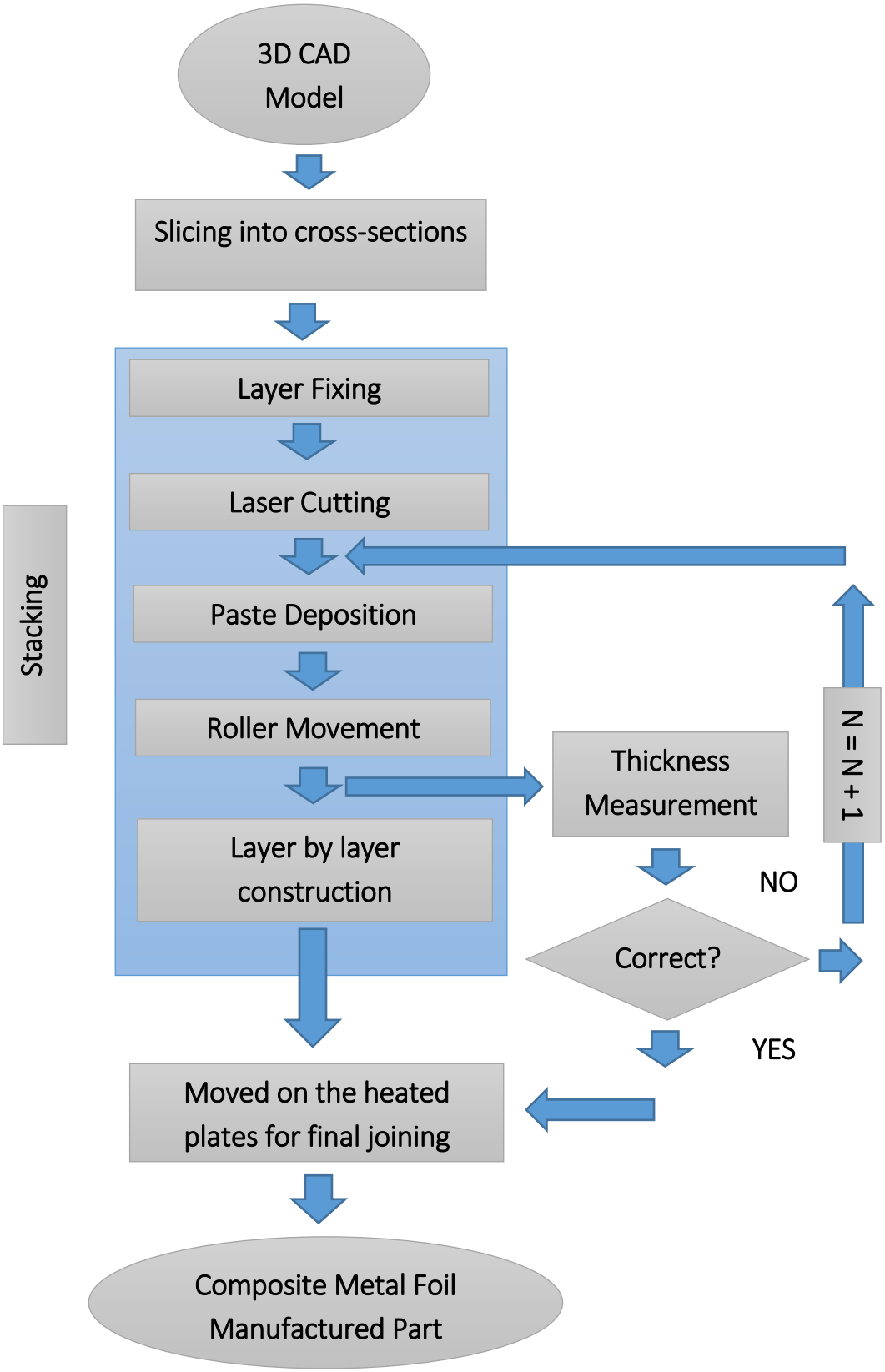

Figure 3.2: Flow chart of CMFM process (N=layer number)

Since metal sheets are not attached to the build platform by any means, the process is slightly different when it comes to fixing the first layer. After the profile outline has been cut for the first layer, the brazing paste is deposited by the dispenser on the defined geometry and the platform stays at its original position. The build platform is capable of moving upwards and downwards just like the feed mechanism. The weight of the paste on the cut-out keeps the metal sheet on the platform as it moves downwards and the remaining of the sheet go to the waste take-up roll. Another sheet is then advanced on top of the previously deposited layer. It is placed on top of the first layer by the feed mechanism. Before the laser cutting, a roller rolls on the surface of the sheet to make a uniform layer of the paste between the first and second layer. It applies a uniform pressure that is essential for a uniform brazing paste layer. The pressure is measured using a wireless system for nip pressure.

The dispenser is a very crucial component of the process. It should be able to provide paste deposit sizes ranging from small dots to continuous stripes of any length. For that reason Model 710 Automatic Applicator from Fusion Automation Inc. was chosen. This compact unit features adjustable time and pressure controls. The amount and time of dispensing is based on the geometric features of the layers and can be controlled both manually and by the main program of the machine. As the laser cuts the metal sheet, the heat produced during the cutting process melts the brazing paste at the edges that keeps the two foils in alignment. The platform is then moved down and adjusts to the thickness of the foils and the paste layer between them. The thickness is measured by two laser sensors that send the information to the system so that no error occurs in lowering the platform. The next sheet then comes in and the platform moves upward. The laser cuts the outline which again melts the paste at the edges. The process is repeated until all the sheets have been cut and deposited with brazing paste. The measurement of thickness during the process is an important aspect as it ensures dimensional accuracy of the part. The Microtrak™ 3 TGS system is designed specifically for

thickness applications. The device can easily interface with PLCs and PCs, or can be used in a standalone configuration. Each module contains an integral LCD display and keypad for setting up and visual display of measurements. Basic input output is provided by discrete lines or a serial interface configured as Modbus® RTU over RS-485 or RS-232. The two sensors are mounted on either sides of the platform to ensure accuracy in thickness measurement.

After the cutting, dispensing and stacking have been done, a stacked structure of brazing paste coated layers is left behind. The structure is stable enough to be moved and so an arm moves the structure onto the heated plate. It is then heated from top and bottom by a heated plate that applies pressure and heat to produce the desired part. The heating plates are set to a temperature of 470 °C so as to allow for quick heating of the product. They apply heat and pressure to ensure proper bonding and dimensional accuracy. The plates are of stainless steel and are fitted with FIREROD cartridge heaters from Watlow and can go up to a maximum of 550 °C. After heating the brazing paste-coated layers for a certain amount of time depending upon the thickness, the part is taken off and is now ready for testing or any other use. Each plate can be controlled individually based on the thickness of the part to be heated. It is better to use one plate when heating thin products in the range of 1-5mm and both plates in case of higher thickness. Using both plates for thin parts may overheat them in a very short span of time and is, therefore, not advised.

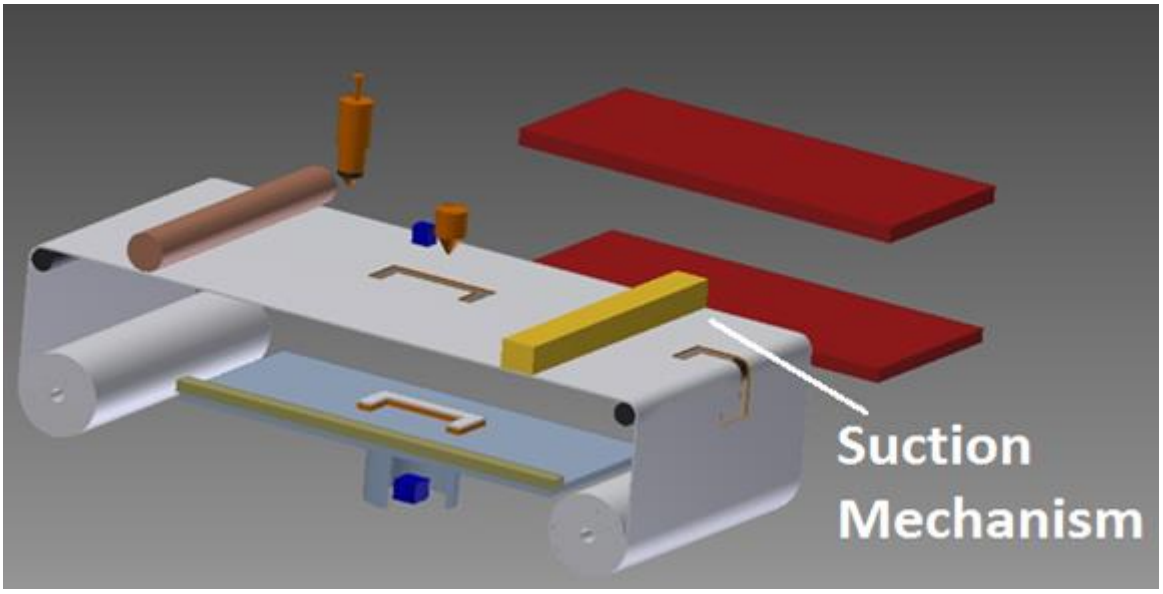

Figure 3.3: CMFM with suction mechanism

The CMFM process should be able to produce different shapes and complex geometries; therefore, a suction mechanism was fitted with it (Fig. 3.3). Sometimes, parts are made with cavities at various points. When cutting metal foil, the material from the cavities need to be removed before the next layer is advanced on top of the previous layer. The drawbacks of leaving extra material in place have been described in Chapter 2 especially with the metal foil LOM process (Section 2.5). For this reason, the software of the CMFM machine has to be programmed in two modes: 'Mode 1' for producing straight geometries as shown in Fig. 3.4a and 'Mode 2' for producing parts with holes as shown in Fig. 3.4b.

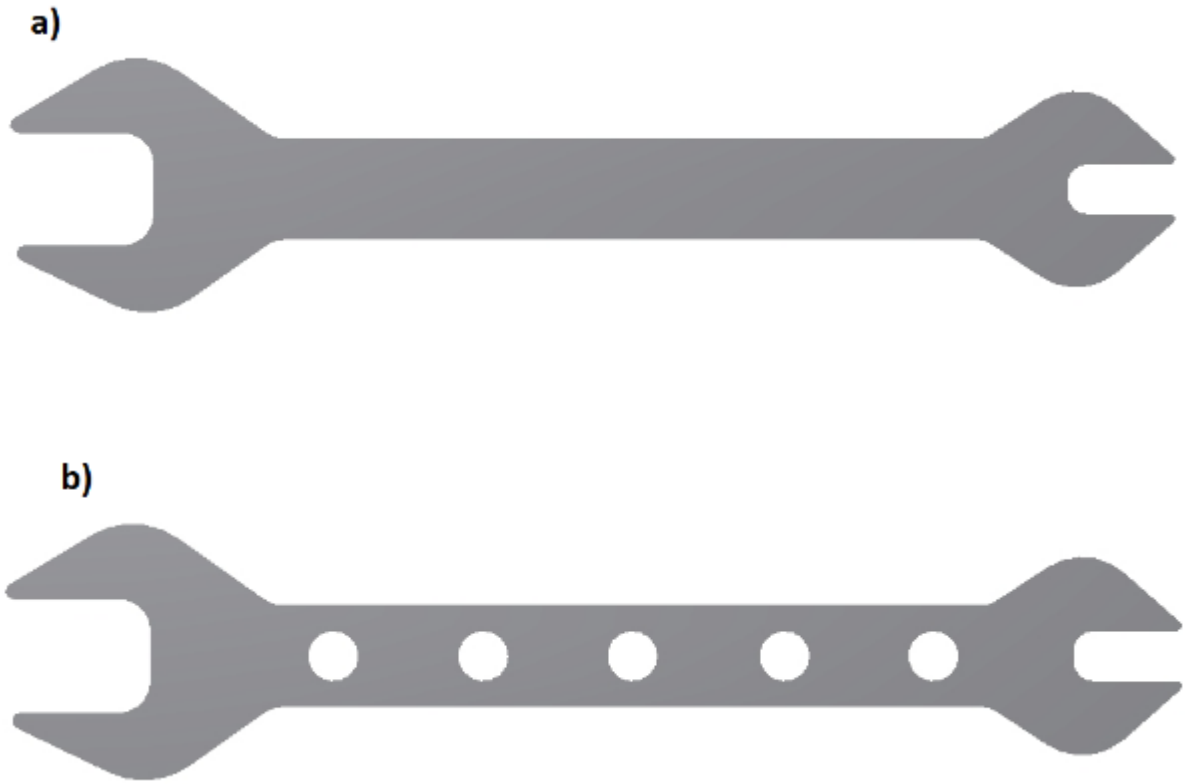

Figure 3.4: CMFM modes demonstration: a) Spanner; b) Spanner with holes

On receiving the information that Mode 2 will be used, the process flow slightly changes. Take the case of the spanner with holes in Fig. 3.4b. The software defines the outside boundary of the part and makes additional layers for holes. The laser cuts the cavities first (Fig. 3.5a) and then the suction mechanism moves over the entire length of the platform (Fig. 3.5b). After the free metal pieces have been removed, the outline boundary of the part is cut by the laser (Fig. 3.5c). Afterwards, the paste is dispensed and the process goes on in the same way until the required height is achieved. It will take more time as compared to producing a spanner without holes but the plus point is that, the entire process is automated and will not lead to significant post processing to remove the holes by drilling or milling. Fig. 3.5 shows the Mode 2 in detail.

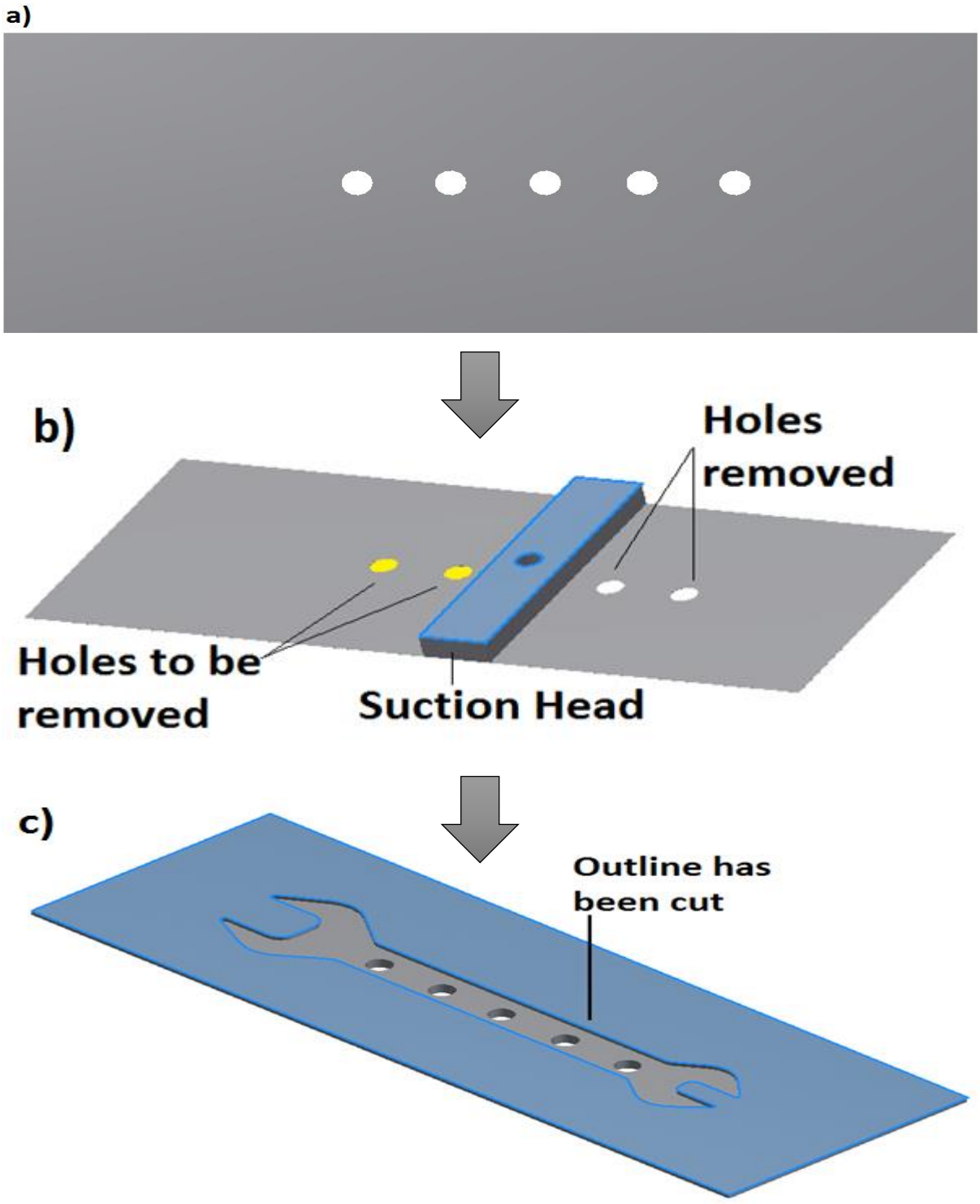

Figure 3.5: Mode 2 of CMFM: a) Cutting of holes; b) Removal of loose metal by the suction head; c) Outline of the spanner is cut

The above description explains the working of the machine and the components. The rest of the chapter will describe the components in more detail. However, the dispenser will be

discussed in later chapters because of its importance to the effectiveness of the process. It should be noted that these individual components call for a large research area in their own right and the information provided here is only to validate their functional capability based on the operation that they are required to perform in the context of the CMFM machine.

3.3 Suction Mechanism for Removal of Extra Material

PIAB Limited, UK have a fully automated 'Flow2' system that is capable of moving along the entire length of the platform and collecting any loose metal. The system consists of an air compressor, a venturi pump and a pneumatic ON/OFF valve as shown in Fig. 3.6.

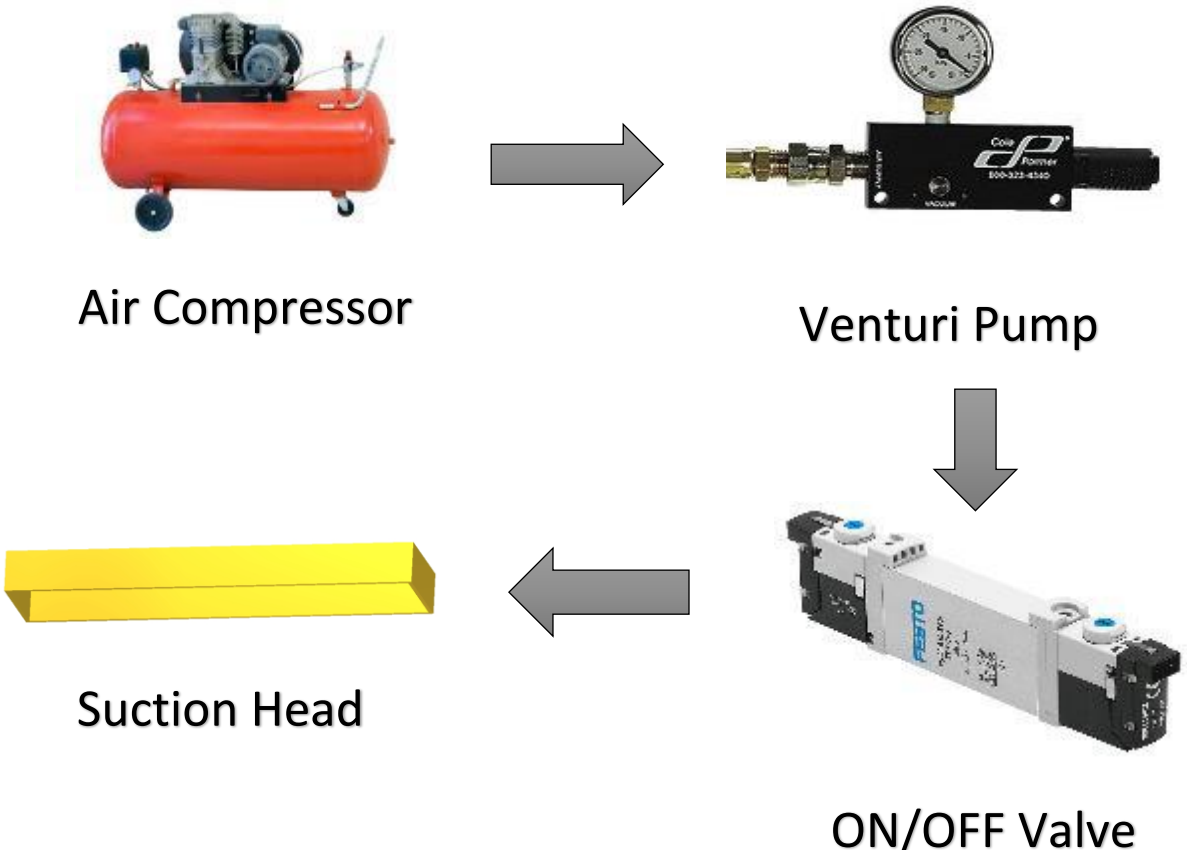

Figure 3.6: Flow chart of the suction mechanism

The process starts when the compressor blows air into the venturi pump at a pressure of around 5 MPa (recommnded value). The pump creates vacuum by taking advantage of the venturi effect. When air passes through a tube that narrows down, its velocity increases, and

because of the venturi effect, its pressure decreases. The fact that a pressure drop accompanies an increased flow velocity is fundamental to the laws of fluid dynamics. This pressure is lower than the ambient pressure (outside the system). This creates suction, vacuum, inside the system. The ambient air pushes itself into the suction head because the pressure inside is lower than the pressure outside. The ON/OFF valve works by receiving information from the software and genreally remains ON as long as the suction head has completed its journey along the entire length of the platform in one direction. It stays OFF during its return to its original position (Piab.com, 2012).

3.4 Fibre Laser for Metal Cutting

The laser works on receiving information about the outline profile of the part and then it starts to cut the metal foil. In general, fibre lasers and pulsed Nd: YAG (neodymium-doped yttrium aluminium garnet) lasers are the two solid state laser options used most for fine cutting of thin material. The fibre laser offers some key advantages over the pulsed Nd: YAG technology, including finer focused spot sizes enabling high resolution, higher repetition rates for faster cutting speeds, and a lower cost of ownership. Moreover, AM processes such as DMLS, EBM etc., use fibre lasers (Frazier, 2014) to sinter powder metal which makes it a very strong candidate for yet another AM process namely CMFM. For these reasons, a 300W fibre laser from MIYACHI is selected as it has the capability to cut metal sheets as thin as 50μm with high dimensional accuracy (Miyachi.com, 2010). The reason for using a 300W laser is that fibre lasers come in a range of 100-500W and after recommendation from the supplier and numerical analysis using ANSYS, it was decided to select a 300W laser as it has the required thermal input to cut through thin aluminium foils. It also offers minimal thermal input, with fine control over how hot the work area gets. This aspect is important because small parts heat up quickly and might otherwise overheat or deform. The laser is highly focusable to about 15μm that makes it feasible to remove the minimum amount of material,

resulting in extremely high precision and accuracy. It is a powerful piece of equipment with little energy loss while cutting and that makes it a perfect component for the required process. It can be operated at various speeds depending upon the thickness of the sheet being used. This laser system along with integration kit is available from AMADA MIYACHI AMERICA. The next section describes the heat transfer using transient thermal analysis of the moving laser on 150mm by 150 mm aluminium 1050 metal sheet.

3.4.1 Transient Thermal Analysis

Heat transfer in the laser cutting process is modelled as transient and three dimensional (3D) with heat flow of 300W and ambient temperature of 10°C. The general mathematical model for transient temperature is written as:

$$\rho c(T)\frac{\partial T}{\partial t} = \frac{\partial}{\partial x}\left(k(T)\frac{\partial T}{\partial x}\right) + \frac{\partial}{\partial y}\left(k(T)\frac{\partial T}{\partial y}\right) + \frac{\partial}{\partial z}\left(k(T)\frac{\partial T}{\partial z}\right) + Q_{int} \qquad (3.1)$$

The temperature distribution during the laser cutting operation is shown in Fig. 3.7.

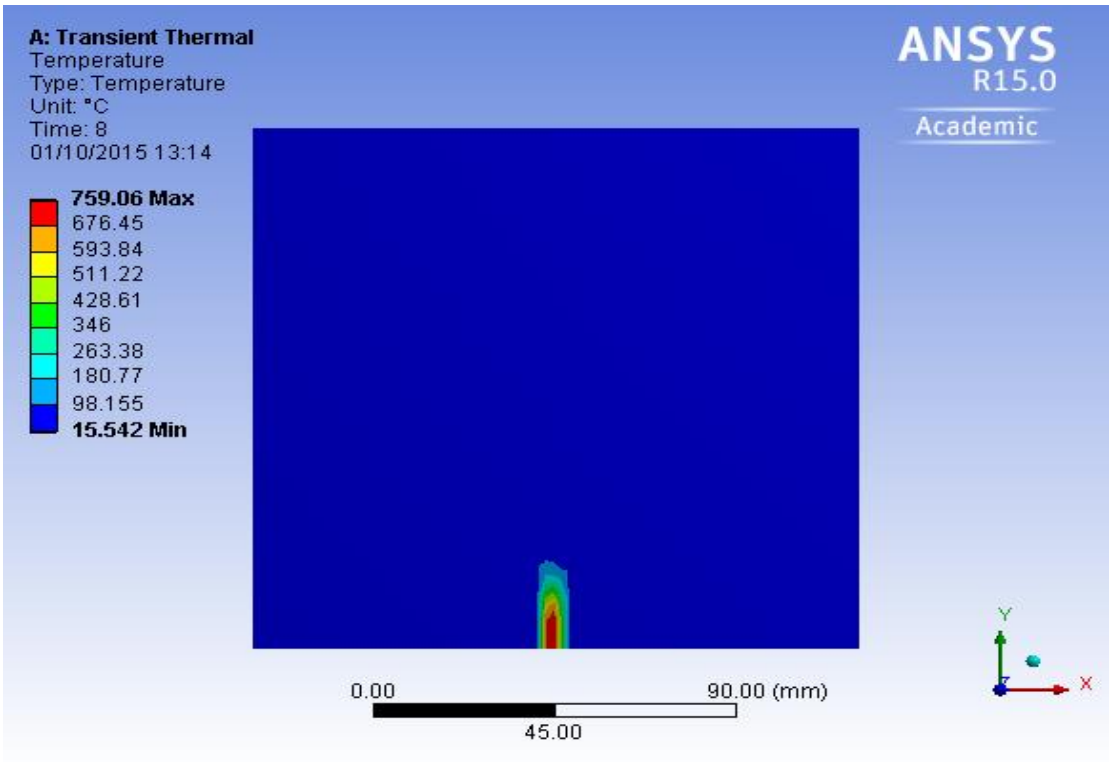

Figure 3.7: Temperature distribution on the aluminium foil during the cutting operation

The fibre laser is highly efficient and the temperature distribution shows a maximum temperature of 759.06 °C which is almost 15% higher than the melting temperature of aluminium (660.3 °C). It shows that the laser is more than capable of cutting aluminium sheets even if it is working at 85% of its capacity (not including energy losses).

3.5 Use of Roller for Uniform Thickness of the Paste

The roller plays a vital role in making the layer of paste uniform and this objective can only be achieved if the roller is capable of applying uniform pressure throughout its entire length. For this reason, the Nip Pressure Measurement System (NPMS) is selected because it is a complete nip pressure and force measurement tool that takes the guesswork out of adjusting rollers (Tekscan.com, 2012). These systems are generally used for pressure measurement between two rollers but to make the CMFM machine more efficient, this system is employed here. As is evident from Fig. 3.8, the roller begins its journey from one end of the machine table that has a smaller roller fitted as part of the feed mechanism. These two rollers come into contact and so a pressure measurement between them lays the foundation for the rest of the process. Fig. 3.9 shows the NPMS2 measuring system that can measure pressure accurately up to 20MPa, weights 2.7kg, has a sensing region of 900mm (300mm more than the width of the platform) and a total of 198 sensing elements along the rows and columns which makes it a very accurate and precise measurement system. The system is fitted with a tactile pressure sensor and data acquisition electronics and its software can be easily integrated with other systems such as the machine in discussion here. The sensor is wireless, ultra-thin, durable, reusable and extremely portable which makes it a suitable option for this type of operation.

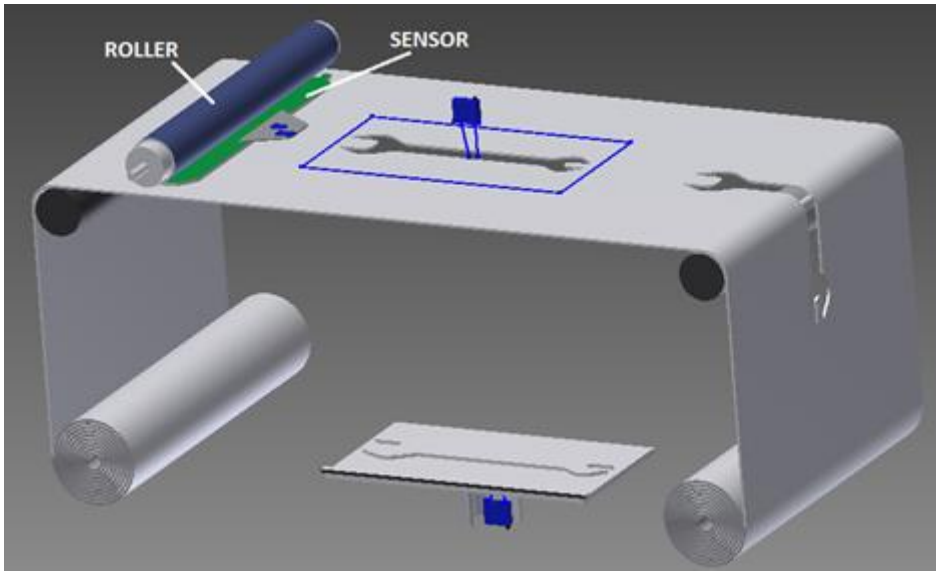

Figure 3.8: Sensor measuring pressure exerted by the roller

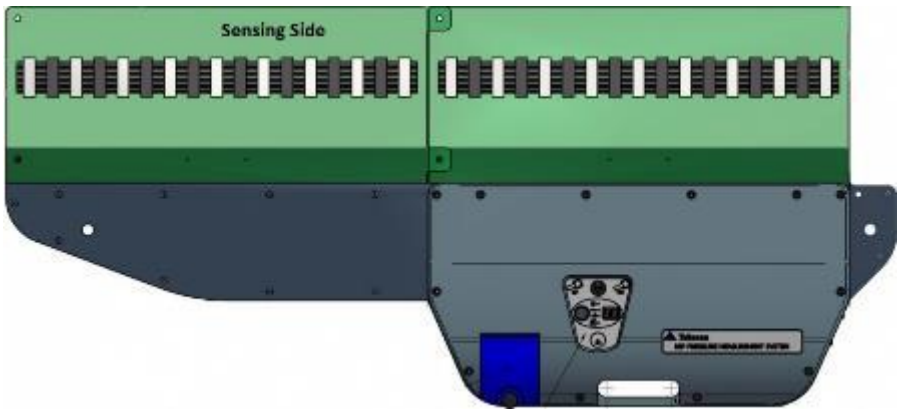

Figure 3.9: NPMS2 measuring system (Tekscan.com, 2012)

Another reason for the use of nip system is that the metal sheets provided are not always of uniform thickness and such a system will help measure any uneven pressure distribution. This will allow the user to set up a realistic pressure value that will give the required results. It eliminates the guesswork involved in adjusting the correct pressure and increases the efficiency of the process. The NPMS sensor and the data acquisition software are available to purchase from Tekscan™.

3.6 Thickness Measurement Mechanism

The foils have uniform thickness but since foils are produced by cold rolling, an inaccuracy in thickness cannot be avoided. Furthermore, to achieve high dimensional accuracy in the Z-direction, it is essential that the layer of paste be of a uniform thickness. As mentioned before, a roller is in operation that applies pressure to ensure a uniform thickness can be obtained. However, due to high temperature of the laser, viscous nature of the paste (Δt_1) and inaccuracy in foil thickness; the difference to the ideal foil thickness is of $\Delta t_2 = \pm 0.1\text{mm}$ (depending on the thickness of the foil being used, this value can change). As a consequence, the real height of the foil stack after N layers can differ by the relation given below:

$$\Delta h = \pm N|(\Delta t_1, \Delta t_2)| \tag{3.2}$$

To solve this issue, the Microtrak™ 3 TGS laser displacement sensors are utilized on either side of the build platform as shown in Fig. 3.10. They are non-contact and use the laser triangulation technology with a solid-state laser light source and a CMOS (complementary metal-oxide semiconductor) detector as shown in Fig. 3.11. A laser beam is projected on the target being measured and a portion of the beam is reflected through focusing optics onto a detector. As the target moves, the laser beam proportionally moves on the detector. The signal from the detector is used to determine the relative distance to the target. These sensors have a sampling frequency of 40 kHz that makes a time period of 50μs which means that the system receives feedback very quickly.

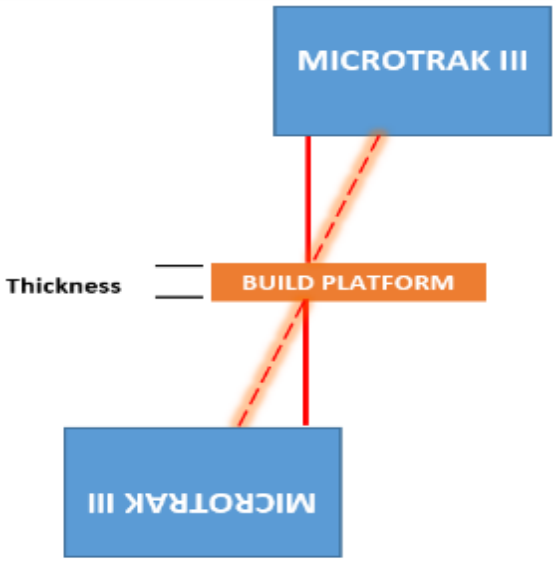

Figure 3.10: Placement of the sensors for thickness measurement

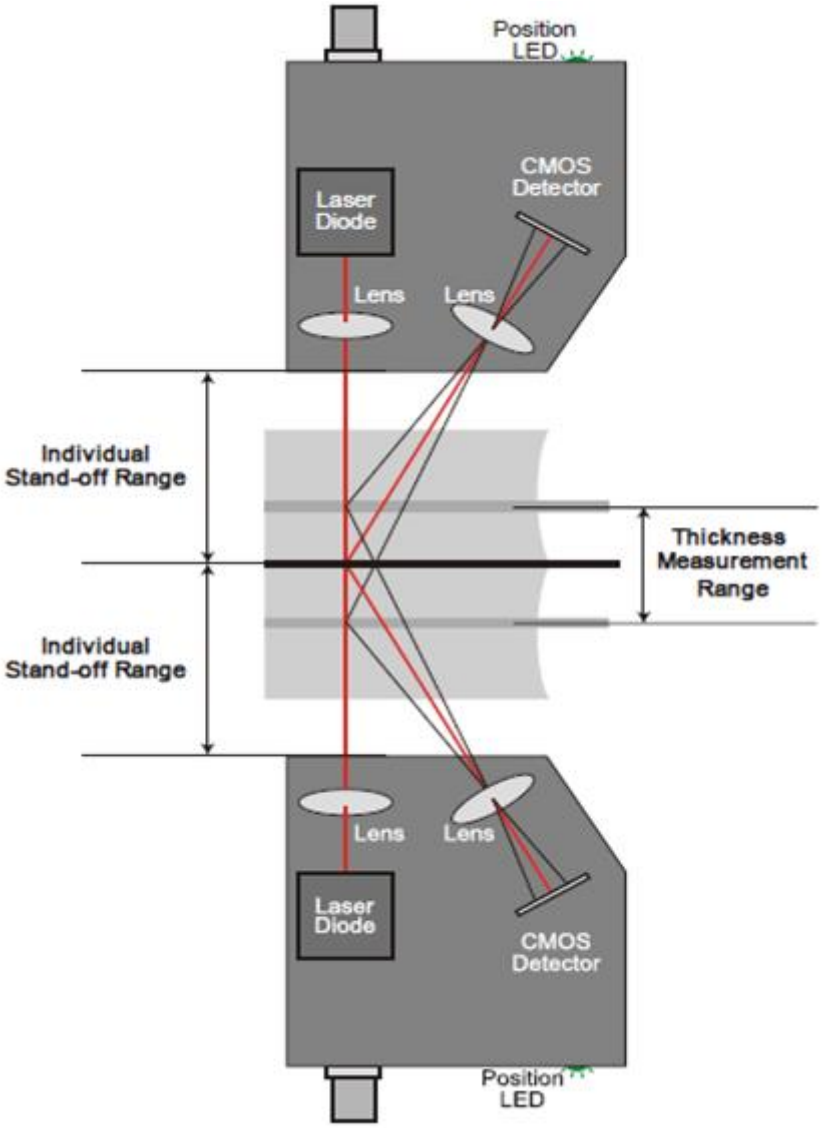

Figure 3.11: Principle of operation (SensorsOnline.com, 2010)

These sensors have an ideal operating point referred to as standoff distance and at this point the laser is at its sharpest focal point and the reflected spot is in the centre of the detector. As the target moves, the spot will move toward the ends of the detector allowing for measurements over a specific range. For the sensors in use, the standoff distance is 200mm, the measuring range is 3-1270mm (the bottom sensor is fixed and the top sensor can move as the part gets built, this range would easily suffice) and measuring resolution is 1µm which covers extremely thin foils easily. The thickness of the foils used for making the parts could have also been measured using one sensor but two sided measurements are preferred. This is because a two sided approach eliminates any errors that might be introduced from the material moving or vibrating (MTIinstruments.com, 2010). The two sensor approach synchronizes the data sampling for both sensors which ensures a correct thickness reading. This type of system provides both analogue and digital outputs connected to LCD display that show both digital (up to 4 decimal places for mm) and analogue (bar representing value) readings. The laser sensors are available to purchase from Microtrak™.

3.7 Operation of Heated Plates

They join the paste-coated foils together by applying heat and pressure. Heated plates are usually custom- built according to the user requirements. Watlow Limited is a world leader in such equipment and was approached by the researcher regarding building two units to which they agreed as it is a common thing for them (Watlow, 2010). Two units have been suggested and the reason is that the current research did not make use of large parts and so a unit with 100mm width and 250mm length seems reasonable. The other unit could be used for large parts having length and width of 400mm. Each rectangular plate should be 20mm thick; it is because of the use of FIREROD cartridge heaters as heating elements. A cartridge heater is a tube-shaped, heavy-duty, industrial joule heating element (electrical resistance) used in the process heating industry, usually custom manufactured to a specific watt density, based on its

intended application. The plates in this case are highly compacted with a surface watt density of up to 60 W/cm² which is very good in terms of the effectiveness of the plates in use. The plates are hollow from the inside with wall thickness of 4mm; it is to allow for rapid heating so that the plates could get to the desired temperature quickly. Each heater is 12mm wide and 120mm long which means that they will be able to cover the entire length of the plate easily. Corresponding holes are drilled along the length to insert the cartridge heaters inside the plates (Watlow, 2010). This configuration allows the heaters to maintain a uniform temperature along the entire length of the plates.

The plates are generally fitted with digital thermocouples, timers and pressure gauges for ease of operation. They are made of stainless steel largely because it has a very high melting temperature (1400-1450 °C) and the operating temperatures for the pastes being utilized go to a maximum value of 500 °C. Based on the cartridge heater from Watlow, the system can go up to a maximum temperature of 550 °C. For the case of the smaller unit (100mm wide and 250mm long), three cartridge heaters are needed and will be fitted at equal distances from each other. A cartridge heater is shown in Fig. 3.12.

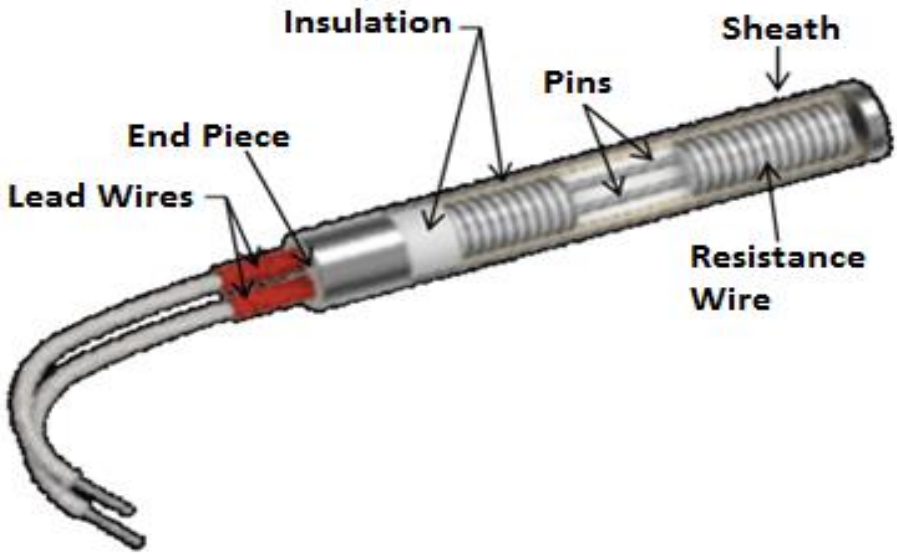

Figure 3.12: A simple illustration of a cartridge heater (Cynebar.com, 2012)

The plates are operating at 240V (maximum) and connected in three phase configuration. The power calculations can be made using the following formula:

$$Watts\ (kW) = \frac{Mass\ (kg) * Specific\ Heat\ Capacity\ \left(\frac{kJ}{kg}\right) * Temperature\ Rise\ (°C)}{Time\ (s)} \qquad (3.3)$$

The next section shows transient thermal analysis of the Al/Cu single lap joint and it can be used as a reference model for future products as well. Foils of 0.1mm thickness are being used and a lap joint was made following BS EN 1465: 2009. The dimensions of the foils were a*b*t=25*100*0.1mm as shown in Fig. 3.13. The lap joint length (l) was 12.5mm and the thickness of the brazing paste (s) was 0.1mm.

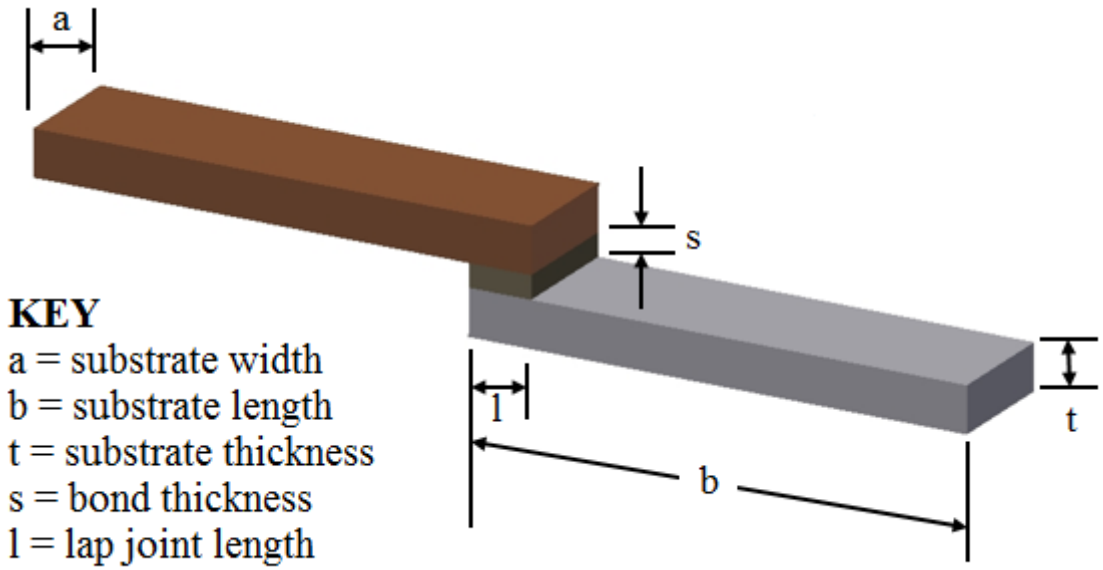

Figure 3.13: Al/Cu single lap joint

3.7.1 Modelling for Numerical Analysis

A three dimensional model has been developed in ANSYS 15.0 to analyse the heat transfer process. The properties of the materials are shown in Table 3.1. They change with temperature and the values given are at room temperature (20°C). The temperatures obtained in thermal analysis have been applied for the structural analysis to analyse the effect of

thermal stress and strain. CMFM requires foils to be joined by sandwiching them between two stainless steel plates (each 250mm long, 100mm wide and 20mm thick). Heat flux has been calculated (0.3825 W/mm^2) and applied as input to the model. One of the plates has been set to a temperature of 470°C as shown in Fig. 3.14.

$$\frac{Q}{A} = \frac{k\,(T_{hot} - T_{cold})}{t} \tag{3.4}$$

$$\frac{Q}{A} = \frac{17 * 10^{-3}\,(470 - 20)}{20}$$

$$\frac{Q}{A} = 0.3825\ {}^{W}/_{mm^2}$$

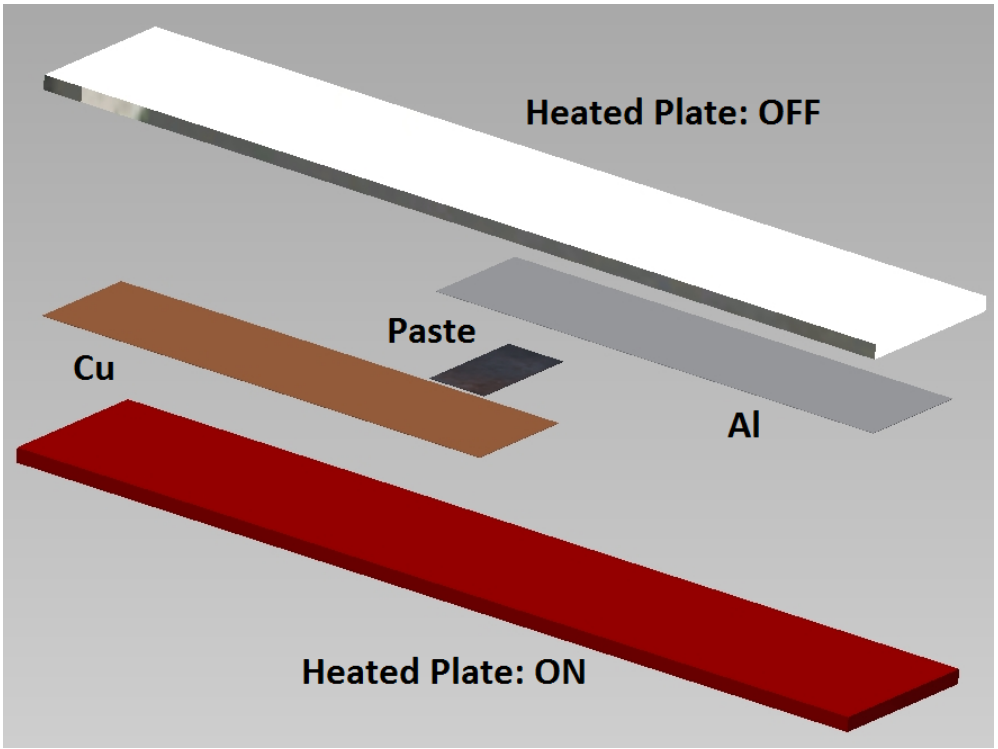

Figure 3.14: Exploded view of the heating operation

The reason for using only one plate is because both plates will heat up the 0.1mm thin metal foils too quickly resulting in pitting or damaging the mechanical integrity of the foil as a

whole. Fig. 3.15 shows the mesh of the Al/Cu single lap joint with copper on the left hand side and aluminium on the right hand side.

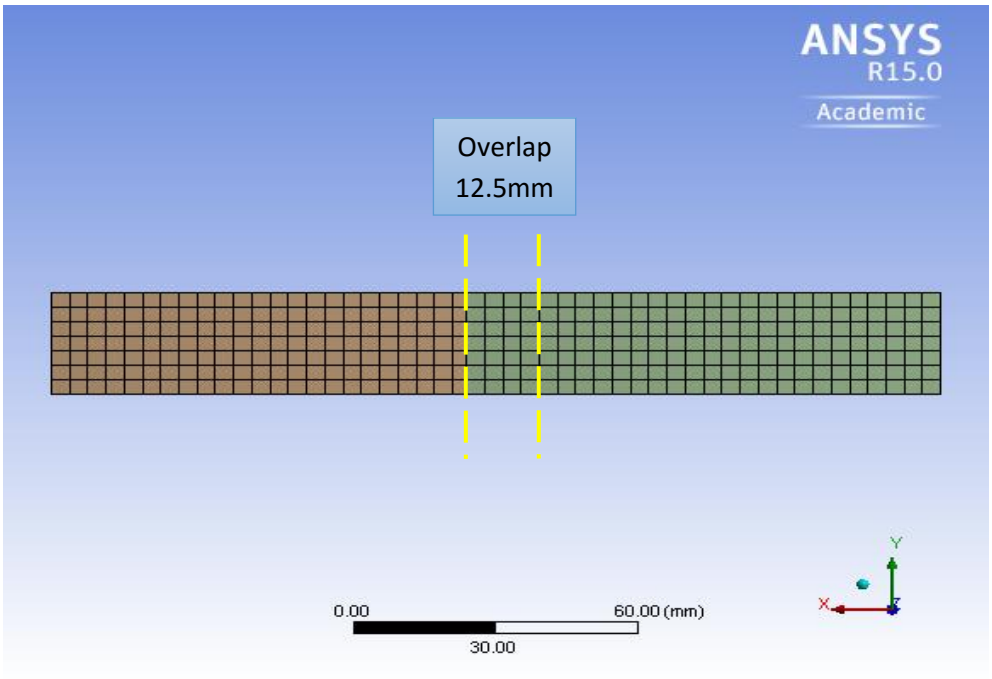

Figure 3.15: Mesh of Al/Cu single lap joint

Table 3.1: Properties of the materials used

Material	Thermal Conductivity (W/m °C)	Specific Heat (J/kg °C)
Brazing Paste	130	480
Stainless Steel 316	21	530
Aluminium 1050	237	900
Copper	398	387

3.7.2 Temperature Distribution

The thermal model has been developed to find the appropriate heating time for the Al/Cu single lap joint. Fig. 3.16 shows the temperature distribution on the plates sandwiching the lap joint between them and Fig. 3.17 shows the temperature distribution on the single lap

joint. It is evident that the temperature of the lap joint is at 470°C after 5 seconds. As soon as the lap joint comes into contact with the heated plate, its temperature gets to 470°C but it has to stay there for three to four seconds to allow the brazing paste to remove the tenacious oxide layer otherwise there will be no bond. But if it is allowed to stay there for longer periods of time, one of two things can happen; (i) the flux in the paste will burn off rendering the paste useless and unable to create a bond or (ii) pitting of the foils because of their thickness. The reason for heating the joint for a few seconds is because the joining area is very small (12.5mm long and 25mm wide). In case of larger joining area or multiple layers stacked on top of each other, the time period will increase comparatively. The maximum temperature is less than the melting temperatures of the base metals but it is close to the annealing temperature of aluminium and copper. The attention is given to aluminium because it is the weaker of the two metals having a lower modulus of elasticity. The foils of aluminium are grade H14 which are work hardened by rolling to half hard and are not annealed afterwards. In the annealing temperature range (300-410°C), the crystalline structure of the material starts to relax, thus making it more malleable. There is also a danger of over-heating which may result in stress relieving, sagging or warping, change in temper, surface conditioning, re-alloying, hot cracking and a worst case scenario is a meltdown of the material in use. The process of brazing uses heat in a localized area (to be joined) and stresses in aluminium from shearing and drawing can change, and result in distortion or deformation. To analyse this effect, structural analysis has been carried out to find out thermal stress, strain and deformation due to the heat transfer process.

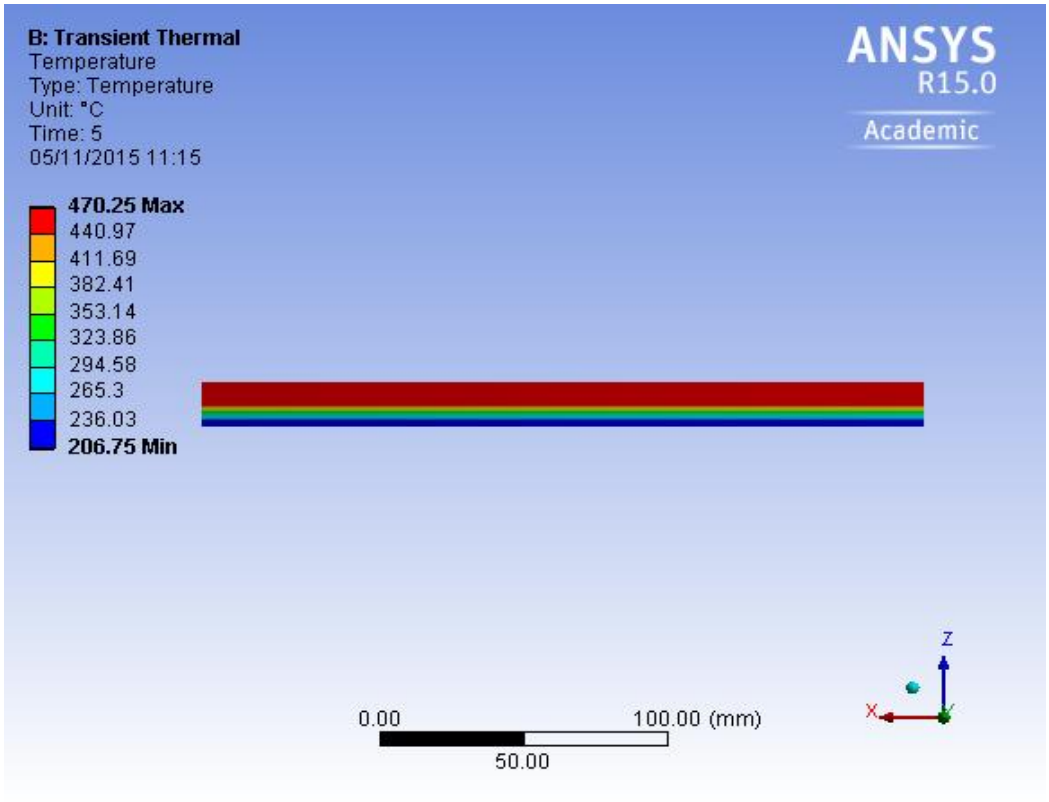

Figure 3.16: Temperature distribution on the plates

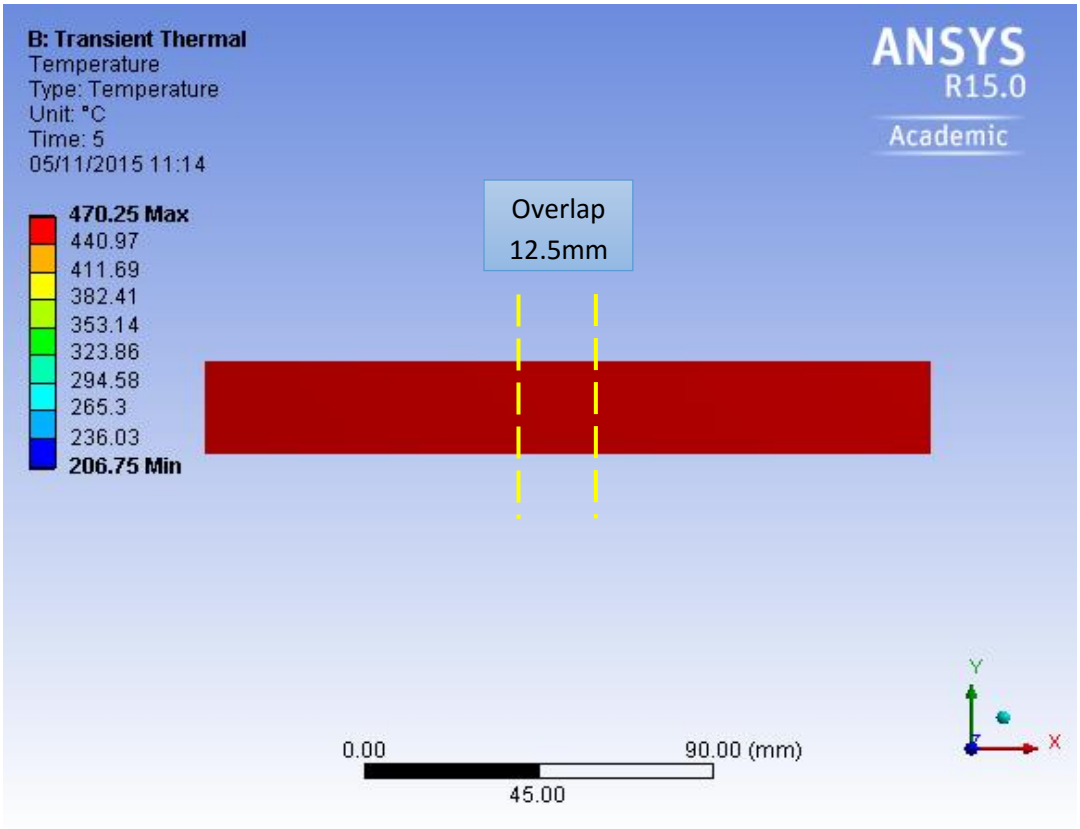

Figure 3.17: Temperature distribution on the Al/Cu single lap joint

The transient thermal analysis was carried out because the temperature is varying with time and to characterize this transient behaviour, the full unsteady equation is needed:

$$\frac{1}{\alpha}\frac{\partial T}{\partial \tau} = \frac{\partial^2 T}{\partial x^2} + \frac{\partial^2 T}{\partial y^2} + \frac{\partial^2 T}{\partial z^2} + \frac{q}{k} \qquad (3.5)$$

In Eq. (3.5), $\alpha = \frac{k}{\rho c}$ = Thermal diffusivity and $\frac{q}{k}$ is the heat source.

In the current scenario, a composite of aluminium, copper and brazing paste is being produced. The equation would have to be solved for each layer separately and then the boundary conditions could be applied. Thermal expansion of the two materials would also result in different set of conditions. The density and viscosity of the brazing paste would have to be incorporated as well. These parameters can be solved analytically but the thermal contact resistance between the layers is a big issue. When it is introduced then the analytical solution becomes significantly more complex. Numerical solutions can, however, be obtained in a relatively simple manner. For these reasons, simulation of the heat transfer process as transient and three dimensional is preferred which can be used as a reference model for future parts.

3.7.3 Thermal Stress and Strain

The temperature values obtained from the thermal model has been used as input for analysing thermal stress, strain and deformation. Since the lap joint was sandwiched between two stainless steel plates, displacement in the Z-direction has been set to zero. Fig. 3.18 shows the deformation caused by the brazing process. The values range from 0.000076731mm to 0.0055414mm. Furthermore, major part of the joint is in the lower range of deformation whereas the maximum value can be seen at the edges of the joint far away from the centre where the bond is present joining the two foils together.

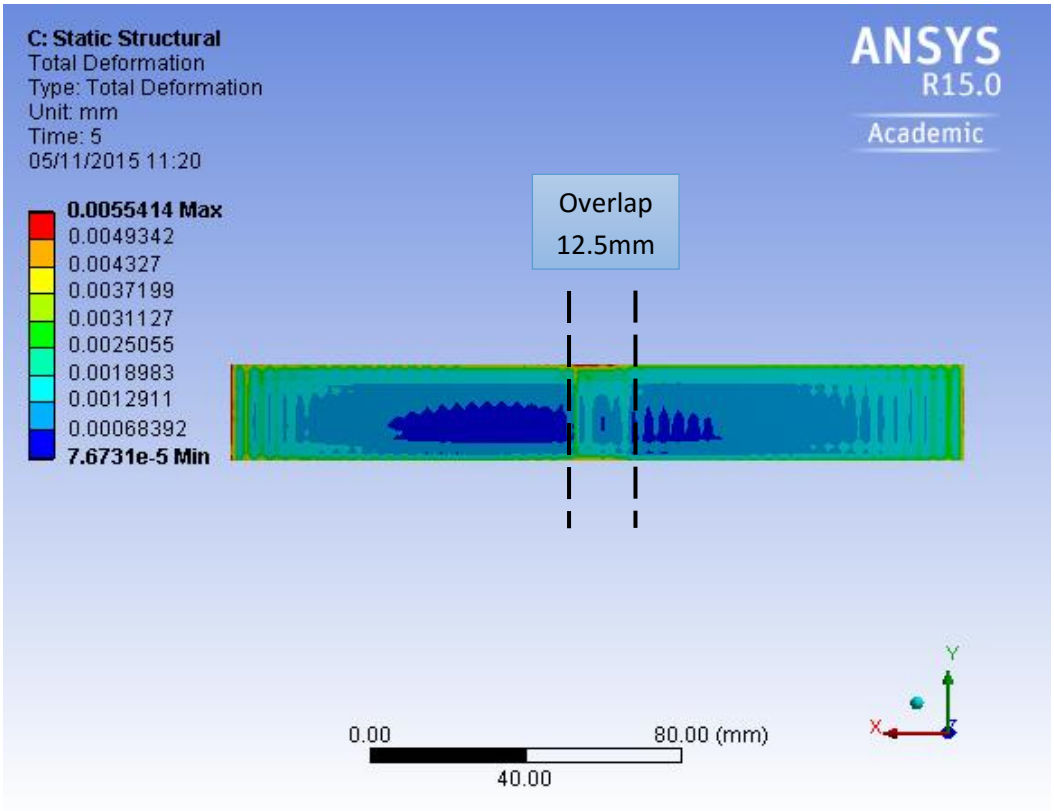

Figure 3.18: Deformation of Al/Cu single lap joint

The effect of thermal stress is shown in Fig. 3.19. In the five seconds that it took to make the single lap joint, the thermal stress value ranges from 0.00094787MPa to 369.59MPa. As was the case with deformation, majority of the joint lies in the low rage and the maximum value can only be observed at the starting edge of the copper foil far away from the bonded area. This goes to show that thermal stress is at minimum in the surrounding area of the bond and that the heat due to the brazing process did not have a significant impact on the mechanical integrity of the foil or the joint.

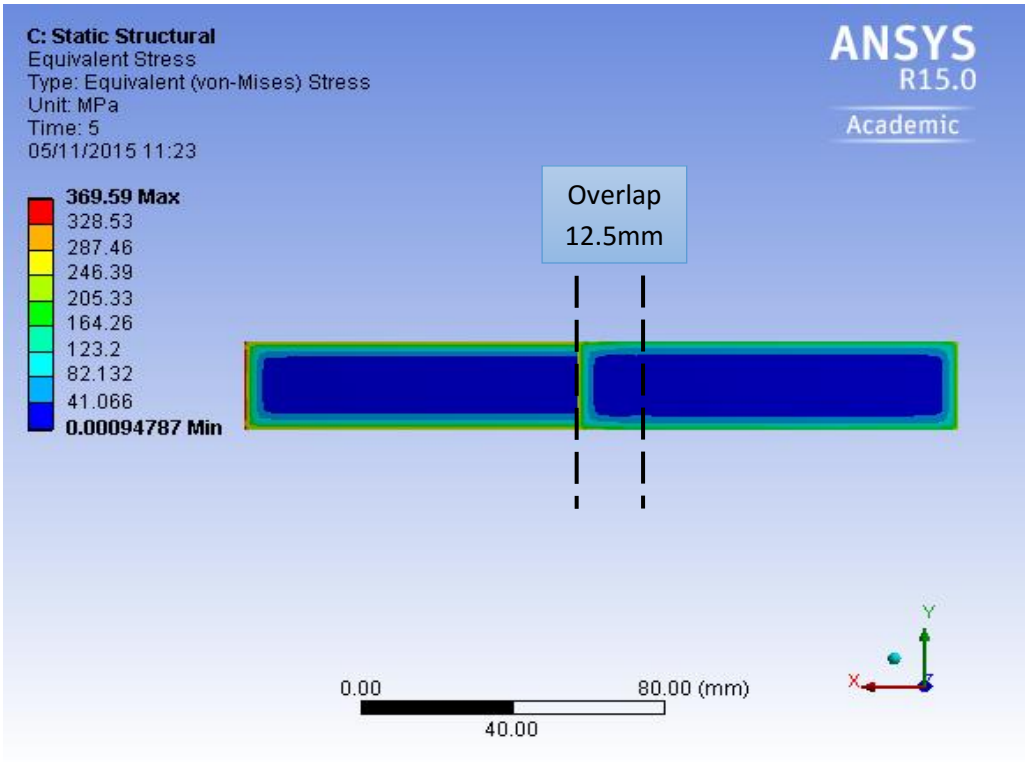

Figure 3.19: Thermal stress in Al/Cu single lap joint

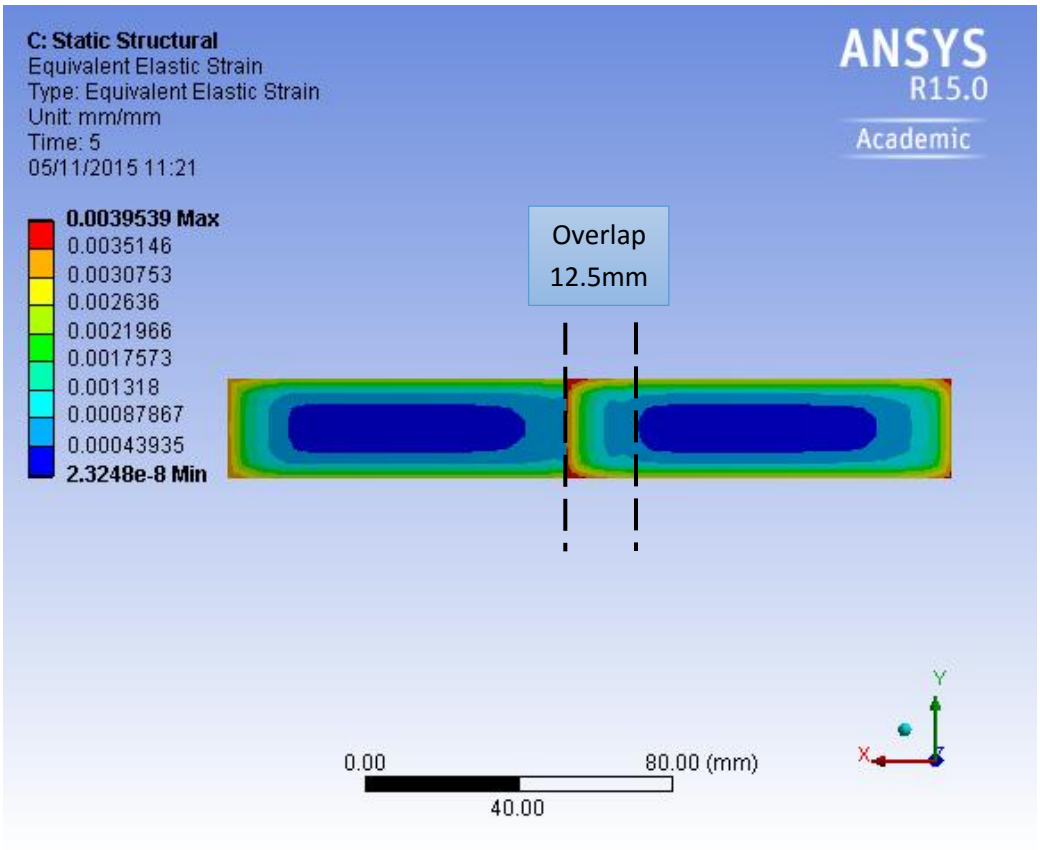

Figure 3.20: Thermal strain in Al/Cu single lap joint

Thermal strain distribution in Fig. 3.20 shows a different distribution compared to the deformation and thermal stress analyses. However, even in this case, the majority of the lap joint is at a low value of strain. The maximum value is 0.0039539 and it is observed at both the short edges of the aluminium foil. The reason behind aluminium experiencing the maximum value is its low strength as compared to copper which makes it more vulnerable to changes in thermal strains. On the other hand, copper did experience the maximum strain value but not to the extent that aluminium had. Using simulation, a heating process window can be established and is shown in Table 3.2. It can be seen that the temperature stays around the 470 °C but it cannot be allowed to stay at this temperature for long periods of time. Applying heat to a single lap joint from 5 to 8 seconds gives the best results.

Table 3.2: Temperature distribution during the heating process

Time (s)	Minimum Temperature (°C)	Maximum. Temperature (°C)
1	25.715	470.12
2	62.952	470.13
3	113.97	470.14
4	163.17	470.15
5	206.78	470.12
6	244.5	470.14
7	276.9	470.12
8	304.66	470.11
9	328.44	470.12
10	348.8	470.12

3.8 Process Advantages

The biggest advantage of CMFM is that the feed-stock is lower in price compared to its competitors. DMLS, EBM make use of metallic powder and depending upon the type of material, the cost varies. The price of the powder is a function of the grain size and required mechanical properties of the final products as well. Such requirements and the recommendation of large companies such as EOS and Arcam to buy their powder for their machines increase the cost of the raw material considerably. EBM can also make use of wire that costs less than powder but is still more expensive in comparison to the price of metal foils. For a single build, the cost ($Cost_B$) can be estimated by the following formula proposed by Ruffo, Tuck and Hague (2006):

$$Cost_B = Cost\ (t_B) + Cost\ (m_B) \qquad (3.4)$$

Where,

$$Cost\ (t_B) = \frac{direct\_Cost}{mass\_unit}\, m_B \qquad (3.5a)$$

$$Cost\ (m_B) = \frac{\sum indirect\_Costs}{working\_time}\, t_B \qquad (3.5b)$$

The time and material used during the build (t_B and m_B respectively) are the main variables of the costing model. Time refers to how long the machine works for the build; part mass (or volume) is an index of the raw material used. CMFM is a lot faster than conventional metal AM methods majorly because of complete process automation and minimal post-processing (Eq. 3.5a). Waste is also considerable less because only the geometry to be joined is cut out from the metal sheet (Eq. 3.5b).

The process of CMFM has the ability to work with a variety of metals and make composites out of them. Current research will show specimens being produced using pure copper sheets

with a thickness of 0.1mm before moving on to difficult metals with poor solderability. Aluminium foil, 1050 grade with a H14 ½ hard temper, of varying thickness (0.05mm, 0.1mm and 0.2mm) was used to produce more specimens for testing. Multiple material parts of copper and aluminium were made and tested as well. Parts produced by additive manufacturing are often criticised for not being strong enough for real world applications but CMFM has the capability to make parts that are comparable with those made by conventional machining methods (Chapter 6). The process can work with various metals provided the right paste is used that has the ability to join the particular metal. This removes the limitation of using different materials which is a big issue with current metal AM methods.

The process of CMFM has the potential to be a strong candidate in the field of metal prototyping as it has reduced a number of limitations related to commercial metal AM methods. A part (15mm wide, 87.5mm long and 2.7mm thick) made by CMFM is shown in Fig. 3.21a and another part with the same dimensions made by DMLS process in an EOS M290 machine is shown in Fig. 3.21b. The figures show the surface finish of the parts immediately after the building operation has finished. For the DMLS part, however, a post-process is required to remove all the excess powder that was not sintered which is time consuming. The CMFM part is ready to be sued for any engineering application but the DMLS part needs to undergo further post-processing as shown in Fig. 3.21c. The part needs to be removed from the base plate and the support structure. Afterwards, it requires grinding and polishing to have a smooth finish as initially it has a very grainy finish as can be seen from Fig. 3.21b. A comparison has been shown in Table 3.3 for the production of the part (dog-bone specimen) shown in Fig. 3.21 with DMLS and CMFM process.

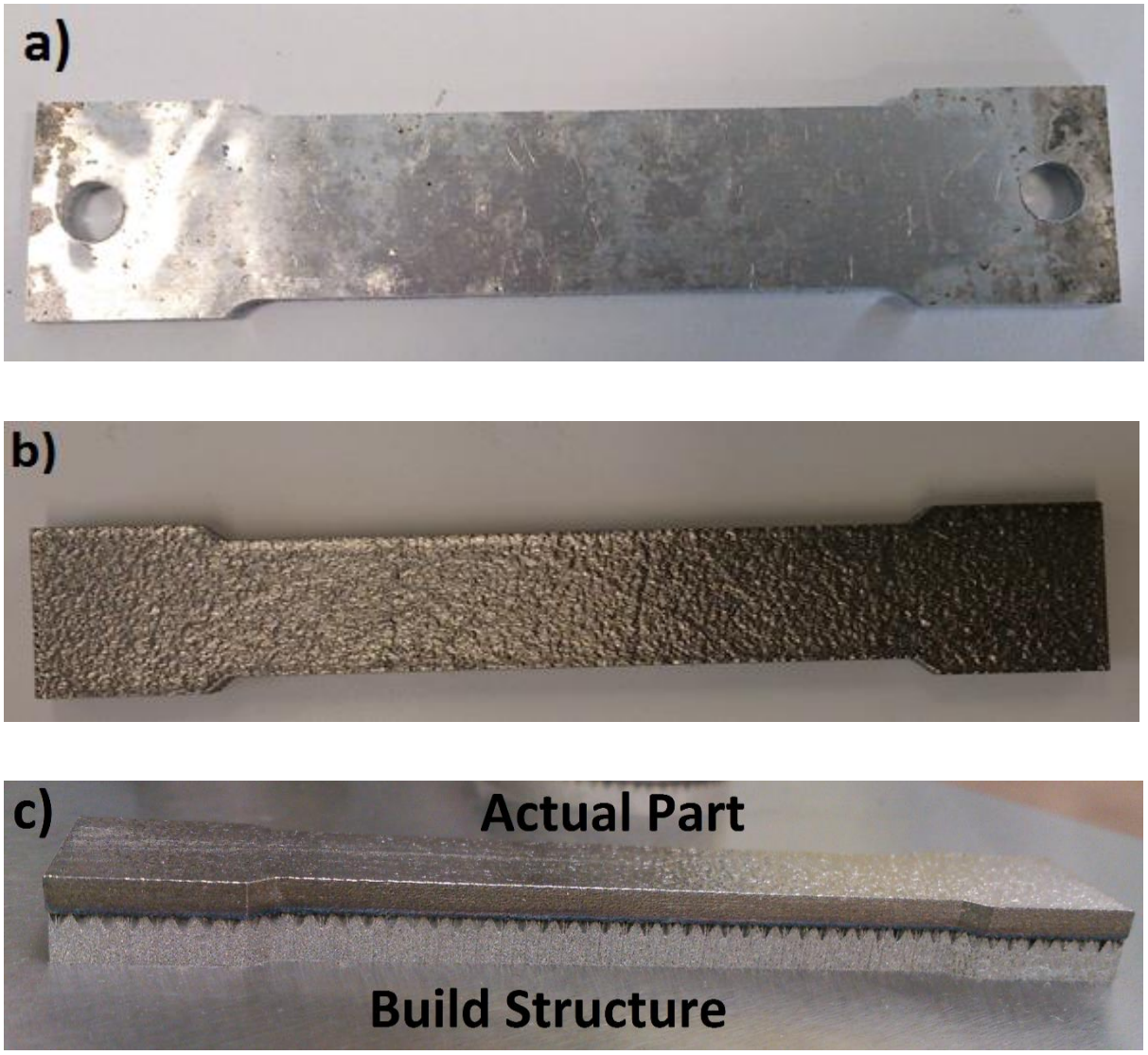

Figure 3.21: Comparison between DMLS part and CMFM part: a) CMFM part; b) DMLS part; c) DMLS part after building operation

Table 3.3: Comparison between DMLS and CMFM process

Limitations	DMLS	CMFM
Machine cost	£500,000	Estimated £30,000
Use of laser	400W fibre laser	300W fibre laser
Single build cost (Fig. 3.21)	£60	Estimated £10
Processing time (Fig. 3.21)	1 hour 45 minutes	Estimated 30 minutes
Surface finish (Fig. 3.21)	Needs post processing	No post processing required
Pre and post-processing	Required	No pre-process and minimal post-processing
Materials	Limited	A wide range provided the appropriate paste is available
Maintenance cost	High	Medium

Further to the comparison in Table 3.3, it should be noted that the price of the DMLS machine mentioned does not include the set up cost raw material cost. DMLS uses a high powdered laser compared to CMFM and thus utilizes more energy during its building operation which increases the running cost of the machine. Companies like EOS and Arcam insist in buying their powders to be used in their machines. For example, one kilogram bag of powdered EOS MaragingSteel MS1 costs around £100 whereas the same material in foil form can be purchased for around £10-£20. The cost of a single build is high for DMLS compared to CMFM based on the initial high cost of the raw material. DMLS has a much longer processing time compared to CMFM. For DMLS, the production run consists of: approximately 40 minutes for the gas to fill the build chamber, 20 minutes for setting up and levelling of the build platform, 45 minutes for the part to be made including a 4mm thick support structure otherwise the actual part would not adhere to the surface, 15 minutes for powder removal after the build, 10 minutes for removing the part from the build platform and

the support structure from the part. Afterwards, grinding, polishing and sometimes heat treatment to impart the required attributes to the products. This requires setting-up of more equipment and machinery. On the other hand, CMFM process requires minimum post processing to remove any ridges formed on the sides of the parts as a result of excess paste and is much less time consuming. In terms of material processing, DMLS has categories of materials and upon moving from one category to the other (for example moving from EOS MaragingSteel MS1 to EOS Aluminium AlSi10Mg or EOS Titanium Ti64), the filters need to be changed due to flammability of the metal powder, thus adding more expenses. CMFM can easily work with different foil materials without having to deal with the extra cost of filters. Both machiens are capable of producing multiple materials in a single build but for DMLS, the base plate can only be used for one build and then it needs to be replaced (£80 for one base plate) which again adds to the operational cost of the DMLS system. CMFM operation is also simpler and does not require extremely strict safety protocols like the DMLS where operators have to wear full body suits and face masks to load and unload the powder before and after each build. All in all, CMFM provides a more flexible approach and notable advantages over the commercially available DMLS process.

CMFM can easily produce light weight composites having (say) aluminium in the middle and a few layers of copper on the top and bottom to make a strong and light weight part as shown in Fig. 3.21. Copper and its alloys (brass, bronze etc.) are natural antimicrobial materials i.e., they kill microorganisms and inhibit their growth. This property of copper has recently become quite important and is under active investigation by scientists (Grass, Rensing and Solioz, 2011). The term ‘contact killing’ has been coined to describe the ability of copper to kill different bacteria, yeasts and viruses upon contact. Stainless steel is generally used in the health care sector due to its clean appearance and corrosion resistance but it does not have any antimicrobial properties. Copper, on the other hand, with their self-sanitizing properties

could potentially make its way in the health care environment as an antibacterial material by providing protection against infectious microbes (Casey, et al., 2010). CMFM has shown that it has the capability to process copper without any issues. The transition of copper to the medical sector can be made much smoother by making copper-based medical instruments using CMFM.

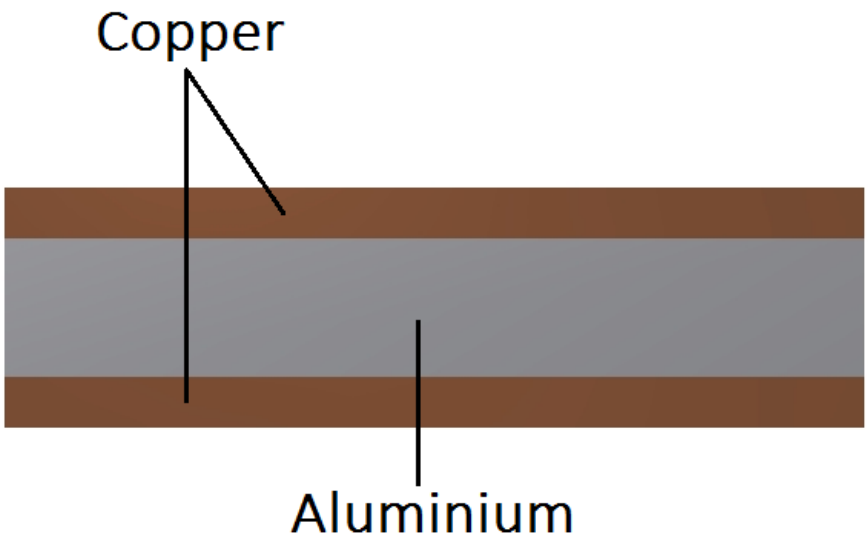

Figure 3.22: Side view of aluminium and copper metal composite

CMFM has the capability to produce complex geometries which might not have been possible using traditional manufacturing techniques, such as:

- undercuts
- channels through sections
- tubes within tubes
- internal voids

It can also be used to produce large moulds with grooves as well as complex cooling systems with cavities and sliders. Generally in such cases the cost for tooling or injection moulding is very high and CMFM can provide cost-effective means of production. Metal foil LOM

suffers from staircase effect and cannot use metal foils that are less than 0.5mm thick (Prechtl, Otto and Geiger, 2005a; 2005b) but CMFM can work with foils of various thickness (Chapter 6) and does not face the same issues. The parts produced by the proposed process have good surface finish compared to some of its rival metal AM methods and require minimum post-processing to improve it. CMFM can produce overhanging parts at different angles with ease whereas DMLS struggles at making anything that is at an angle of more than 25° (Fig. 3.22) and needs support material which as mentioned before results in a time consuming post-process.

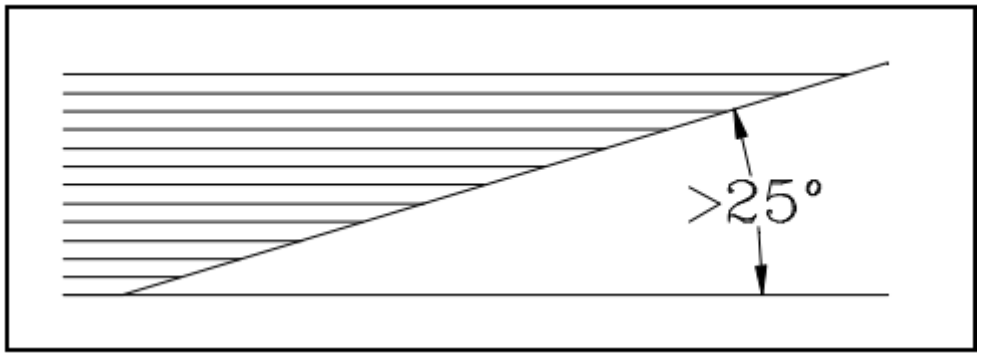

Figure 3.23: Limit for overhanging parts requiring support material for DMLS

3.9 Process Limitations

The process has the capability to produce parts as strong if not stronger compared to conventional machining methods (Chapter 6) but in doing so the parts lose their ductility. The reason is that the layer of paste prohibits the metal atoms from slipping when stress is applied and thus prohibiting any dislocations resulting in a smaller deformation range. However, it can be considered as a trade-off for getting a stronger but less ductile metal part. The build size has always been a limitation for metal AM methods and it prevails with the current setup as well. Machines with larger build volume are expensive as well but they are also capable of handling most parts. Even though the build volume for the CMFM machine has been set at 600mm wide, 1000mm long and 1000mm in height which is a lot more than most rival metal

AM processes but there are still some machines that have a comparatively larger working area (Table 2.3). The software used for AM machines is complex and needs further development as the manufacturing process advances. This could pose problems of interfacing and troubleshooting can become harder to carry out. Expert handling of the software would be required to carry out maintenance activities. Another issue is the reliability of the dimension in the Z-direction. Even though every effort is being made to ensure that the thickness/height of the part being produced remains unaltered, it is highly unlikely to happen. The pressure from the roller ensures a uniform layer of paste but when the part is placed on the heated plates then there is a high probability that the heat and pressure applied could reduce the thickness from what it was before it was heated. Therefore, experimentation is needed in this regard to offer a shrinkage factor or set a tolerance limit to avoid dimensional inaccuracies.

This research work carried out here deals with lap-shear, peel, tensile testing and microstructural analysis under different settings to keep the focus on tension forces. The test results obtained have been compared with those of established AM methods to establish the effectiveness of the new process (Chapter 6). In addition, a large number of tests could have been performed to analyse the behaviour of the parts under different conditions. They include but are not limited to hardness, bending, torsion, compression, creep and stress rupture, fracture toughness, notch-toughness, impact toughness, fatigue, thermal fatigue and fatigue crack growth rate. The list is long but is by no means an exhaustive one and additions could be made based on the type of forces acting on the tested part. The additional tests were not performed because they are a separate research field in their own right and would have required a lot of time and resources; therefore, they were set aside for future.

3.10 Summary

This chapter presents the new proposed additive manufacturing process termed as Composite Metal Foil Manufacturing. A conceptual model of a machine based on the principle of CMFM has been shown. The process details along with the flow chart of operation have been presented. The main components of the machine include suction mechanism, fibre laser, roller, thickness measuring laser sensors, dispenser (Chapter 4) and heated plates. These components have been carefully selected and explained for their functional capabilities in context of their role in the process. 3D transient thermal analysis has also been carried out that will serve as a reference model for future parts. This chapter also discussed the advantages and limitations of the proposed process.

CHAPTER 4

4 Dispensing Mechanism

The accurate dispensing of the solder or brazing paste is crucially important as it will ensure the proper bonding of the metal foils and avoid waste. This chapter will introduce 710 dispenser that came highly recommended by Fusion Inc., the same company from which the brazing paste was purchased. CFD analysis of the dispenser has been carried out with the ASN-892-600 brazing paste as it can join aluminium as well as composite of aluminium and copper. The electrical connections and C++ code to establish communication between the dispenser and the main machine have been presented.

A detailed description of another type of dispenser has been presented in Appendix A. It is a powder dispenser which has been integrated to a fully functional 3D printer (Butt, 2011). Its integration with an external machine (3D printer), electrical connections and programming is very similar to the one done for 710 dispenser which makes it a very good second option. It can serve as a substitute to the 710 dispenser or can be used in addition to it.

4.1 Introduction to 710 Dispenser

The dispenser is responsible for dispensing the brazing paste and it should be able to dispense precise and minute quantities of the paste without any wastage. 710 dispenser from Fusion Inc. is chosen for the job as it is a compact unit featuring adjustable time and pressure controls to provide paste deposit sizes ranging from small dots to continuous stripes of any length (Fig. 4.1). Each paste deposit is precisely measured, ensuring controlled filler metal costs without waste. Fig 4.2 shows the cross-section of the dispenser gun and reservoir.

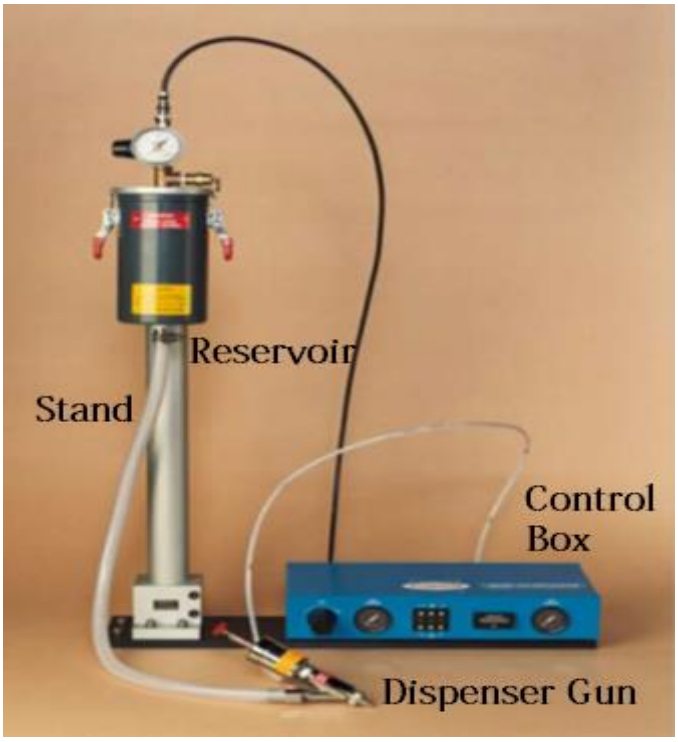

Figure 4.1: 710 paste dispenser (Fusion-Inc.com, 2013)

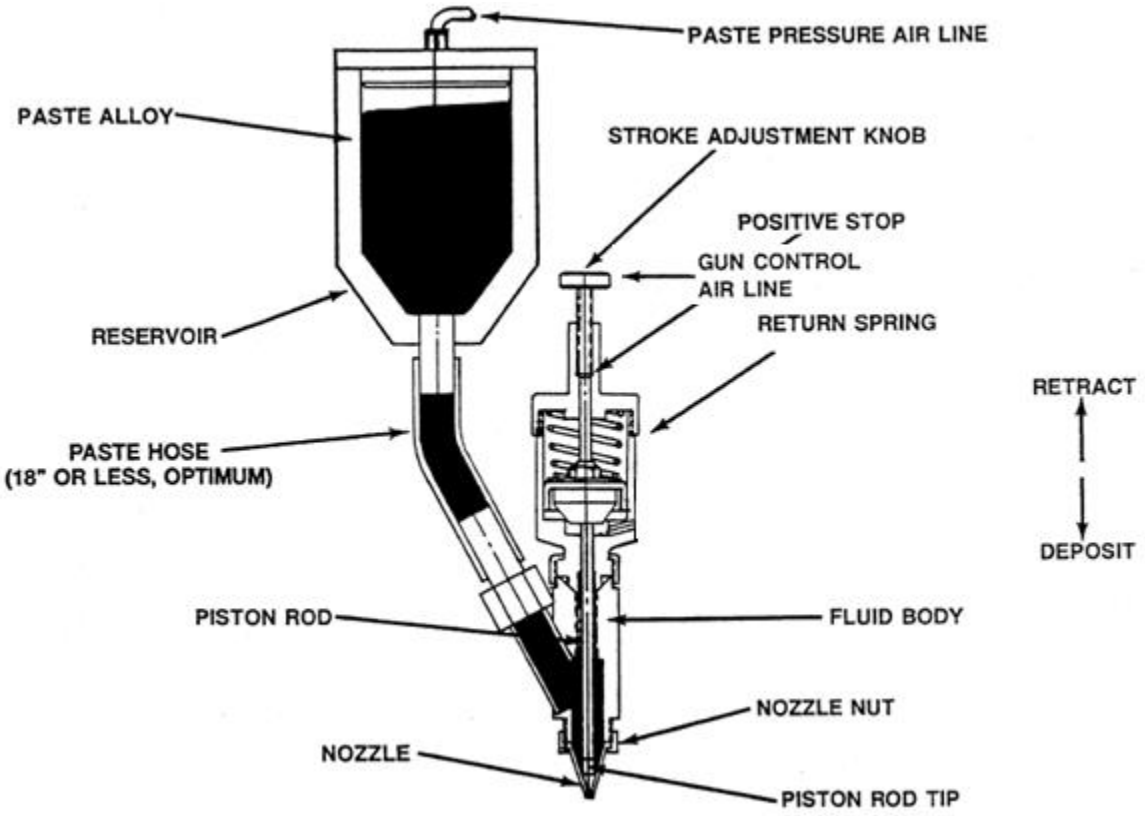

Figure 4.2: Cross-section of the gun and reservoir of the 710 paste dispenser (Fusion-Inc.com, 2013)

As the sketch indicates, pressure is supplied to the paste alloy in the reservoir through the paste pressure air-line. The amount of air pressure in this line is controlled by the regulator located on the applicator control panel and designated there as paste pressure. This air pressure keeps the paste alloy flowing through the system for eventual deposit through the applicator nozzle. Air also passes to the cylinder of the applicator gun through the gun pressure air-line. The pressure gauge is also located on the applicator control panel and designated there as gun pressure. This gun pressure is factory set depending on the operation. The pressure on the piston causes the movement of the piston rod within the cylinder. The piston rod in the gun extends down into the fluid body and the tip is attached to the piston rod. The stroke and retraction of the piston rod dispenses the paste alloy through the nozzle orifice on a positive displacement principle. As the piston rod retracts, paste flows into the void created within the nozzle. When the rod comes forward, the amount displaced is dispensed through the nozzle orifice. The nozzle orifice is available in a variety of sizes. The next section calculates the precise amount of dispensed paste from the nozzle using CFD (Computational Fluid Dynamics) analysis. For the CFD analysis, a nozzle orifice size of 3mm has been used.

4.1.1 CFD Analysis of the 710 Dispenser

It should be noted that the dispenser gun is being modelled in CFD and not the entire reservoir. Although the pressure value from the reservoir will be taken into account while modelling as it is responsible for pushing the paste forward. The ASN-892-600 brazing paste has a density of 7200 kg/m^3 and a viscosity of 150 kg/m-s. These two properties are required for calculation of mass flow rate of the paste using CFD analysis. Mass flow rate will then be used to calculate the thickness of a continuous stripe on the metal sheet with the help of the following formula:

$$\text{Thickness} = \frac{\text{Mass flow rate}}{(Density\ of\ the\ paste)(\text{Width of exit})(\text{Speed of the dispenser})} \quad (1)$$

The dispenser comes with recommended factory pressure settings for optimal performance. Those settings were put to the test by the CFD analysis. The gun pressure is at 310.264kPa (45 psi) and the paste pressure is at 155.132kPa (22.5 psi: half of the gun pressure) as shown in Fig. 4.3.

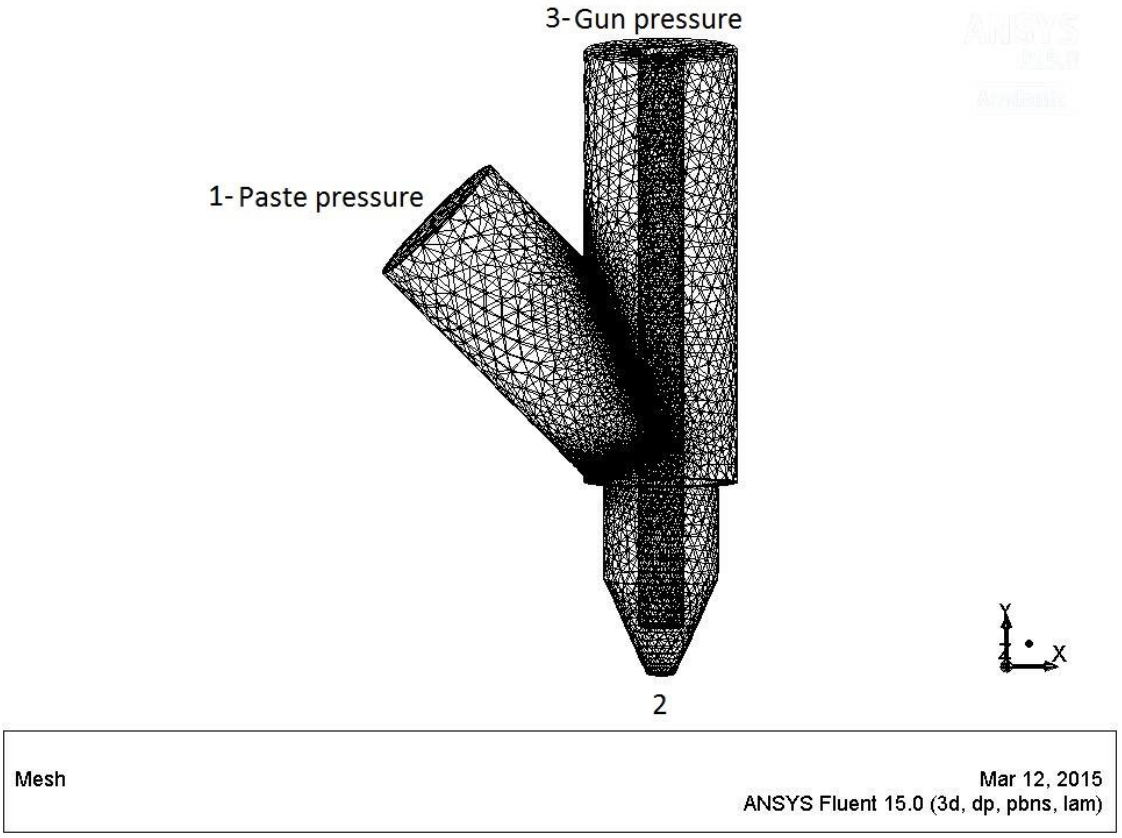

Figure 4.3: Mesh for the 710 paste dispenser gun

The paste in use is a highly viscous non-Newtonian fluid meaning that its viscosity is dependent on shear rate or shear rate history. The paste is not stirred and the dispensing is done at room temperature. The parameters of interest include velocity and pressure as non-uniformity in any of these two will result in improper dispensing. Fig. 4.4 shows the path lines for the velocity magnitude of the dispenser and Fig. 4.5 shows the same for the nozzle.

As is evident from these figures, the velocity is uniform and there are no abrupt changes throughout the body of the dispenser which makes the dispensing operation smooth and dependable.

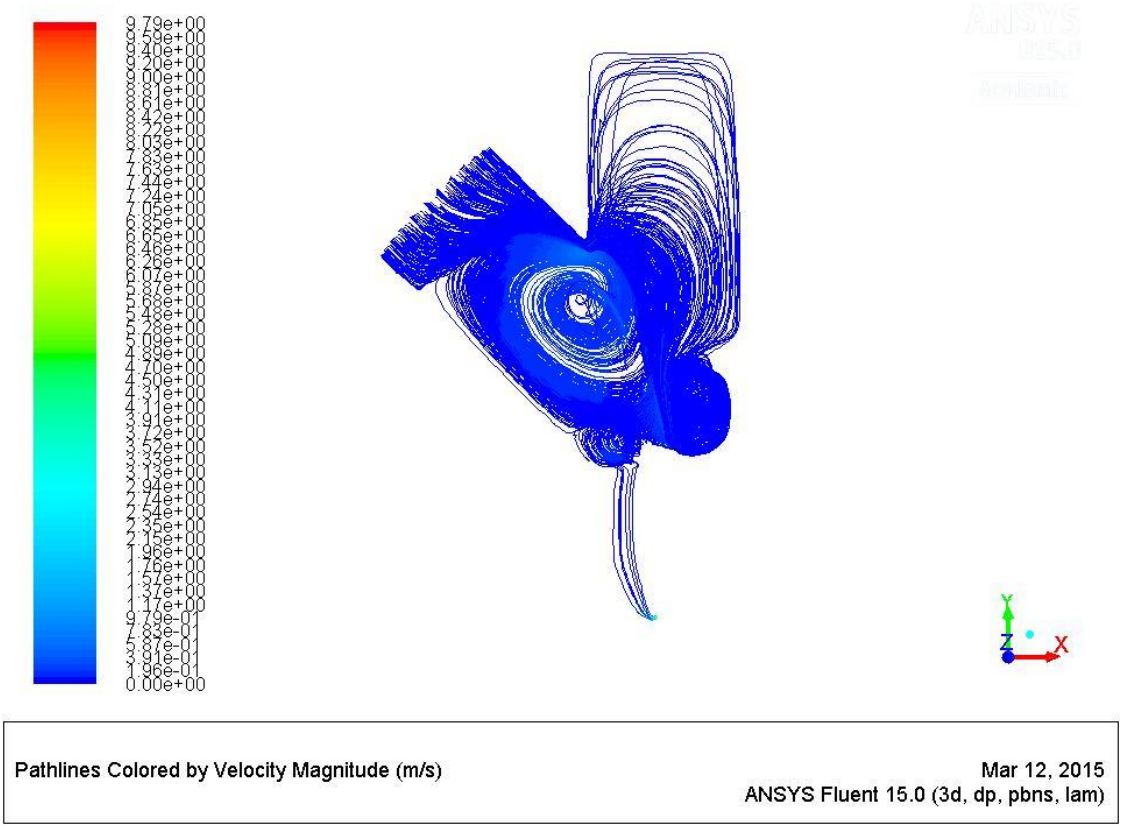

Figure 4.4: Velocity path lines for dispenser

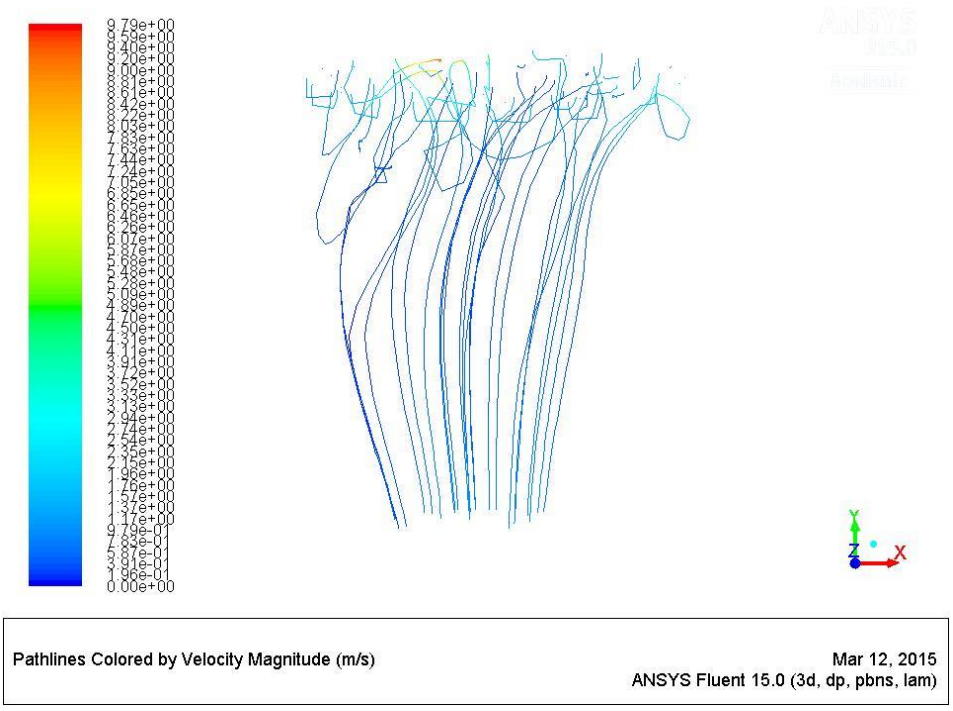

Figure 4.5: Velocity path lines for nozzle

A uniform velocity ensures proper dispensing and a more in-depth analysis of the cross-section of the dispenser showed the same results as is evident from Fig. 4.6 and Fig. 4.7.

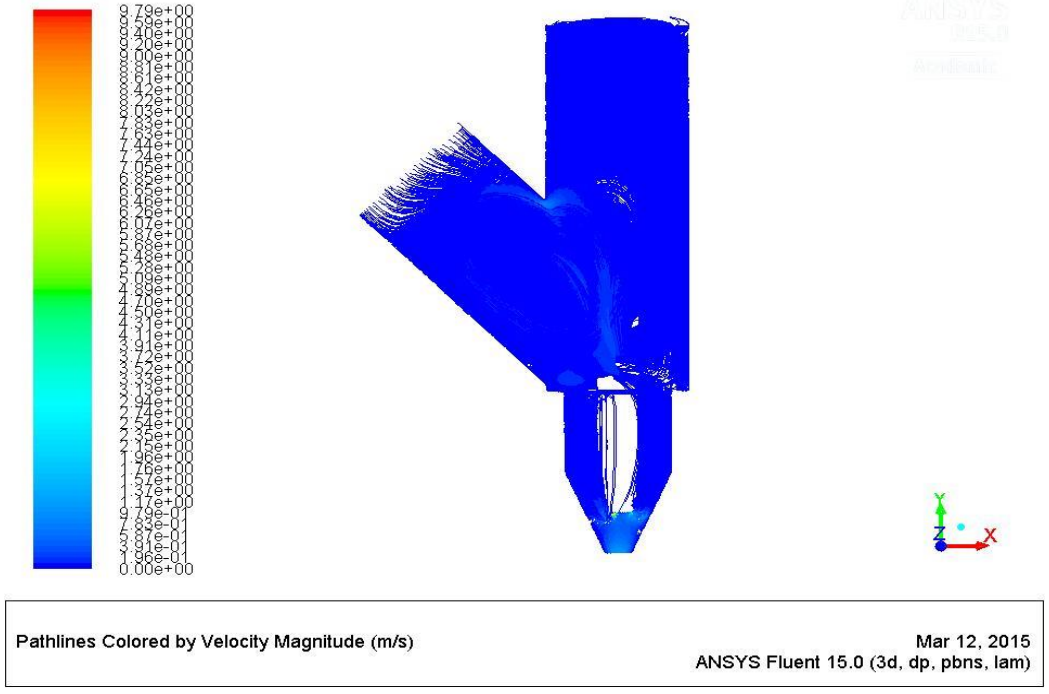

Figure 4.6: Cross-sectional velocity path lines for dispenser

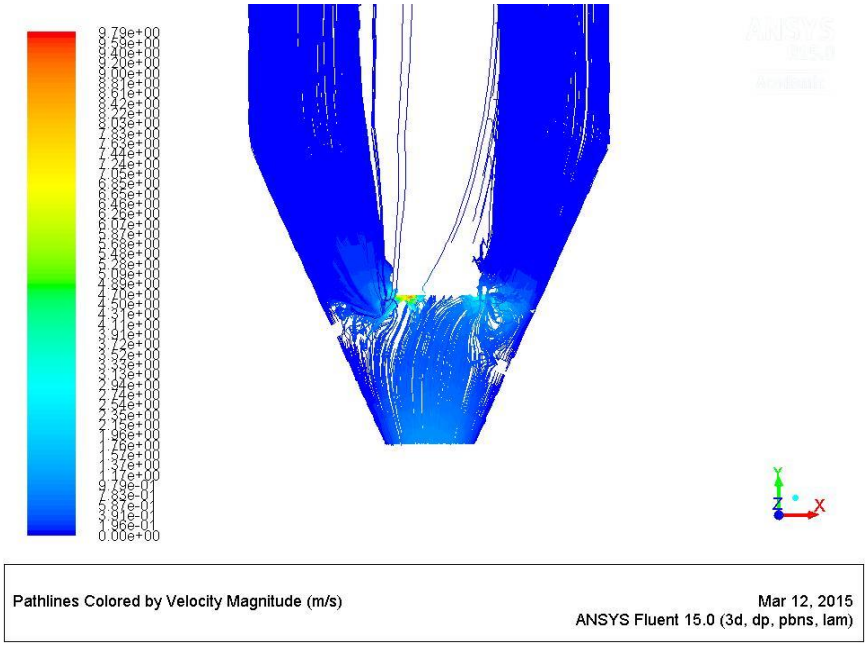

Figure 4.7: Closer look at the cross-sectional velocity path lines for dispenser

Pressure is also an important factor as it is something that is being given to the system. The values of 310.264kPa and 155.132kPa should not create disturbance in the fluid flow. If a large disturbance is observed then the pressures would have to be changed for optimization. However, the pressure contours (Fig. 4.8) do not show a drastic change in pressure. Although a small variation can be observed towards the bend of the nozzle which is expected (Fig. 4.9).

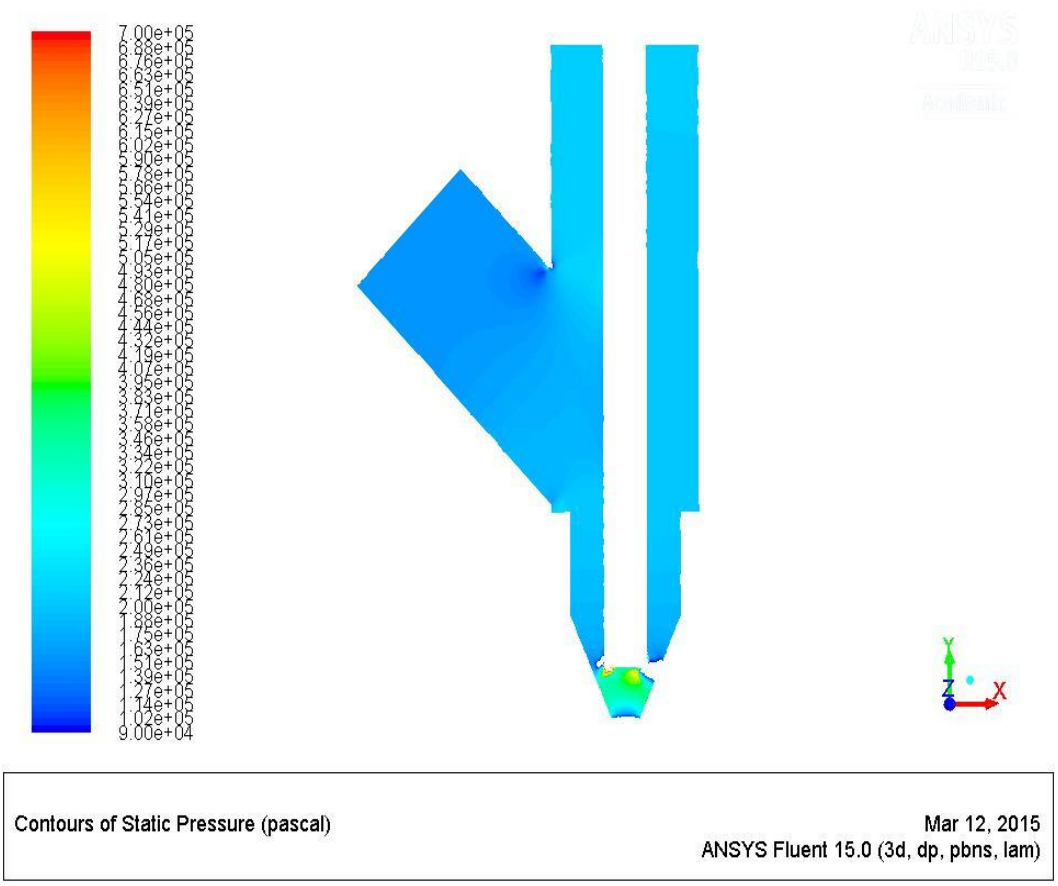

Figure 4.8: Pressure contours for dispenser

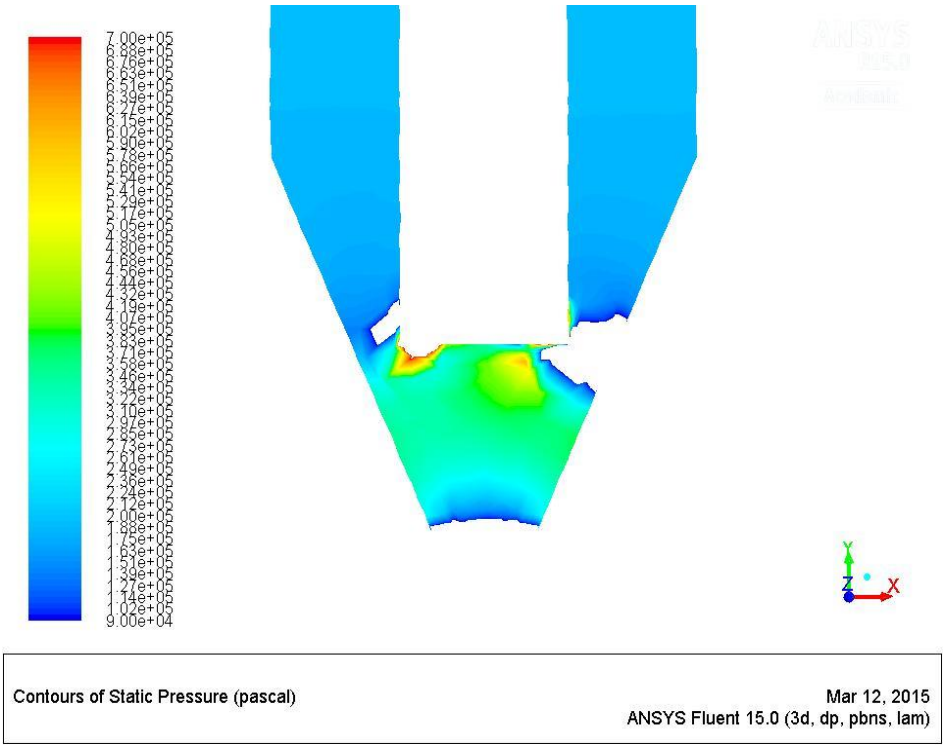

Figure 4.9: Closer look at the pressure contours of the dispenser

CFD analysis gives the mass flow rate in kg/s for the three areas shown in Fig. 4.3. For area 1, it is 0.0007909932, the value for area 2 is -0.0016624 (because it is the exit, therefore, the negative value) and for area 3, the value is 0.0008612468. The value at area 2 is to be used in Eq. 1 as the mass flow rate, width of the nozzle (exit) is 3mm, speed is 30mm/s and the density of the paste is 7.2×10^{-6} kg/mm^3. Upon calculation, the thickness of the paste coming out of the 3mm nozzle is 2.6 mm. By using the CFD analysis, the dispenser can be modelled for different pressure values, nozzle diameters and then using Eq. 1, the correct thickness of the paste to be dispensed can be calculated.

4.1.2 Components for Installing 710 Dispenser

After it has been established that 710 paste dispenser is fully capable of working according to the requirements of the process, additional components for its connection to the main machine were sorted out. Table 4.1 lists down the components needed for the dispenser's installation along with their part numbers and sources from where the components can be purchased.

Table 4.1: Components for electrical connections of the 710 paste dispenser

Components	Part Number	Source
710 Applicator with finger switch	710	Fusion Automation Inc.
1 pint reservoir for the paste	3P0133Q	
FE71 paste gun	FE71	
Nozzle	SINGLE-N	
Arduino Uno	Uno	Arduino Website
RLY-108 TTL Relay Board	RLY-108	Auric Solutions
5V Power Supply	PS-5	Spark Fun

4.1.2.1 Arduino Uno

Arduino Uno is being used to provide a digital signal to run the applicator. It is an electronics platform with a microcontroller board based on the ATmega328. It has 14 digital input/output pins (of which 6 can be used as PWM outputs), 6 analogue inputs, a 16 MHz ceramic resonator, a USB connection, a power jack, an ICSP header, and a reset button as shown in Fig. 4.10. It contains everything needed to support the microcontroller.

Figure 4.10: Arduino Uno

The Arduino Uno can be powered via the USB connection or with an external power supply. The power source is selected automatically. External (non-USB) power can come either from an AC-to-DC adapter (wall-wart) or battery. The adapter can be connected by plugging a 2.1mm centre-positive plug into the board's power jack. Leads from a battery can be inserted in the GND and VIN pin headers of the POWER connector. Arduino Uno can supply a voltage of 5V which will be required to power the relay.

4.1.2.2 Relay

Relays are used wherever it is necessary to control a high power or high voltage circuit with a low power circuit. Its use here is to isolate the applicator from the computer and will be wired between Pins 1 and 2 of the 710 applicator. Pin 1 is the trigger signal which will cycle the applicator. This input is a TTL signal, low-true logic. The chosen relay is RLY-108, 8-Channel TTL Relay Board as shown in Fig. 4.11. The reason for choosing an eight channel relay is that it would be able to handle more than one component if needed.

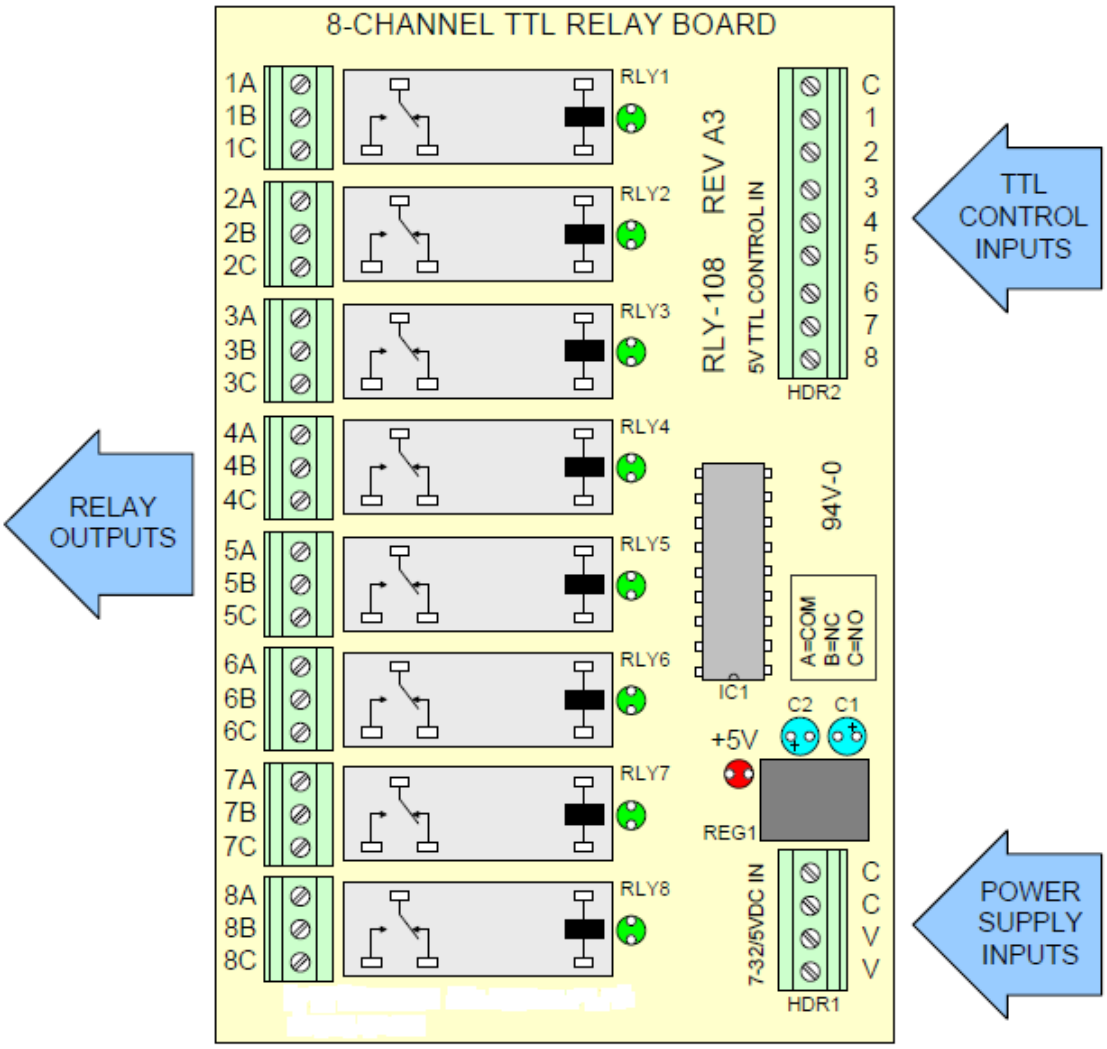

Figure 4.11: Component layout on the RLY-108 relay board (AuricSolutions.com, 2009)

A relay is an electromagnetic switch and one of its important parts is the coil which converts electrical current into an electromagnetic flux. The main problem with relay coils is that they are “highly inductive loads” as they are made from coils of wire. Any coil of wire has an impedance value made up of resistance (R) and inductance (L) in series. As the current flows through the coil a self-induced magnetic field is generated around it. When the current in the coil is turned “OFF”, a large back EMF (electromotive force) voltage is produced as the magnetic flux collapses within the coil (transformer theory). This induced reverse voltage value may be very high in comparison to the switching voltage, and may damage any semiconductor device such as a transistor, FET or micro-controller used to operate the relay coil. One way of preventing damage to the transistor or any switching semiconductor device, is to connect a reverse biased diode across the relay coil. When the current flowing through the coil is switched “OFF”, an induced back EMF is generated as the magnetic flux collapses in the coil. This reverse voltage forward biases the diode which conducts and dissipates the stored energy preventing any damage to the semiconductor transistor. When used in this type of application the diode is generally known as a Flywheel Diode, Free-wheeling Diode and even Fly-back Diode, but they all mean the same thing. Other types of inductive loads which require a flywheel diode for protection are solenoids, motors and inductive coils. As well as using flywheel Diodes for protection of semiconductor components, other devices used for protection include RC Snubber Networks, Metal Oxide Varistors or MOV and Zener Diodes. This particular relay is already fitted with a flywheel diode which makes it perfect for the application at hand.

The relays on the RLY-108 board are Single Pole Double Throw (SPDT) Relays meaning that each relay has its own 3-terminal connector. The A terminal is the COMMON. The B terminal is the NORMALLY CLOSED (NC). The C terminal is the NORMALLY OPEN (NO). Normally the COMMON relay pin is connected to the NO terminal when the relay is

turned on, and to the NC terminal when it is off. The relay's LED will illuminate when the relay is energised.

4.1.3 Electrical Connections for 710 Dispenser

The 710 applicator has a 9 pin 'D' connector on the rear of the unit that allows the unit to be controlled by an external system, which in this case is a computer. Table 4.2 shows the pins of the applicator.

Table 4.2: Pins of 710 Applicator

PIN	FUNCTION
1	Initiate + Start cycle (contact closure at TTL input)
2	Ground
3	Output + TTL Output (200mA Max)
4	Ground
5	Initiate + Start cycle (contact closure at TTL input)
6	Ground
7	Ground
8	Ground
9	Ground

Pin 1 is the trigger signal which will cycle the applicator. This input is a TTL signal, low-true logic. Like everything else in the machine setup, the computer is controlling every aspect of the process. Arduino Uno is connected to the computer via USB cable and is being controlled by it. The relay receives its input from the Arduino being controlled by the computer. On receiving an input signal, the relay is turned ON and goes into NO position. This in turn makes the 710 applicator dispense paste. The dispensing will keep going until the previous signal is stopped or a new input is sent to stop the process of dispensing.

Fig. 4.12 shows the relay in NO position. The signal is coming from the computer through serial communication into the Arduino Uno board. Pin 2 of the board is a digital pin and is

responsible for relaying the signal to the inverter or (NOT gate). When the signal from Pin 2 of the Arduino is low true logic (or 0V) then the NOT gate will invert it and low high logic (or 5V) is given to the relay (Fig. 4.13). The LED lights up showing that the relay is energized and the dispenser starts to dispense as long as the signal remains the same. The dispenser is connected to its own 220 VAC power supply. Pins 1 and 2 of the dispenser are connected to the NO and COM contacts of the relay. The Arduino is being powered by the 5V USB power and the operating voltage of the relay is also 5V which makes everything at the same voltage. Connecting the relay to Arduino's 5V pin means that the both the trigger current and the current to drive the relay coil are being supplied by the Arduino board. From the datasheet for the relay (AuricSolutions.com, 2009), it is 420mA and Arduino is capable of supplying this current with ease. The relay moves in NC position when there is no activity and the signal is high true logic.

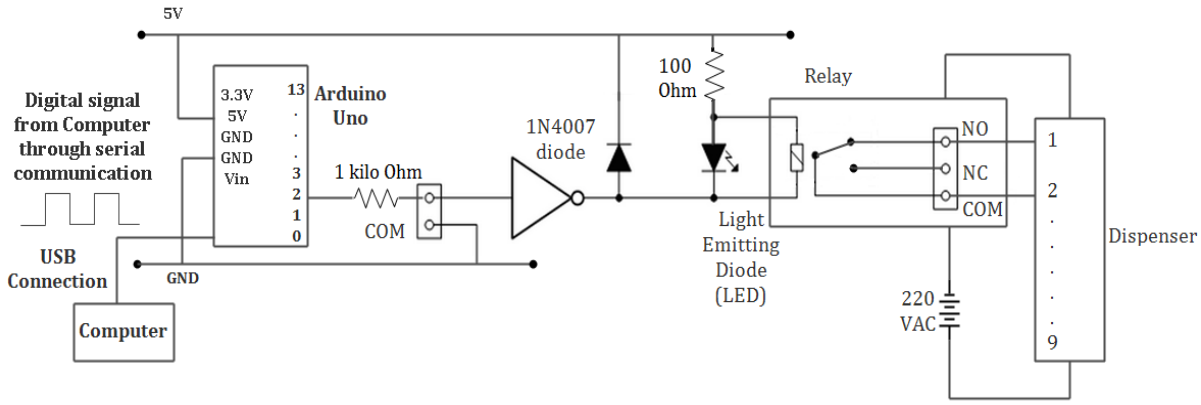

Figure 4.12: Relay in NO position

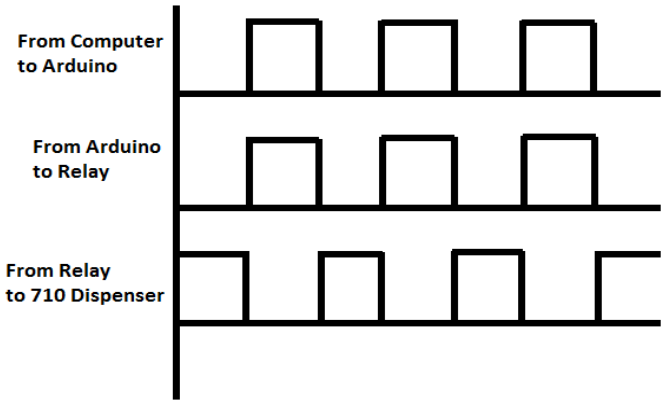

Figure 4.13: Signal Processing from computer to the dispenser

The following code will be uploaded into the Arduino Uno that will allow the computer to control it and in turn control the dispensing operation.

```
#include "SPI.h" // necessary library
int ledPin = 2;              // LED connected to digital pin 2
word outputValue = 0; // a word is a 16-bit number
byte data = 0; // and a byte is an 8-bit number
void setup()
{
 pinMode(ledPin, INPUT);     // sets the digital pin as input
 //set pin(s) to input and output
 pinMode(10, OUTPUT);
 SPI.begin(); // wake up the SPI bus.
 SPI.setBitOrder(MSBFIRST);
}

void loop()
{
 for (int a=0; a<=4095; a++)
 {
  outputValue = 2000;
  digitalWrite(10, LOW);
  data = highByte(outputValue);
  data = 0b00001111 & data;
  data = 0b00110000 | data;
  SPI.transfer(data);
  data = lowByte(outputValue);
  byte x = SPI.transfer(data);
  digitalWrite(10, HIGH);

 }

 for (int a=4095; a>=0; --a)
 {
  outputValue = 2000;
  digitalWrite(10, LOW);
  data = highByte(outputValue);
  data = 0b00001111 & data;
  data = 0b00110000 | data;
  byte x = SPI.transfer(data);
  data = lowByte(outputValue);
```

```
   SPI.transfer(data);
   digitalWrite(10, HIGH);

  }
}
```

4.2 Summary

The 710 applicator is a modern day and versatile piece of equipment that comes highly recommended from the company Fusion Inc. CFD analysis on the paste flow showed uniform velocity and pressure distribution without any abrupt changes. The analysis also helped in calculating the exact amount of paste dispensed and it can serve as a reference model for incorporating changes in pressure, dispenser moving speed, nozzle diameter etc., for future analyses. Electrical connections for integrating the 710 applicator to the main machine along with the C++ code needed to establish communication has also been presented.

CHAPTER 5

5 Process Practices

5.1 Introduction

The previous two chapters (Chapter 3 and 4) have given the description of the components for the automated machine based on the principles of CMFM. But for practicality, the process was systematically broken down into simple steps so that parts could be produced and tested for their mechanical properties. Since every step was performed independently, it was important to make sure that the process utilizes the minimum resources as one of the objectives is to make this process as cost-effective as possible. Laminated Object Manufacturing has not been integrated with soldering/brazing to form a process that is 'additive' in nature for the production of metal parts. The process of soldering/brazing can be tricky for certain metals but it was crucial to make the process as adaptable as possible so that it can handle difficult metals. The experimental heating time has been validated by numerical analysis and a three dimensional reference model has been presented, using ANSYS that can be used for future parts.

Each and every step was performed by making use of the resources available at the university facilities without compromising the end result. The flow chart in Fig. 5.1 gives the step by step description of the experimental setup created for the production of sample parts and Table 5.1 shows the processes that took the place of the machine components described in Chapter 3 and 4.

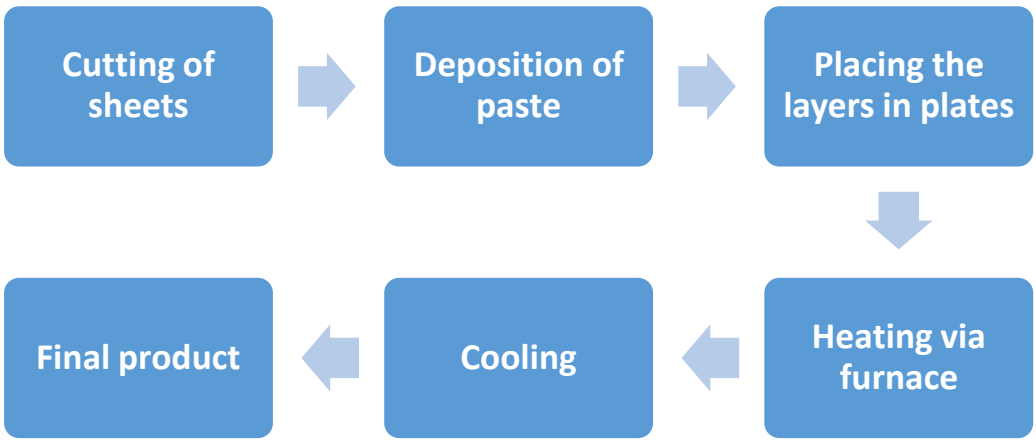

Figure 5.1: Flow chart of the process

Table 5.1: Comparison of the machine components and the replacement practices used

Process	CMFM machine	Replacement Practices
Cutting of metal foil	300W MIYACHI fibre laser	Punch and die tool
Deposition of paste	710 paste dispenser	Manual application
Thickness measurement	Microtrak™ 3 TGS laser displacement sensors and NPMS2 measuring system	Use of torque wrench to ensure uniform thickness of the paste
Moving the paste coated foils on the heating plates	Automatic with the use of a part moving arm	Manual positioning of the paste coated foils on stainless steel plates fitted with nuts and bolts
Heating for final joining	Pre-programmed industrial plates heating the paste coated metal foils	Pate coated metal foils sandwiched between two 4mm thick stainless steel plates heated in Carbolite CWF1200 Chamber Furnace
Post-processing	Manual removal of any ridges	Manual removal of any ridges

5.2 Cutting of Metal Sheets

The metal sheets selected for the process included pure copper foils and Aluminium 1050 grade foils with a H14 ½ hard temper of varying thicknesses (0.05mm, 0.1mm and 0.2mm). After the selection of the material, the next step was to cut the sheets according to the shape required. For the sake of clarity, a copper dog-bone specimen is being made as shown in Fig. 5.2 (BS EN ISO 6892-1: 2009, 2009) using the direct aluminium solder paste and the specimen will follow all the steps shown in Fig. 5.1.

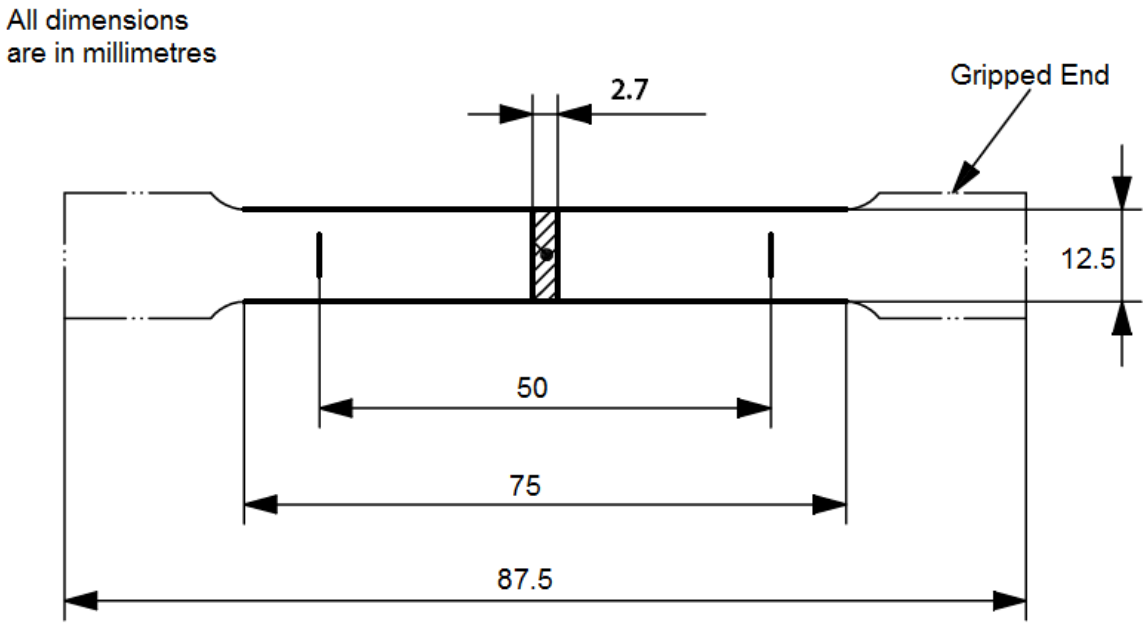

Figure 5.2: Dimensions of the dog-bone specimen

A punch and die tool (Fig. 5.3c) was used for cutting the copper sheets. It consists of two parts; one is a solid block, called the punch (Fig. 5.3a) and the other is a hollow part, called die (Fig. 5.3b).

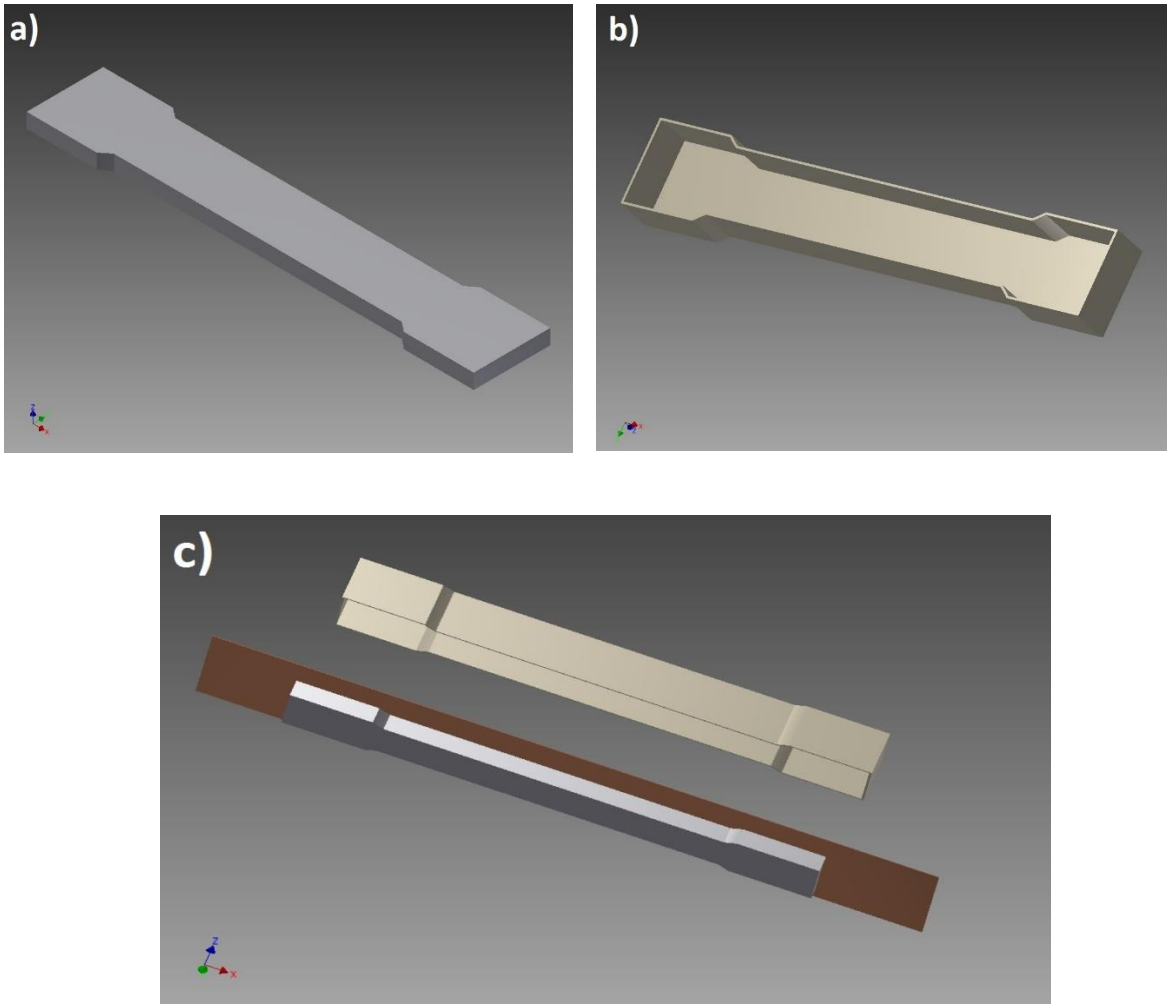

Figure 5.3: Punch and die tool: a) Punch; b) Die; c) Assembly of the tool

The punch was made out of stainless steel plate but making of the die was more involving. The required dog-bone shape was first cut out using milling operation and then the part was heat treated for strength followed by grinding so that it could be able to cut the metal sheet on impact. The corners of the die were made 1mm larger so that they can easily perform the cutting operation without damaging the metal sheet and can fit into the punch when brought down with force. Fig. 5.4 shows a dog-bone shape punched out from the 0.1mm thin copper sheet and it is evident that the punch and die tool are working to a satisfactory level as very little distortion of the metal sheet is observed.

Figure 5.4: Specimen punched out from the metal sheet using punch and die tool

5.3 Deposition of Paste

The solder paste was deposited manually to each and every layer (Fig. 5.5). There was a concern over the thickness of the solder paste as being non-uniform because of the manual application. Therefore, a torque wrench was used to ensure uniform paste distribution.

Figure 5.5: Foils after the deposition of solder paste

5.4 Placing the Layers in Plates

The copper sheets used for the production of dog-bone specimen are very thin (0.1mm) which means that heat cannot be applied directly to them so stainless steel plates were used to sandwich the layers. The plates were cut out from a 4mm thick Stainless Steel 316 plate according to the dimensions of the part to be made so that they can cover the entire product

and will act as a heated plate that will transfer heat gradually to the metal foils coated with solder paste sandwiched between them. The plates were 150mm long and 35mm wide. Holes of 7mm were drilled in the plates at equal intervals which were then fitted with stainless steel nuts and bolts (Fig. 5.6) so that appropriate pressure could be applied at all times. The major reason for using stainless steel 316 is because of its melting point (1400 °C) which is higher than the operating temperatures of the soldering process, and its availability.

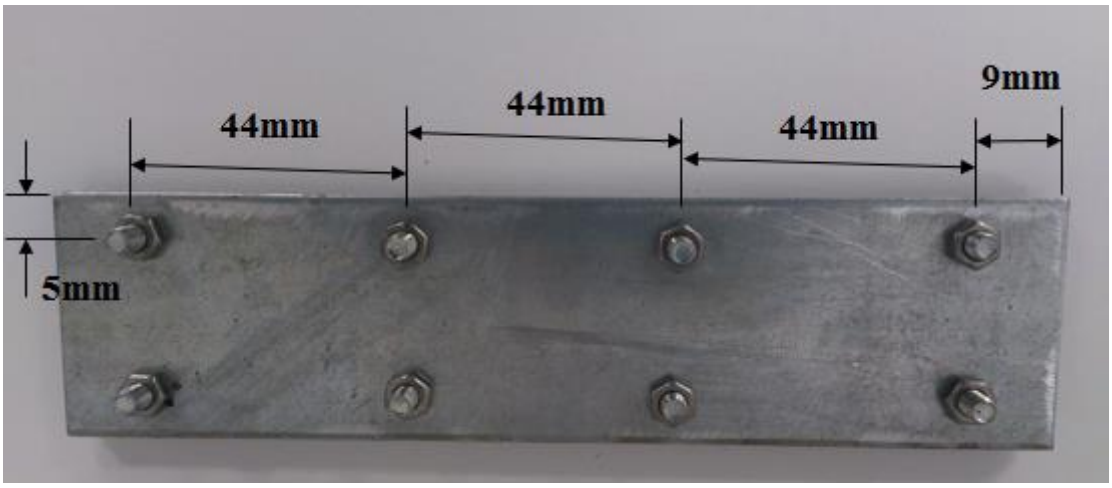

Figure 5.6: Stainless steel plates fitted with nuts and bolts

The stainless steel plates serve three purposes:

- They smooth out the solder paste layer among foils of metal. This is achieved when the nuts and bolts are tightened with a torque wrench (Fig. 5.7a) at a value of 60Nm (Fig. 5.7b). This process expels all the extra paste leaving behind a uniform and smooth layer. The paste is then cleaned so that it will not get attached to the plate and cause problems afterwards. The torque wrench was utilized for every part that was made to ensure repeatability. The value of 60 Nm was not selected at random. It was observed while experimentation, that if more torque is applied then it resulted in shearing of the bolts which renders the bolt useless.

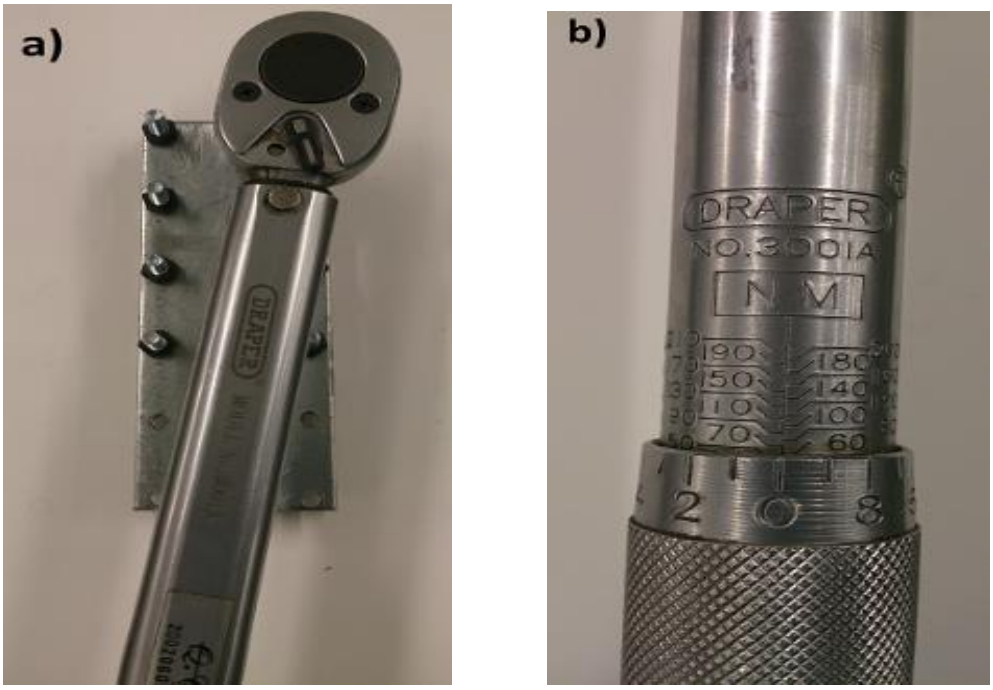

Figure 5.7: Torque wrench: a) Tightening the nuts; b) Constant value of 60 Nm

The torque of 60 Nm resulted in a pressure of 3.2MPa as seen from the following calculation:

The nut has a diameter of 7mm wide which makes the radius equal to 3.5mm or 0.0035m and the force then becomes 60/0.0035=17142N. The plates are 0.15m (150mm) long and 0.035m (35mm) wide which makes the area equal to 0.00525m^2. Therefore, the pressure will be 17142/0.00525=3.2MN/m^2 or 3.2MPa.

- These plates also keep the layers of foils aligned as they have stoppers (Fig. 5.8) fitted according to the geometry of the part being made.

Figure 5.8: Alignment of foils inside the stainless steel plates

- They serve as heat plates when the entire assembly (paste-coated foils and plates) are placed in the furnace. The heat from the surroundings gradually sets in the plates and reaches the solder paste to melt it so that the layers can be soldered together. The paste has a soldering range of 280-380 °C.

The nuts and bolts used are of stainless steel because they are readily available and also because of their ability to sustain high temperatures. Since the stainless steel plates fitted with nuts and bolts are to be placed inside the furnace, it is necessary that satisfactory elevated temperature clamping force is maintained at all times. The first step in ensuring it is to determine the change in thickness, Δt, of the structure from room to maximum operating temperature (Bickford, 1998).

For stainless steel 316 material (Fig. 5.9):

$$\Delta t_1 = t_1(T_2 - T_1)\alpha \qquad (5.1)$$

$$\alpha = \frac{17.5\mu m}{m.K}$$

$$t_1 = 0.004m$$

$$T_2 = 400\ ℃ \text{ and } T_1 = 20\ ℃$$

$$\Delta t_1 = 26.6\ \mu m$$

Because there are two plates of stainless steel 316 of the same thickness, the total increase in thickness for the joint members is twice the value of Δt_1 which comes out to be $53.2\ \mu m$. This value clearly indicates that the change in thickness due to heat is very small compared to the overall thickness (0.004m or 4mm) for each plate.

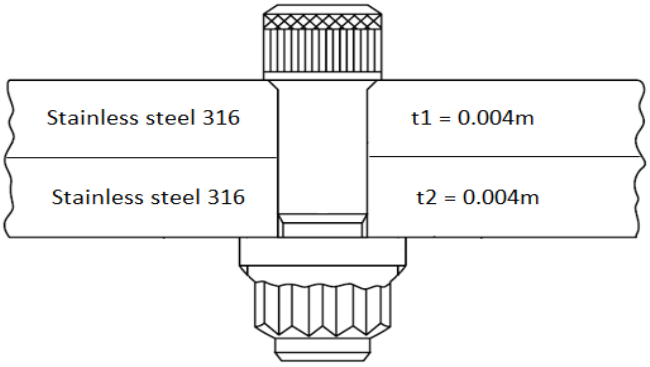

Figure 5.9: High temperature effects

The total effective bolt length equals the total joint thickness plus one-third of the threads engaged by the nut (Bickford, 1998).

$$L = t_1 + t_2 + (1/3\,d) \qquad (5.2)$$

Diameter of the bolt = 0.007m

$$L = 0.010 \text{ m or } 10 \text{ mm}$$

A bolt of at least 10mm length should be used to ensure satisfactory clamping force but since there was a 2.7mm thick dog-bone specimen sandwiched between the plates, a 15mm long bolt was utilized. The ideal coefficient of thermal expansion of the bolt material is found by dividing the total change in joint thickness by the bolt length times the change in temperature.

$$\alpha = \frac{53.2\mu m}{0.01m\,(400 - 20)}$$

$$\alpha = \frac{14\mu m}{m.K}$$

The coefficient of thermal expansion of stainless steel is in the range of 12 to 18.5 depending on the temperature of the metal at any given time (Ashby and Cebon, 1993). Therefore, the choice of stainless steel 316 is justified as it has the capability to withstand the thermal effects of the process.

5.5 Heating via Furnace

The foils of metal need to be deposited with solder paste and then put in the furnace for the paste to melt and solder the foils together. The furnace used was a Carbolite CWF1200 Chamber Furnace (Fig. 5.10) that can go up to a maximum temperature of 1200 degree Celsius. Another good option was the use of a heated plate which had to be custom-made to fit the requirements of the process as different pastes work at different temperatures and the heated plates are quite expensive. Therefore, using the furnace that can go up to 1200 °C was a suitable option.

Figure 5.10: CWF 1200 furnace used for heating

The furnace was first tested for usage as it is a new process and requires precise measurements of temperature and time. The furnace was set at a temperature of 400 °C and its door was opened at regular intervals to see the drop in temperature after putting the structure (stainless steel plates with nuts and bolts) inside it. The drop was noted as well as the temperature of the furnace floor and the structure, with infrared temperature gun, to get an

idea of the difference in temperature as seen from the furnace display and as measured on the surface of the structure as it is the main source of heat transfer to the specimen. The thickness, material, area, and temperature difference are all factors that can affect the heat transfer to the specimen sandwiched between the plates. It is evident from Fig. 5.11 that the temperature of the structure increased gradually which is expected as the heat takes time to increase the temperature of the 4mm thick stainless steel 316 plates.

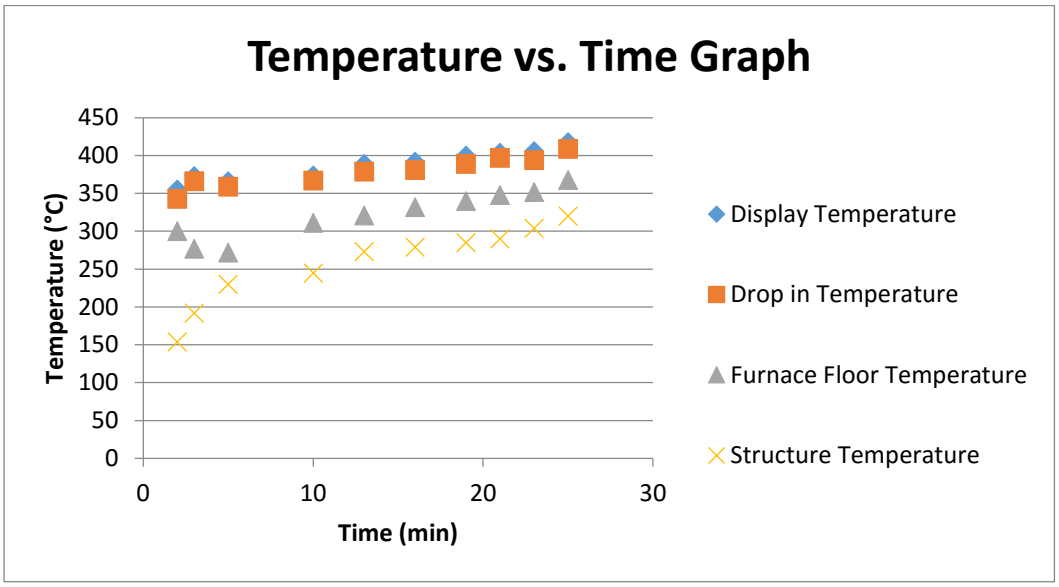

Figure 5.11: Furnace temperature drop testing

Since the foils were very thin, it was very difficult to measure the exact temperature as they are sandwiched between the plates. The best thing was the use of a thermocouple that would measure the temperature of the specimen. It was done and will be described at the end of this chapter as it helped in developing a three dimensional model using ANSYS. Using the model, the time required to produce a part was determined which eliminated trial and error approach. However, for the present case of a 2.7mm thick dog-bone specimen, the heating time was three minutes. The furnace heats up the air inside its doors which will then heat the structure that is placed in it but because this operation needed precision to ensure the melting of the

solder paste, it was essential to understand the heat losses and the factors affecting the transfer of heat to the plates with the specimen inside.

5.5.1 Heat Losses

- Heat storage in the furnace structure.
- Losses from the furnace outside walls or structure.
- Heat loss due to conduction.
- Radiation losses from openings, hot exposed parts, etc.
- Heat carried by the cold air infiltration into the furnace.

5.5.2 Factors Affecting Heat Transfer

There are three main methods of heat transfer - conduction, convection and radiation. In case of a furnace, the heat exchange is via convection which is defined as the transfer of thermal energy from one place to another by the movement of fluids.

There are two types of convective heat transfers namely:

- **Free or natural convection:** when fluid motion is caused by buoyancy forces that result from the density variations due to variations of thermal temperature in the fluid. In the absence of an external source, when the fluid is in contact with a hot surface, its molecules separate and scatter, causing the fluid to be less dense. As a consequence, the fluid is displaced while the cooler fluid gets denser and the fluid sinks. Thus, the hotter volume transfers heat towards the cooler volume of that fluid (Churchill and Chu, 1975).

- **Forced Convection:** when a fluid is forced to flow over the surface by an external source such as fans, by stirring, and pumps, creating an artificially induced convection current (Shah and London, 2014).

In this case, the convection is free or natural as no external source is affecting the heat transfer and the rate of heat transfer can be expressed by the following relation (Bejan, 2013):

$$\boldsymbol{Rate} = \frac{\boldsymbol{h_c A dT}}{\boldsymbol{t}} \quad (5.3)$$

The equation shows the factors that affect the rate of transfer:

- Temperature difference
- Area
- Material
- Thickness

5.5.2.1 Difference in Temperature

Heat continues to flow from a location of hot temperature to cold one. In case of the dog-bone specimen where 14 layers of copper foil coated with solder paste are placed between two stainless steel plates, it is vital to understand the role that the temperature difference will play. The time taken for the air inside the furnace to melt the solder paste between foils of metal while being sandwiched between stainless steel plates is of the utmost importance. This time defines whether or not a bond will be formed between the foils. When the display setting of the furnace is set at 550 °C, it means that the air inside is at that temperature. As the structure (stainless steel plates and the foils) is at ambient temperature, when it is placed inside the furnace, the hot air attacks it from all directions. As long as there is a temperature difference, the heat transfer will continue and once the difference has been nullified then the system will reach an equilibrium state. It is not necessary to reach equilibrium stage as the goal is only to form a bond between the foils so that a part can be produced. Furthermore, if the paste is kept at high temperatures for prolonged periods of time then it will burn the flux in the paste and the paste will not be able to bond the metal foils together. It is also important

to speed up the soldering process so that the foils will not be damaged by excessive heat. Experimentally, it took three minutes to produce a dog-bone composite copper specimen with 14 layers at the furnace display temperature of 550 °C.

5.5.2.2 Area for Heat Transfer

This section focusses on the area of the specimen or in this case, the area of the stainless steel plates. The larger the area, the more heat transfer as there is a direct relationship between the two. The plates used were 150mm long, 35mm wide and 4mm thick. It is also worth mentioning that if very large plates are to be used, for example, to make large parts then the area of the plates will largely affect the rate of heat transfer. The fitted nuts and bolts also add to the rate of heat transfer but that has minimal effect as the specimen is always in the centre of the plates so the specimen is directly affected by the thickness of the stainless steel plate rather than the number of nuts and bolts fitted to the plate (Fig. 5.12).

Figure 5.12: Stainless steel plates

5.5.2.3 Effect of Materials Used

The materials involved in the heat transfer process hold a key importance as they dictate the flow of heat. The effect of different materials on heat transfer rates is often expressed in terms of a number known as the thermal conductivity. These are numerical values that are determined by experimentation. The heat transfer depends directly on this value as the higher

it is, the more rapidly heat will be transferred. The materials involved along with their thermal conductivity values are given in Table 5.2.

Table 5.2: Thermal conductivity of the materials used

Material	Thermal Conductivity (W/m. K)
Stainless Steel	21
Copper	398
Aluminium 1050	237
Solder Paste	78

As is obvious from the values given in Table 5.2 that stainless steel does not have very good thermal conductivity and this effect is minimized by using thin plates (4mm) so that heat will take less time to get to the specimen inside the plates.

5.5.2.4 Impact of Thickness of the Materials

The thickness of the plate is inversely proportional to the rate of heat transfer which means that a thin plate will allow for more heat transfer, therefore, plates of 4mm thickness were used. Although the thickness was reduced, it was essential that the plates did not bend so much as to relieve the pressure from the specimen inside. A balance was sought out between the thickness and the straightness of the plates that would allow appropriate pressure to be exerted and aid the heat transfer.

Based on the factors discussed, the display setting was kept at 550 °C whereas the structure was kept inside the furnace for a total of three minutes. During that time, the door of the furnace was not opened to allow continuous heat transfer.

5.6 Cooling of the Final Product

After three minutes, the structure was taken out of the furnace and allowed to be air cooled. Once the structure is at room temperature, the nuts are loosened to remove the top plate. The product is ready and is then removed from the bottom plate for testing purposes.

Fig. 5.13 shows the cooling process of the 2.7mm thick, 87.5mm long and 15mm wide dog-bone specimen. The structure consists of two stainless steel plates 4mm thick, 35mm wide and 150mm long fitted with nuts and bolts. The structure was allowed to air cool and when it was at room temperature, the nuts were unscrewed and the specimen was taken out. Temperatures were noted for both the top plate and the specimen for 17 minutes at 1 minute intervals.

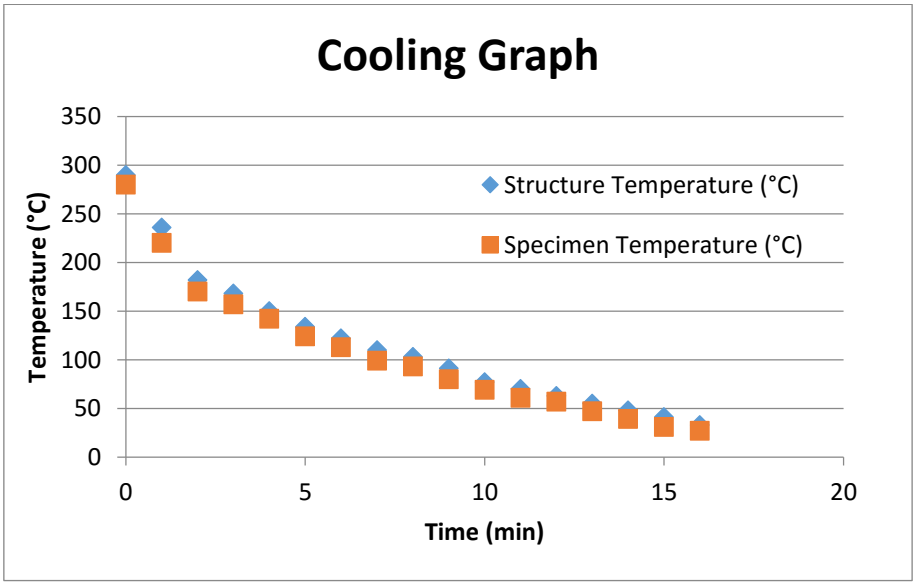

Figure 5.13: Time vs. Temperature Graph

5.7 Final Product

There is minimum post-process cleaning involved. Slight discoloration is observed due to the application of heat but other than that the product is in good shape (Fig. 5.14). No additional process is needed to enhance the mechanical properties or surface quality.

Figure 5.14: Dog-bone specimen produced by CMFM

A number of specimens were produced using the practices identified including single lap joints, peel specimens and dog bone specimens. A couple of open-ended spanners, each having a thickness of 7mm, were also produced using brazing paste. One was made up of aluminium foils and the other was a composite of aluminium and copper. They are shown in Fig. 5.15 along with SEM analysis showing the layers of metal foil and paste.

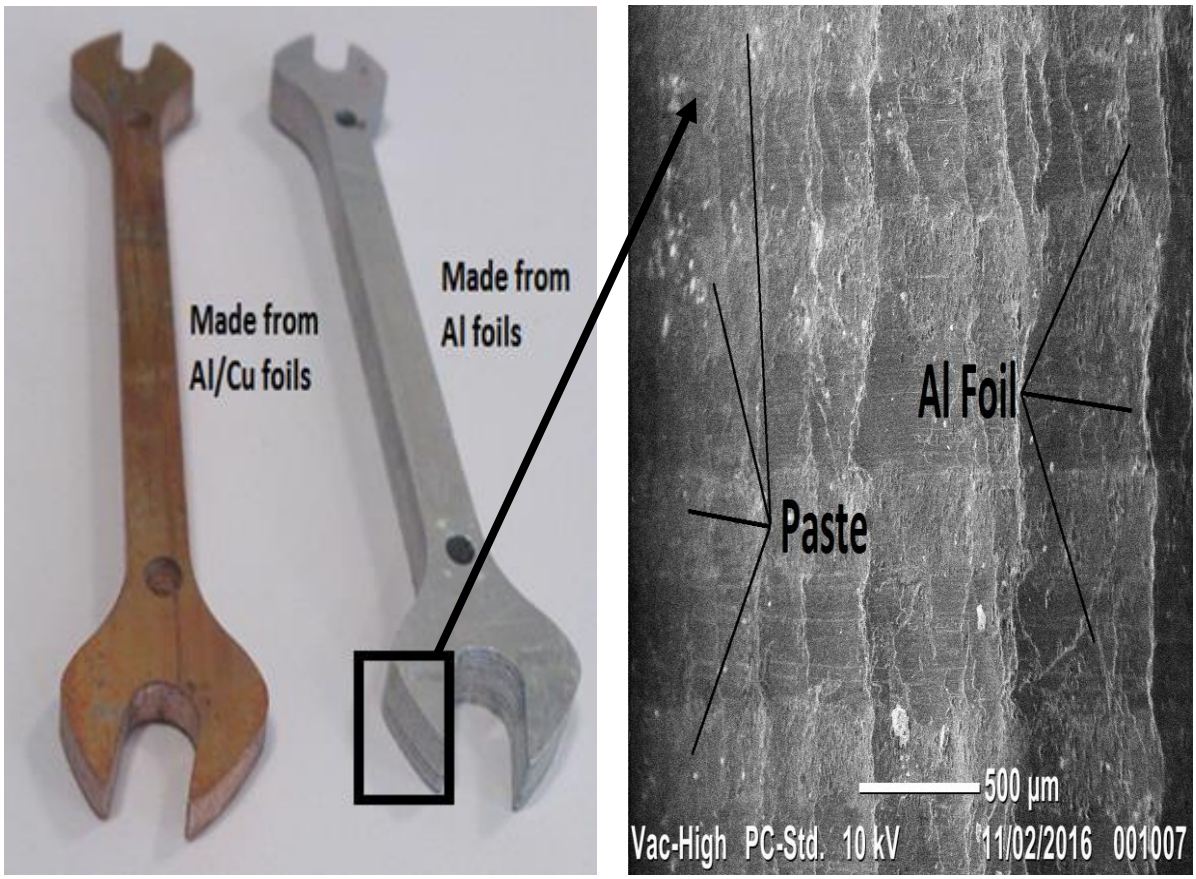

Figure 5.15: Spanners made by CMFM (left) and SEM analysis of the spanner made from Al foils (right)

5.8 Validation of Heating Time

This section will present the experimental data obtained while making a single lap joint of aluminium foil (0.1mm thick) using brazing paste. The dimensions of the foils were W*L*t=25*100*0.1mm (Fig. 5.16). The lap joint length (l) was 12.5mm and the thickness of the brazing paste was kept at 0.1mm using torque wrench.

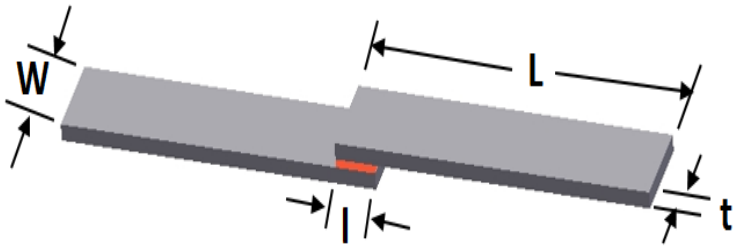

Figure 5.16: Aluminium single lap joint

The single lap joint was sandwiched between two stainless steel plates and placed inside the furnace for one minute and forty seconds (100 seconds). After this duration, the structure was taken out and allowed to be cooled. A thermocouple connected to a digital display was used to measure the values of temperature at every second. Table 5.3 shows the components needed to carry out the measurements inside the furnace.

Table 5.3: Components for temperature measurement

Components	Part Number	Source
NEXTEL insulated type K thermocouple	XC-20-K-12	Omega Engineering Limited
Handheld thermocouple indicator (Digital display)	HH11B	
Male/female connector	SMPW-K-MF	

OMEGA® Nextel ceramic-insulated thermocouples are easy-to-use precise temperature elements manufactured to meet the highest industry standards. The Nextel ceramic insulation is rated for 1200°C (2200°F) continuous use, or 1425°C (2600°F) short term. These highly

versatile elements are ideal for many high-temperature applications. Since the furnace was set at a temperature of 950°C, it was important that the thermocouple should be insulated and capable of working properly at such high temperature. It has a flexible design that can be bent to reach tough spots without breaking or compromising accuracy. The thermocouple had two ends; one for sensing the temperature and the other has to be wired to the connector so that it could be attached to the digital display as shown in Fig. 5.17. After the appropriate connections were made, the sensing end of the thermocouple was placed on the aluminium foil (Fig. 5.18a) and then another foil was placed on top of it in the configuration of a lap joint as shown in Fig. 5. 18b. After tightening the nuts on the stainless steel plates with the foils and thermocouple (Fig. 5.18c), the structure was placed inside the furnace and a video was recorded showing the digital display with time shown in Fig. 5. 18d. The atmospheric temperature was 22 °C and the furnace temperature was set at 950 °C.

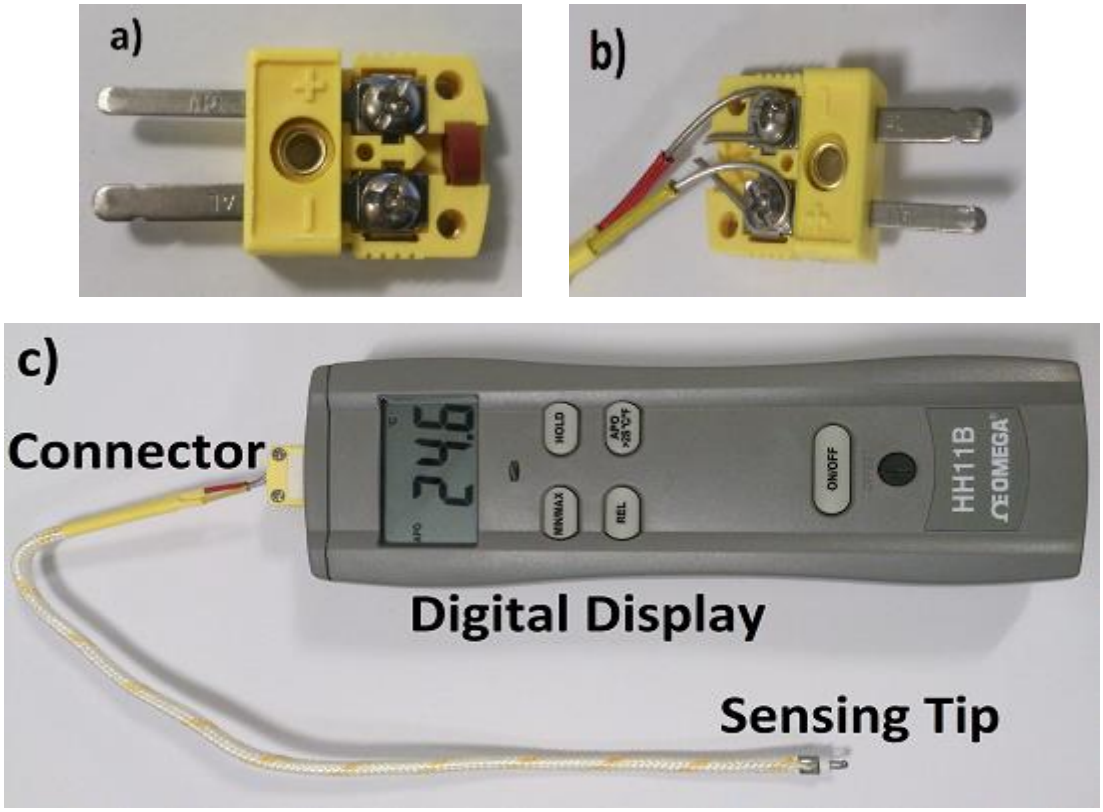

Figure 5.17: Thermocouple connections: a) Connector; b) Wiring the thermocouple with connector; c) Thermocouple attached to the digital display

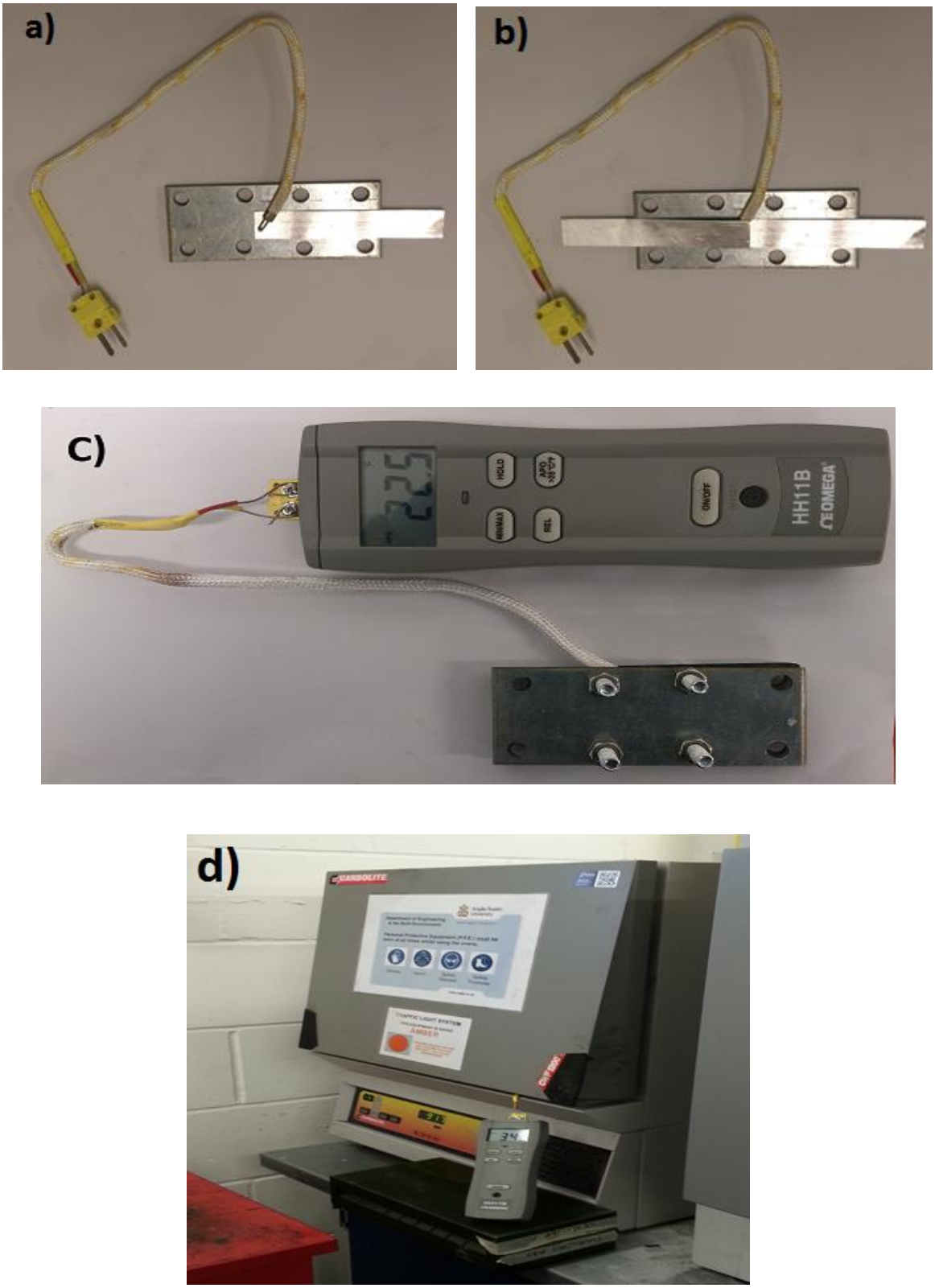

Figure 5.18: Thermocouple for temperature measurement: a) Sensing head with the foil; b) Sensing head sandwiched between foils; c) Foils and thermocouple sandwiched between stainless steel plates; d) Thermocouple taking readings

After taking measurements inside the plates, the thermocouple was then attached on the outer surface of the stainless steel plate so that the heating time could be verified using numerical method. Fig. 5.19 shows the graph obtained from the experiment for the inside and outside temperatures.

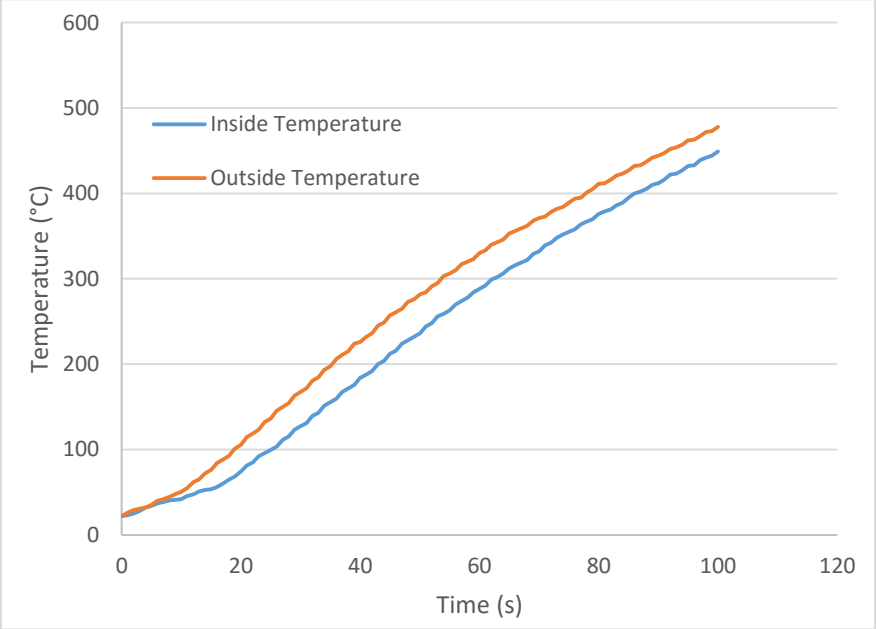

Figure 5.19: Temperature measurements from inside and outside the stainless steel plates

5.8.1 Transient Thermal Analysis

A 3D finite element model was made in ANSYS to carry out the transient thermal analysis for making a single lap joint using aluminium foil. The experiment took 100 seconds to make the joint and the same time was inserted for the analysis as well. The initial temperature was set at 22 °C and the data obtained from the outside temperature measurement was inserted as temperature input to the upper and bottom plates as shown in Fig. 5.20.

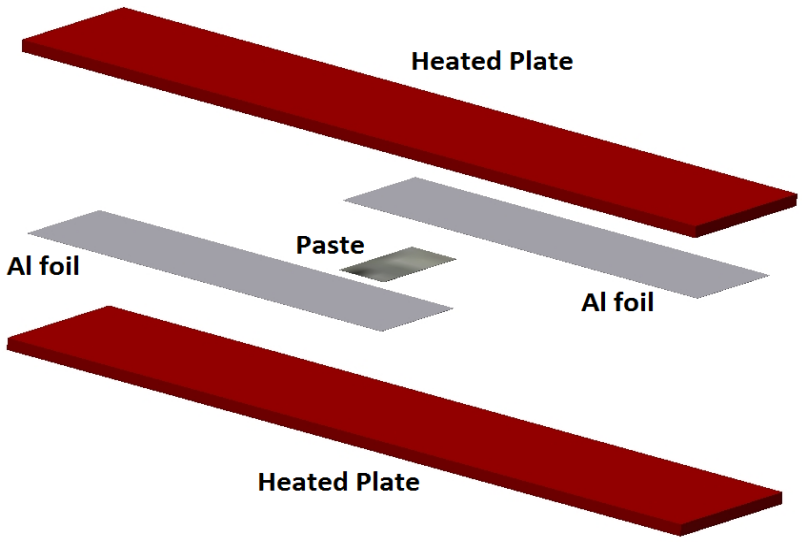

Figure 5.20: Exploded view for the transient thermal analysis

The connections were set to 'No Separation' as this is how the foils become when nuts and bolts have been tightened. The analysis yielded a minimum temperature of 450.28 °C which can be seen on the inside of one of the stainless steel plates in Fig. 5.21. It is the same area where the lap joint is placed; therefore, it is also at a temperature of 450.28 °C after 100 seconds (Fig. 5.22). The brazing paste has an operating range from 410-470 °C and the minimum temperature after the set time (100 seconds) falls within this range. Therefore, it has been verified both experimentally and numerically that it takes 100 seconds to make a single lap joint using aluminium foils of 0.1mm thickness. The values obtained from the analysis have been plotted with the experimental values that were obtained by putting the thermocouple inside the two stainless steel plates. The graph is shown in Fig. 5.23 and it can be seen that there is a good agreement between the two temperature values i.e., experimental (Exp.) and numerical (FEM). The maximum temperature that was achieved experimentally is 449 °C and the numerical maximum temperature is 450.28 °C on the lap joint. The analysis clearly validates the experimental approach and can be used as a reference model to produce different parts in the future with ease.

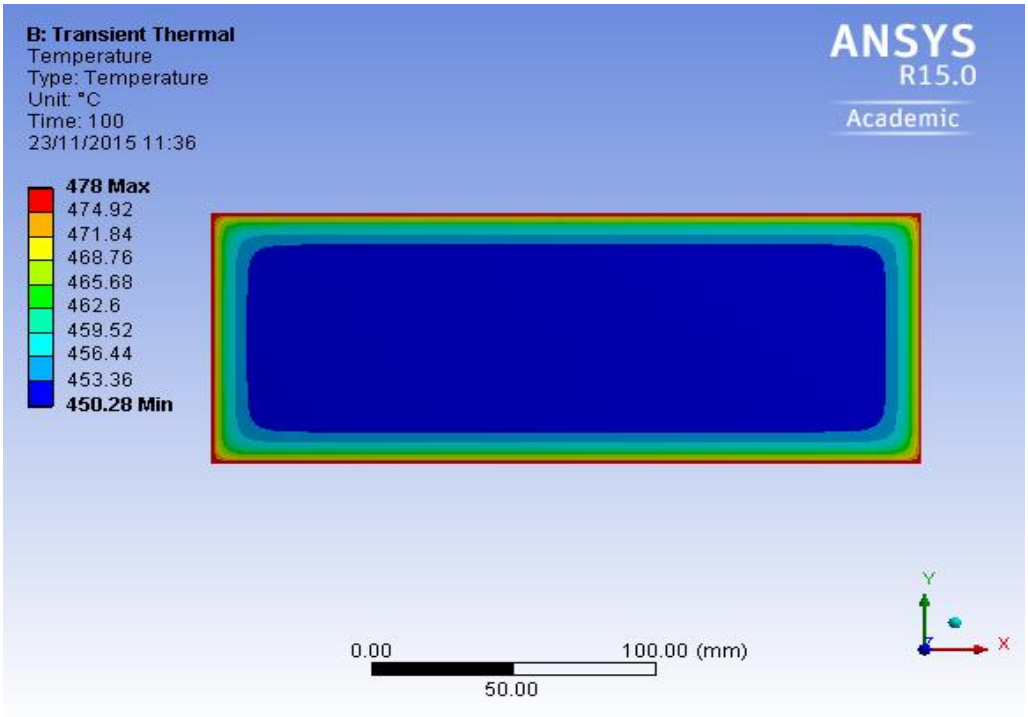

Figure 5.21: Transient thermal analysis on the plate

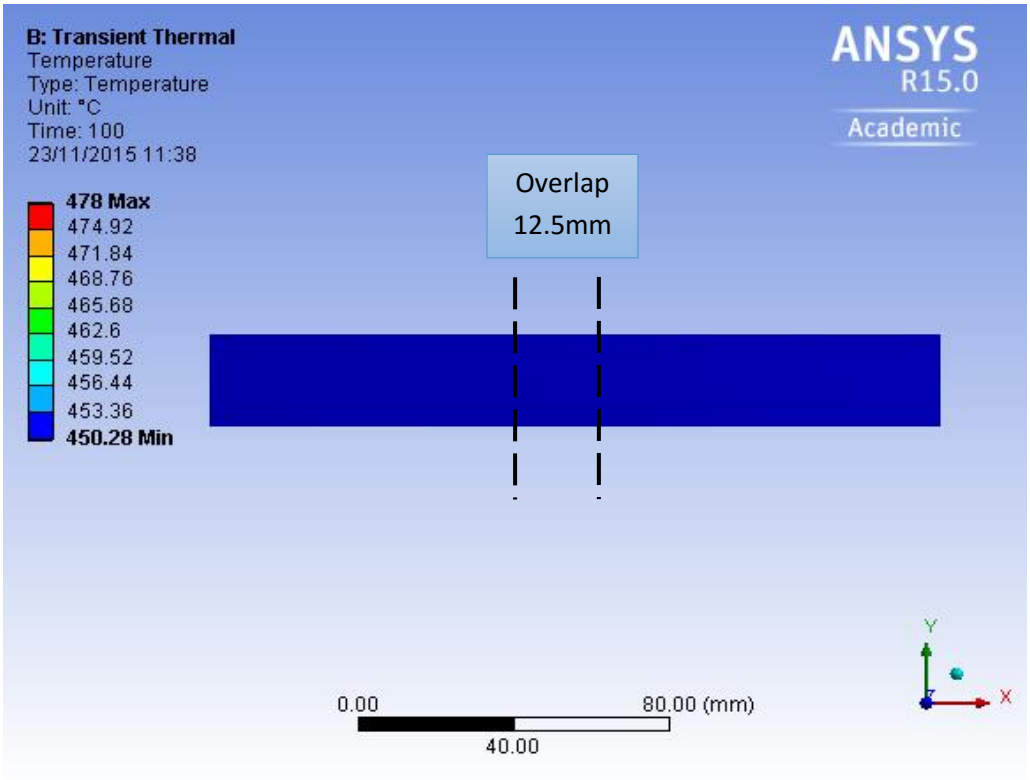

Figure 5.22: Temperature distribution on the single lap joint

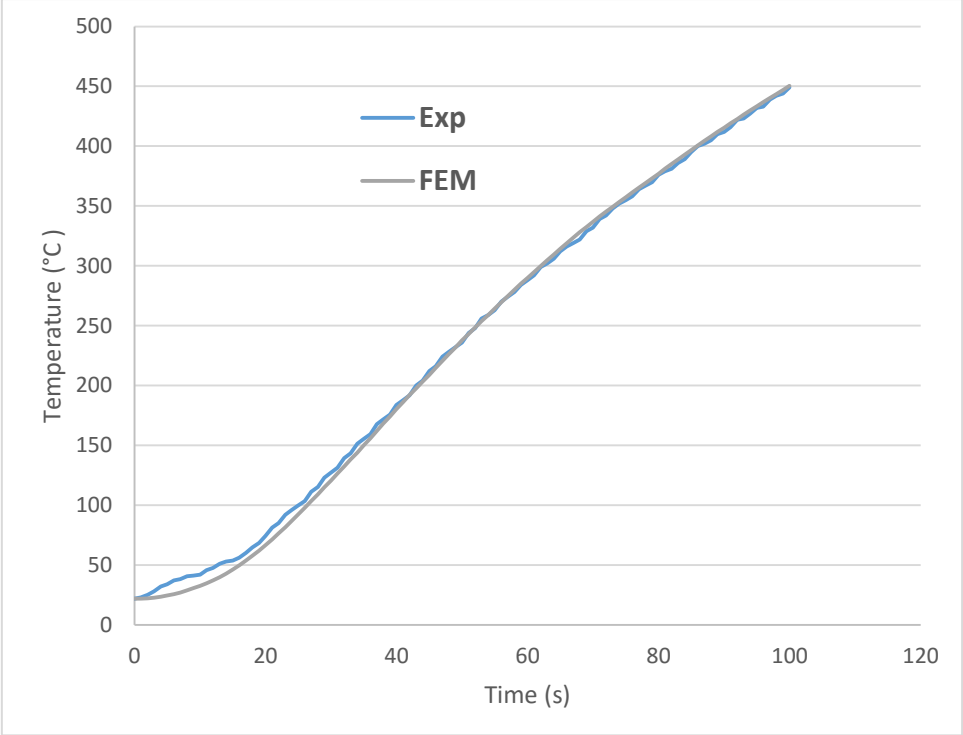

Figure 5.23: Comparison between the experimental and numerical temperature

A single lap joint is shown in Fig. 5.24 following the experimental setup. However, the joint should not be heated for a prolonged period of time after 100 seconds as it will result in pitting due to overheating because of the thin nature of the foils as shown in Fig. 5.25. Therefore, the timing should be kept within 100-110 seconds to obtain good results.

Figure 5.24: Aluminium single lap joint

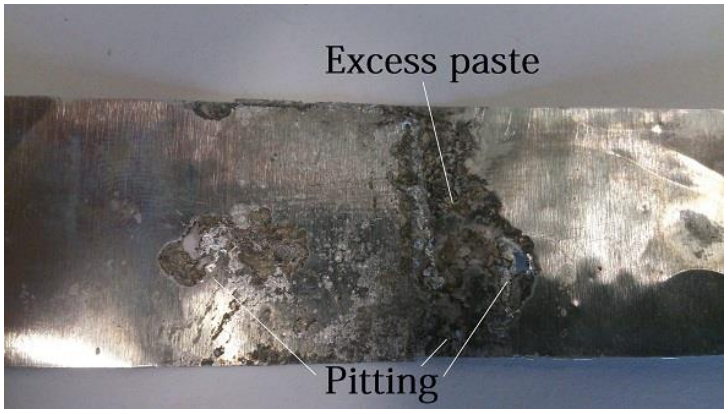

Figure 5.25: Pitting of an aluminium single lap joint due to overheating

5.8.2 Thermal Stress and Strain Analysis

Static structural analysis was carried out in ANSYS to observe the thermal stress and strain on the aluminium single lap joint. The temperature obtained from the transient thermal analysis was inserted as input and the connections were set to 'No Separation' as before. A torque wrench was used to make the thickness of the paste as 0.1mm as explained in Section 5.4. Since the nuts and bolts on the stainless steel plates were tightened by the wrench, the displacement in Z-direction was assumed to be zero. Displacements in X and Y directions were set to 'Free' during the analysis. Fig. 5.26 shows the stress distribution on the single lap joint due to heating for 100 seconds. As is evident, it is uniform throughout the entire length of the joint and is in the range of 685.25 MPa to 913.66 MPa. A generic equation for calculating thermal stress is given below:

$$Thermal\ stress = \alpha \Delta T E \tag{5.4}$$

$$Coefficient\ of\ thermal\ expansion, \alpha = 23.1\ K^{-1}$$

$$Change\ in\ tempaeature, \Delta T = 427\ K$$

$$Modulus\ of\ elasticity, E = 70\ GPa$$

Putting the values in Eq. 5.4 gives:

$$Thermal\ stress = 690.459\ MPa$$

This value is within the range given by the numerical analysis. It is a very rudimentary calculation and more sophisticated instruments or analytical methods should be employed to get a more exact value.

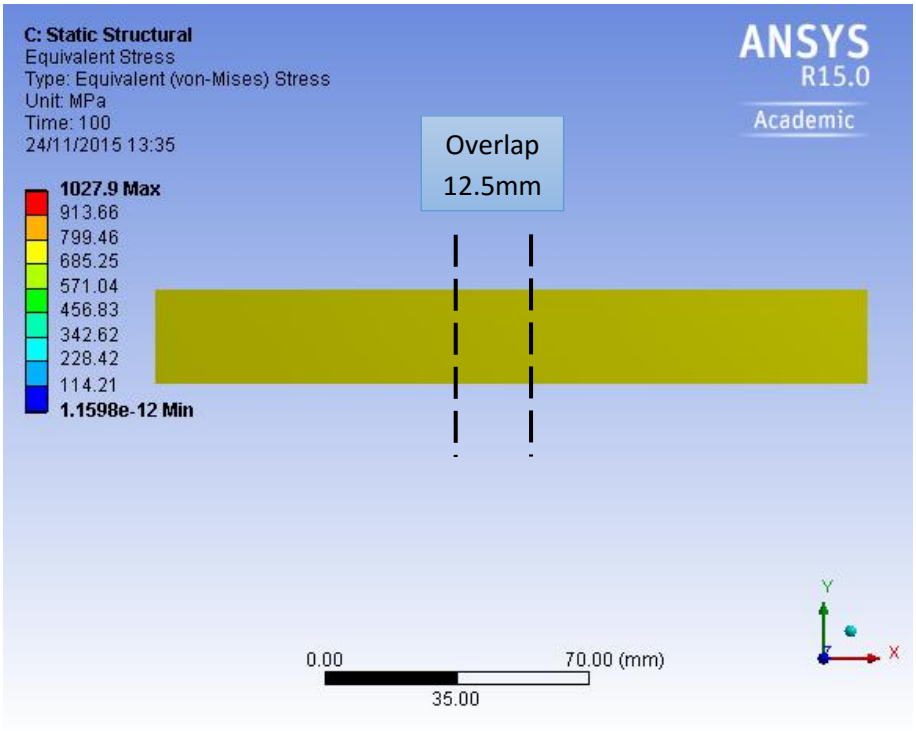

Figure 5.26: Thermal stress distribution in aluminium single lap joint

The maximum stress was observed for the layer of paste as shown in Fig. 5.27 which is expected as it underwent a phase change from a viscous fluid to liquid and then solidifying by forming an intermetallic bond with the metal surface.

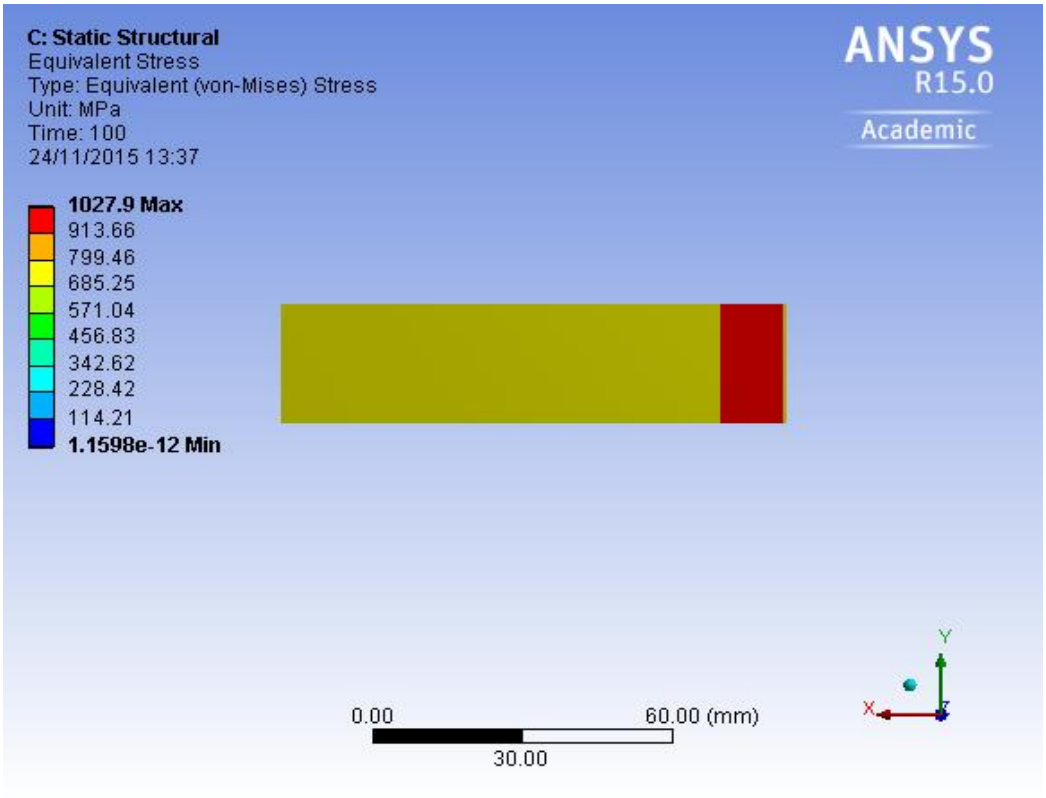

Figure 5.27: Paste layer showing the maximum thermal stress

The thermal strain on the lap joint is shown in Fig. 5.28. The lap joint is experiencing the highest strain value of 0.0098504 but it is very small as compared to the overall length of the joint (187.5mm). Strain in the range of 0.004378-0.0054725 is being experienced by the paste layer (Fig. 5.29) which is sandwiched between the two aluminium foils.

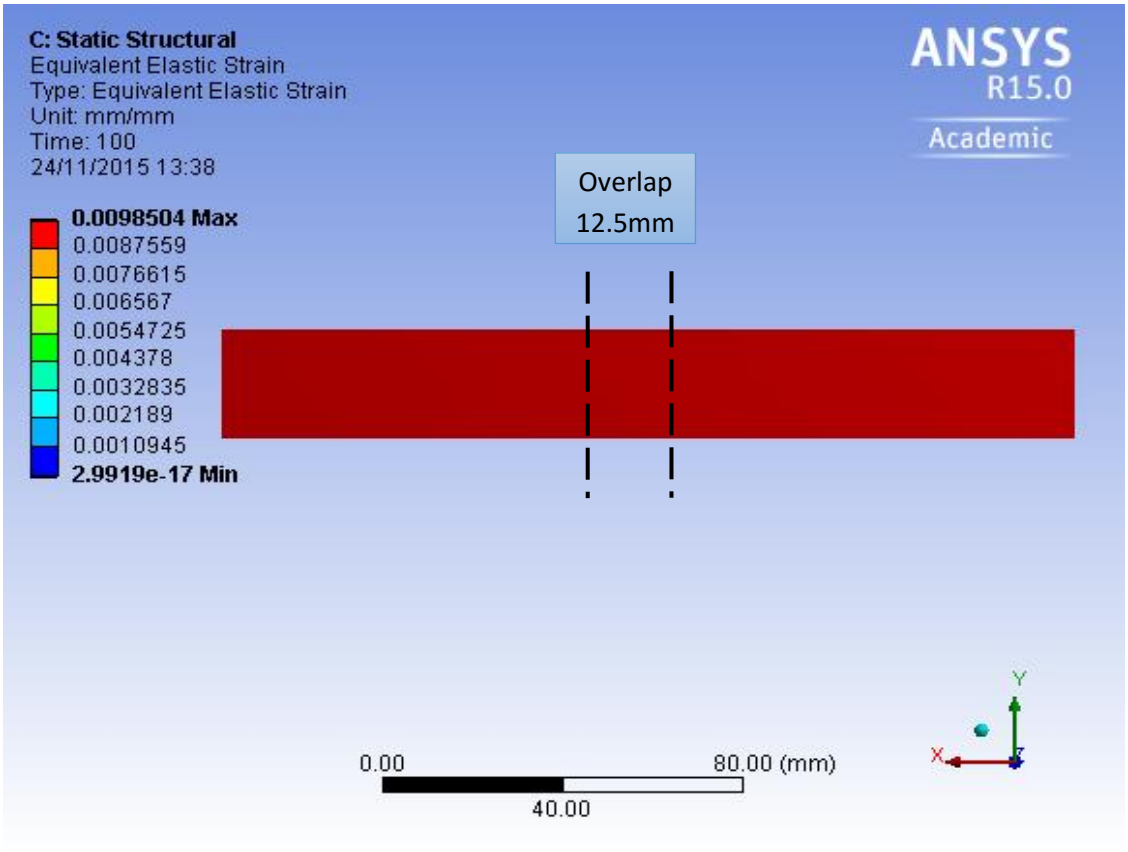

Figure 5.28: Thermal strain in the aluminium single lap joint

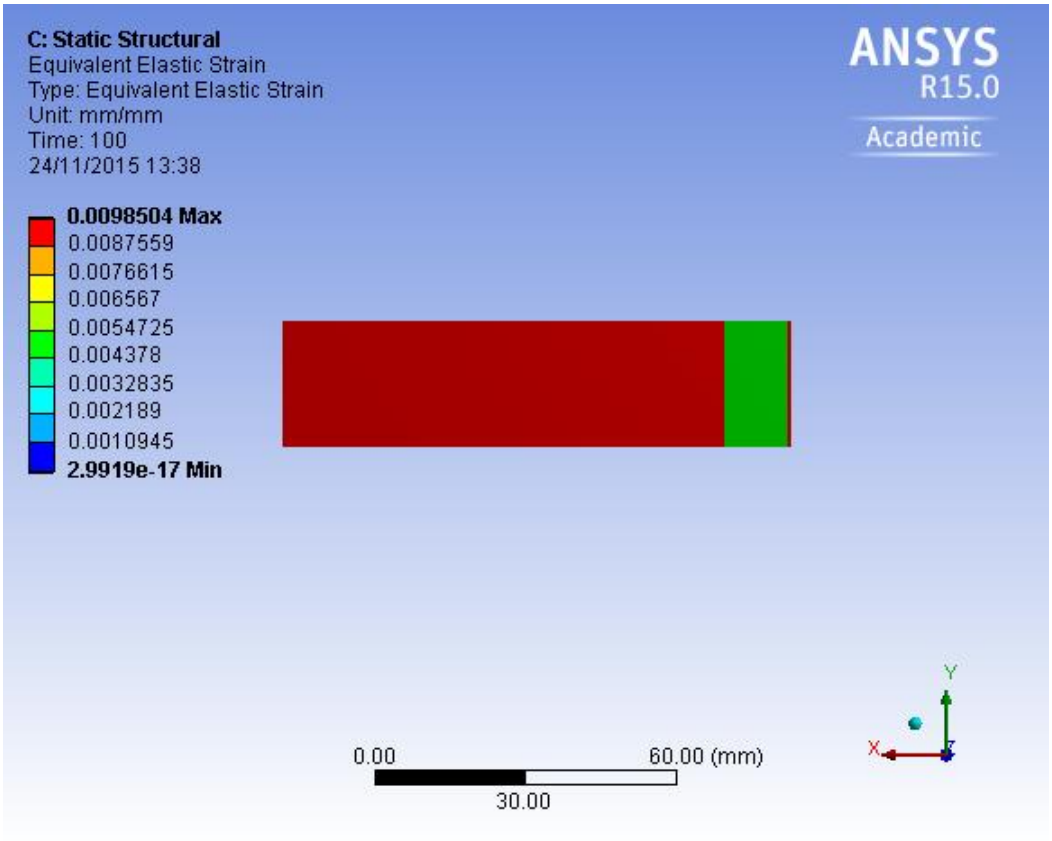

Figure 5.29: Thermal strain in the paste layer

5.8.3 Other Validation Methods

The reference model created in Section 5.8 has validated the experimental and numerical heating time and can be used to create parts in the future. There are some other validation methods that could have been carried out like calculating the convective heat transfer co-efficient and then using that value for transient thermal analysis. It would have required taking a large number of temperature readings at different positions on the surface of the stainless steel plates. Those values would then have to be incorporated in a CFD model to get a temperature vs. convective heat transfer co-efficient graph. A linear equation would have been obtained from that graph and used for transient thermal analysis.

Another method would be to randomly select convective heat transfer co-efficient values and carry out transient thermal analysis. Whichever value gives the closest curve could be adopted and used for future production of parts. Both the methods hold merit and could have been employed but in the light of the comparison obtained in Fig. 5.23 between experimental and numerical temperature values, it was decided not to continue in that direction as an appropriate validation has already been achieved.

5.9 Summary

This chapter gives a step-by-step guide of the practices that were utilized for the production of metal parts. An experimental setup was created by keeping in mind the proposed process. Each step was carried out in such a way that it closely resembles the flow of operation of the conceptual automated machine based on the principles of CMFM. All the materials, equipment and tools used for the production of parts have been justified. A number of parts including single lap joints from varying thickness (0.05mm, 0.1mm, 0.2mm and 10mm), peel specimens and dog-bone specimens were produced for mechanical testing so as to validate the effectiveness of the proposed process. The heating time for the production of a single

aluminium lap joint has been validated using numerical analysis. Firstly, the actual temperature on the inside and outside of the stainless steel plates was recorded. A 3D model was created in ANSYS and the recorded temperature from outside the plate was used as input for transient thermal analysis. The simulation gave temperature distribution on the inside of the plate which was then plotted alongside the recorded temperature obtained from the thermocouple. A good agreement was observed between the experimental and numerical temperature values. This 3D model can be used as a reference for future parts and will remove guesswork for heating time inside the furnace.

CHAPTER 6

6 Experimental Testing, Results and Analysis

Lap shear testing, peel testing, microstructural analysis and tensile testing have been carried out under different settings to analyse the effectiveness of the new process. This chapter describes the test settings, the results and discuss their significance with regards to other methods. There are three sets of test results for:

1- Pure copper foils

2- Aluminium 1050 grade foils with a H14 ½ hard temper

3- Composites of pure copper foils and aluminium 1050 foils (Al/Cu)

Aluminium 1050 grade foils with a H14 ½ hard temper foils and pure copper foils of different thicknesses (0.05mm, 0.1mm and 0.2mm) were used for the experimental testing and were cut according to the dimensions of the desired specimens. Table 6.1 shows the chemical composition of the foils and Table 6.2 shows their mechanical properties.

Table 6.1: Chemical composition of materials

Materials	**Chemical composition (in weight %)**							
	Cu	**Si**	**Fe**	**Mn**	**Mg**	**V**	**O**	**Al**
Al 1050	0.05	0.25	0.40	0.05	0.05	0.05	-	Balance
Copper	Balance	0.007	0.009	-	-	-	0.01	-

Table 6.2: Mechanical properties of materials

Mechanical Properties	**Materials**			
	Al 1050 H14	**Copper**	**Solder Paste**	**Brazing Paste**
Yield Strength (MPa)	105-145	70	40	45
Tensile Strength (MPa)	120	200	55	60
Young's Modulus (GPa)	70	120	50	60

All the specimens were made and tested according to British and International Standards where applicable. They included single lap joints, peel testing specimens and dog-bone specimens. Microstructure analysis was also carried out to investigate the bonding between the layers of foils.

It should be noted that specific testing standards for additively manufactured parts were under discussion at the time of carrying out the experiments (as cited by Information Specialist Knowledge Centre, Jonathon Lyons at British Standards Institution). It was also mentioned that the committee members who develop standards are representatives of various professional bodies and associations and they do not actually work for British Standards Institution (BSI) so contacting associated members was one option but the response was the same that the standards are under discussion. AMT/8 was the Additive Manufacturing committee responsible for the generation of a specific standard, (BS ISO 17296-3: 2014, 2014) that would give general principles for appearance, surface texture, colour, dimensional tolerances etc. However, it was recommended that it is better to work with the existing standards and interpret them according to the testing needed rather than waiting for a committee to approve a particular standard. The Director of Developmental Operations, Pat A. Picariello, at American Society for Testing and Materials (ASTM) was contacted who was helpful enough to send a document that they have been using to test additively manufactured parts (NISTIR 7847: Mechanical properties testing for metal parts made via additive manufacturing: A review of the state of the art of mechanical property testing). The document contained information of the BSI/ASTM standards to be used for different testing methods and was very helpful in choosing the correct ones for testing. Currently, some standards have been approved (BS ISO 17296-2:2015, 2015; BS ISO 17296-4:2014, 2014) but they find their basis from the previous versions and mostly describe the principles of AM processes.

The next section describes the tests performed and the dimensions of the parts according to the standards.

6.1 Tensile Lap-Shear Test

Testing was done with foils of varying thicknesses (0.05mm, 0.1mm and 0.2mm) but there is no lap-shear testing standard for foils of such low thickness values. The standard (BS EN 1465: 2009, 2009) was followed where possible even though it relates to thicker foils of metal (1.6±0.1mm). This particular standards was used because it was stated in the document sent over by ASTM Director and also because literature review has showed the use of this standard for foils as thin as the ones being used to make single lap joints. The Tinius Olsen tensile testing machine and INSTRON 5582 machine was used for carrying out the lap-shear testing with appropriate load cell (5kN, 10kN and 50kN). The machine was operated at various speeds (10mm/min, 50mm/min and 100mm/min) with the 200mm long and 25mm wide specimens at an overlap length of 12.5mm (Fig. 6.1).

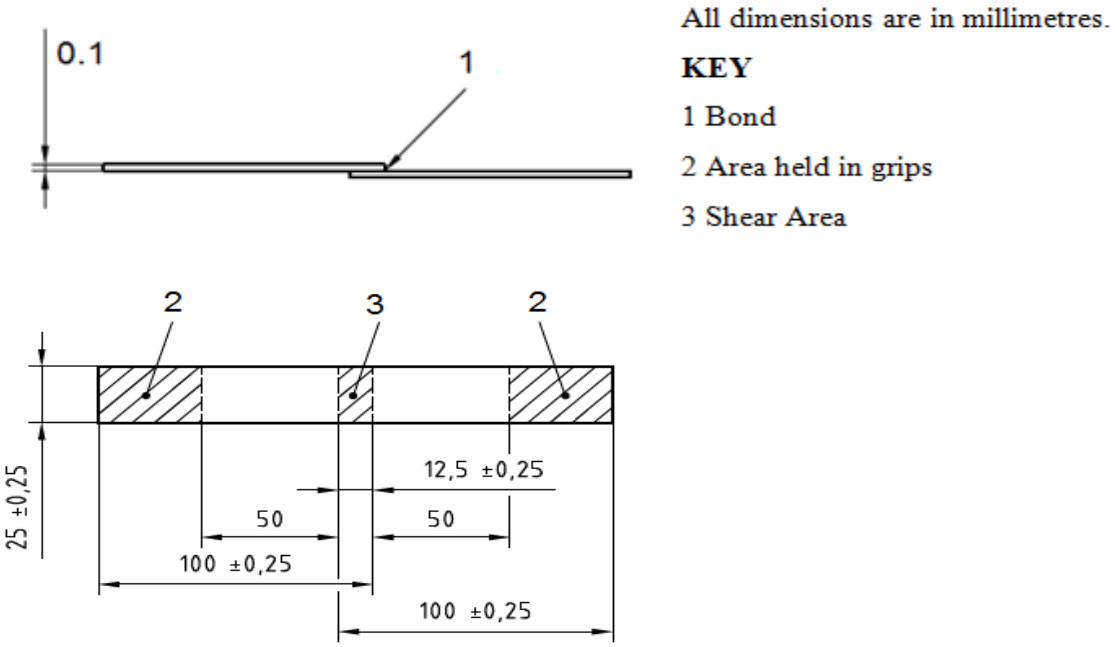

Figure 6.1: Dimensions of lap-shear specimen

6.2 Peel Test

The peel test was performed in accordance with the standard (BS EN ISO 11339:2010, 2010), which was designed for the determination of the strength of adhesives on flexible-to-flexible bonded assemblies based on the maximum load specimens can withstand under peeling action. The specimens were 200mm long and 25mm wide. Out of the 200mm length, 150mm was bonded with the solder/brazing paste (Fig. 6.2). The tests were carried out at different peel rates (10mm/min, 50mm/min and 100mm/min).

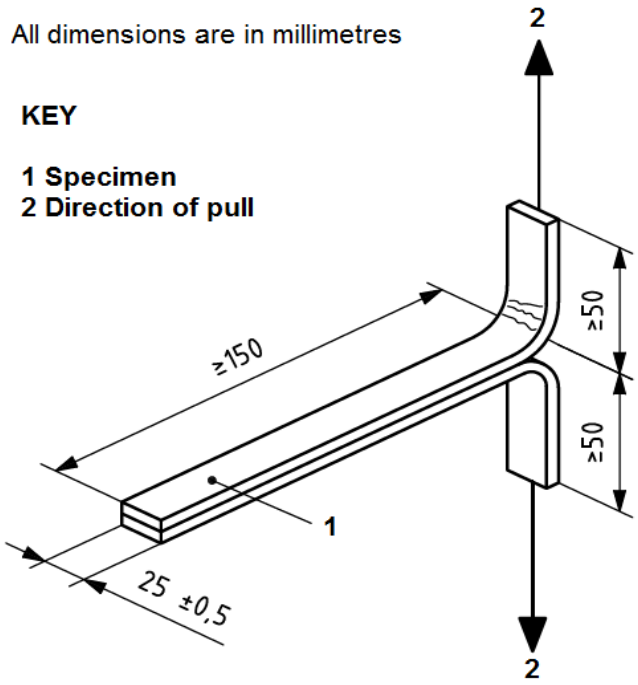

Figure 6.2: Dimensions of peel test specimen

6.3 Corrosion Test of Aluminium Specimens

The corrosion test was performed in accordance with the standard (BS EN ISO 11130:2010, 2010). It was only performed on aluminium peel specimens so as to assess the effect of galvanic corrosion on the bond/foil interface. The peel specimens of 1050 aluminium were immersed in a solution of 35 grams of sodium chloride dissolved in 1 litre of distilled water

for 24 hours. Afterwards, they were dried for 24 hours and then tested on the Hounsfield Tinius Olsen Tensile Testing machine at a peeling rate of 10mm/min.

6.4 Microstructural Analysis

The aim of the microstructural analysis was to establish the proportion of bonded to unbounded area in a specimen. This means that the higher the proportion of the soldered/brazed zone, the stronger the bond and vice versa. For cross-sectional analysis, specimens were cut from the centre portion (approx. 20 mm from where the soldered/brazed zone commenced). They were then mounted one by one on the platform of the scanning electron microscope (SEM) for analysis.

6.5 Tensile Testing for Dog-bone Specimen

Dog-bone specimens were produced by following the standard (BS EN ISO 6892-1: 2009, 2009). The specimens made by CMFM were first tested and then compared to the same shaped specimens machined out of copper and 1050 aluminium blocks. All the specimens were 2.7mm thick, 87.5mm long, 12.5mm wide and had a gauge length of 50mm (Fig. 6.3). The composite specimens (specimens produced by CMFM) were made up of 14 layers stacked on top of each other with a uniform paste thickness of 0.1mm.

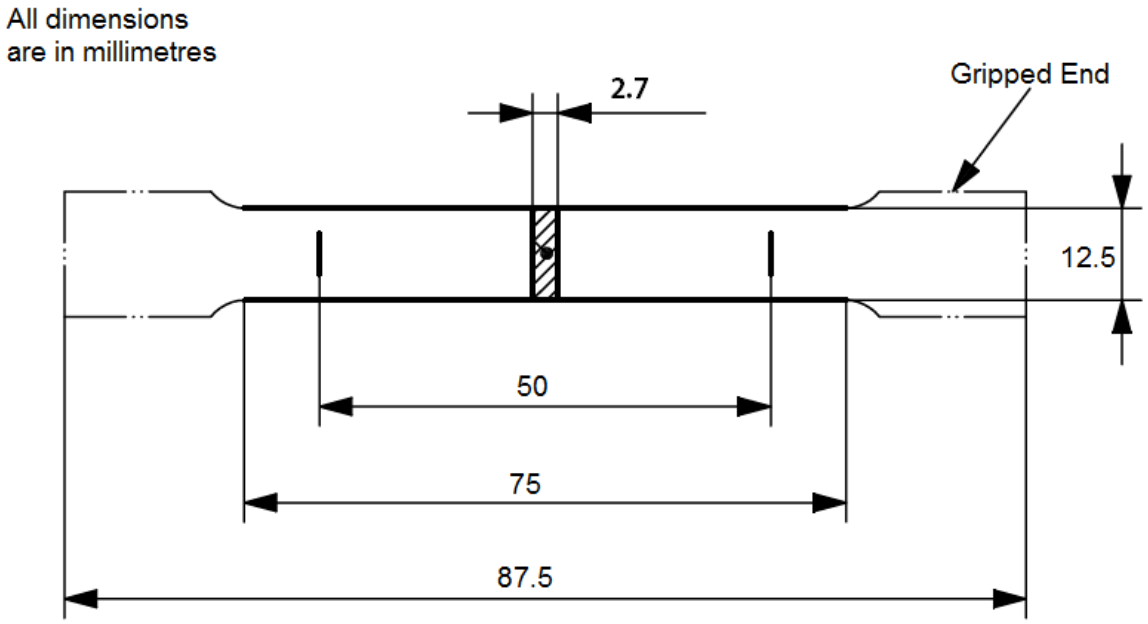

Figure 6.3: Dimensions of the dog-bone specimen

6.6 Other Tests

The lap-shear test was done for shear strength, peel test for peel strength, tensile test for tensile strength and microstructure analysis to access the proportion of bonded/un-bonded soldered/brazed region. These tests gave an insight into the mechanical behaviour of parts produced by the proposed process. However, there are a number of other tests including hardness, bending, torsion, compression, creep and stress rupture, fracture toughness, notch-toughness, impact toughness, fatigue, fatigue crack growth rate etc., which could also be performed on parts made by the proposed process. The researcher limited his testing to the mechanical failures due to tension forces and the other tests can be performed in the future to get a better understanding of their corresponding failure types. Instead of carrying out a number of different tests, only tension related testing was performed to understand the effect of tension forces on the parts produced. The tests performed during the course of the research form the basis upon which further testing should be carried out so as to establish the effectiveness of CMFM as a strong candidate in the field of metal AM methods.

6.7 Results from Copper Foils

Copper foils of 0.1mm thickness were joined together as single lap joints, peel specimens and dog-bone specimens using the direct aluminium solder paste. The foils were used as provided with no surface treatment.

6.7.1 Results from Lap-shear Test

The test was carried out at a speed of 100mm/min according to the standard. From the specimens tested, all broke within the base metal adjacent to the bonded area (Fig. 6.4). In none of the specimens did breaks occur within the soldered area/zone. As in tensile testing, specimens failed at locations with minimum cross-sectional area (i.e. the base metal, instead of the lapped region which had twice the cross-sectional area).

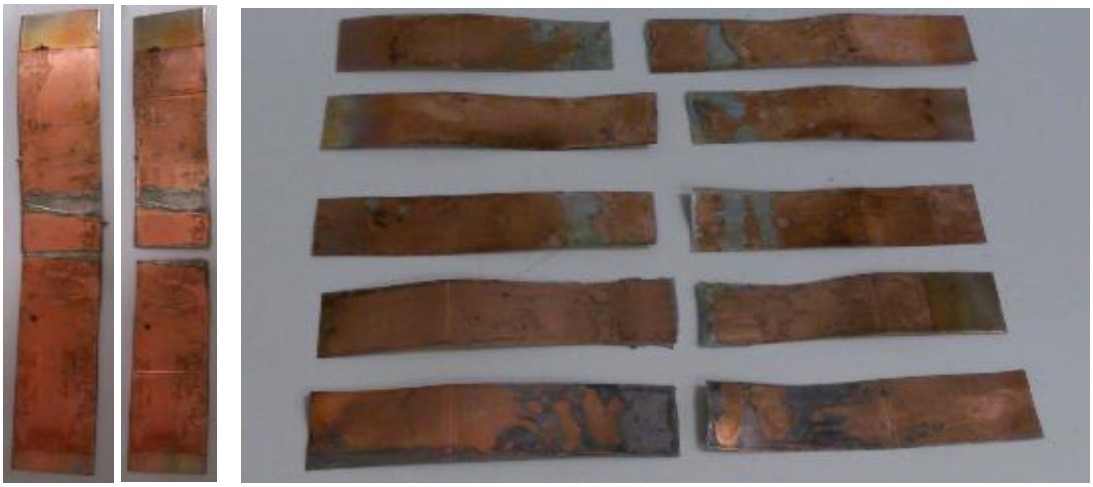

Figure 6.4: Failure modes of copper lap-shear specimens

The results show the effectiveness of the bond and in all the specimens the failure was recorded according to the standard (BS EN ISO 10365:1995, 1995). The failure pattern was always substrate failure with the designation SF. There are a number of factors that can affect the outcome of the test results. They include lap joint length, gage length and asymmetric loading. To make sure that repeatability was observed in the test results, careful measures were taken. The lap joint was kept at a length of 12.5mm consistent with the standard. The

test specimens were symmetrically placed in the grips, with each grip 50 ± 1 mm from the nearest edge of the overlap. Additional foils were used in the grips so that the applied force will be in the plane of the bond. Fig. 6.5 shows the test results of the lap-shear specimens. The numbers of samples are denoted by S1, S2, S3, S4 and S5.

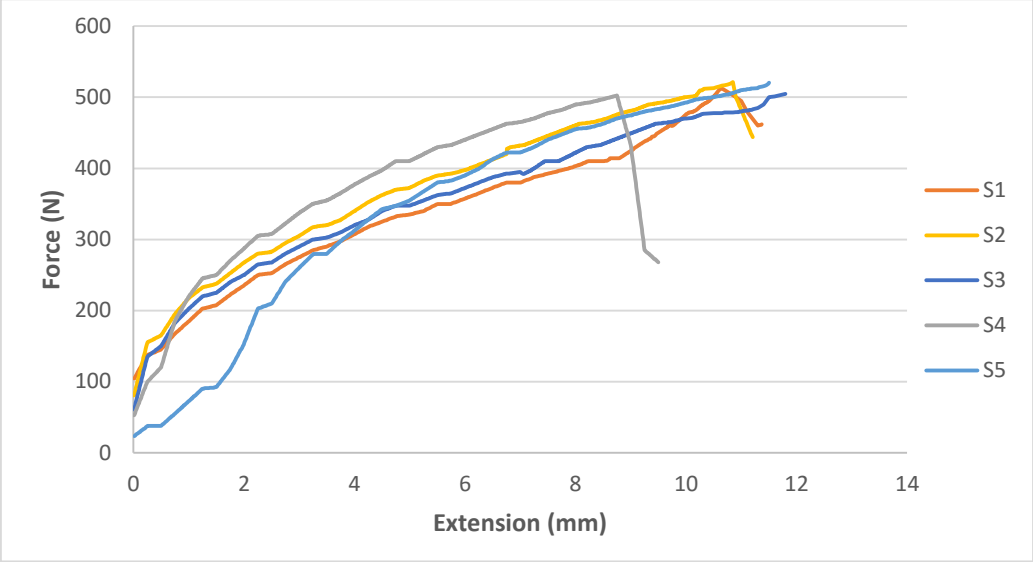

Figure 6.5: Lap-shear test results of copper specimens

6.7.2 Results from Peel Test

The peel test was found to be effective in determining the bond effectiveness. From the specimens tested, two categories of failure mode were observed as shown in Fig. 6.6.

Figure 6.6: Fracture modes of copper peel test

Two failure modes were observed as seen graphically in Fig. 6.7:

1. Where there was a clear break at the beginning of a soldered region (when a load was applied) indicating an effective bond giving a high load ranging from 382-432N.

2. Where a sample did not break at the beginning of soldered region but failed as the breaking points grew under loading. Typically such failure resulted in soldered loads of around 337N.

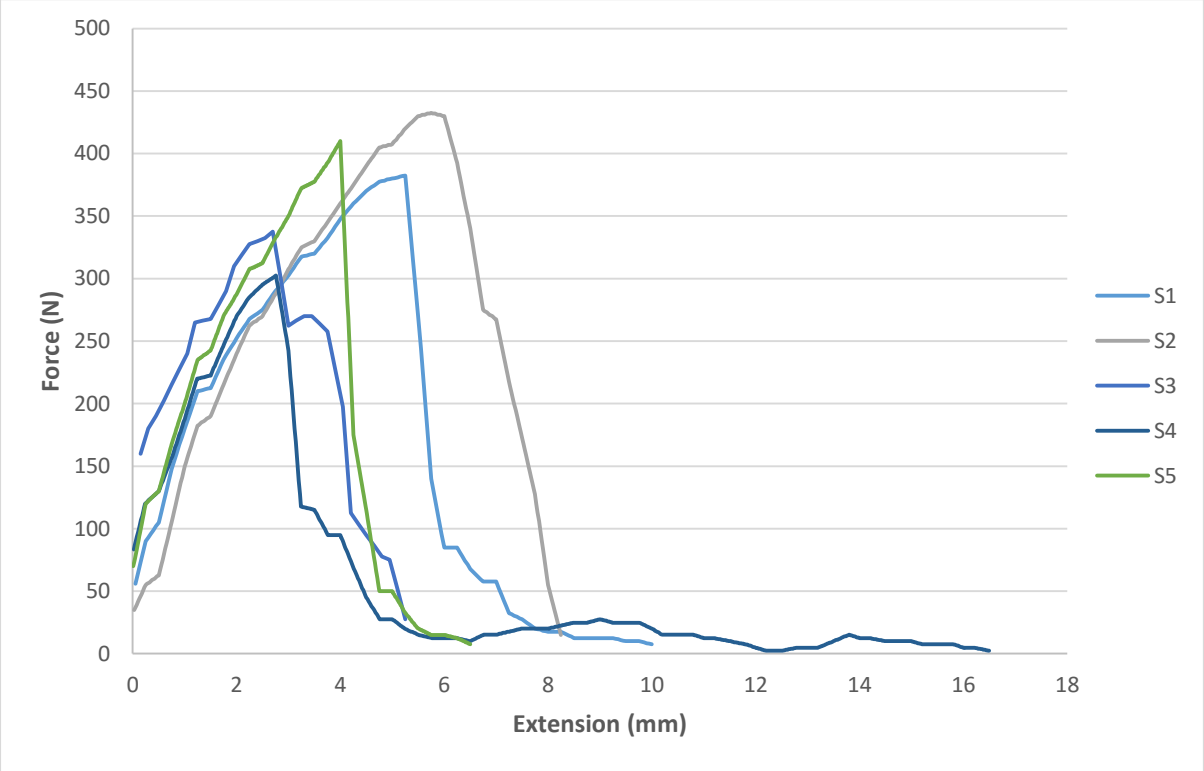

Figure 6.7: T-peel test results of copper specimens

The peel test used in the experiments did not behave in the same way as a peel test applied to adhesive bonds which tend to fail uniformly across the bond interface. When applied to soldered specimens the method of failure was different and tended to propagate from a series of 'contact points'. A contact point is defined as a small region within the soldered zone that was fully bonded. Under peeling action a contact point remains bonded with un-bonded material around it tearing during failure to give the effect of 'teeth'. The more contact points present in a soldered sample the higher the resistance to peeling with shorter 'teeth' being

observed. This indicated that even though soldering was done, there may still be regions where no atomic bond was present either through insufficient force being applied or through the presence of oxide at the interface. The peel test results were essentially indications of a qualitative measure of failure of the many contact points within a soldered interface (with contact points failing at differing loads). However, the test proved useful as an indication of overall soldering effectiveness and did produce a proportional load response. In all the specimens, the failure was recorded according to the standard (BS EN ISO 10365:1995, 1995). The failure pattern was always delamination failure with the designation DF meaning that the substrate failed by splitting in layers. The true nature of a soldered interface could only be ascertained through microscopic observation.

6.7.3 Results from Microstructural Analysis

This test was important to identify the proportion of bonded to unbounded area within the specimen. Fig. 6.8 shows a foil of copper deposited with solder paste. It clearly indicates the presence of an intermetallic bond at the surface and thus proving that there is a great proportion of area where the paste has bonded with the metal.

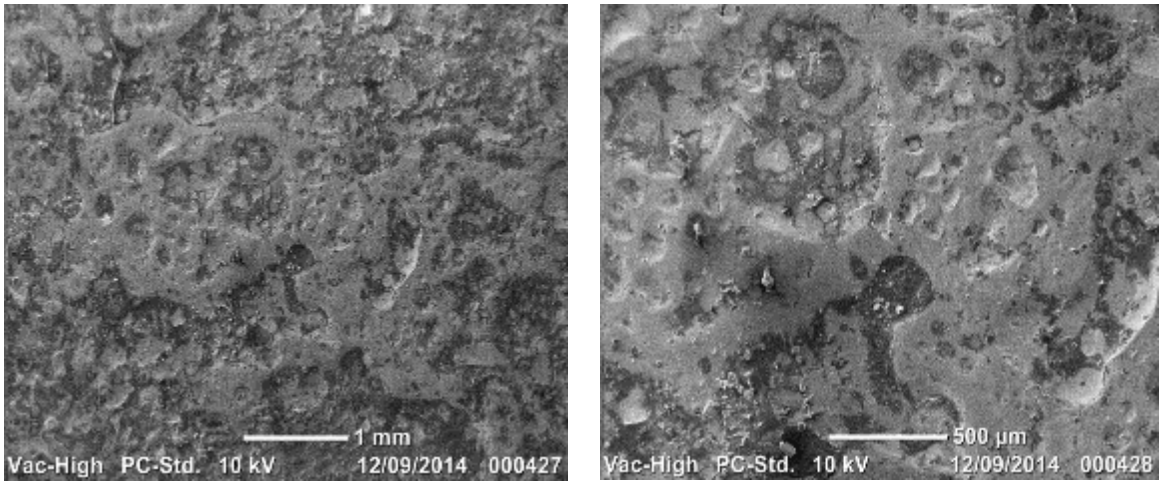

Figure 6.8: SEM analysis of copper foil

There are, however, areas where cracks are present as shown in Fig. 6.9. These cracks can cause wetting issues which will lead to no-bonded zones in the specimen. This is not a good thing when talking about the integrity of the specimen produced. Such zones tend to give false readings and can cause abrupt failures.

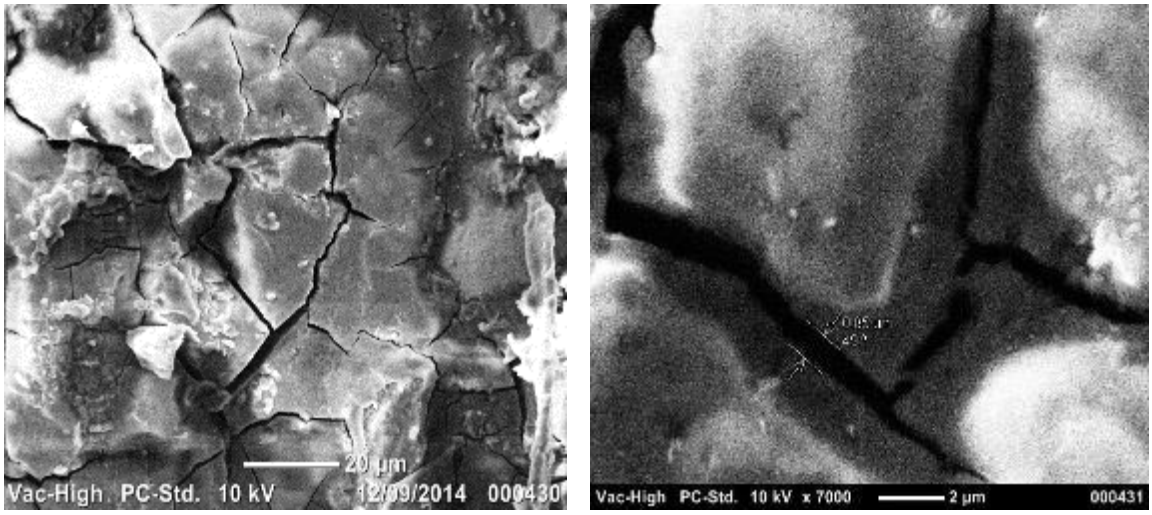

Figure 6.9: SEM crack analysis of copper foil

One way of overcoming this issue is to make sure that there is a uniform layer of paste on the surfaces to be soldered so that when the solder paste starts to melt, it could easily wet the entire surface rather than just the areas where the paste is present. Copper has excellent solderability which helps the wetting process but other factors need to be considered as well including applying appropriate pressure so that the molten paste seeps into the surface of the metal quickly and forms an intermetallic bond.

A sample was cut from a peel specimen and mounted on the platform of an optical microscope to observe the layers of copper and solder. Fig. 6.10 shows the cross-section at 100 times magnification. The shiny yellow lines indicate the copper metal whereas the black line in the middle indicates the solder. The results are expected as they clearly show the presence of solder paste between the two layers of metal.

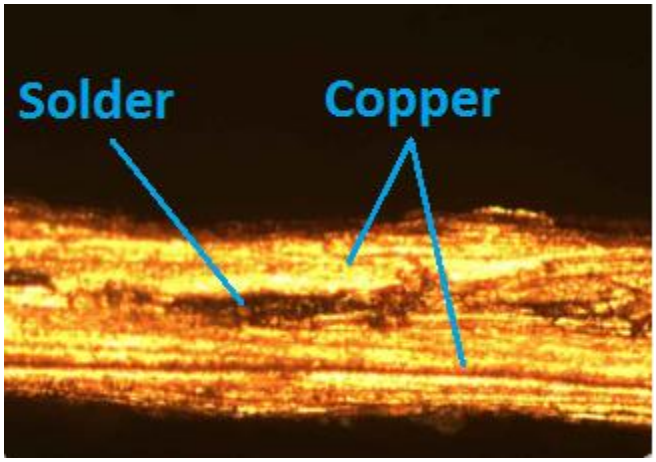

Figure 6.10: Microscopic analysis of copper single lap joint

6.7.4 Results from Dog-bone Tensile Test

The test showed that the strength of the composite copper is higher than the parent copper. It is evident from the results that the specimen produced by CMFM is 11% stronger than the product manufactured from traditional methods. Fig. 6.11 shows the two specimens and Fig. 6.12 shows the comparison between the two specimens.

Figure 6.11: Copper tensile test specimens

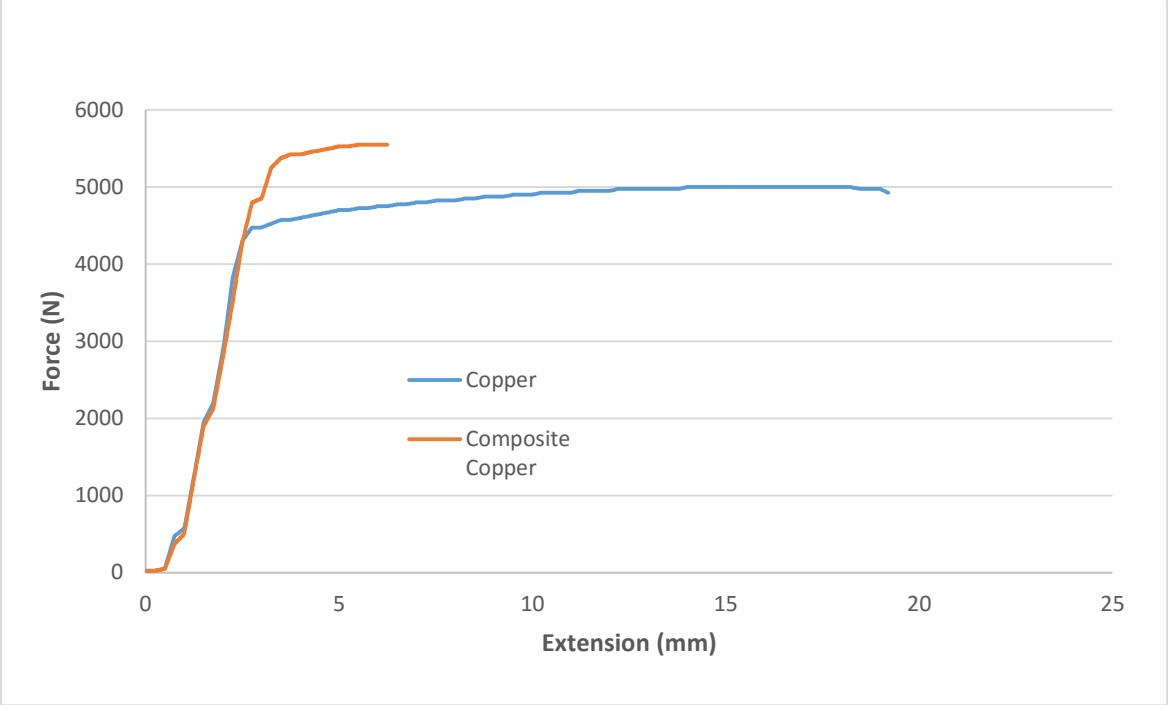

Figure 6.12: Comparative tensile test between copper and composite copper

The maximum force for failure is 5550N for the composite whereas it is 5000N for the parent copper. There was no failure of individual layers but a complete failure of the specimen proving that the fourteen layers that were bonded together were actually functioning as a single unit rather than individual layers and that added to the strength of the specimen. The reason for the high strength of copper is very basic. The yield strength of copper is 70 MPa whereas the yield strength of the paste used is 40 MPa and because the paste is forming an intermetallic bond with the metal, these strengths tend to add up theoretically (Shirvani, 2000; ExtremeTech.com, 2013). In theory, the strength keeps on increasing with the increase in the number of layers. Practical testing does not show the same increase in strength as in theory but there is some improvement in strength nonetheless which is evident from the Fig. 6.12. Furthermore, the layer of solder stops the metal atoms from slipping when stress is applied and thus prohibiting any dislocations.

Both the specimens follow the same elastic region and show almost identical behaviour. Copper being a ductile metal has a large plastic deformation range before fracturing whereas the composite copper does not behave in the same manner. It has high strength but a smaller plastic deformation range before fracturing due to the presence of intermetallic bonds among the layers. The bonds prevent the copper layers to follow their ductile nature resulting in a rather smaller plastic deformation range. The presence of bonds is also responsible for a much less percentage elongation of the composite copper specimen (9.6%) as compared to the parent copper (38.8%).

Copper being a ductile metal shows the presence of inclusions (Fig. 6.13), which act as tiny stress concentrations. They either fracture or separate from the matrix, nucleating voids that grow and link up, ultimately causing fracture.

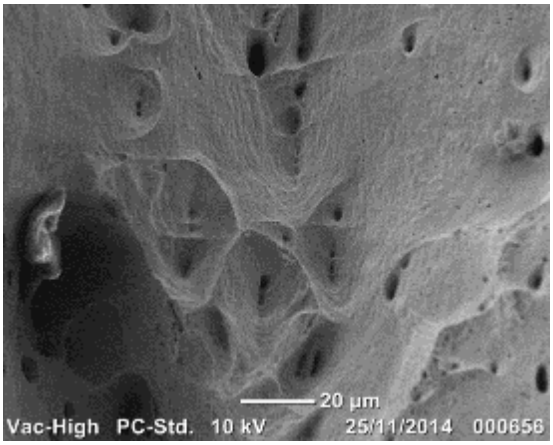

Figure 6.13: Fracture mode of copper specimen at x800

The composite copper has less pronounced fracture characteristics compared to solid copper (Fig.6.14) that allows it to have a smaller plastic deformation region.

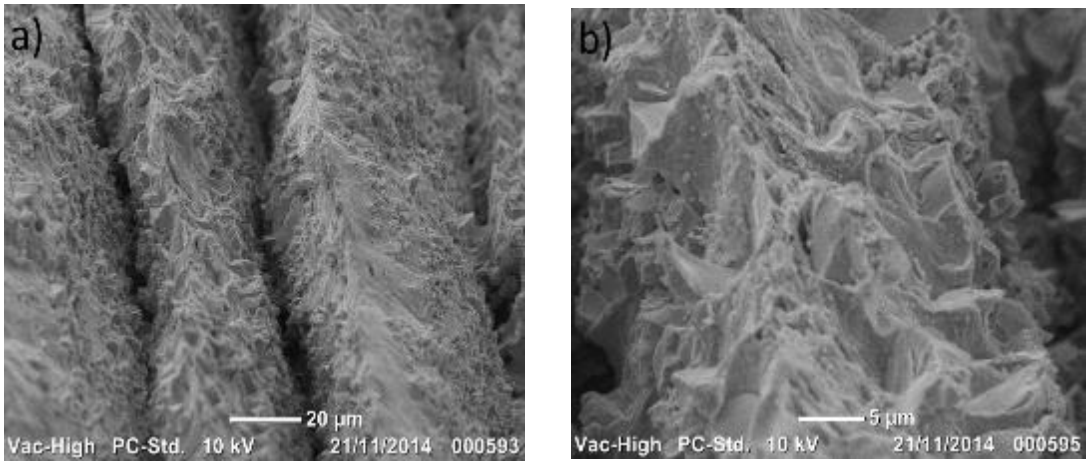

Figure 6.14: Fracture modes of the composite copper specimen: a) Layers at x800; b) Layer at x3000

6.8 Results from Aluminium 1050 Foils

The testing was focussed more on aluminium because of its use in industries owing to its high strength and low weight. Aluminium 1050 foils were joined together as single lap joints, peel specimens and dog-bone specimens using the ASN-892-600 brazing paste. The foils were used as provided with no surface treatment.

6.8.1 Results from Lap-shear Test

The lap-shear test was conducted to study the effect of three parameters on the single lap joints:

I. **Test Speed:** Specimens at an overlap length of 12.5mm subjected to cross-head speeds of 10mm/min, 50mm/min and 100mm/min.

II. **Material Thickness:** Specimens of 0.05mm, 0.1mm and 0.2mm thickness at an overlap length of 12.5mm subjected to a speed of 10mm/min.

III. **Lap Length:** 10mm thick specimens were subjected to cross-head speed of 100mm/min at overlap lengths of 3mm, 6mm and 12mm.

6.8.1.1 Effect of Test Speed

Like the previous test with copper foils, all the tested specimens failed at the base metal and not at the bonded area. The failure pattern was always substrate failure (SF) meaning that the substrate fractured before the bond. Fig. 6.15 shows the test results of the single lap joints carried out at different speeds.

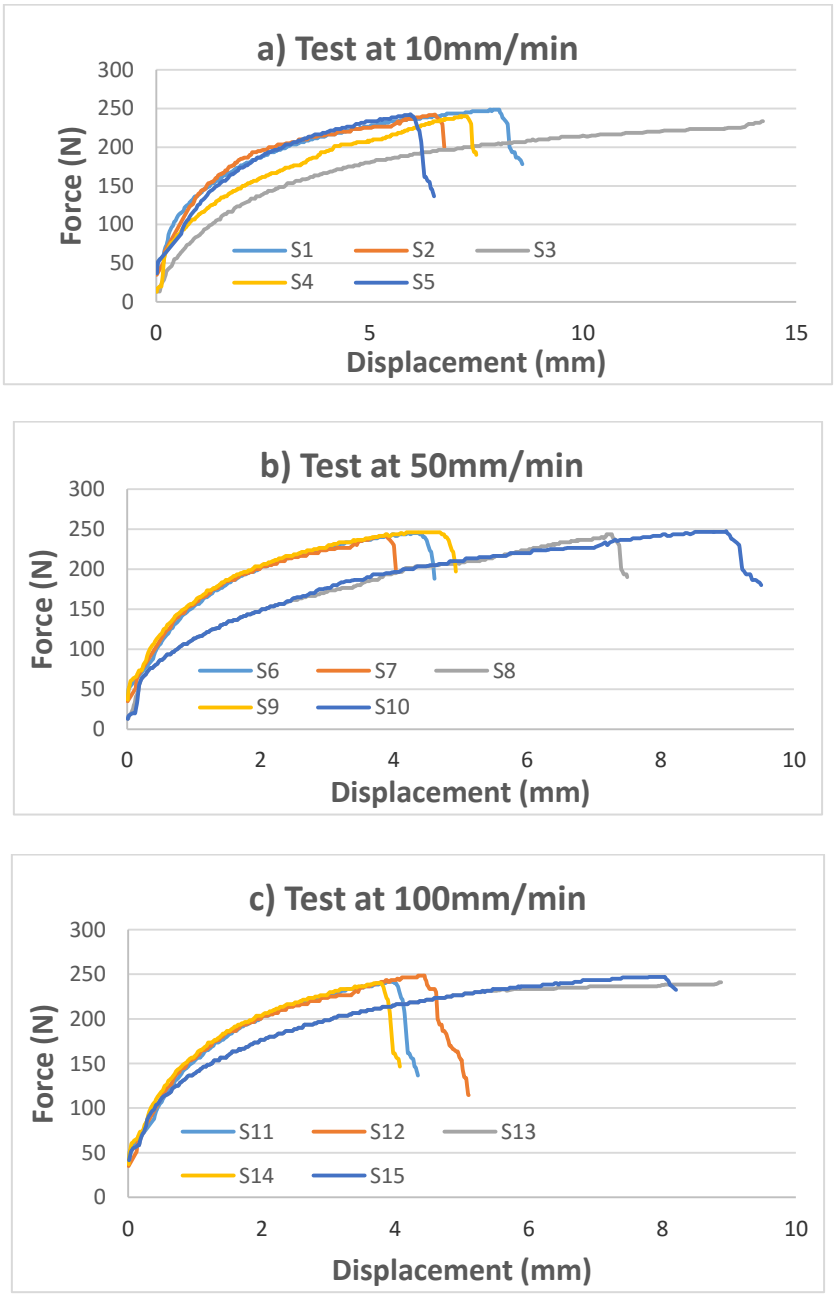

Figure 6.15: Test results of Al single lap joints carried out at different speeds: a) 10mm/min; b) 50mm/min; c) 100mm/min

From the tested specimens, two categories of failure mode were observed and their behaviour is shown in Fig. 6.16 (a).

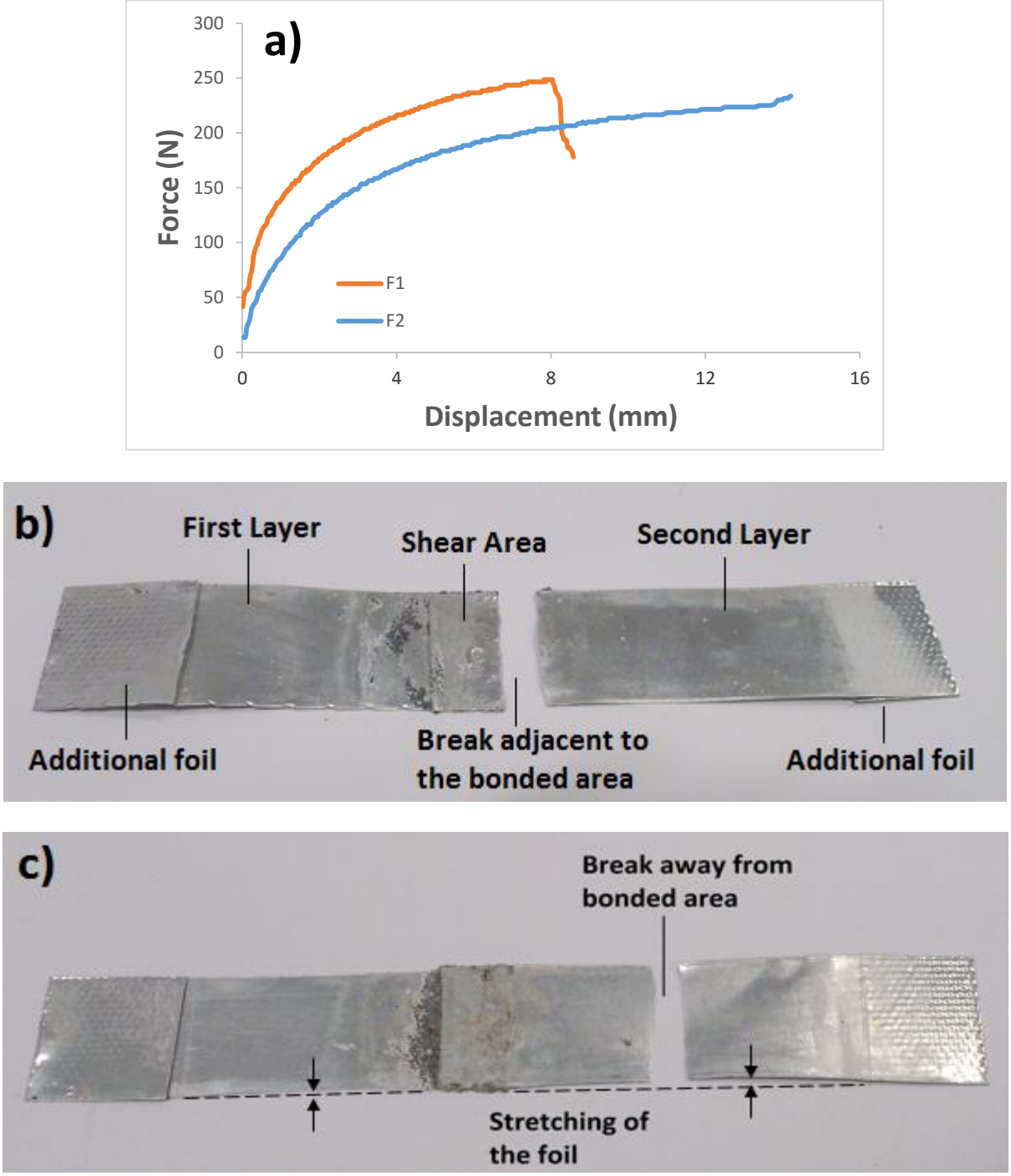

Figure 6.16: Failure modes Al single lap joints: a) Force vs. displacement curve showing two failure modes of Al 1050; b) First mode of failure, F1; c) Second mode of failure, F2

The two failure modes were:

1) Where there was a break at the base metal adjacent to the bonded area shown in Fig. 6.16 (b) as F1. Such a failure is characterised by a smaller displacement range to failure as exhibited by most of the specimens (S1, S2, S4, S5, S6, S7, S9, S11, S12 and S14). Smaller displacement range resulted in smaller plastic deformation of the foil before failure. Once a crack was initiated, it ran across the width of the foil to cause fracture.
2) Where a break occur away from the bonded area shown in Fig. 6.16 (c) as F2 where stretching of the foil can be seen on either ends of the bonded area that led to a fairly larger displacement range in the case of S3, S8, S10, S13 and S15.

It is worth noting that all the testing speeds yielded similar results and the fracture was always due to substrate failure. None of the specimens broke within the bonded area showing that the bond is stronger than the material itself. It shows that the lap joints are not affected by the cross-head speeds and this is consistent with the work done by Da Silva, et al. (2009). The specimens failed at values approaching the tensile strength of the metal (100 MPa) as shown in Fig. 6.17.

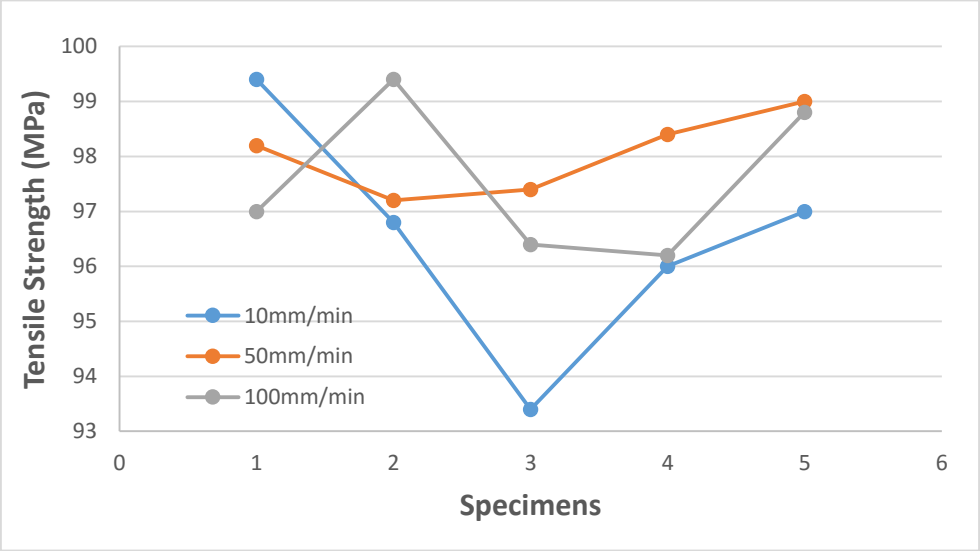

Figure 6.17: Lap-shear test results of Al single lap joints

The test results show similar pattern as compared to the work done by Kong, Soar and Dickens (2002) using UC to produce aluminium single lap joints. They used aluminium 3003-H18 foils (tensile load=570N) that were 0.1mm thick and this research was carried out using aluminium 1050 H14 ½ hard temper foils (tensile load=250N) of the same thickness. In case of UC, as contact force (pressure) and amplitude were increased, the level of deformation became significant resulting in weld failure at lower loads showing that as process parameters increase (weld speed and pressure), the failure measurements became more and more faulty (Fig. 6.18). All the specimens were tested at same speed of 2mm/min but based on the decrease in failure measurements as the process parameters were increased, the researchers had to abandon the lap shear test. This goes to show that UC is not capable of producing high quality lap joints without optimization of its process parameters and hence the specimens produced at high speed and pressure cannot sustain their material properties when subjected to testing. The results fell from force values of 570N to around 300N showing the inconsistency at higher process parameters. On the other hand, CMFM is fully capable of producing consistent lap joints and does not need optimization studies for better results. All the lap joints were produced under same conditions and yielded similar values while testing at different speeds without compromising the integrity of the material properties. A good cluster of breaking force values was observed ranging from 233N to 248N showing consistency of results. In addition to the experimental results, major differences lie in the actual processes as well. UC relies heavily on the optimization of the amplitude, weld speed and contact pressure whereas CMFM is a straight forward process as it does not require optimization in terms of its control parameters. UC requires milling operations to achieve the required geometry and surface finish whereas CMFM produces parts after cutting them into shape and there is minimal post-processing to enhance surface finish.

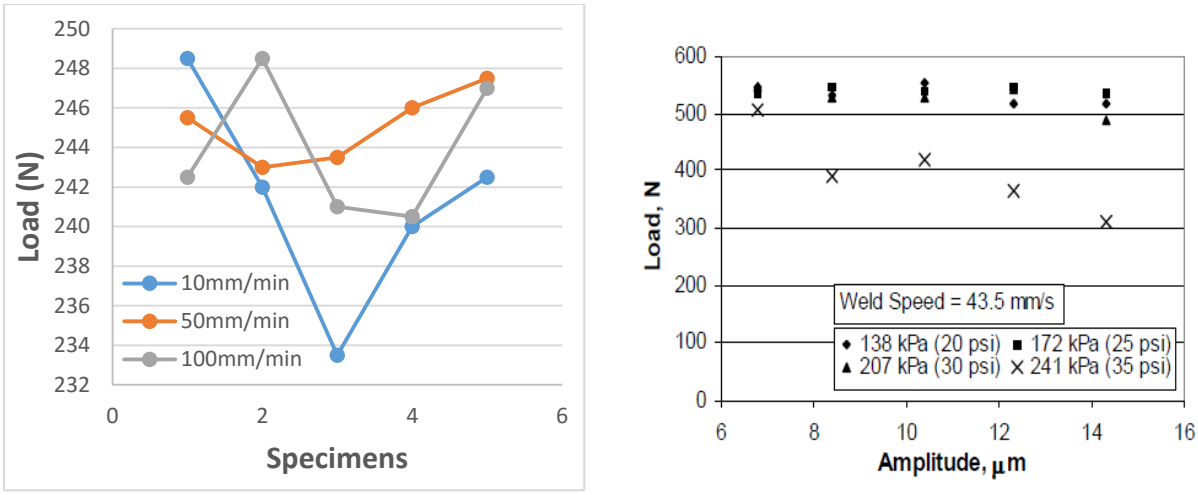

Figure 6.18: Comparison between CMFM and UC lap-shear test results

6.8.1.2 Effect of Material Thickness

After analysing the effect of testing speed with 0.1mm thin Aluminium 1050 foils, the effect of material thickness was investigated. These tests were carried out at a cross-head speed of 10mm/min as more consistent results were obtained previously at this speed. The failure modes were similar to the previous tests and the type of failure was substrate failure. Fig. 6.19 and 6.20 show the test results for 0.2mm and 0.05mm thin metal foils respectively.

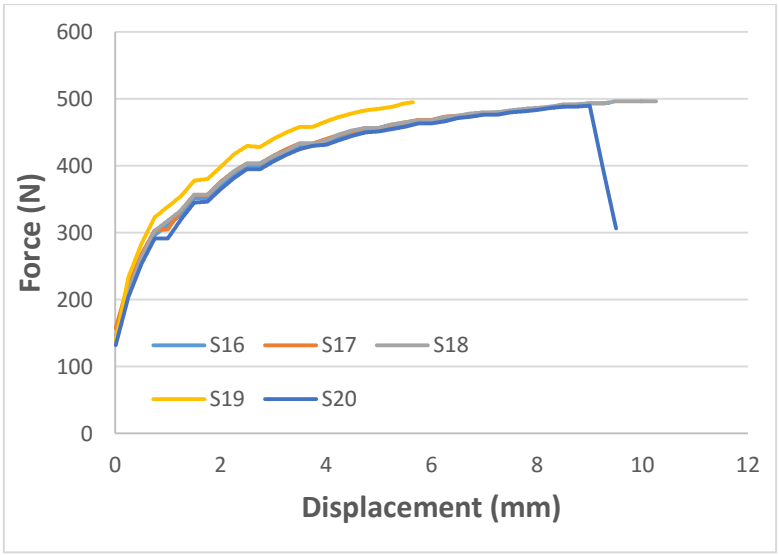

Figure 6.19: Test results of 0.2mm Al single lap joints

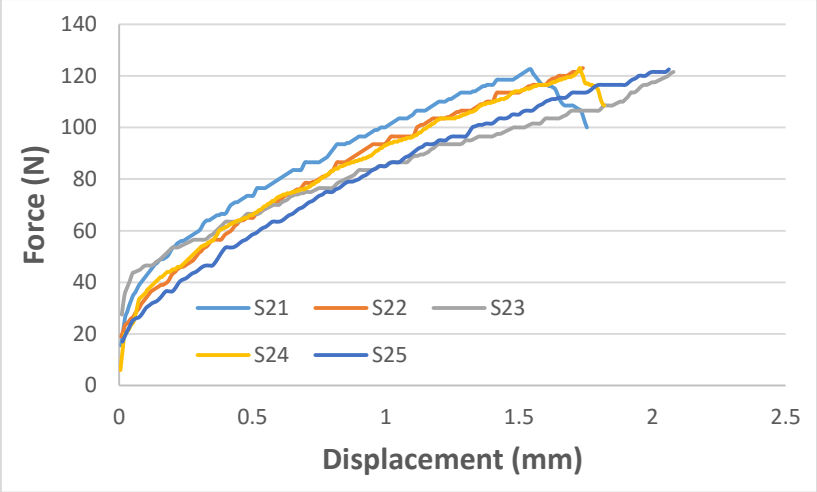

Figure 6.20: Test results of 0.05mm Al single lap joints

Upon comparing the three different thickness values from Fig. 6.15 (a), Fig. 6.19 and Fig. 6.20, an almost linear relationship is observed. For 0.05mm, the force values are approaching 125N, for 0.1mm, they are approaching 250N and for 0.2mm, they are approaching 500N. Therefore, the force values are almost doubled as the thickness is doubled. This goes to show that with increase in the thickness of the material, the breaking force needed for failure also increases. This can be easily explained by the fact that as the thickness increases, the resistant area is also increased and thus more force is required to cause failure. Furthermore, it is important to note that the breaking force values in all the cases are still approaching the tensile strength values for a particular cross-sectional area as shown in Fig. 6.21.

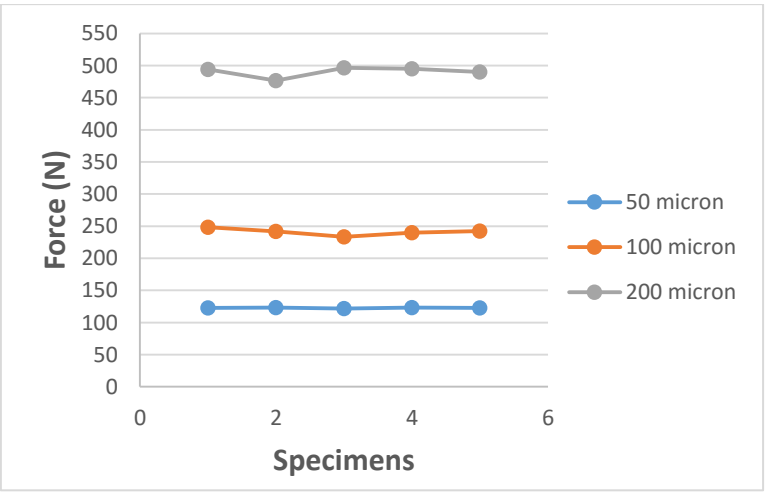

Figure 6.21: Comparison of test results for different Al foil thickness values

6.8.1.3 Effect of Lap Length

The above test results are for very thin Aluminium 1050 foils and the effect of lap length would not be evident from them as they would result in substrate failure. Hence, thick plates of the same grade metal were utilized. Aluminium plates of 10mm thickness were bonded together in lap lengths of 12mm, 6mm and 3mm. This is because anything less than 10mm had resulted in substrate failure. To fully investigate this effect, cohesion failure was observed for the specimens. Cohesion bond failure resulted in fracture of the bond and is characterised by the clear presence of brazing paste on the matching faces of both plates as shown in Fig. 6.22.

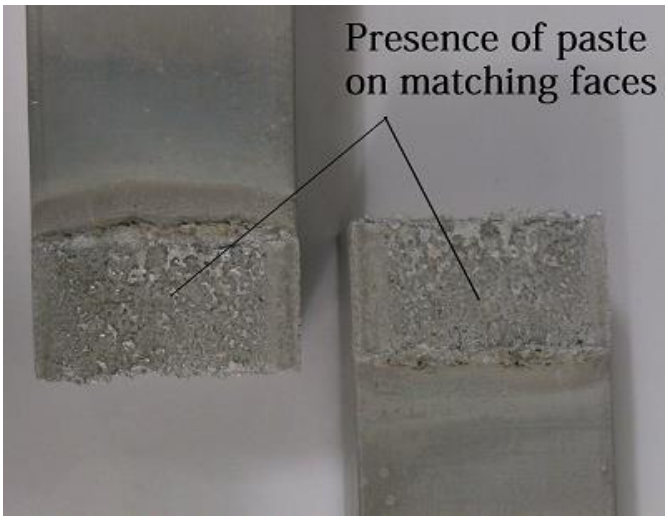

Figure 6.22: Cohesion failure on aluminium plates

A comparison of the breaking forces for the different lap lengths is shown in Fig. 6.23. It is evident that the joint strength increases almost linearly with overlap. The overlap is the factor that has the biggest impact in the joint strength. This is due to the fact that when the overlap length is increased then the force has to overcome more bonded area which results in a much higher breaking force value. The breaking forces for 12mm lap lengths are around 16kN whereas the ones for 6mm lap length are around 8kN showing that almost half the force is needed when lap length is decreased by the same factor. However, the same linear

relationship cannot be observed for 3mm lap length and 6mm. The reason being the fact that now the difference between the two lengths is not large enough to provide linearity but the breaking forces of around 6kN still give a pretty good picture of the effect of lap length. It is clear from the results that lap length has significant impact on the joint strength as the breaking force values increase with increase and decreases with decrease in lap length.

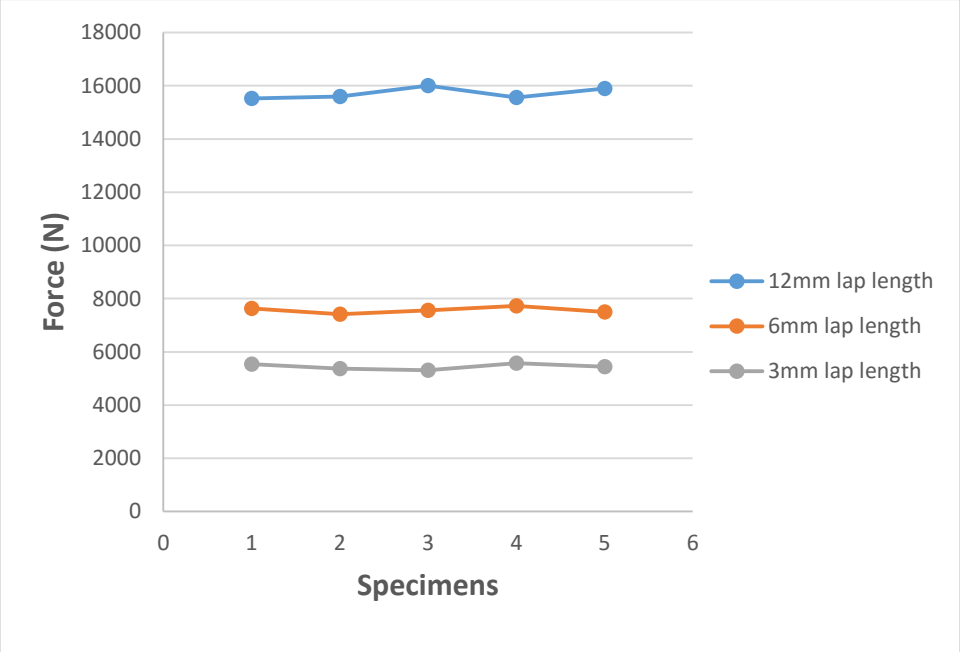

Figure 6.23: Comparison of different lap lengths for Al plates

6.8.1.4 Calculation of Lap-shear Strength

For industrial applications, tensile lap-shear strength of the bond or in other words joint tensile strength (σ) is important, therefore, the results from 12mm long lap length joints are being used to calculate this value.

The bond strength (τa) has been calculated as a maximum shear stress achieved in the bond layer, based on recorded maximum tensile forces for each tested joint:

$$\tau a = \text{Fmax} / \text{Length of the lap joint} * \text{Width of the substrate} \quad (6.1)$$

The joint tensile strength (σ) as a maximum tensile stress transferred crossover the joint:

$$\sigma = \text{Fmax} / \text{Thickness of the substrate} * \text{Width of the substrate} \quad (6.2)$$

The values of the bond shear strength and joint tensile strength are calculated by using equations (6.1) and (6.2). They are presented in Table 6.3.

Table 6.3: Calculation of joint tensile strength at 12mm overlap length

Specimens	F_{max} (N)	Bond Shear Strength (MPa)	Joint Tensile Strength (MPa)
S26	15520	51.73	62.08
S27	15600	52	62.4
S28	16000	53.3	64
S29	15560	51.86	62.24
S30	15900	53	63.6
		Average = **52.378**	Average = **62.864**

The experimental calculation yields shear strength of 52.378 MPa (N/mm^2) for the bond produced by the brazing paste used. This value is quite high as compared to some of the industrial adhesives (Da Silva, et al., 2009) including a very ductile polyurethane adhesive (Sikaflex-255 FC with a shear strength of 8.26 MPa); a very brittle two-component epoxy adhesive (Araldite® AV138/HV998, with a shear strength of 30.2 MPa, from Huntsman), and an intermediate two-component epoxy adhesive (Araldite® 2015, with a shear strength of 15.9 MPa, from Huntsman). The joint tensile strength is 62.864 N/mm^2 and must be kept in mind while designing products using CMFM.

6.9 Results from T-peel Test of Aluminium Specimens

The peel test was found to be effective in determining the bond effectiveness. The specimens had a bond thickness of 0.1 mm, therefore, the thickness of each specimen became 0.3 mm after it had been produced and was ready for testing. The results of a peel test are generally influenced by peel angle and peel rate. The peel angle was kept constant as shown in Fig. 6.24b whereby the peel rate was varied. Since the specimen was stiff enough to form a

perfect ‘T’ shape after being loaded into the machine, the angle of separation was constant for all the tests.

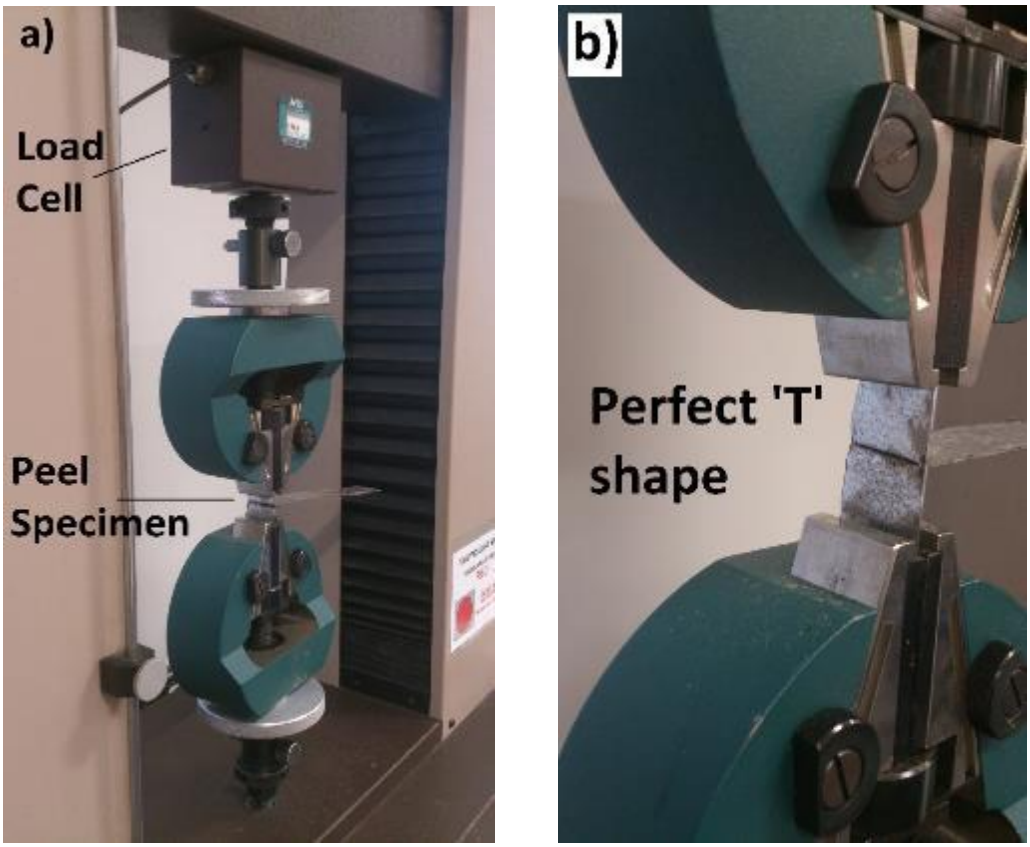

Figure 6.24: Peel testing of Al specimens: a) Testing apparatus; b) Alignment of the specimen

From the specimens tested at three different peel rates, two categories of failure modes were observed and are shown in Fig. 6.25.

Figure 6.25: Fracture modes of aluminium peel test

The two failure modes:

1. When there was a clear break at the beginning of a soldered region (when a load was applied) indicating an effective bond giving a high load ranging from 61.5-56N.

2. When a sample did not break at the beginning of soldered region but failed as the breaking points grew under loading. Typically such failure resulted in soldered loads of around 45.5N.

As mentioned for the copper specimen peel testing, the test did not behave in the same way as a peel test applied to adhesive bonds which tend to fail uniformly across the bond interface. The reason is that adhesives do not make a strong enough bond with the metal as does a brazing paste; therefore, contact points appear giving the effect of teeth. Shorter teeth mean higher resistance to peeling and longer mean a small degree of resistance. The peel test results were essentially a qualitative measure of failure of the many contact points within a brazed interface (with contact points failing at differing loads). However, the test proved useful as an indication of overall metal joining effectiveness and did produce a proportional load response. In all the specimens, the failure was recorded according to the standard (BS EN ISO 10365:1995, 1995). The failure pattern was always cohesive substrate failure (CSF) meaning that one of the substrates failed.

6.9.1 Crosshead Speed of 10mm/min

The results of the peel test at a peel rate of 10mm/min yielded a maximum peeling force of 55.5N and a minimum peeling force of 45.5N as shown in Fig. 6.26.

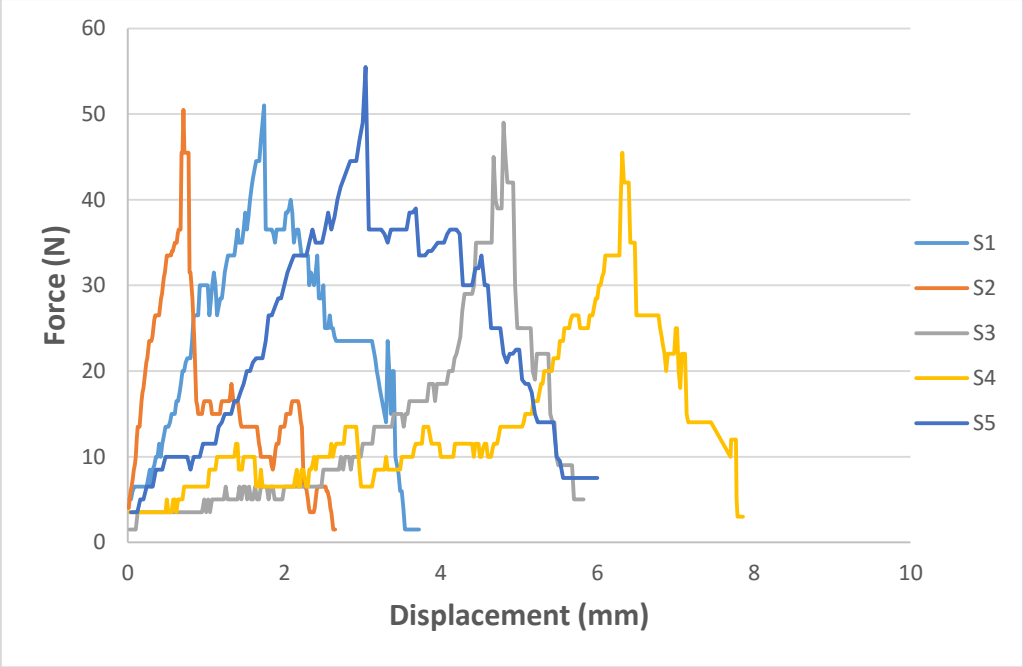

Figure 6.26: Peel test of Al specimens at 10mm/min

Table 6.4 calculates the average force (from the graph) and peel strength which is obtained by dividing the maximum force with the cross-sectional area (0.1 mm x 25 mm = 2.5 mm^2) of each specimen.

Table 6.4: Peel test calculations of Al specimens at 10mm/min

Specimens	Maximum Peeling Force (N)	Average Peeling Force (N)	Peel Strength (N/mm^2)	Type of Failure
S1	51	23.80	20.4	Cohesive Substrate Failure
S2	50.5	16.85	20.2	
S3	49	13.04	19.6	
S4	45.5	13.56	18.2	
S5	55.5	23.86	22.2	
Average Peel Strength = 20.12 N/mm^2				

6.9.2 Crosshead Speed of 50mm/min

The results of the peel test at a peel rate of 50mm/min yielded a maximum peeling force of 61.5N and a minimum peeling force of 45.5N as shown in Fig. 6.27. Table 6.5 calculates the average force and peel strength of each specimen.

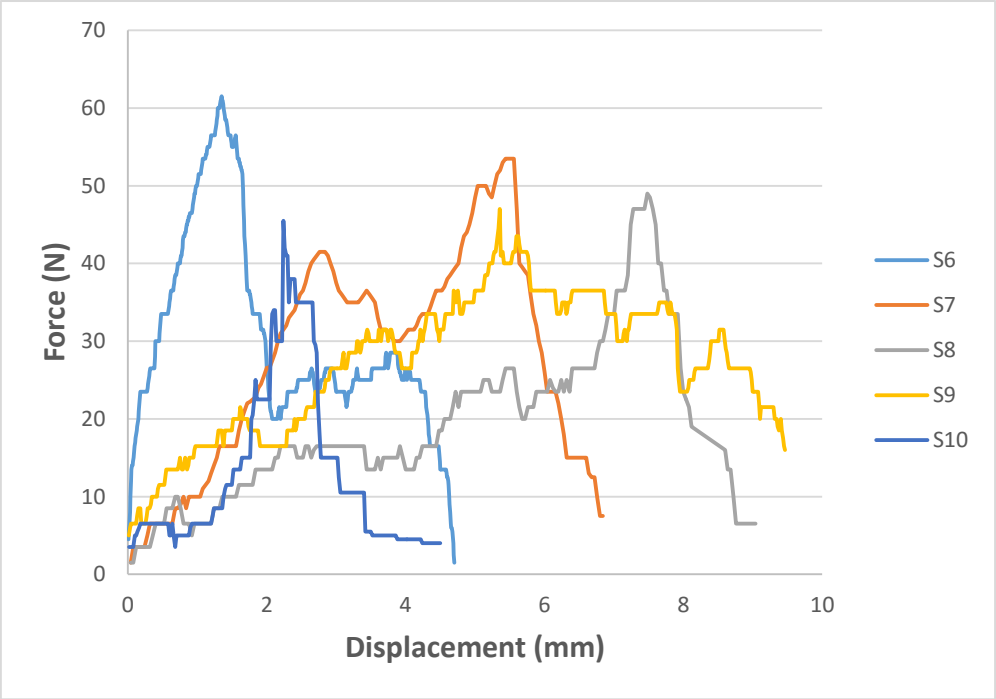

Figure 6.27: Peel test of Al specimens at 50mm/min

Table 6.5: Peel test calculations of Al specimens at 50mm/min

Specimens	Maximum Peeling Force (N)	Average Peeling Force (N)	Peel Strength (N/mm^2)	Type of Failure
S1	61.5	30.33	24.6	Cohesive Substrate Failure
S2	53.5	27.70	21.4	
S3	49	18.97	19.6	
S4	47	26.99	18.8	
S5	45.5	12.74	18.2	
Average Peel Strength = 20.52 N/mm^2				

6.9.3 Crosshead Speed of 100mm/min

The results of the peel test at a peel rate of 100mm/min yielded a maximum peeling force of 56N and a minimum peeling force of 46N as shown in Fig. 6.28. Table 6.6 calculates the average force and peel strength of each specimen.

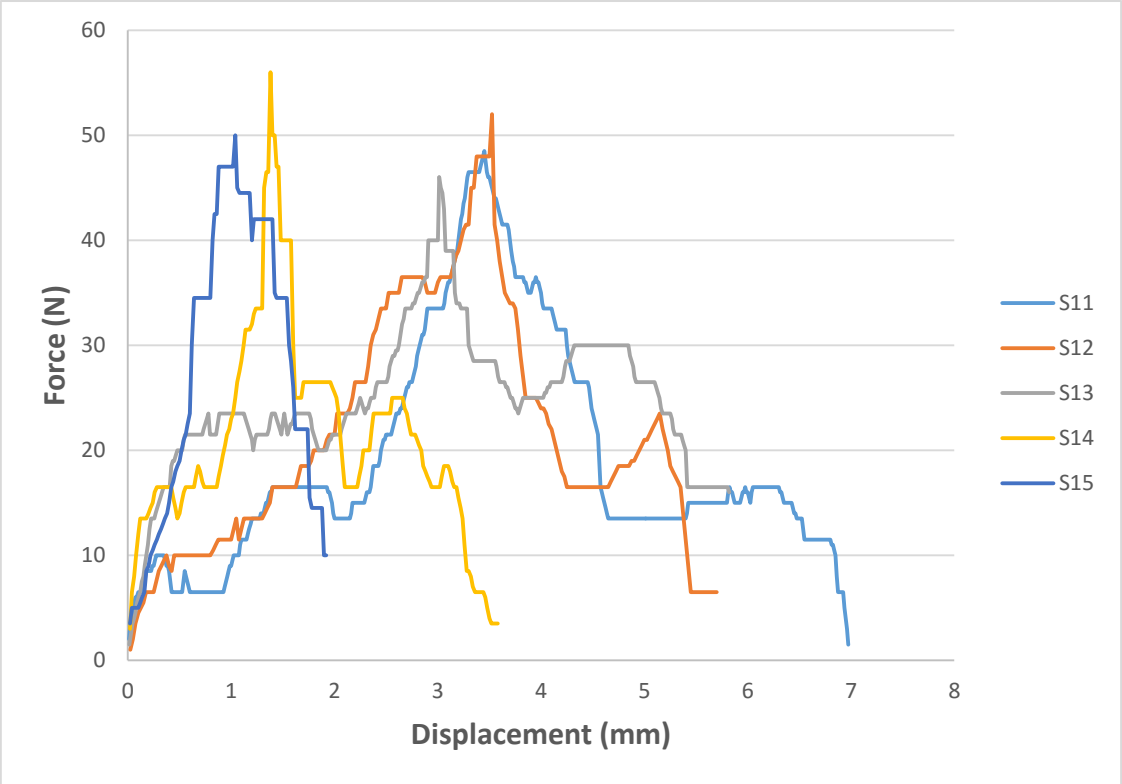

Figure 6.28: Peel test of Al specimens at 100mm/min

Table 6.6: Peel test calculations of Al specimens at 100mm/min

Specimens	Maximum Peeling Force (N)	Average Peeling Force (N)	Peel Strength (N/mm^2)	Type of Failure
S1	48.5	19.14	19.4	Cohesive Substrate Failure
S2	52	21.41	20.8	
S3	46	24.62	18.4	
S4	56	20.78	22.4	
S5	50	27.56	20	
Average Peel Strength = 20.2 N/mm^2				

The test results show similar pattern as compared to the work done by Kong, Soar and Dickens (2005) using UC to produce aluminium specimens for peel testing. They used aluminium 6061 foils (tensile strength=310MPa) that were 100 micron thick and this research was done using Al 99.5 grade 1050 H14 ½ hard temper foils (tensile strength=100MPa) of the same thickness. In case of UC, at high contact pressures (241kPa) and slow weld speeds (34.5 mm/s), the specimens failed through a crack-like geometry at the beginning of the weld region, at around 71.7 N, and represented failure in the single foil and not the welded region. This value was termed by the researchers as 'critical peeling load'. Some specimens, however, tear within the weld region, propagating from the various contact points. The specimens were produced at different amplitudes corresponding to the minimum, medium and maximum amplitude of the UC equipment. All the specimens were tested at a cross-head speed of 50mm/min. Since the peel test was unable to indicate the weld strength of the specimens beyond the critical peeling load, peel strength was calculated at this point and it comes out to be 28.68N/mm^2 or 28.68MPa (71.7N/2.5mm^2=28.68 N/mm^2). However, in comparison, the peel strength is roughly 0.0925 times the tensile strength of aluminium 6061. The specimens produced by CMFM were tested at three different cross-head speeds and one of those speeds was 50mm/min. All the results yielded failure modes similar to each other and to the tests performed by Kong, Soar and Dickens (2005). The speed had no effect on the peeling loads and the peeling strength was a constant 20N/mm^2 for all the three sets of tests. This value of peel strength, in comparison comes out to be 0.2 times the tensile strength of Al 99.5. This goes to show that the specimens produced by CMFM have relatively higher peel strength as compared to the specimens produced by UC (Fig. 6.29).

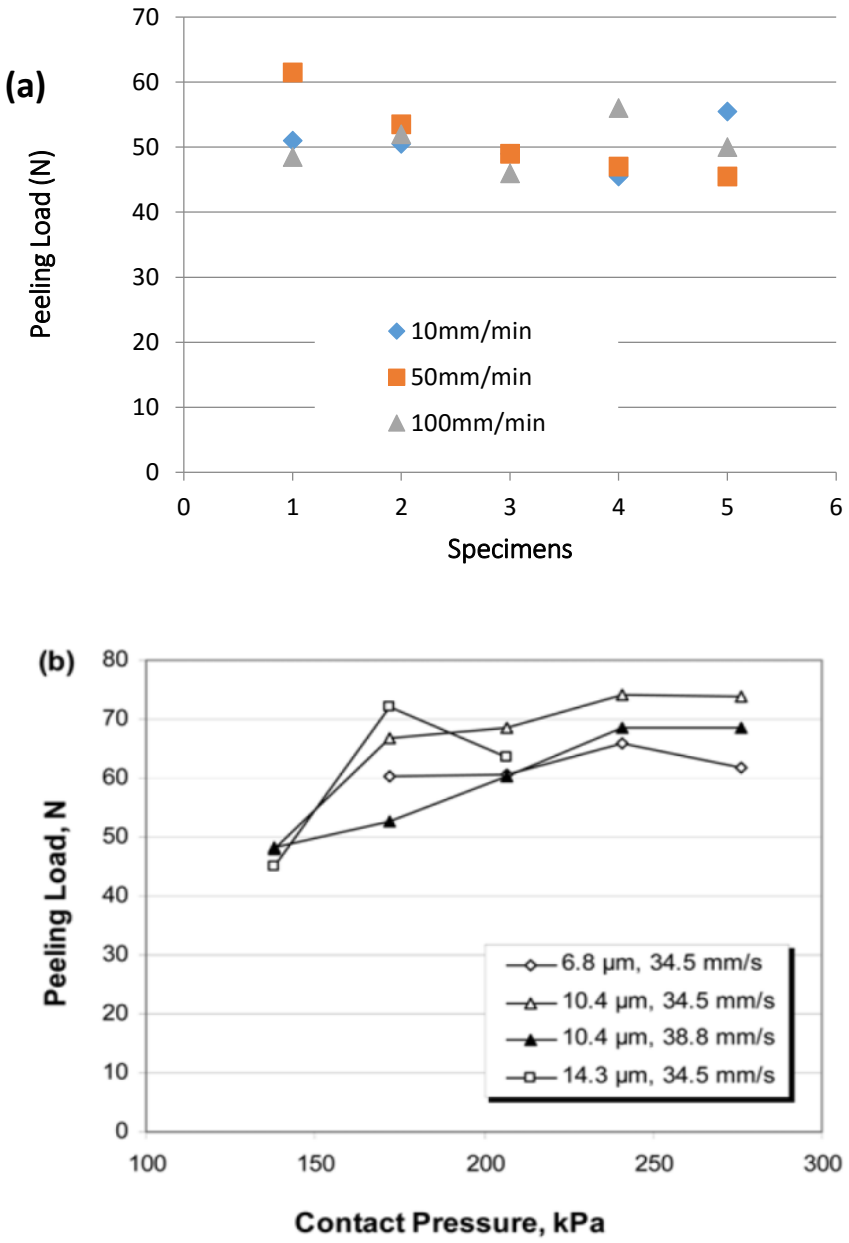

Figure 6.29: Comparison of peel tests: a) CMFM test results; b) UC test results

6.9.4 Corrosion Test of Aluminium Specimens

As mentioned before, galvanic corrosion is a major concern and any corrosion in the bond/foil interface would seriously undermine the strength of the specimen. This test was performed to assess the peel strength of the specimens and whether or not it is affected by corrosion. The aluminium peel specimens were put in a cylindrical container for 24 hours as shown in Fig. 6.30.

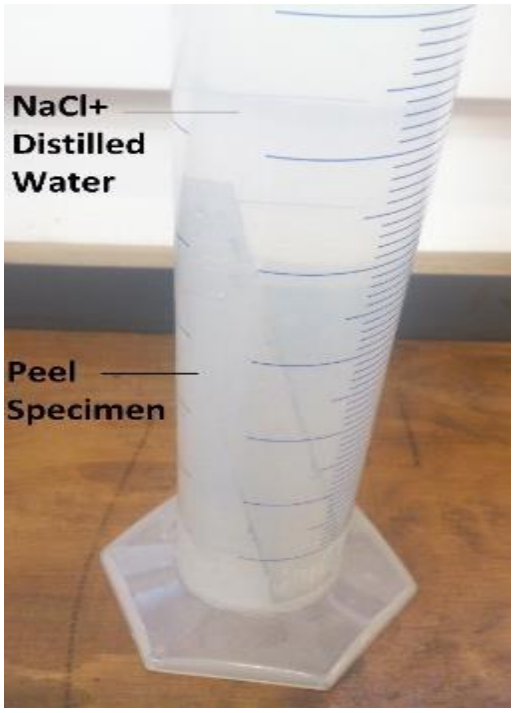

Figure 6.30: Corrosion testing of Al specimen

The pH of the solution was checked, by the use of pH strips, when the specimen was put in the container and when it was taken out. The value was 7.0 in both cases and is in the acceptable range. Afterwards, the specimens were tested on the tensile testing machine at a peel rate of 10mm/min and yielded similar fracture modes (Fig. 6.31) as previous peel test specimens. The resulting maximum peeling force for the tests was 55N and the minimum peeling force 45.5N (Fig. 6.32). The peel strength calculation is shown in Table 6.7.

Figure 6.31: Fracture modes of aluminium peel test after corrosion testing

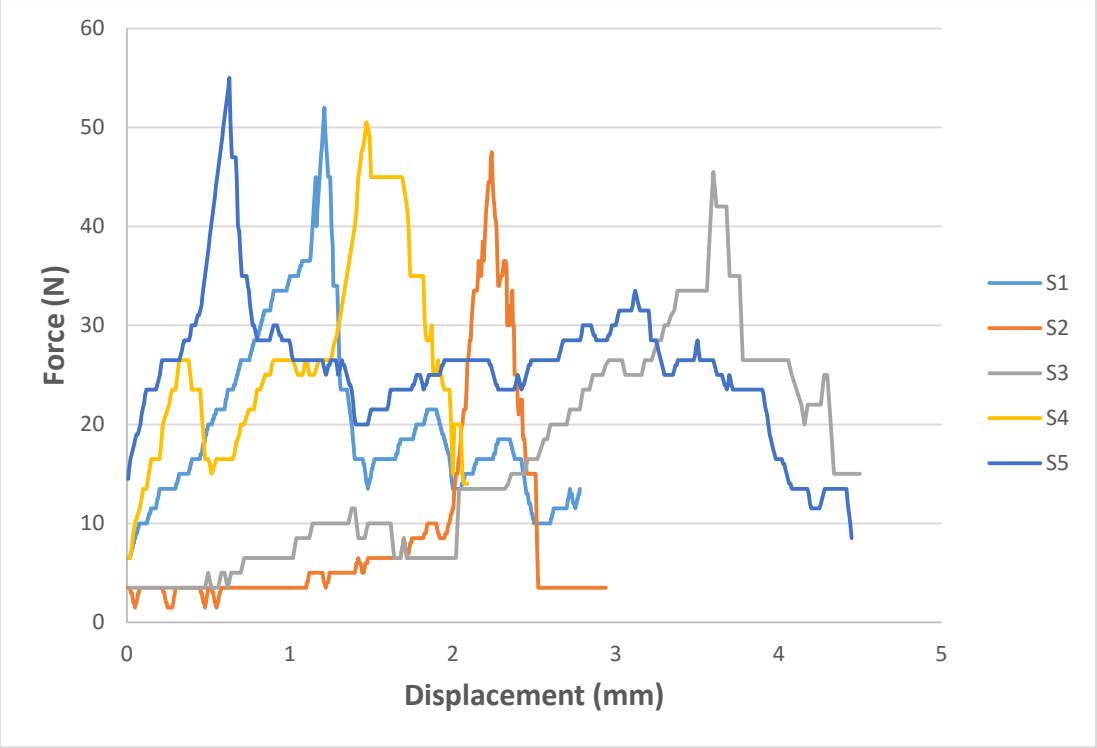

Figure 6.32: Peel test of Al specimens at 10mm/min after corrosion testing

Table 6.7: Peel test calculations of Al specimens at 10mm/min after corrosion testing

Specimens	Maximum Peeling Force (N)	Average Peeling Force (N)	Peel Strength (N/mm^2)	Type of Failure
S1	45.5	16	18.2	Cohesive Substrate Failure
S2	50.5	26.35	20.2	
S3	52	20.15	20.8	
S4	55	25.67	22	
S5	47.5	18.69	19	
Average Peel Strength = 20.04 N/mm^2				

An average peel strength of 20.04 N/mm^2 shows that the mechanical properties of the specimens were not affected by corrosion.

6.10 Results from Microstructural Analysis

This test was important to identify the proportion of bonded to unbounded area within the specimen. Fig. 6.33 shows a single foil of aluminium deposited with brazing paste. It clearly indicates the presence of an intermetallic bond at the surface and thus proving that there is a great proportion of area where the paste has bonded with the metal. But the problem arises when another foil of aluminium is joined and it is largely due to the presence of the oxide layer that hinders the production of a bond on the metal surface.

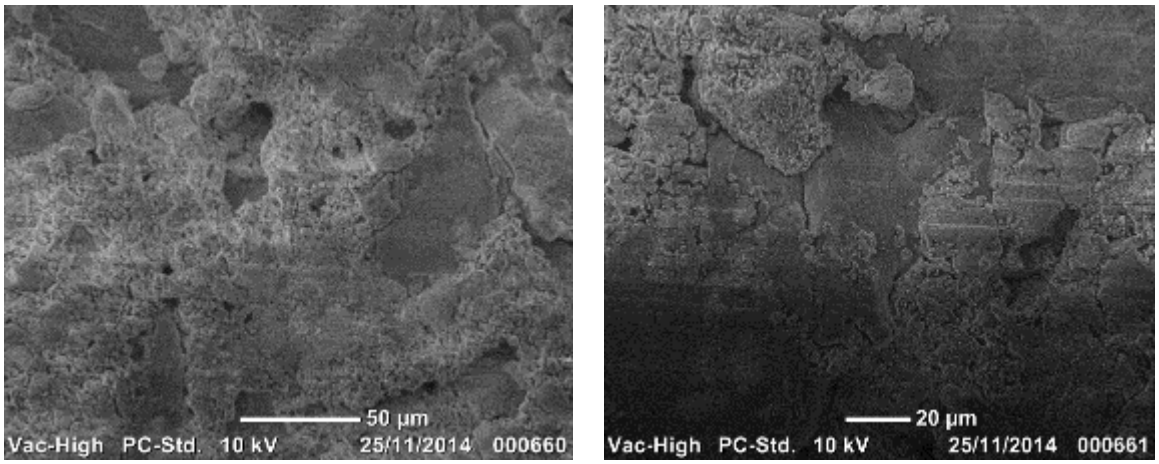

Figure 6.33: SEM analysis of aluminium foil surface coated with brazing paste at x500 and x700

A peel specimen is a sandwich of two layers brazed together and the presence of an intermetallic bond is essential for them to stay bonded. Fig. 6.34 shows a specimen with a uniform layer of brazing paste sandwiched between the two 1050 aluminium foils. A good proportion of bonded area can be observed which is essential for product development.

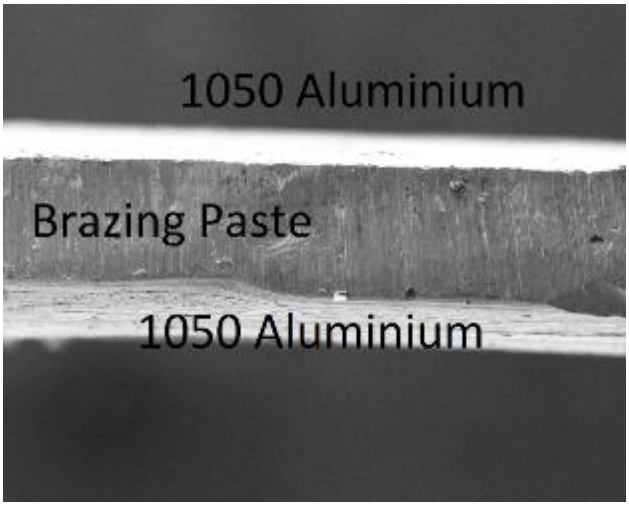

Figure 6.34: SEM image showing layers of the Al peel specimen

There are, however, areas where cracks are present as shown in Fig. 6.35a. These cracks can cause issues which will lead to no-bonded zones in the specimen as is observed in the fracture modes of the peel specimens. The crack in this case is 0.029mm wide (Fig. 6.35b) and cracks of similar dimensions were observed in some places along the length of the specimen. The areas with such cracks can cause abrupt failures; therefore, a more in-depth analysis is required where multiple layers are scanned so as to get a better picture of the bond integrity.

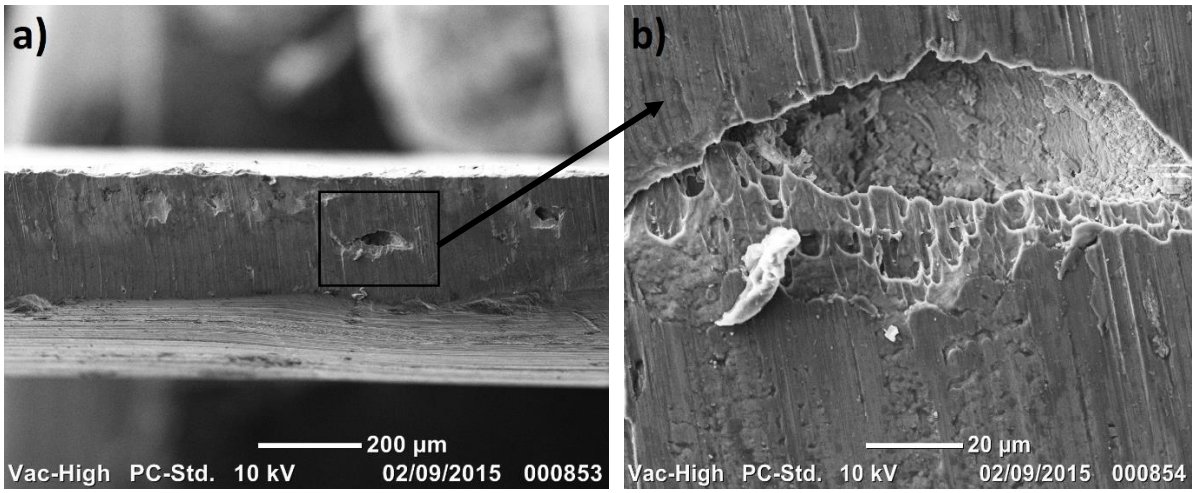

Figure 6.35: SEM analysis of Al peel specimen: a) Cracks in the paste layer; b) Enhanced image of the crack in the layer

6.11 Results from Dog-bone Tensile Test

This test was performed to analyse the strength of the bond produced by the proposed process with aluminium foils. A dog-bone specimen was machined out of solid aluminium 1050 block. Three dog-bone specimens (S1, S2 and S3) were then made using the process of CMFM. Each specimen was a multi-layered structure with 14 layers stacked on top of each other and brazing on either side. The very first observation was the absence of necking in case of the composite specimens. Aluminium, being a ductile material, showed considerable necking but it was not the case with the specimens made from CMFM. The fracture modes of Al 1050 and one of the specimens is shown in Fig. 6.36 and Fig. 6.37 shows the comparison of their tensile test.

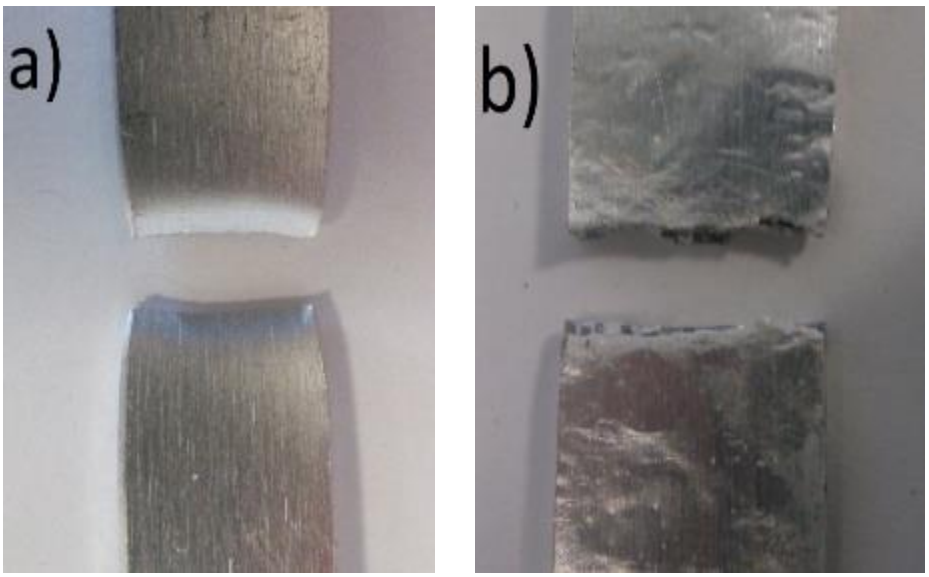

Figure 6.36: Fracture modes of the test specimens: a) 1050 Aluminium; b) Composite specimen

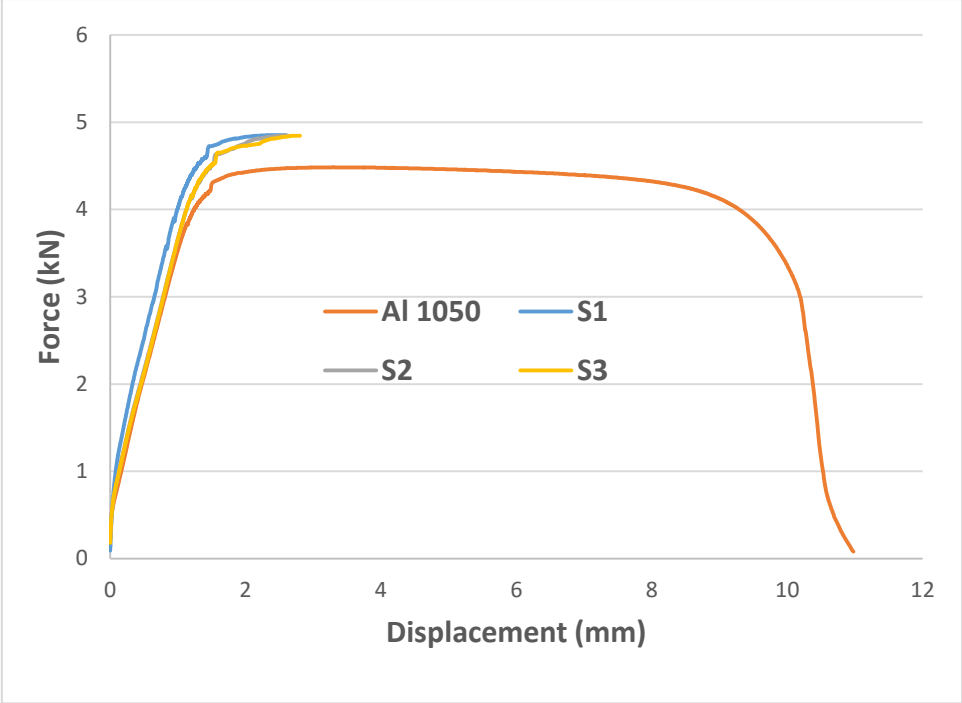

Figure 6.37: Comparative tensile test of Al specimens

The maximum force value for the solid aluminium 1050 specimen is 4.483kN and its curve has well defined elastic and plastic regions as is expected from an aluminium alloy. On the other hand, the three specimens produced by the proposed process showed maximum force values of 4.853kN, 4.845kN and 4.849kN respectively. There was no failure of individual layers but a complete failure of the specimen proving that the fourteen layers that were bonded together were actually functioning as a single unit rather than individual layers and that added to the strength of the specimens. The fracture values of the three specimens are very close to each other showing the ability of the process to produce consistent parts. The three composite specimens are 8.25%, 8.07% and 8.16% higher in strength as compared to the parent aluminium of the same thickness (2.7mm). This test clearly demonstrates that parts produced by the proposed process are stronger than the product manufactured from traditional machining (subtractive) methods. The reason for the high strength of the specimens is the same as the reason for high strength of composite copper i.e., the addition of

strength on increasing the number of layers. The yield strength of aluminium is 105 MPa whereas the yield strength of the paste used is 45 MPa and because the paste is forming an intermetallic bond with the metal, these strengths tend to add up theoretically. Practical testing does not show the same increase in strength as in theory but there is some addition in strength nonetheless which is evident from Fig. 6.37.

All the specimens follow the same elastic region and show almost identical behaviour. Aluminium being a ductile metal has a large plastic deformation range before fracturing whereas the composite specimens do not behave in the same manner. They have high strength but a smaller plastic deformation range before fracturing due to the presence of intermetallic bonds among the layers. The bonds prevent the aluminium layers from following their ductile nature resulting in a rather smaller plastic deformation range. The presence of bonds is also responsible for a much less percentage elongation of the specimens as compared to the parent aluminium as is evident from Table 6.8.

Table 6.8: Values obtained from tensile test

Specimens	Total Elongation (%)	Ultimate Tensile Strength (MPa)
Al 1050	21.5	132.8
S1	2.8	143.79
S2	3.1	143.55
S3	2.7	143.67

Aluminium shows inclusions that act as tiny stress concentrations as shown in Fig. 6.38. They either fracture or separate from the matrix, nucleating voids that grow and link up, ultimately causing fracture.

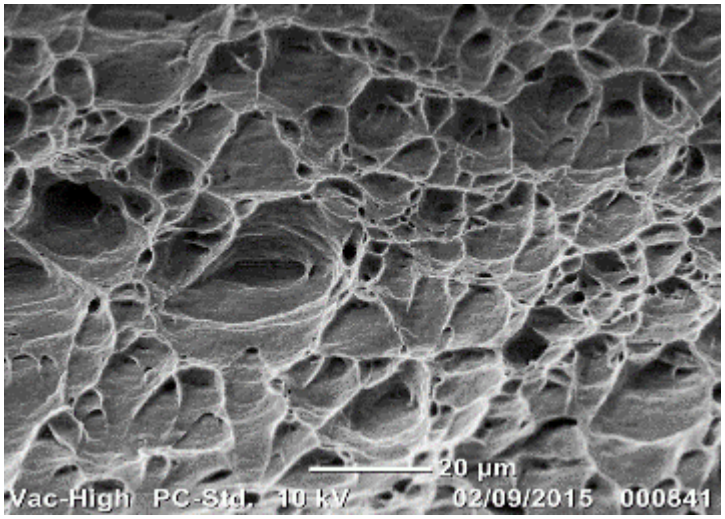

Figure 6.38: SEM analysis of 1050 aluminium at x1000

The composite specimen shows the aluminium foil between two layers of brazing paste (Fig. 6.39a). The inclusions that were seen in case of solid aluminium are visible in Fig. 6.39b but not to the same extent. The paste has made an intermetallic bond with the metal and the result is a high strength product that has better properties compared to its parent metal.

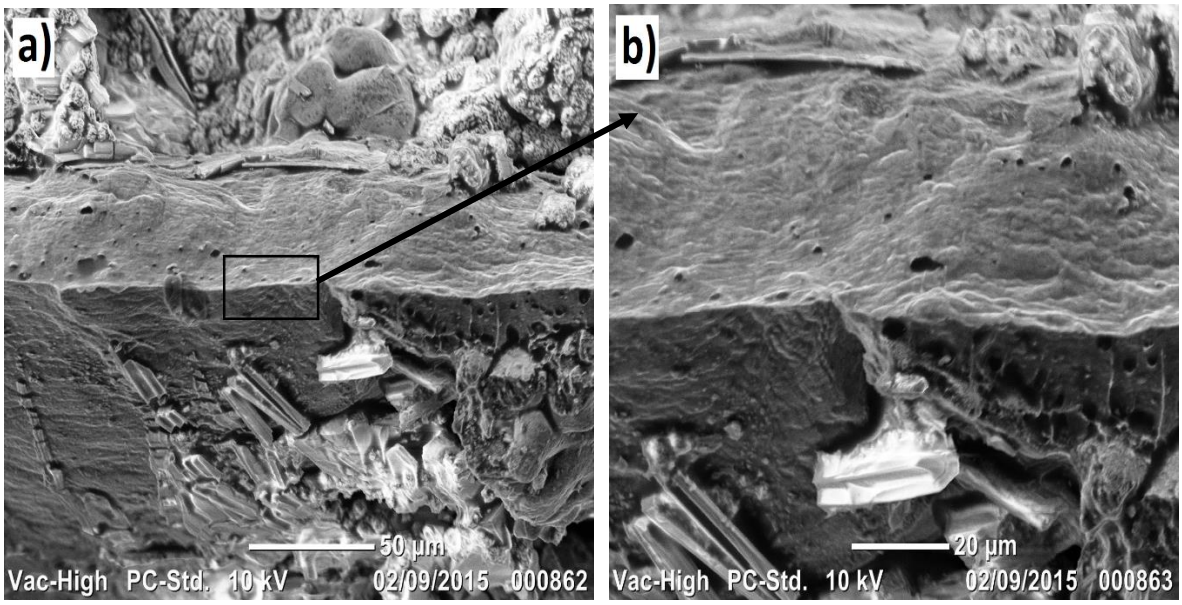

Figure 6.39: SEM analysis of CMFM part: a) Fractured foil at x500; b) Fractured foil at x1000

6.12 Shear Strength of Aluminium Dog-bone Specimens

Torsion test is not being performed as a part of this research and has been set aside for future testing. One important material property that is calculated by torsion test is the ultimate shear strength. There exists a relationship between ultimate tensile strength (UTS) and ultimate shear strength given by the following equation (Conry, 1976):

$$USS = 0.65 * UTS \qquad (6.3)$$

Therefore, by using UTS values from Table 6.8, USS of the aluminium specimens is calculated as shown in Table 6.9.

Table 6.9: Calculation of ultimate shear strength for Al specimens

Specimens	Ultimate Tensile Strength (MPa)	Ultimate Shear Strength (MPa)
Al 1050	132.8	86.32
S1	143.79	93.46
S2	143.55	93.30
S3	143.67	93.38

6.13 Results from Tensile Test of Different Layers

It has been established that higher number of layers result in high strength. To further verify this effect, tensile test was carried out on three dog-bone specimens made by using foils of different thickness. Each specimen was 2.7mm thick and the thickness of the paste layer was 0.1mm. Table 6.10 shows the number of layers and thickness of the foils used.

Table 6.10: Specification of the Al specimens for tensile test

Thickness (mm)	Number of foils
0.05	18
0.1	14
0.2	9

In theory, the more the number of foils used for a particular thickness, the more the strength should be. Using different number of foil layers (of different thickness) to make testing specimens of the same thickness (2.7mm) is one way to study the effect and analyse whether or not a linear relation exists between number of foils and strength. Fig. 6.40 shows the result of the tensile test carried out on the three specimens in comparison with the Al 1050.

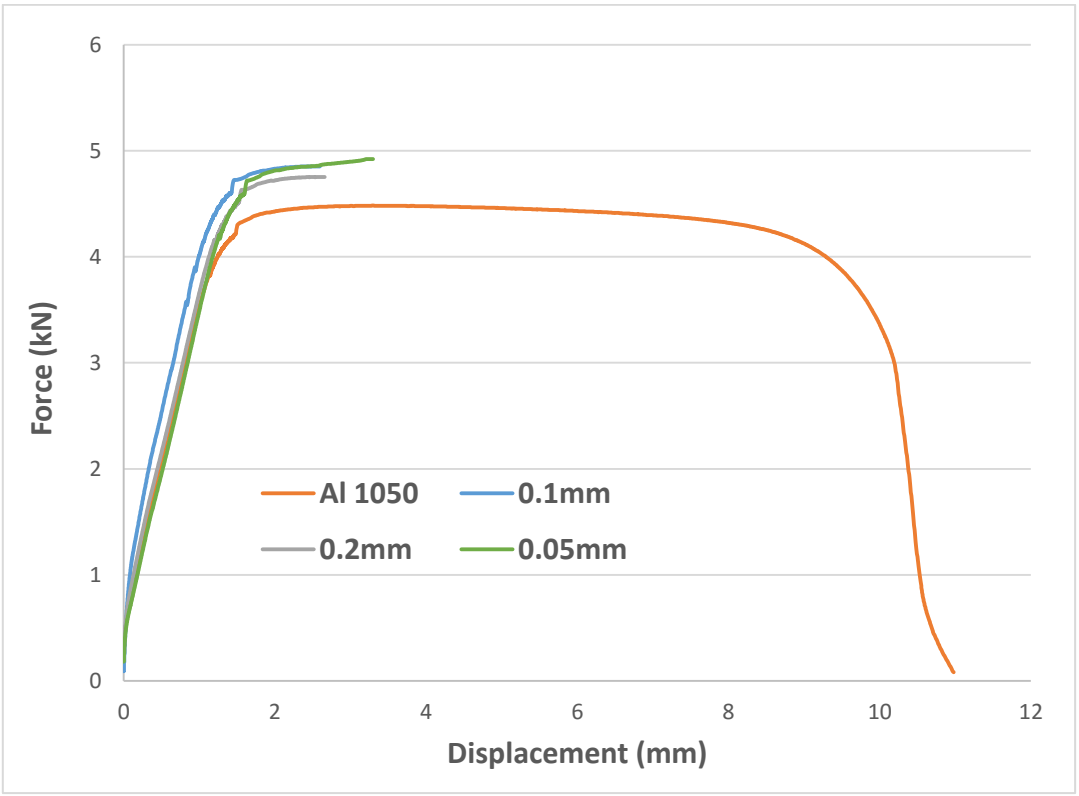

Figure 6.40: Tensile test results of Al foils with different thickness

The values obtained from the tensile test are plotted in Fig. 6.41 which shows a linear relationship between number of layers and force values. It clearly indicates that the more the number of layers used for a particular thickness, the more force is required to fracture the part.

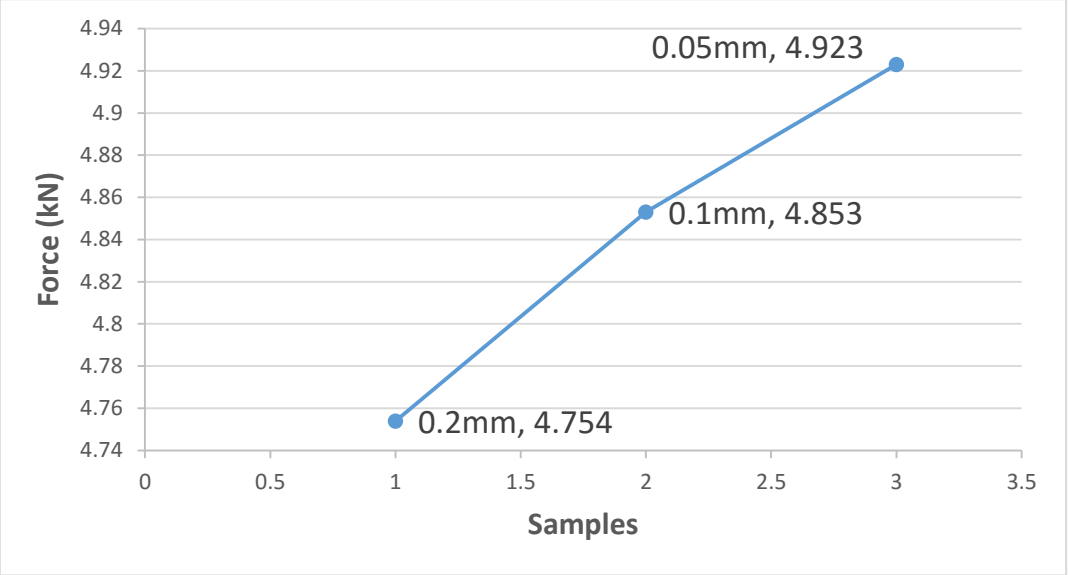

Figure 6.41: Relationship between strength and Al foils of different thickness

6.14 Results from Al/Cu Lap-shear Test

Single lap joints of Al/Cu composite using various thickness foils were produced and tested at a speed of 10mm/min. The reason for testing foils of different thickness values at the same speed was to analyse the effectiveness of the bond and whether or not the fracture values correspond to the tensile force for each thickness. A total of five specimens were tested for each thickness value. All fractured within the base metal and not at the bonded area. As in tensile testing, specimens failed at locations with minimum cross-sectional area (i.e. the base metal, instead of the lapped region which had twice the cross-sectional area). Since copper is stiffer than aluminium, it was held in the movable gripper as recommended by the standard. Aluminium foil fractured in each test because copper is stronger than aluminium having a

greater modulus of elasticity. All the special measures were taken to ensure repeatability of results by carefully monitoring factors such as lap joint length, gauge length and asymmetric loading. The lap joint was kept at a length of 12.5mm for the samples according to the standard. The test specimens were symmetrically placed in the grips, with each grip (50 ± 1) mm from the nearest edge of the overlap. Additional foils were used in the grips so that the applied force will be in the plane of the bond as shown in Fig. 6.40.

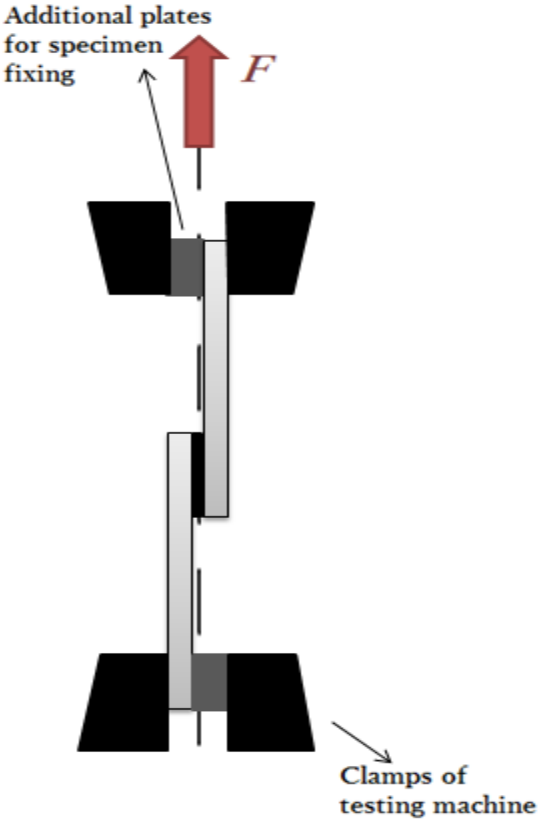

Figure 6.42: Schematic drawing showing single lap joint in clamps

Fig. 6.41 shows the failure mode of the lap-shear specimens and Fig. 6.42 shows the graphs for the three thicknesses. All the specimens failed at breaking forces approaching the tensile force needed to cause fracture in a particular thickness of the aluminium foil. The failure pattern was always substrate failure (SF).

Figure 6.43: Failure modes of Al/Cu single lap-shear specimens

6.14.1 Effect of Material Thickness

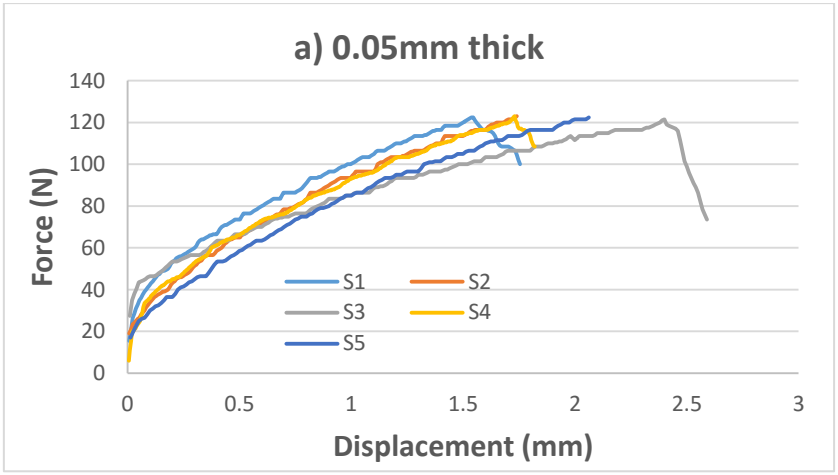

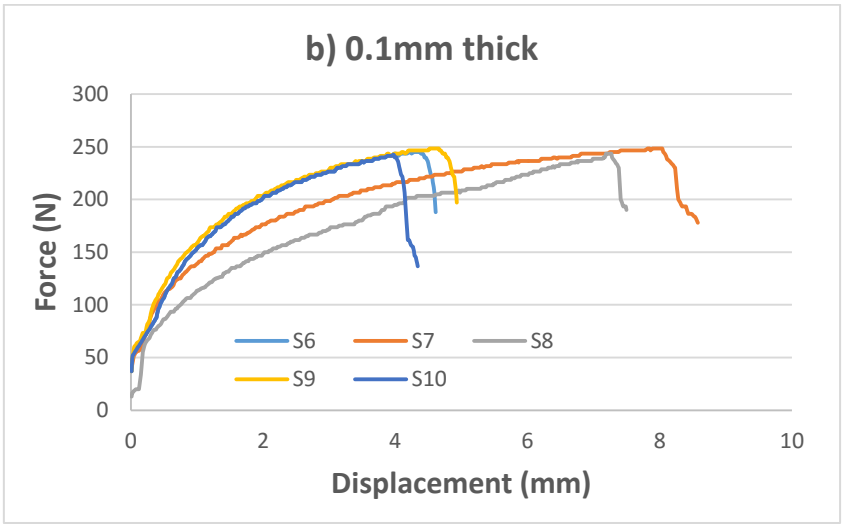

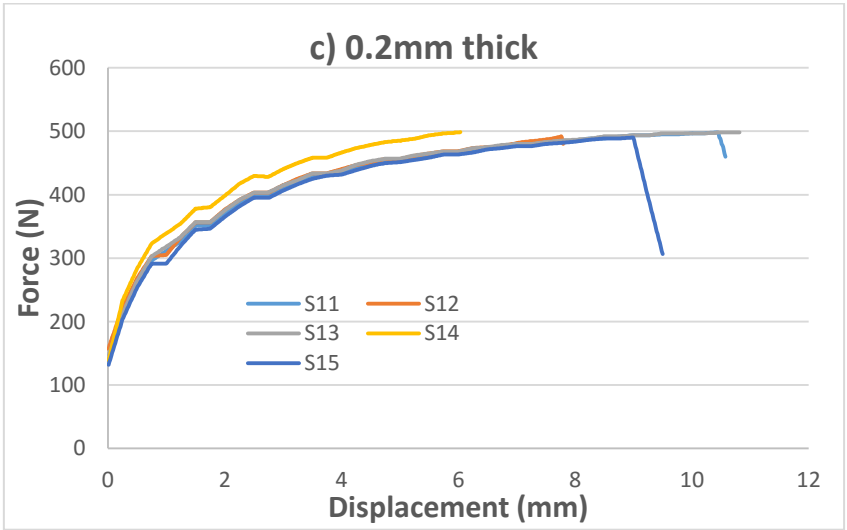

Figure 6.44: Lap shear test results of Al/Cu specimens: a) 0.05mm foil; b) 0.1mm foil; c) 0.2mm foil

6.14.2 Calculation of Lap-shear Strength

All the tests resulted in substrate failure which does not provide the value of lap-shear strength of the bond or in other words joint tensile strength (6). Cohesion failure is required to experimentally calculate this value and could only be achieved by using thicker plates (10mm) rather than thin foils. Cohesion bond failures result in fracture of the bond and are characterised by the clear presence of the brazing paste on the matching faces of both substrates. Aluminium 1050 and copper plates were cut according to the dimensions. Five specimens were tested at 100mm/min (Fig. 6.44) to get a mean value of the joint tensile strength produced by the proposed process of CMFM. Fig. 6.43 shows the cohesion failure of one of the five specimens.

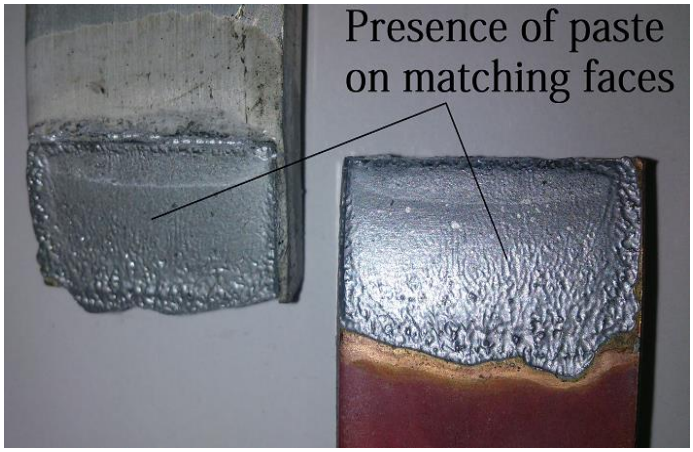

Figure 6.45: Cohesion failure of Al/Cu specimen

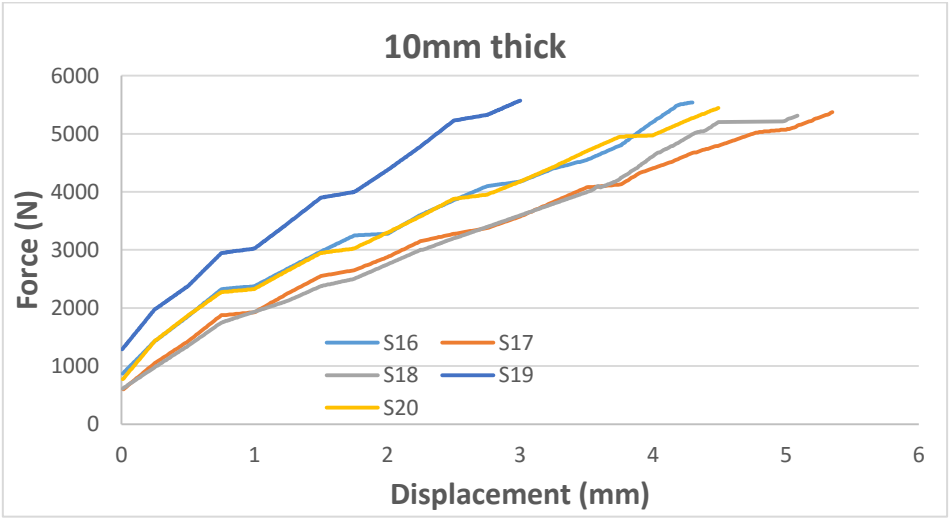

Figure 6.46: Lap shear test of Al/Cu specimen resulting in cohesion failure

The values of the bond shear strength and joint tensile strength are calculated by using equations (6.1) and (6.2). They are presented in Table 6.9.

Table 6.11: Calculation of joint tensile strength for Al/Cu specimens

Specimens	F_{max} (N)	Bond Shear Strength (N/mm^2)	Joint Tensile Strength (N/mm^2)
S16	5540	17.728	22.16
S17	5370	17.184	21.48
S18	5310	16.992	21.24
S19	5572.5	17.832	22.29
S20	5445	17.424	21.78
		Average = **17.432**	Average = **21.79**

The experimental calculation yields shear strength of 17.432 MPa (N/mm^2) for the bond produced by the brazing paste used. This value is relatively high as compared to some of the industrial adhesives (Da Silva, et al., 2009) including a very ductile polyurethane adhesive (Sikaflex-255 FC with a shear strength of 8.26 MPa) and an intermediate two-component epoxy adhesive (Araldite® 2015, with a shear strength of 15.9 MPa, from Huntsman). The joint tensile strength is 21.79 MPa and must be kept in mind while designing products using CMFM.

6.15 Results from Peel Test

In a peel test, when the two ends of the specimen are pulled apart, all stress is concentrated in a single line at the end where the bond is being destroyed. Stiffness of the substrates has significant effects on the results: the stiffer the substrate, the more the load tends to be distributed away from the centre line at the leading edge of the bond, causing the apparatus to measure cleavage rather than peel. Since copper is more stiff than aluminium, it was held in the movable gripper as recommended by the standard (BS EN ISO 11339:2010, 2010). The test was carried out at a peel rate of 10mm/min and similar fracture modes were observed as with aluminium peel test specimens (Fig. 6.45). It is evident that aluminium caused the

fracture of the specimen and not copper because copper is stronger than aluminium having a greater modulus of elasticity.

Figure 6.47: Fracture modes of Al/Cu peel test

The two failure modes were (Fig. 6.46):

1. When there was a clear break at the beginning of a soldered region (when a load was applied) indicating an effective bond giving a high load ranging from 56.5-52N.

2. When a sample did not break at the beginning of soldered region but failed as the breaking points grew under loading. Typically such failure resulted in soldered loads of around 50.5N.

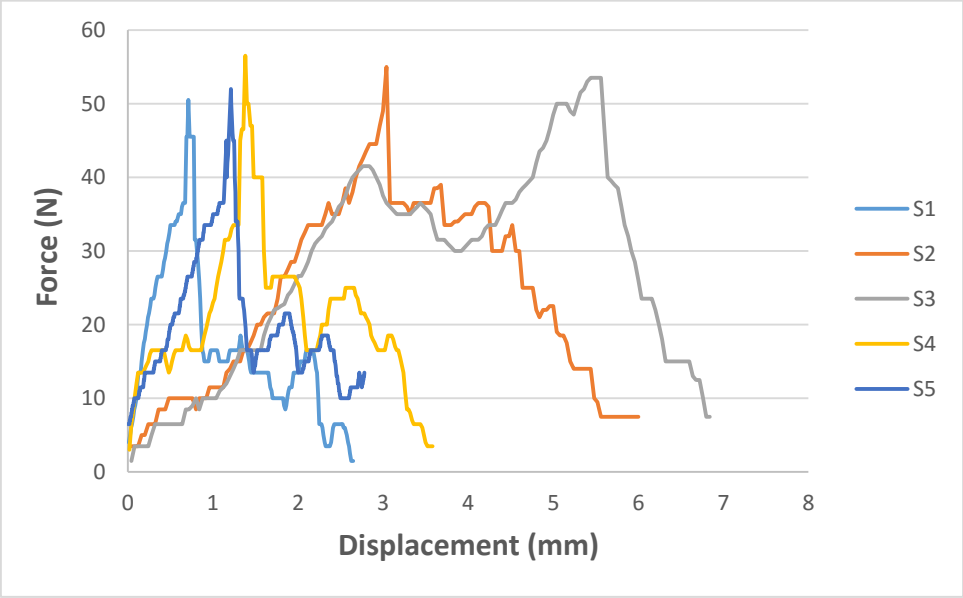

Figure 6.48: Peel test of Al/Cu specimens

Table 6.10 calculates the average force (from the graph) and peel strength which is obtained by dividing the maximum force with the cross-sectional area (0.1 mm x 25 mm = 2.5 mm^2) of each specimen.

Table 6.12: Peel test calculations of Al/Cu specimens

Specimens	Maximum Peeling Force (N)	Average Peeling Force (N)	Peel Strength (N/mm^2)	Type of Failure
S1	50.5	16.85	20.2	Cohesive Substrate Failure
S2	55	23.2	22	
S3	53.5	21.24	21.4	
S4	56.5	20.78	22.6	
S5	52	20.15	20.8	
Average Peel Strength = 21.4 N/mm^2				

The maximum force for the peel tests was much lower than the maximum force for Al 99.5 which is 250N (100MPa or 100N/mm^2) for a cross-sectional area of 2.5 mm^2 (25 mm x 0.1 mm). Aluminium failed in every test because of having less strength as compared to copper and the same was observed with lap testing as well where aluminium failed during testing and not copper. The failure pattern was always delamination failure with the designation DF meaning that the substrate failed by splitting in layers.

6.16 Results from Microstructural Analysis

This test was important to identify the proportion of bonded to unbounded area within the peel specimen. At this point, it is a sandwich of two layers brazed together which makes the analysis simpler and will give an estimation of the bonding capabilities of the process using dissimilar metal foils. Fig. 6.47 shows a specimen with a uniform layer of brazing paste sandwiched between copper and 1050 aluminium foils. As it is evident, there are no holes in the layer of the paste indicating a good bonded area which is essential for product development.

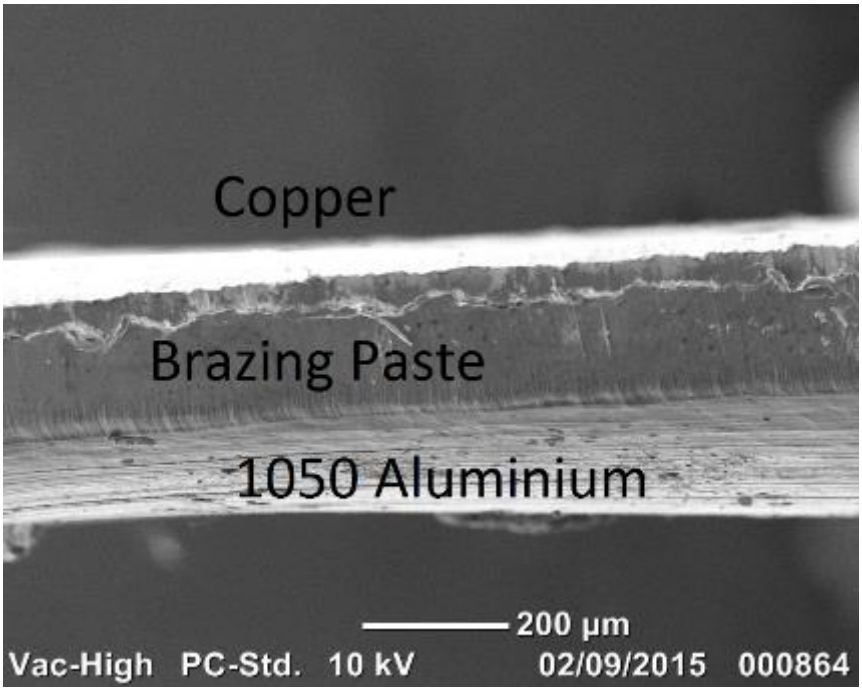

Figure 6.49: SEM image showing layers of Al/Cu peel specimen

There are, however, areas where cracks are present as shown in Fig. 6.48a. These cracks can cause issues which will lead to no-bonded zones in the specimen as is observed in the fracture modes of the peel specimens. The crack in this case is 0.035mm wide (Fig. 6.48b) and cracks of similar dimensions were observed in some places along the length of the specimen. The areas with such cracks can cause abrupt failures; therefore, a more in-depth analysis is required where multiple layers are scanned so as to get a better picture of the bond integrity produced by the process.

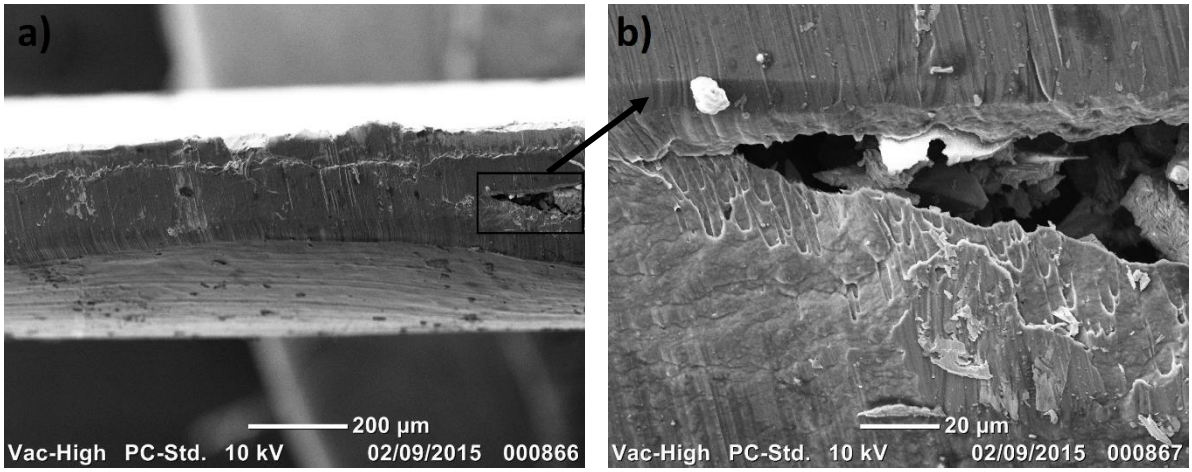

Figure 6.50: SEM analysis of Al/Cu peel specimen: a) Cracks in the paste layer; b) Enhanced image of the crack in the layer

6.17 Results from Dog-bone Tensile Test

This test was very important to demonstrate the effectiveness of the process. In the lap test, only 12.5mm of the foil was joined to another foil. In the peel test, although 150mm length was joined, there were still only two foils involved. Those tests gave an indication of the bond integrity and strength but to gain a better understanding, a multi-layer structure is needed. In a multi-layer structure, brazing is on both sides of the foil and it will truly test the integrity of the bond among the layers when subjected to tensile loading. A dog-bone specimen with aluminium and copper foils bonded alternately was made and tested. Fig. 6.49 shows the fracture modes of the specimens. As expected, both aluminium and copper showed considerable necking but the composite specimen did not show any such characteristics.

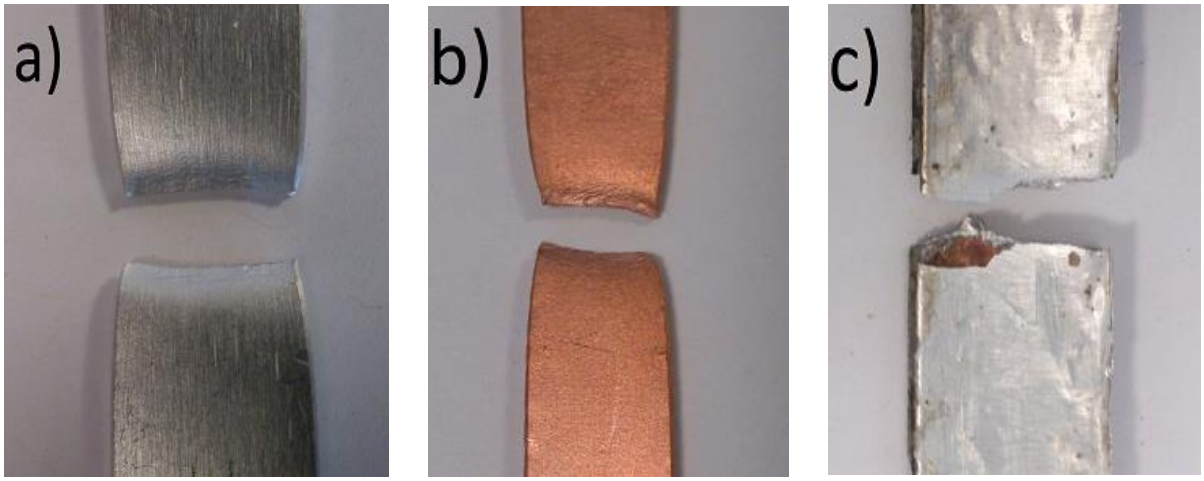

Figure 6.51: Fracture modes of the test specimens: a) 1050 Aluminium; b) Copper; c) Composite

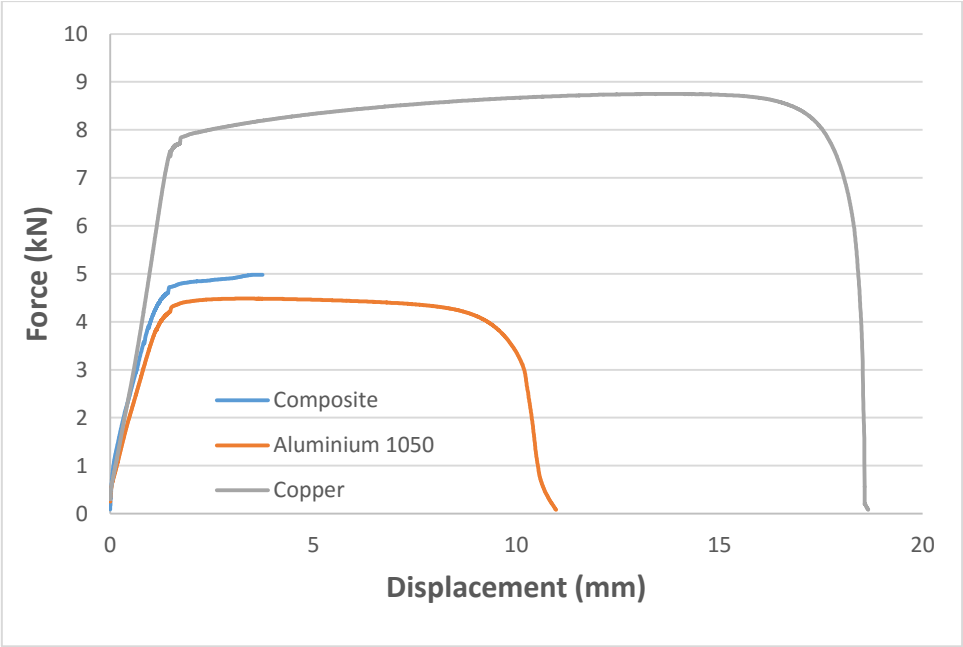

Figure 6.52: Comparative tensile test among Al, Cu and Al/Cu specimens

A composite of two materials is expected to have properties that either lie somewhere between the two or is completely different from the two materials from which it was made. Fig. 6.50 shows the curves for the three tested specimens. Both copper and aluminium, being ductile materials show a curve with well-defined elastic and plastic regions whereas it is not the case with the composite specimen. It showed an elastic region but the plastic region is much shorter as compared to the other two curves on the graph. It is important to note that the

maximum force value for the solid 1050 aluminium specimen is 4.484 kN whereas the composite specimen showed maximum force value of 4.98 kN, making it 11% stronger in comparison. It also has a higher modulus of elasticity (75 GPa) as compared to 1050 aluminium (69 GPa). This test demonstrates that the process is capable of producing composite specimen that is stronger than the weaker of the two metals from which it was produced. The reason for the high strength of the specimens is the same as with the other tensile tests that the yield strengths of the metal and the paste add up in theory. An increase of 11% in case of a composite is proof that a different part is produced otherwise the increase should have been around 8% as seen with aluminium dog-bone specimens. The extra 3% is because of the presence of copper that makes for an exciting new prospect for composite production using CMFM.

Copper (Fig. 6.51a) and 1050 aluminium (Fig. 6.51b), being ductile material show inclusions that act as tiny stress concentrations. They either fracture or separate from the matrix, nucleating voids that grow and link up, ultimately causing fracture.

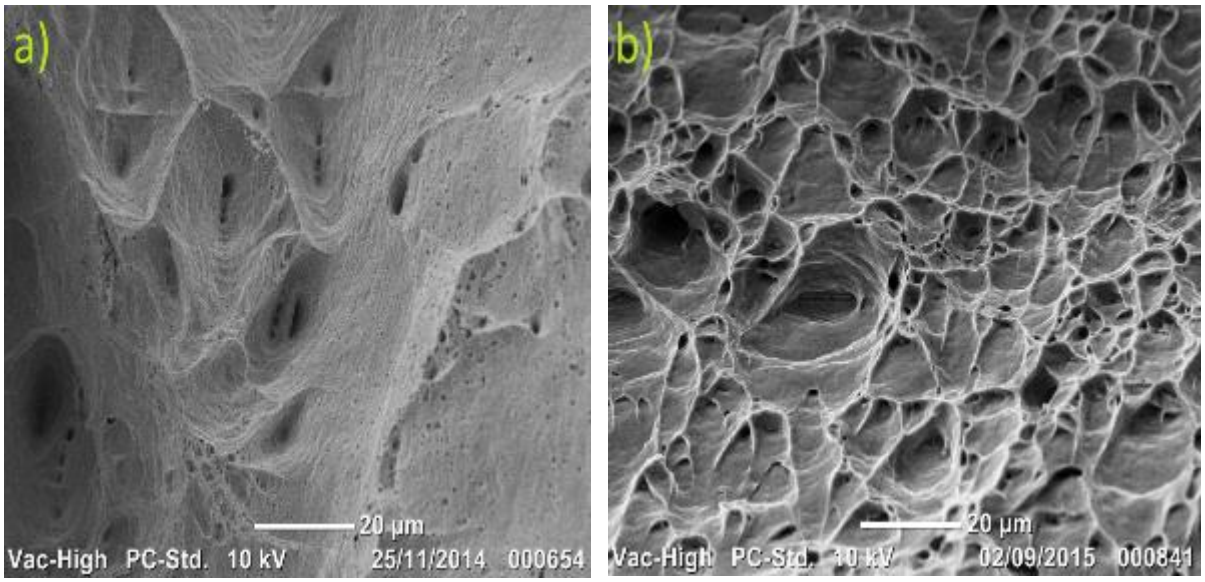

Figure 6.53: SEM analysis of parent metals: a) Copper; b) 1050 Aluminium

The composite specimen (Fig. 6.52a) shows the layer of paste sandwiched between copper and aluminium. The layer of paste has cracks and holes as were seen in the SEM analysis of the peel specimens. However, the result is a specimen that is 11% stronger than aluminium but weaker than copper. Fig. 6.52b and 6.52c show the SEM analysis of the two metal foils covered with paste and showing some inclusions at the fractured region.

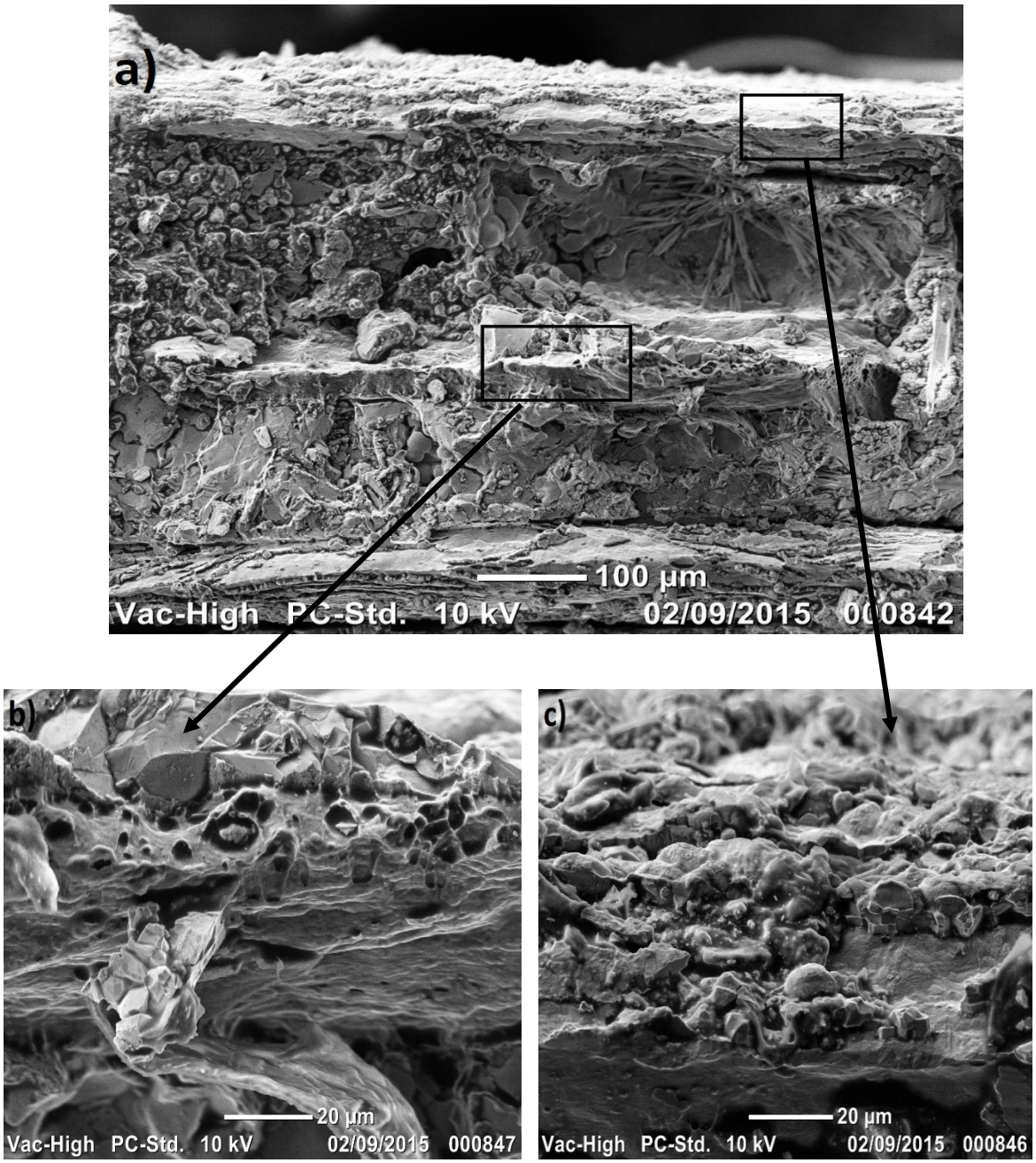

Figure 6.54: SEM analysis of Al/Cu specimen: a) Composite specimen; b) Copper layer; c) Aluminium layer

6.18 Summary

This chapter presented details on all the testing specimens produced and experimentation done following relevant British and International Standards. Three sets of tests were conducted using foils of; (i) copper, (ii) aluminium 1050 and (iii) composite of aluminium 1050 and copper. Tensile lap-shear testing, peel testing, comparative tensile testing and microstructural analysis was carried out on all the specimens. The testing for copper, using 0.1mm thin foils, demonstrated the capability of the process. Copper specimens were produced using direct aluminium solder paste. Tensile lap-shear test and peel test showed promising results. Microstructural analysis showed the presence of an intermetallic bond necessary for joining operation and the comparative tensile test showed that the composite copper (part produced by CMFM) is 11% stronger than the part produced by conventional methods (machining from a solid copper block). After establishing that the process is capable of working with copper, tougher metals with poor solderability were used to ensure flexibility and efficiency of the process.

Aluminium is one of the most difficult metals to join because of the presence of a tenacious oxide layer. The process was able to remove the oxide layer from the thin foils (0.05mm, 0.1mm and 0.2mm) with ease and join aluminium 1050 foils together using a special, 80% zinc and 20% aluminium, brazing paste. Aluminium single lap joints were subjected to various tests; testing speed did not have any effect but changes in thickness and lap length greatly influenced the failure force values. These results are in agreement with the work done by Da Silva, et al. (2009). Shear strength of the bond produced by the brazing paste was also calculated by using 10mm thick plates and observing cohesion failure. The value was calculated to be 52.378 MPa (N/mm^2) which is quite high as compared to some industrial adhesives (Da Silva, et al., 2009). The test results were also compared to the work done by Kong, Soar and Dickens (2002) and it was observed that the single lap joints produced by

CMFM are not influenced by changes in parameters and do not require optimization in the same way as joints produced by UC do. Aluminium peel specimens were also tested at different peeling rates but showed consistent failure modes and force values. Upon comparison with the work done by Kong, Soar and Dickens (2005), it was observed that the peel strength of specimens produced by CMFM is twice the peel strength of specimens produced by UC. These comparisons clearly show the superiority of CMFM over UC. Galvanic corrosion is considered to be a major concern and any corrosion in the bond/foil interface would seriously undermine the strength of the specimen. Therefore, peel specimens were kept in a solution of sodium chloride plus water and tested to analyse whether or not the peel strength has been affected. The peel strength was the same as with other peel testes (20 MPa) showing that the parts produced by CMFM do not face the problem of galvanic corrosion. Microstructural analysis showed good proportion of bonded to un-bonded area which is essential to ensure proper bonding. The comparative tensile test showed that the composite aluminium is 8.25% stronger than part machined out of an aluminium 1050 solid block. The ability to join thin aluminium foils which is a tough task using conventional methods and produce stronger parts, has brought CMFM to the fore-front of technological advancements.

In addition to working with aluminium, CMFM is also capable of producing composites in the same way as producing same material parts. It is a big advantage and does not require the use of additional equipment or machinery. The same tests were conducted as with copper and aluminium. Copper is stronger than aluminium and it was evident from the testing as in single lap joints and peel specimens, the failure was always due to the fracture of aluminium. Microstructural analysis showed the two metals bonding very well with the presence of an intermetallic bond. The comparative tensile test of the composite with aluminium and copper specimens showed that the composite is 11% stronger than aluminium, the weaker of the two

parent metals. This implies the production of a composite with entirely different properties than the metals from which it was produced. The 11% increase in strength is the reason for that otherwise the increase should have been 8.25% as seen with composite aluminium specimen which is not the case here. The experimental test results are promising and prove that CMFM has a sound potential to be a strong candidate in the field of metal additive manufacturing.

CHAPTER 7

7 Conclusions and Future Work

In this research, a new additive manufacturing process for the production of low-cost and high quality metal parts was introduced. It is termed as Composite Metal Foil Manufacturing which is a combination of Laminated Object Manufacturing and soldering/brazing techniques. A conceptual model of a machine based on the principles of the proposed process was presented along with a flow chart of operation. All the major components involved in the manufacturing of metal parts was described in detail for their functional capabilities either by experimental work or numerical analyses. The thermal effects due to heating via stainless steel plates to produce parts was modelled in a three dimensional environment using transient thermal analysis and it could serve as a reference model for future parts that will eliminate guess work for heating time. Dispensing of the paste is a crucial part of the process. The capabilities of the 710 applicator were analysed by making use of CFD analysis to calculate the exact amount of paste dispensed at any given time. The practices utilized to produce metal parts were justified for every step and the materials used. A transient thermal analysis model was also presented verifying the time taken to produce a single lap joint which could also be used for future parts. Metal parts were produced from pure copper foils, aluminium 1050 with H14 ½ hard temper and composites of the two metals using foils of various thicknesses. They were made as single lap joints, T-peel specimen and dog-bone specimens to investigate their mechanical properties. Microstructural analysis was also carried out to assess the proportion of bonded to un-bonded area which was essential for proper bonding of the foils. The tests were promising and showed that the process is not only capable of producing high quality parts but can also produce stronger parts compared to conventional machining/subtractive methods.

7.1 Answers to Research Questions

- Can LOM effectively work with joining methods such as brazing and soldering?

Chapter 3 and 5 have shown that a process based on the integration of LOM with soldering/brazing is possible. The process has been termed as Composite Metal Foil Manufacturing and is capable of producing metal parts as well as composites effectively.

- How will the proposed process be automated?

Chapter 3 gives a conceptual model of a machine based on the principle of CMFM. A fully automated flow chart involving every component in operation has also been presented.

- What type of geometries can be made using the proposed process?

CMFM can easily produce large parts and is not restricted to the production of flat parts only. It can produce parts with complex geometries, cavities, over-hanging elements, circular parts etc., as has been explained in Chapter 3.

- How much post-processing will be involved?

CMFM involve minimal post processing to remove ridges due to excess paste but does not require any secondary operation for enhancing the mechanical properties. The part after passing through the heated plates is ready to use for any engineering application.

- Will the produced parts be of satisfactory quality for comparison with other processes?

Chapter 6 has given extensive comparisons of the parts made by CMFM to other processes. Single lap joints showed consistent results as compared to joints produced by UC. The peel strength of t-peel specimens produced by CMFM was twice the peel strength of specimens produced by UC. The comparative tensile tests showed increase in strengths compared to conventional machining methods. The parts produced by CMFM showed 11%, 8.25% and 11% increase for copper, aluminium and composite specimens respectively.

- Will produced parts be free from cracks, voids and cavities as a result of thermal stresses?

The effects of thermal stress and strain were briefly described in Chapter 3 and 5 using ANSYS. The simulated results show that the effects were not causing major damage to the mechanical integrity of the parts. Microstructural analysis, however, showed voids at areas where there was no bond. Heating did not cause any voids, cracks or cavities in the parts.

- How fast will the proposed process be able to produce parts?

Chapter 5 gave a timeline for the production of a 7mm thick aluminium spanner that took 20±3 minutes to be produced using CMFM. On the other hand, same product in a DMLS machine would take more than an hour; 15 minutes to fill the machine chamber with an inert gas, 5 minutes mounting and levelling the build platform, 10 minutes for part production, with another 30 to 40 for cleaning up after and setting up for the next batch.

- How will the material properties be affected in the proposed process?

The material properties were affected due to heating as the operating temperatures reach the annealing temperatures for both aluminium and copper. More attention is given to aluminium because it is the weaker of the two metals having a lower modulus of elasticity. The foils of aluminium are grade H14 which are work hardened by rolling to half hard and are not annealed afterwards. In the annealing temperature range (300-410°C), the crystalline structure of the material starts to relax, thus making it more malleable. There is also a danger of over-heating which may result in stress relieving, sagging or warping, change in temper, surface conditioning, re-alloying, hot cracking and a worst case scenario is a meltdown of the material in use. The process of brazing uses heat in a localized area (to be joined) and stresses in aluminium from shearing and drawing can change, and result in distortion or deformation. In Chapter 3, structural analysis has been carried out to analyse the effect of thermal stress, strain and deformation due to the heat transfer process on a single lap joint of

aluminium/copper. Also, the results from tensile testing of dog-bone specimens in Chapter 6 show that the strength increases with increase in the number of layers. Since the paste is making an intermetallic bond with the metal foil, the foil becomes alloyed and that is the reason for the higher strength of the bonded dog-bone specimens compared to solid ones. These results show that the material properties are affected in such a way that they make the mechanical properties of the parts better.

- To what extent can the proposed process reduce cost of production?

As explained in Chapter 3, the usage of metal foil has largely reduced the cost of production because foils are very low-cost compared to metal powder and metal wire that other metal additive manufacturing processes utilize for the production of parts. Furthermore, there is minimal post-processing involved and no need for additional machinery to produce multiple materials parts. This adds flexibility and versatility to the system which is something that other processes struggle with.

- Does the proposed process have the capability to compete with rival metal prototyping technologies?

  CMFM is still in its early stages and would need more testing and numerical analysis to establish itself as a competitor but the initial testing has been promising as shown in Chapter 3, 5 and 6. With more research work, the proposed process has the potential to be a strong candidate in the field of metal prototyping.

7.2 Novel Contributions to Knowledge

The emphasis on the production of metal parts with additive manufacturing led to this research. A new process was required to overcome the limitations that existing AM technologies face. LOM and soldering/brazing techniques were integrated together to form a new additive manufacturing process called Composite Metal Foil Manufacturing. The aim and objectives outlined in Chapter 1 have all been met by the subsequent chapters. Chapter 2

reviews and analyses the existing metal prototyping processes along with their limitations. LOM was selected to be a part of the new proposed process based on its simplicity and ease of operation in terms of automated cutting and stacking. The chapter also sheds light on the choice of soldering/brazing as a suitable metal joining operation. Chapter 3 gives an in-depth description of a conceptual model of an automated machine based on the process along with a flow chart of operation. All the components of the machine are validated for their functional capabilities either by experimental work or numerical analyses. A three dimensional model for analysing the heat transfer process has also been presented in this chapter that would serve as a reference model for future parts. Dispensing of paste is a very important part of the process and Chapter 4 gives the description of 710 applicator appropriate for the brazing paste. CFD analysis has been carried out that calculates the exact amount of paste being dispensed at any given time. The electrical connections and C++ programming to establish communication between the dispenser and the main machine has also been presented. Appendix A describes the working of another dispenser that could be used instead of or in addition to the 710 applicator. The information presented in Chapter 3 and 4 can be used to buy the components and build a machine based on the principles of CMFM.

The process was broken down in to simple independent steps so that without the actual automated machine, the parts can still be produced for mechanical testing. Chapter 5 gives a detailed explanation and justification of every step, materials and equipment used. A three dimensional model has been presented to validate the heating time for the production of parts which can be used as a reference for future parts using the practices. The experimental data presented in Chapter 6 is based on the use of British and International Standards. This chapter gives information of the specific standards used for tensile lap-shear testing, peel testing, corrosion testing, microstructural analysis and tensile testing. The tests provide

promising results with the parts produced by CMFM showing better experimental consistency and strength values after testing as compared to parts produced by UC. These results show the superiority of the new proposed process in comparison to UC which has been researched upon for years. The parts produced by CMFM are cost effective and high quality. They can withstand high temperatures (based on the operational temperature of the paste used) and are stronger than the parts joined by industrial adhesives. Galvanic corrosion which is a major problem with aluminium is not a factor and does not affect the bond/foil interface. The dog-bone specimens produced by CMFM showed 11%, 8.25% and 11% increase for copper, aluminium and composite specimens respectively, when compared with parts machined out of corresponding solid metal blocks.

7.3 Future Work

The approaches described in this thesis are supported by literature and experimental work. It is clear from the work done that the process of CMFM is an interdisciplinary research integrating mechanical, materials science, thermos-mechanical engineering, process planning, electrical aspects. Significant research and further understanding are required to better establish CMFM as a strong candidate in the field of metal prototyping.

7.3.1 Building the Automated Machine

A conceptual model of an automated machine based on the principle of CMFM has been presented in Chapter 3. All the components have been identified and validated for their functional capabilities. It is to be noted that building a machine from scratch is a resource and time consuming process especially with such an automated machine. It would generally take a large company working with all its resources and having the expertise of different departments. This process of building the machine can easily branch out into different research areas including mechanical, electrical, programming, integration etc., which clearly makes it something to be done in the future.

The 300W fibre laser from MIYACHI is a state of the art piece of equipment capable of focussing to about 15μm that makes it feasible to remove the minimum amount of material, resulting in extremely high precision and accuracy. It also offers minimal thermal input, with fine control over how hot the work area gets. This aspect is important because small parts heat up quickly and might otherwise overheat or deform. It is a powerful piece of equipment with little energy loss while cutting and that makes it a perfect component for the required process. It can be operated at various speeds depending upon the thickness of the sheet being used. The dispensing mechanism has been explained in Chapter 4 with CFD analysis of the versatile 710 applicator capable of depositing precise and accurate amount of paste at any given time. The electrical connections and the C++ code to establish communication has also been presented. The roller is fitted with Nip Pressure Measurement System (NPMS) to measure nip pressure and force which takes the guesswork out of adjusting rollers leaving behind a smooth and uniform layer of paste necessary to ensure dimensional accuracy. The Microtrak™ 3 TGS laser displacement sensors are utilized on either side of the build platform to measure thickness of the part being produced at all times. They are non-contact and use the laser triangulation technology with a solid-state laser light source and a CMOS (complementary metal-oxide semiconductor) detector. These sensors have a sampling frequency of 40 kHz that makes a time period of 50μs which makes feedback to the system very quick. The system keeps track of the thickness reading and if required sends a command to add more foils to the previously calculated layer data to ensure accuracy in the Z-direction. The heated plates are available from Watlow and are fitted with FIREROD cartridge heaters. They are made of stainless steel and both can be operated independently. They join the paste-coated foils together by applying heat and pressure. There are two versions of the plates with different dimensions; 150mm by 300mm and 400mm by 400mm with a thickness of 8mm. They can go up to a maximum of 550 °C and provides constant pressure throughout the entire

length of the plates. The information presented can be utilized to build an automated machine capable of producing stronger metal and composite parts compared to conventional methods.

7.3.2 Transverse Tensile Testing

The tested parts in the research include single lap joints, t-peel specimens and dog-bone specimens as shown in Chapter 6. More parts can be produced and tested to analyse the effects on various aspects of the parts. For example, the tensile test was carried out on the dog-bone specimen in the longitudinal direction as it is the most common tensile test performed on all types of materials. The results were highly in favour CMFM. Transverse tensile test can also be performed on the same specimen to measure the transverse tensile strength, yield strength, proof stress, elongation and reduction in area (Fig. 7.1). However, special care must be given while adjusting the specimen in the grippers of the machine as it is important to hold the same thickness at both ends to ensure a valid result. It is expected that the result would be cohesive substrate failure as was observed during peel testing of the t-peel specimens. It is a rather uncommon scenario and generally specimens are not tested in transverse direction, but there is a possibility that transverse testing might reveal interesting results that may or may not be in favour of the efficient of the process. Hence it is something that should definitely be done in the future.

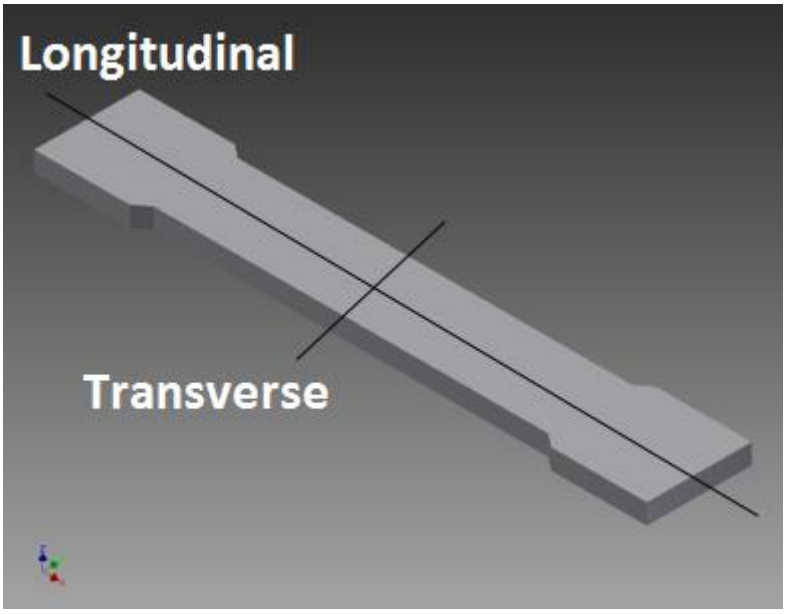

Figure 7.1: Transverse and longitudinal direction for tensile testing

7.3.3 Testing in Different Orientations

The current tensile test was done by laying down layers in XY plane and height in the Z-direction as shown in Fig. 7.2, option 3. Two different orientations can also be tested to analyse their effect on the mechanical properties of the material. It is to be noted that option 3 from Fig. 7.2 was chosen because it is the most common type of specimen and it takes less number of layers as compared to options 1 and 2. The other orientations were avoided as Z-direction oriented specimens tend to be more expensive and time consuming because of the high number of layers (Pilipovic, Raos and Sercer, 2011). Different orientation of layers will yield different results that would make for an exciting extension to the tensile properties of parts produced by CMFM.

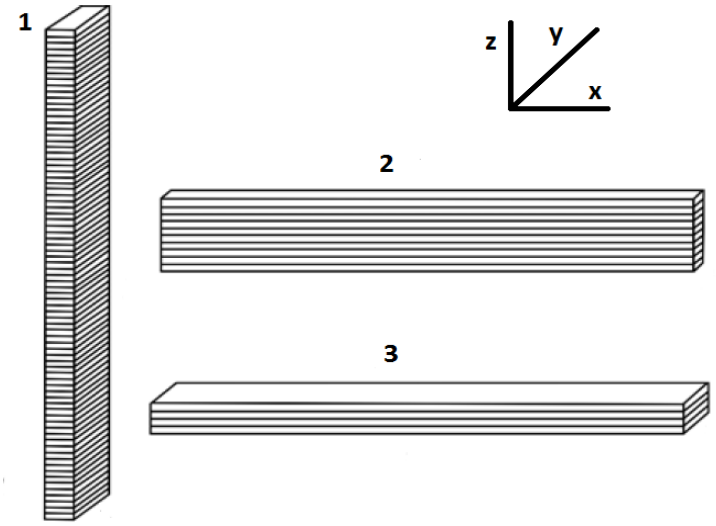

Figure 7.2: Different orientation of layers for the production of parts

7.3.4 Additional Tests

The reason for limiting the tests to lap-shear, peel and tensile properties was to gain an understanding of the mechanical integrity of the parts produced by CMFM. But to establish this process as a viable candidate, it is necessary to perform tests in other appropriate conditions and scenarios as well. Testing the specimen under different loading conditions is one way of achieving that goal. The tensile test has already taken care of the tension mode of loading; the others include compression, bending and torsion (Fig. 7.3). Compression testing was not performed because the foils were already pressed down by sandwiching them between two stainless steel plates fitted with nuts and bolts. A constant torque of 60Nm was applied for the production of each specimen. Bending was not done because the tests showed the parts produced by CMFM have higher fracture values as compared to parts produced by conventional machining methods. They behave in the same way as wood laminates do that can be bent without any loss of strength (Barbu, Reh and Irle, 2013). One of the parameters from torsion test is the calculation of shear strength and it has been shown in Section 6.13 without performing the test by using an existing relationship between the tensile and shear strength. The problem with torsional testing is that a number of assumptions have to be made

for the results to be valid (Khokhar, 2011). The parts produced by CMFM are first and foremost composites of metal foil and paste. Both have different characteristics and don't fulfil the assumption of being homogeneous, isotropic and linearly elastic. Fatigue testing was also set aside for future as it takes a long time to perform HCF and even at LCF, parts produced by CMFM would have had a number of problems. Fatigue life is largely influenced by microstructure, presence of oxidizing or inert chemicals, surface finish, temperature, frequency of operation (Forrest, 2013). In terms of microstructure, parts produced by CMFM are composites of metal foils and solder/brazing paste. They have been heat treated and then allowed to cool. They also have inclusions and voids not to mention some imperfections as the process is still in its earlier stages. The use of brazing paste which cannot be fully put down as an isotropic or anisotropic material causes a lot of confusion while assessing its impact on the fatigue assessment (Van and Paradopoulos, 2014). There are simply too many factors to consider for fatigue testing that could affect the outcome. One major issue is the time and frequency of testing (Lee, Barkey and Knad, 2011). As CMFM is a new process and functional parts have not been produced using this process, setting up the frequency will be based on trial and error method. The testing would have to go through LCF and then HCF to have a clear picture of the effects of fatigue which will require time (days, weeks or even months for 10^9 cycles) and resources (Wycisk, et al., 2015).

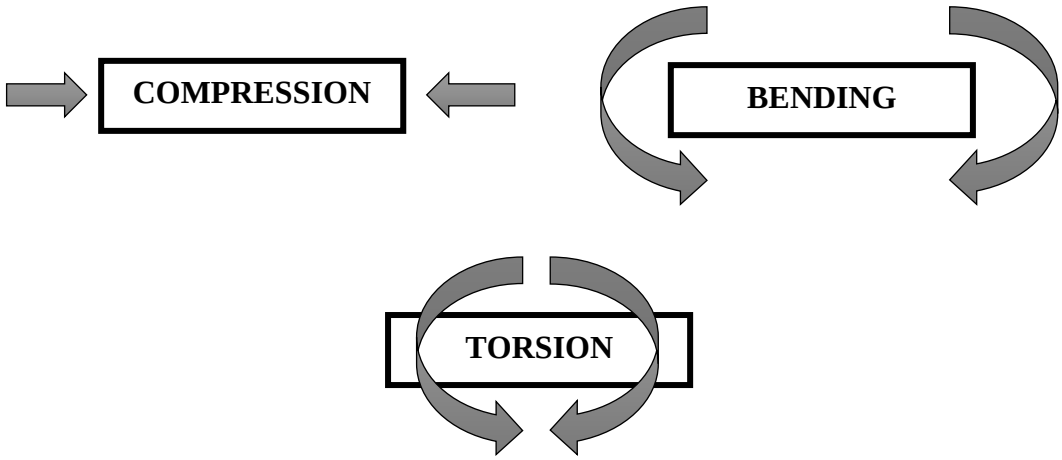

Figure 7.3: Different types of loads

In addition to analysing the effects of different types of loadings, there are a number of tests that are commonly used to examine the mechanical integrity of parts. They include tests such as hardness, creep and stress rupture, fracture toughness, notch-toughness, impact toughness, fatigue, fatigue crack growth rate etc. The fatigue test is particularly of importance as it would indicate the effect of cyclic loading on the parts produced by CMFM and it will be an interesting advancement in understanding their capabilities.

7.3.5 Heat Transfer Analysis

Two 3D models have been presented showing the heat transfer process for producing metal parts in Chapter 3 and 5. The same chapters also contain models for analysing the effects of thermal stress and strain on the parts. The researcher did not formulate analytical solutions because of the complexity posed by the governing equations. The same goes for thermal stress and strain analyses. A future area of research could include the use of sophisticated equipment to experimentally measure these values. Tests conducted in Chapter 6 have indicated that thermal stress and strain did not have any adverse effects on the parts. They were present but the values were not high enough to cause issues. The researcher has touched upon some basic formulae for them but an in-depth analysis using analytical methods could prove to be a very interesting phase of research in the future.

7.4 Concluding Remarks

The process of CMFM has the potential to be a strong candidate in the field of metal prototyping which has been shown by this research work. The process could be optimised for better performance which would result in better quality parts. Additional analytical, computational and experimental work could help in bringing this process from the academic sector to the mainstream manufacturing industries.

References

Adams, R.D., Comyn, J. and Wake, W.C., 1997. *Structural adhesive joints in engineering*. Springer Science & Business Media.

Arduino.com, 2010. *Arduino Uno.* [online] Available at: <https://www.arduino.cc/en/Main/ArduinoBoardUno> [Accessed 30 June 2015].

Armstrong, K.B., 1997. Long-term durability in water of aluminium alloy adhesive joints bonded with epoxy adhesives. *International Journal of Adhesion and Adhesives*, *17*(2), pp.89-105.

Ashby, M. F. and Cebon, D., 1993. Materials selection in mechanical design. *Le Journal de Physique IV*, *3*(C7), pp. C7-1.

ASTM F2792-10:2010, 2010. *Standard Terminology for Additive Manufacturing Technologies.* ASTM International, West Conshohocken, PA, USA.

AuricSolutions.com, 2009. *RLY 108, 8-channel TTL relay board.* [pdf] Auric. Available at: <http://www.auricsolutions.com/downloads/Relay%20Board%20Leaflet.pdf> [Accessed 30 July 2015].

Avery, W. F., 2011. *Direct Aluminium Soldering Paste*. Cleveland, OH, USA: Superior Flux and Manufacturing.

Banerjee, R., Genc, A., Collins, P.C. and Fraser, H.L., 2004. Comparison of microstructural evolution in laser-deposited and arc-melted In-Situ Ti-TiB composites. *Metallurgical and Materials Transactions A*, *35*(7), pp.2143-2152.

Barbu, M.C., Reh, R. and Irle, M., 2013. Wood-Based Composites. *Research Developments in Wood Engineering and Technology, edited by Alfredo Aguilera and J. Paulo Davim. Wood-Based Composites*, pp.1-45.

Baufeld, B., Brandl, E. and Van der Biest, O., 2011. Wire based additive layer manufacturing: Comparison of microstructure and mechanical properties of Ti–6Al–4V components fabricated by laser-beam deposition and shaped metal deposition. *Journal of Materials Processing Technology*, *211*(6), pp.1146-1158.

Bejan, A., 2013. *Convection heat transfer.* John Wiley & Sons.

Bickford, J. ed., 1998. *Handbook of bolt and bolted joints.* CRC Press.

BS EN 1465:2009, 2009. *Adhesives. Determination of tensile lap-shear strength of bonded assemblies*. British and European Standard, London, UK.

BS EN ISO 10365:1995, 1995. *Adhesives. Designation of main failure patterns.* British, European and International Standard, London, UK.

BS EN ISO 11130:2010, 2010. *Corrosion of metals and alloys. Alternate immersion test in salt solution.* British, European and International Standard, London, UK.

BS EN ISO 11339:2010, 2010. *Adhesives. T-peel test for flexible-to-flexible bonded assemblies*. British, European and International Standard, London, UK.

BS EN ISO 6892-1:2009, 2009. *Metallic materials. Tensile testing. Method of test at ambient temperature*. British, European and International Standard, London, UK.

BS ISO 17296-2:2015, 2015. *Additive Manufacturing—General Principles—Part 2: Overview of process categories and feedstock*. British and International Standard, London, UK.

BS ISO 17296-3:2014, 2014. *Additive Manufacturing—General Principles—Part 3: Main characteristics and corresponding test methods*. British and International Standard, London, UK.

BS ISO 17296-4:2014, 2014. *Additive Manufacturing—General Principles—Part 3: Overview of data processing*. British and International Standard, London, UK.

BS ISO 18338:2015, 2015. *Metallic materials. Torsion test at ambient temperature*. British and International Standard, London, UK.

Butt, J., 2011. *A 3D printer using dry powder dispensing device.* MSc Thesis, University of Southampton.

Butt, J., Mebrahtu, H. and Shirvani, H., 2015. A novel rapid prototyping process for the production of metal parts. *International Journal of Advancements in Mechanical and Aeronautical Engineering – IJAMAE, 2*(1), pp.15-18.

Butt, J., Mebrahtu, H. and Shirvani, H., 2015. Peel and tensile test investigation of aluminium 1050 foil parts made with a new additive manufacturing process. *International Journal of Rapid Manufacturing*, *5*(1), pp.95-115.

Butt, J., Mebrahtu, H. and Shirvani, H., 2015. Rapid prototyping by heat diffusion of metal foil and related mechanical testing. *The International Journal of Advanced Manufacturing Technology*, pp.1-10.

Butt, J., Mebrahtu, H. and Shirvani, H., 2015. Thermo-Mechanical Analysis of Dissimilar Al/Cu Foil Single Lap Joints Made by Composite Metal Foil Manufacturing. *World Academy of Science, Engineering and Technology, International Journal of Mechanical, Aerospace, Industrial, Mechatronic and Manufacturing Engineering*, *10*(1), pp.41-46.

Butt, J., Mebrahtu, H. and Shirvani, H., 2016. Microstructure and mechanical properties of dissimilar 1050 aluminium/pure copper foil composites made with a new additive manufacturing process. *Journal of Materials Processing Technology*, *238*, pp.96-107.

Butt, J., Mebrahtu, H. and Shirvani, H., 2016. Strength analysis of aluminium foil parts made by composite metal foil manufacturing. *Progress in Additive Manufacturing*, *1*(1), pp.93-103.

Butt, J., Mebrahtu, H. and Shirvani, H., 2016. Metal Rapid Prototyping Technologies. In: V. M. Petrova, ed. 2016. *Advances in Engineering Research. Volume 14.* New York, USA: Nova Science Publishers, Inc. Ch.2. ISBN: 978-1-63485-930-1.

Byrnes Jr, E.R., 1971. Vacuum flux-less brazing of aluminium. *Weld J.*, 50(10), pp.712-716.

Calignano, F., Manfredi, D., Ambrosio, E.P., Iuliano, L. and Fino, P., 2013. Influence of process parameters on surface roughness of aluminium parts produced by DMLS. *The International Journal of Advanced Manufacturing Technology*, *67*(9-12), pp.2743-2751.

Casey, A.L., Adams, D., Karpanen, T.J., Lambert, P.A., Cookson, B.D., Nightingale, P., Miruszenko, L., Shillam, R., Christian, P. and Elliott, T.S.J., 2010. Role of copper in reducing hospital environment contamination. *Journal of Hospital Infection*, *74*(1), pp.72-77.

Choi, J.W. and Oh, T.S., 2001. Peel strength and peel angle measured by the T-peel test on Cr/BPDA-PDA interfaces. *Journal of adhesion science and technology*, *15*(2), pp.139-152.

Churchill, S.W. and Chu, H.H., 1975. Correlating equations for laminar and turbulent free convection from a horizontal cylinder. *International Journal of Heat and Mass Transfer*, *18*(9), pp.1049-1053.

Connelly, L.M., 2009. Mixed methods studies. *Medsurg Nursing,* 18(1), pp.31-33.

Cormier, D., Harrysson, O. and West, H., 2004. Characterization of H13 steel produced via electron beam melting. *Rapid Prototyping Journal*, *10*(1), pp.35-41.

Custom Part, 2009. *Direct Metal Laser Sintering*. [online] Available at: <http://www.custompartnet.com/wu/direct-metal-laser-sintering> [Accessed 20 July 2015].

Cynebar.com, 2012. *Cartridge Heating Elements.* [online] Available at: <http://www.cynebar.com.au/cartridge-heater.php> [Accessed 12 May 2015].

Da Silva, L.F., Carbas, R.J.C., Critchlow, G.W., Figueiredo, M.A.V. and Brown, K., 2009. Effect of material, geometry, surface treatment and environment on the shear strength of single lap joints. *International Journal of Adhesion and Adhesives*, *29*(6), pp.621-632.

Davis, J.R. ed., 1993. *Aluminum and aluminium alloys.* ASM international.

Davis, J.R. ed., 2001. *Copper and copper alloys*. ASM international.

Davis, J.R. ed., 2004. *Tensile testing.* ASM international.

Deckard, L. and Claar, T.D., 1993. Fabrication of ceramic and metal matrix composites from selective laser sintered ceramic preforms. In: *Solid Freeform Fabrication Symposium* (pp. 215-222).

Dickens, P.M., 1995. Research developments in rapid prototyping. *Proceedings of the Institution of Mechanical Engineers, Part B: Journal of Engineering Manufacture*, *209*(4), pp.261-266.

Ding, D., Pan, Z., Cuiuri, D. and Li, H., 2015. Wire-feed additive manufacturing of metal components: technologies, developments and future interests. *The International Journal of Advanced Manufacturing Technology*, *81*(1-4), pp.1-17.

DuPont, J.N. and Marder, A.R., 1995. Thermal efficiency of arc welding processes. *Welding Journal-Including Welding Research Supplement*, *74*(12), p.406s.

ExtremeTech.com, 2013. *Graphene used to make graphene-copper composite that's 500 times stronger*. [online] Available at: <http://www.extremetech.com/extreme/164961-graphene-used-to-make-graphene-copper-composite-thats-500-times-stronger> [Accessed 20 July 2013].

Facchini, L., Magalini, E., Robotti, P., Molinari, A., Höges, S. and Wissenbach, K., 2010. Ductility of a Ti-6Al-4V alloy produced by selective laser melting of pre-alloyed powders. *Rapid Prototyping Journal, 16*(6), pp.450-459.

Forrest, P.G., 2013. *Fatigue of metals*. Elsevier.

Frazier, W.E., 2014. Metal additive manufacturing: A review. *Journal of Materials Engineering and Performance, 23*(6), pp.1917-1928.

Fumo, M. and Noorani, R., 2015, January. Development of an Expert System for the Selection of Rapid Prototyping and 3D Printing Systems. In: *International Conference on Computer Science Education Innovation & Technology (CSEIT). Proceedings* (p. 14). Global Science and Technology Forum.

Fusion-Inc.com, 2013. *Operations manual, Model 710, Digital dispensing system.* [pdf] Fusion-Inc. Available at: <http://www.fusion-inc.com/wp-content/uploads/2013/10/FusionApplicatorManualLap.pdf > [Accessed 30 June 2015].

Fusion-inc.com, 2013. *Safety Data Sheet ASN-892-XXX*. [online] Available at: <http://www.fusion-inc.com/brazing/alloys-and-paste/aluminum/> [Accessed 20 July 2015].

Gao, Z., Niu, J.T., Yang, S.C., Wang, X.T. and Cheng, D.F., 2013. Soldering of Aluminum matrix composites SiCp/A356 and Kovar alloy. *Engineering Review, 33*(2), pp.123-128.

Gietzelt, T., Toth, V., Lambach, H. and Dittmeyer, R., 2013. Considerations of Microstructural Influences for Diffusion Welding of Metals in Microsystem Technology. *Advanced Engineering Materials, 15*(8), pp.669-683.

Gomes, C.M., Rambo, C.R., De Oliveira, A.P.N., Hotza, D., Gouveˆa, D., Travitzky, N. and Greil, P., 2009. Colloidal processing of glass–ceramics for laminated object manufacturing. *Journal of the American Ceramic Society*, *92*(6), pp.1186-1191.

Gomez, L.P.C., Spangenberg, A., Ton, X.A., Fuchs, Y., Bokeloh, F., Malval, J.P., Tse Sum Bui, B., Thuau, D., Ayela, C., Haupt, K. and Soppera, O., 2016. Rapid Prototyping of

Chemical Microsensors Based on Molecularly Imprinted Polymers Synthesized by Two-Photon Stereolithography .*Advanced Materials*.

Grass, G., Rensing, C. and Solioz, M., 2011. Metallic copper as an antimicrobial surface. *Applied and environmental microbiology*, *77*(5), pp.1541-1547.

Grimm, T., 2004. *User's guide to rapid prototyping*. Society of Manufacturing Engineers.

Gu, D. and Shen, Y., 2006. WC–Co particulate reinforcing Cu matrix composites produced by direct laser sintering. *Materials Letters*, *60*(29), pp.3664-3668.

Gu, D., Shen, Y., Zhao, L., Xiao, J., Wu, P. and Zhu, Y., 2007. Effect of rare earth oxide addition on microstructures of ultra-fine WC–Co particulate reinforced Cu matrix composites prepared by direct laser sintering. *Materials Science and Engineering: A*, *445*, pp.316-322.

Hatch, J.E. ed., 1984. *Aluminum: properties and physical metallurgy*. ASM International.

He, H.Y., Zhang, J.Y., Mi, X., Hu, Y. and Gu, X.Y., 2015. Rapid prototyping for tissue-engineered bone scaffold by 3D printing and biocompatibility study. *International journal of clinical and experimental medicine*, *8*(7), p.11777.

Her, S.C., 1999. Stress analysis of adhesively-bonded lap joints. *Composite structures*, *47*(1), pp.673-678.

Himmer, T., Nakagawa, T. and Noguchi, H., 1997, August. Stereolithography of ceramics. In: *International Solid Freeform Fabrication Symposium, Austin, TX* (pp. 363-369).

Janaki Ram, G.D., Robinson, C., Yang, Y. and Stucker, B.E., 2007. Use of ultrasonic consolidation for fabrication of multi-material structures. *Rapid Prototyping Journal*, *13*(4), pp.226-235.

Jones, D.A., 1996. High-and low-frequency fatigue revisited. *Acta Physiologica Scandinavica*, *156*(3), pp.265-270.

Kai, C.C., 1994. Three-dimensional rapid prototyping technologies and key development areas. *Computing & Control Engineering Journal*, *5*(4), pp.200-206.

Kamitani, T., Yamada, O. and Marutani, Y., 2000, November. Selective laser sintering with heat of formation by using reactive materials. In: *First International Symposium on Laser*

Precision Microfabrication (LPM2000) (pp. 299-302). International Society for Optics and Photonics.

Kearns, W.H., 1980. Adhesive Bonding of Metals. In *Welding Handbook* (pp. 337-365). Macmillan Education UK.

Khaing, M.W., Fuh, J.Y.H. and Lu, L., 2001. Direct metal laser sintering for rapid tooling: processing and characterisation of EOS parts. *Journal of Materials Processing Technology*, *113*(1), pp.269-272.

Khokhar, A.M., 2011. *The evaluation of shear properties of timber beams using torsion test method*. PhD Thesis, Edinburgh Napier University Edinburgh, Scotland, United Kingdom.

Kim, J., Kim, K.S. and Kim, Y.H., 1989. Mechanical effects in peel adhesion test. *Journal of adhesion science and technology*, *3*(1), pp.175-187.

Kinloch, A.J., 2003. Toughening epoxy adhesives to meet today's challenges. *MRS bulletin*, *28*(6), pp.445-448.

Kong, C.Y. and Soar, R.C., 2005. Fabrication of metal–matrix composites and adaptive composites using ultrasonic consolidation process. *Materials Science and Engineering: A*, *412*(1), pp.12-18.

Kong, C.Y., Soar, R.C. and Dickens, P.M., 2002, August. An investigation of the control parameters for aluminium 3003 under ultrasonic consolidation. In: *Proceedings of the 13th Solid Freeform Fabrication Symposium* (pp. 199-210).

Kong, C.Y., Soar, R.C. and Dickens, P.M., 2003. Characterisation of aluminium alloy 6061 for the ultrasonic consolidation process. *Materials Science and Engineering: A*, *363*(1), pp.99-106.

Kong, C.Y., Soar, R.C. and Dickens, P.M., 2004. Optimum process parameters for ultrasonic consolidation of 3003 aluminium. *Journal of Materials Processing Technology*, *146*(2), pp.181-187.

Kong, C.Y., Soar, R.C. and Dickens, P.M., 2005. A model for weld strength in ultrasonically consolidated components. *Proceedings of the Institution of Mechanical Engineers, Part C: Journal of Mechanical Engineering Science*, *219*(1), pp.83-91.

Kumar, S. and Kruth, J.P., 2010. Composites by rapid prototyping technology. *Materials & Design, 31*(2), pp.850-856.

Laoui, T., Froyen, L. and Kruth, J.P., 1999. Effect of mechanical alloying on selective laser sintering of WC-9Co powder. *Powder Metallurgy, 42*(3), pp.203-205.

Lapcevic, A.R., Jevremovic, D.P., Puskar, T.M., Williams, R.J. and Eggbeer, D., 2016. Comparative analysis of structure and hardness of cast and direct metal laser sintering produced Co-Cr alloys used for dental devices. *Rapid Prototyping Journal, 22*(1), pp.144-151.

Law, C.M.T., Wu, C.M.L., Yu, D.Q., Wang, L. and Lai, J.K.L., 2006. Microstructure, solderability, and growth of intermetallic compounds of Sn-Ag-Cu-RE lead-free solder *alloys. Journal of electronic materials, 35*(1), pp.89-93.

Lee, Y.L., Barkey, M.E. and Kang, H.T., 2011. *Metal fatigue analysis handbook: practical problem-solving techniques for computer-aided engineering*. Elsevier.

Liu, B., Bai, P. and Cheng, J., 2008. Microstructure evolution of Mo-based composites during selective laser sintering and thermal processing. *Journal of Computational and Theoretical Nanoscience, 5*(8), pp.1565-1569.

Maeda, K. and Childs, T.H.C., 2004. Laser sintering (SLS) of hard metal powders for abrasion resistant coatings. *Journal of Materials Processing Technology*, *149*(1), pp.609-615.

Marchese, G., Bassini, E., Calandri, M., Ambrosio, E.P., Calignano, F., Lorusso, M., Manfredi, D., Pavese, M., Biamino, S. and Fino, P., 2016. Microstructural investigation of as-fabricated and heat-treated Inconel 625 and Inconel 718 fabricated by direct metal laser sintering: contribution of Politecnico di Torino and Istituto Italiano di Tecnologia (IIT) di Torino. *Metal Powder Report.*

Metal AM, 2010. *Metal Additive Manufacturing Processes*. [online] Available at: <http://www.metal-am.com/introduction_to_metal-additive_manufacturing/processes> [Accessed 20 July 2015].

Mitchell, A., 1999. The electron beam melting and refining of titanium alloys. *Materials Science and Engineering: A, 263*(2), pp.217-223.

Miyachi, 2010. *High speed thin metal cutting using fibre laser technology*. [pdf] Miyachi. Available at: <http://www.amadamiyachi.com/servlet/servlet.FileDownload?retURL=%2Fapex%2Feducationalresources_articles&file=01580000001akdt> [Accessed 30 June 2015].

Mok, S.H., Bi, G., Folkes, J., Pashby, I. and Segal, J., 2008. Deposition of Ti–6Al–4V using a high power diode laser and wire, Part II: Investigation on the mechanical properties. *Surface and Coatings Technology*, *202*(19), pp.4613-4619.

Moures, F., Cicală, E., Sallamand, P., Grevey, D., Vannes, B. and Ignat, S., 2005. Optimisation of refractory coatings realised with cored wire addition using a high-power diode laser. *Surface and Coatings Technology*, *200*(7), pp.2283-2292.

MTIinstruments, 2010. *Microtrak 3*. [online] Available at: <http://www.mtiinstruments.com/products/Microtrak3.aspx> [Accessed 2 July 2015].

Mueller, B. and Kochan, D., 1999. Laminated object manufacturing for rapid tooling and patternmaking in foundry industry. *Computers in Industry*, *39*(1), pp.47-53.

Murr, L.E., Gaytan, S.M., Ceylan, A., Martinez, E., Martinez, J.L., Hernandez, D.H., Machado, B.I., Ramirez, D.A., Medina, F., Collins, S. and Wicker, R.B., 2010. Characterization of titanium aluminide alloy components fabricated by additive manufacturing using electron beam melting. *Acta materialia*, *58*(5), pp.1887-1894.

Park, J., Tari, M.J. and Hahn, H.T., 2000. Characterization of the laminated object manufacturing (LOM) process. *Rapid Prototyping Journal*, *6*(1), pp.36-50.

Pham, D.T. and Gault, R.S., 1998. A comparison of rapid prototyping technologies. *International Journal of Machine Tools and Manufacture*, *38*(10), pp.1257-1287.

Piab, 2012. *Flow2*. [online] Available at: <https://www.piab.com/Products/Flow2/> [Accessed 30 June 2015].

Pilipović, A., Raos, P. and Šercer, M., 2011. Experimental testing of quality of polymer parts produced by laminated object manufacturing–LOM. *Tehnički vjesnik*, *18*(2), pp.253-260.

Piva, E., Azevedo, E.C., Ogliari, A.O., Pilownic, K.J., Pinto, M.B., Camacho, G.B., Petzhold, C.L. and Ogliari, F.A., 2015. Evaluation of experimental phosphate and sulfur-based primer

bonding to metal casting alloys. *International Journal of Adhesion and Adhesives*, *58*, pp.59-62.

Ponader, S., Vairaktaris, E., Heinl, P., Wilmowsky, C.V., Rottmair, A., Körner, C., Singer, R.F., Holst, S., Schlegel, K.A., Neukam, F.W. and Nkenke, E., 2008. Effects of topographical surface modifications of electron beam melted Ti-6Al-4V titanium on human fetal osteoblasts. *Journal of Biomedical Materials Research Part A*, *84*(4), pp.1111-1119.

Prechtl, M., Otto, A. and Geiger, M., 2005. Rapid tooling by laminated object manufacturing of metal foil. In: *Advanced Materials Research* (Vol. 6, pp. 303-312).

Prechtl, M., Otto, A. and Geiger, M., 2005. *Laminated Object Manufacturing of Metal Foil—Process Chain and System Technology* (pp. 597-606). Springer Vienna.

Ram, G.J., Yang, Y. and Stucker, B.E., 2006. Effect of process parameters on bond formation during ultrasonic consolidation of aluminium alloy 3003. *Journal of Manufacturing Systems*, *25*(3), pp.221-238.

*R*ambo, C.R., Travitzky, N., Zimmermann, K. and Greil, P., 2005. Synthesis of TiC/Ti–Cu composites by pressureless reactive infiltration of TiCu alloy into carbon preforms fabricated by 3D-printing. *Materials Letters*, *59*(8), pp.1028-1031.

Rännar, L.E., Glad, A. and Gustafson, C.G., 2007. Efficient cooling with tool inserts manufactured by electron beam melting. *Rapid Prototyping Journal*, *13*(3), pp.128-135.

Ruffo, M., Tuck, C. and Hague, R., 2006. Cost estimation for rapid manufacturing-laser sintering production for low to medium volumes. *Proceedings of the Institution of Mechanical Engineers, Part B: Journal of Engineering Manufacture*, *220*(9), pp.1417-1427.

Scott-Emuakpor, O., Holycross, C., George, T., Knapp, K. and Beck, J., 2016. Fatigue and Strength Studies of Titanium 6Al–4V Fabricated by Direct Metal Laser Sintering. *Journal of Engineering for Gas Turbines and Power*, *138*(2), p.022101.

Sellars, C.M., Barraclough, D.R., Whittaker, H.J. and Nair, K.D., 1973. Effect of specimen geometry on hot torsion test results for solid and tubular specimens. *Journal of testing and evaluation*, *1*(3), pp.220-226.

Sensors Online, 2010. *Motion/velocity/displacement: Thickness measurement using laser triangulation.* [online] Available at: <http://www.sensorsmag.com/sensors/motion-velocity-

displacement/thickness-measurements-using-laser-triangulation-7050> [Accessed 2 July 2015].

Shah, R.K. and London, A.L., 2014. *Laminar flow forced convection in ducts: a source book for compact heat exchanger analytical data* (Vol. 1). Academic press.

Shirvani, H., 2000. Honeycomb structure, method of forming a honeycomb structure and method of joining aluminium or aluminium alloy bodies. *Anglia Polytechnic University, GB Patent: WO0033997 (A1).*

Siddique, S., Imran, M., Wycisk, E., Emmelmann, C. and Walther, F., 2015. Fatigue Assessment of Laser Additive Manufactured AlSi12 Eutectic Alloy in the Very High Cycle Fatigue (VHCF) Range up to 10^9 cycles. *Materials Science*, *2214*(7853).

Simchi, A., 2006. Direct laser sintering of metal powders: Mechanism, kinetics and microstructural features. *Materials Science and Engineering: A*, *428*(1), pp.148-158.

Simchi, A., Petzoldt, F. and Pohl, H., 2003. On the development of direct metal laser sintering for rapid tooling. *Journal of Materials Processing Technology*, *141*(3), pp.319-328.

Slocombe, A. and Li, L., 2001. Selective laser sintering of TiC–Al 2 O 3 composite with self-propagating high-temperature synthesis. *Journal of materials processing technology*, *118*(1), pp.173-178.

Sonmez, F.O. and Hahn, H.T., 1998. Thermomechanical analysis of the laminated object manufacturing (LOM) process. *Rapid Prototyping Journal*, *4*(1), pp.26-36.

Stenbacka, N., Choquet, I. and Hurtig, K., 2012. Review of arc efficiency values for gas tungsten arc welding. In: *IIW Commission IV-XII-SG212, Intermediate Meeting, BAM, Berlin, Germany* (pp. 1-21).

Suganuma, K., 2003. *Lead-Free Soldering in Electronics: Science, Technology, and Environmental Impact*. CRC Press.

Tekscan, 2012. *Nip pinch roller pressure measurement.* [online] Available at: <https://www.tekscan.com/applications/nip-pinch-roller-pressure-measurement> [Accessed 30 June 2015].

TheKneeslider.com, 2012. *Casting the musket V-twin engine.* [online] Available at: <http://thekneeslider.com/casting-the-musket-v-twin-engine/> [Accessed 10 June 2015].

Unocic, R.R. and DuPont, J.N., 2004. Process efficiency measurements in the laser engineered net shaping process. *Metallurgical and materials transactions B*, *35*(1), pp.143-152.

Van, K.D. and Paradopoulos, I.V. eds., 2014. *High-cycle metal fatigue: from theory to applications* (Vol. 392). Springer.

Vandenbroucke, B. and Kruth, J.P., 2007. Selective laser melting of biocompatible metals for rapid manufacturing of medical parts. *Rapid Prototyping Journal*, *13*(4), pp.196-203.

Vianco, P.T., 1999. An overview of surface finishes and their role in printed circuit board solderability and solder joint performance. *Circuit World*, *25*(1), pp.6-24.

Wang, J.X., Xue, S.B., Han, Z.J., Yu, S.L., Chen, Y., Shi, Y.P. and Wang, H., 2009. Effects of rare earth Ce on microstructures, solderability of Sn–Ag–Cu and Sn–Cu–Ni solders as well as mechanical properties of soldered joints. *Journal of Alloys and Compounds*, *467*(1), pp.219-226.

Wang, Q.Y., Kawagoishi, N. and Chen, Q., 2006. Fatigue and fracture behaviour of structural Al-alloys up to very long life regimes. *International journal of fatigue*, *28*(11), pp.1572-1576.

Watlow, 2010. *Cartridge/Insertion Heaters*. [online] Available at: <http://www.watlow.co.uk/products/heaters/ht_cart.cfm> [Accessed 5 July 2015].

Wei, D., Zhou, R., Cheng, S., Feng, W., Yang, H., Du, Q., Li, B., Wang, Y., Jia, D. and Zhou, Y., 2014. MC3T3-E1 cells' response and osseointegration of bioactive sphene–titanium oxide composite coatings fabricated by a hybrid technique of microarc oxidation and heat treatment on titanium. *Journal of Materials Chemistry B*, *2*(20), pp.2993-3008.

Wei, S.T., Lv, D., Liu, R.D., Lin, L., Xu, R.J., Guo, J.Y. and Wang, K.Q., 2014. Similar and dissimilar resistance spot welding of advanced high strength steels: welding and heat treatment procedures, structure and mechanical properties. *Science and Technology of Welding and Joining*, *19*(5), pp.427-435.

Weisensel, L., Travitzky, N., Sieber, H. and Greil, P., 2004. Laminated object manufacturing (LOM) of SiSiC composites. *Advanced Engineering Materials*, *6*(11), pp.899-903.

Wycisk, E., Siddique, S., Herzog, D., Walther, F. and Emmelmann, C., 2015. Fatigue Performance of Laser Additive Manufactured Ti–6Al–4V in Very High Cycle Fatigue Regime up to 10^9 Cycles. *Frontiers in Materials*, *2*, p.72.

Xiao, R., Chen, K., Zuo, T., Ambrosy, G. and Huegel, H., 2002, September. Influence of wire addition direction in C02 laser welding of aluminium. In *Photonics Asia 2002* (pp. 128-137). International Society for Optics and Photonics.

Xiong, Y., Smugeresky, J.E. and Schoenung, J.M., 2009. The influence of working distance on laser deposited WC–Co. *Journal of Materials Processing Technology*, *209*(10), pp.4935-4941.

Yang, Y., Ram, G.J. and Stucker, B.E., 2007. An Experimental Determination of Optimum Processing Parameters for Al/ SiC Metal Matrix Composites Made Using Ultrasonic Consolidation. *Journal of Engineering Materials and Technology*, *129*(4), pp.538-549.

Yang, Y., Ram, G.J. and Stucker, B.E., 2009. Bond formation and fiber embedment during ultrasonic consolidation. *Journal of Materials Processing Technology*, *209*(10), pp.4915-4924.

Yasa, E., Poyraz, O., Solakoglu, E.U., Akbulut, G. and Oren, S., 2016. A Study on the Stair Stepping Effect in Direct Metal Laser Sintering of a Nickel-based Super-alloy. *Procedia CIRP*, *45*, pp.175-178.

Zhang, Y., Han, J., Zhang, X., He, X., Li, Z. and Du, S., 2001. Rapid prototyping and combustion synthesis of TiC/Ni functionally gradient materials. *Materials Science and Engineering: A*, *299*(1), pp.218-224.

Zhang, Y., He, X., Du, S. and Zhang, J., 2001. Al2O3 ceramics preparation by LOM (laminated object manufacturing). *The International Journal of Advanced Manufacturing Technology*, *17*(7), pp.531-534.

Zhang, Y., He, X., Han, J. and Du, S., 1999. Ceramic green tape extrusion for laminated object manufacturing. *Materials Letters*, *40*(6), pp.275-279.

Appendix A: Powder Dispenser

A.1 Introduction to Powder Dispenser

This powder dispenser was designed and used for dispensing powder in dots and in continuous lines with accuracy and control. It was part of the researcher's Masters Project and is fully capable of working with both powder and paste (Butt, 2011). This dispenser will be referred to as a powder dispenser from here onwards to distinguish it from the 710 paste dispenser. It was integrated with a 3D printer in the same way as the 710 dispenser is being integrated with the machine. The protocols are the same and it can be used in addition to or instead of the 710 dispenser as it is capable of dispensing a viscous non-Newtonian fluid like the brazing paste. Fig. A.1 shows the setup that was created for the integration of the powder dispenser to the 3D printer.

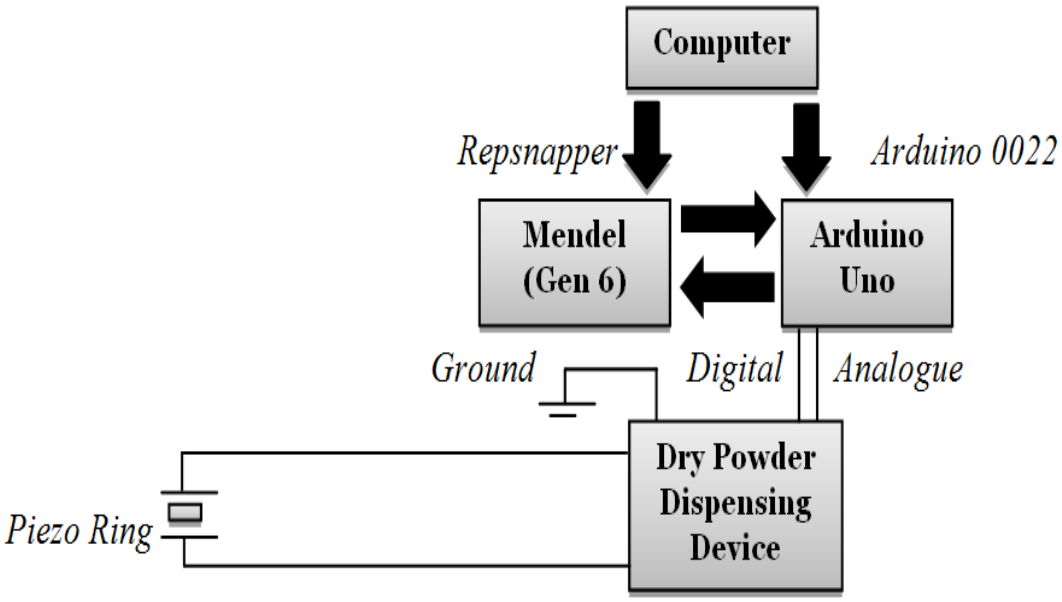

Figure A.1: Block diagram showing communication among device

The 3D printer (Mendel) was connected to computer via USB cable. The host software used is called Repsnapper and it could send G-codes or STL (STereoLithography) files from the computer to the printer to print them. The software was directly communicating with the Gen 6 board of the printer having an ATMEGA644A microcontroller with RS485 connectors. Arduino Uno, with an ATMEGA328 microcontroller, was also connected to the computer via USB cable and Arduino 0022 environment was installed which had the libraries needed to run the 3D printer. The computer was controlling the printer using Repsnapper and Arduino Uno by using Arduino 0022 software. Communication between Gen 6 board of the 3D printer and Arduino was established by making use of the ICSP (In Chip Serial Programming) port at the Gen 6 board. A closed loop setup was created where every device was able to communicate with the other in order to ensure the functionality of the system as a singular cohesive unit. On the other hand, the dry power dispensing device needed one digital and one analogue signal to run. There was no physical space available to connect anything on the Gen 6 board to get the two signals. That was the reason for the introduction of Arduino Uno into the setup. It is an electronics platform with very flexible hardware and software along with some efficient protocols suitable for this study.

A.2 Working of the Powder Dispenser

The dispenser consists of a glass tank with a piezo ring attached at the bottom and enclosing a capillary tube fitted with a rubber stopper (Fig. A.2). The hole at the bottom of the capillary had a diameter of 0.2mm depending on the particle size of the powder used (solder powder of 45 micron). The glass tank was open at the top and had a hole at the bottom which was closed in order to make the system leak proof. The piezo ring acts as an actuator and was connected with wires on both sides which will be connected to a power supply. The tank was filled with water as it transmits vibrations onto the capillary for dispensing powder.

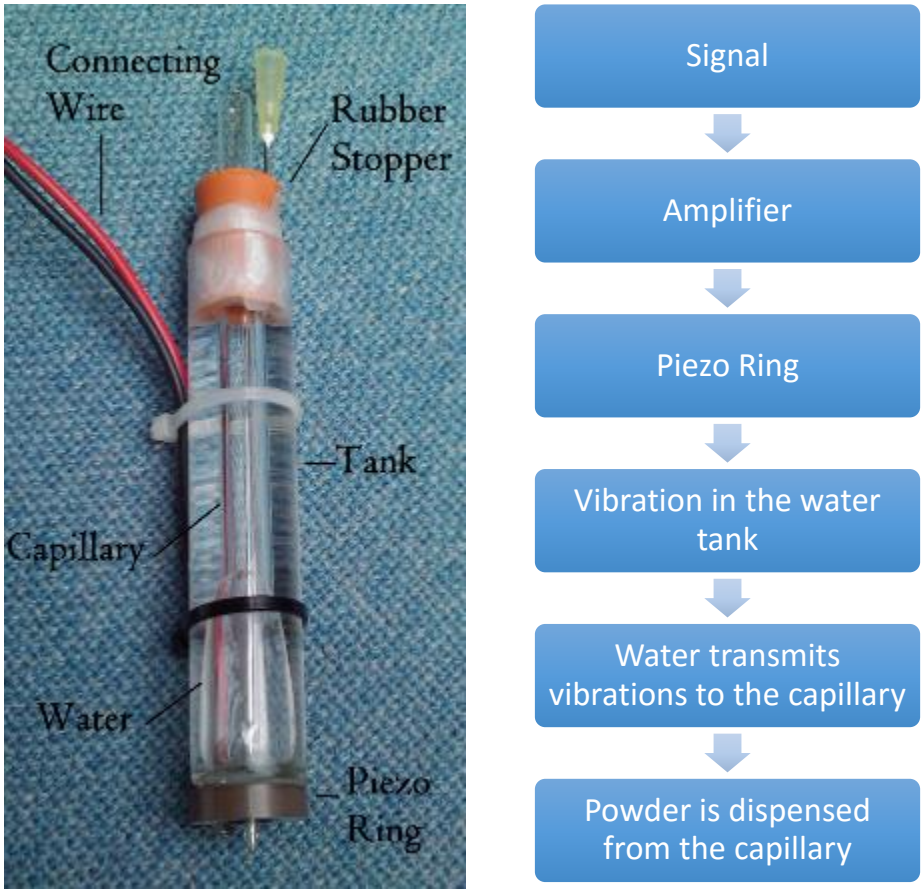

Figure A.2: Construction and working of dry powder dispensing device

The dispenser needed two signals to run i.e., one digital and one analogue (Fig. A.3). The analogue signal controls the amplitude or in simple words the amount of powder dispensed. For example, to completely fill a square, the voltage value will be kept higher so that the dispenser can dispense powder quickly and completely cover the area of the square. On the other hand, if very fine lines are to be drawn like a maze or a bespoke electric circuit on a printed plastic part, the voltage will be kept lower to allow for fine and proper dispensing. The analogue signal can have any value in the defined range. Also, in analogue, the amplitude and frequency vary continuously. However, depending on the nature of dispensing only a fixed value of voltage was chosen.

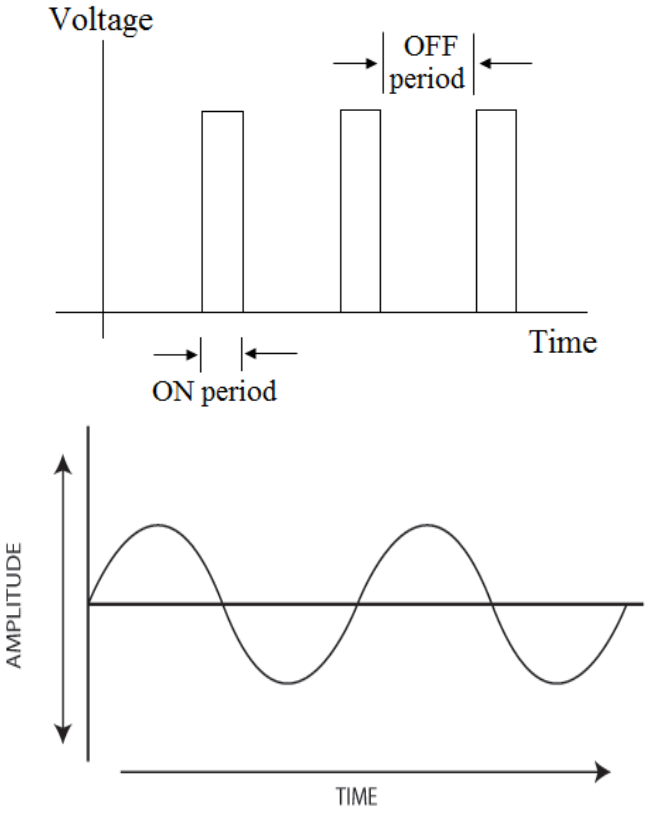

Figure A.3: Digital & analogue signal representation

The digital signal will be working as ON/OFF for the dispenser. Therefore, when the digital signal is logic 1, the dispenser will be printing or dispensing and when the signal is logic 0, no powder will be dispensed. Logic 1 and logic 0 defines the "ON" and "OFF" states of the dry powder dispensing device. In addition to logic 0, when there is no analogue signal, there will be no dispensing as well. The frequency and the "ON" and "OFF" time periods can be varied according to the requirements.

A.3 Analogue Signal for the Dispenser

The analogue signal was achieved by making use of a 12 bit MCP4921 DAC (digital to analogue converter) chip. The digital signal from the Arduino was converted into analogue signal by the chip using SPI protocol and by loading a conversion program into the Arduino. SPI communication is a synchronous serial data protocol used by microcontrollers for communicating with one or more peripheral devices quickly over short distances.

Four pins on the Arduino Uno support the SPI communication by making use of the SPI library. These pins are:

Pin 10: Serial Select (SS) - The pin on each device that the master can use to enable and disable specific devices.

Pin 11: Master Out Slave in (MOSI) - The Master line for sending data to the peripherals.

Pin 12: Master In Slave out (MISO) - The Slave line for sending data to the master.

Pin 13: Serial Clock (SCK) - The clock pulses which synchronize data transmission generated by the master.

Fig. A.4 shows the connections of Arduino Uno with MCP 4921 chip with pin 8 being the required output signal:

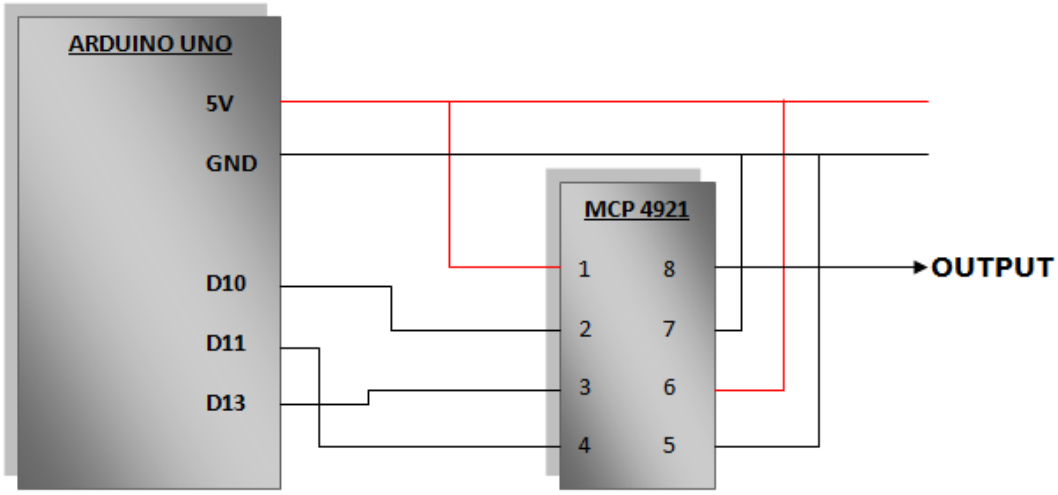

Figure A.4: Connections of Arduino Uno & MCP 4921 chip

A.4 Digital Signal for the Dispenser

ICSP port was used for communication between the Gen 6 and Arduino. It has 6 pins in total and just one pin was toggled high and low in order to get the required digital signal for the powder dispenser. Figure A.5 shows the pins of the ICSP port.

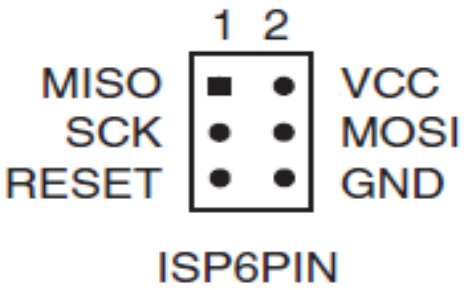

Figure A.5: Pins of ICSP port

The MISO (Master-In Slave Out) and MOSI (Master-Out Slave In) pins were the two options available that could be utilized as they were not used for anything else during the operation of the printer. Therefore, the MISO pin was declared as output in the main code of Gen 6 and new g-codes were introduced into the Gen 6 program that toggled the MISO pin high and low whenever they were sent by Repsnapper. Modifications were made in the main program of the 3D printer by defining the MISO pin and introducing new g-codes corresponding to the switching of the powder dispenser.

#define miso 6

MISO was declared as static variable so that its lifetime would run over the entire length of the program. The new g-codes were defined in the following format:

```
case 100:
        pinMode(miso, OUTPUT); //set pin as output
        digitalWrite(miso, HIGH);
 break;
```

According to this newly added code, whenever G100 would be sent by Repsnapper to the printer, the MISO pin would turn HIGH and in terms of dry powder dispensing device, it meant that the dispenser would be ON.

case 101:

pinMode(miso, OUTPUT); //set pin as output

digitalWrite(miso, LOW);

break;

In the same way, whenever G101 would be sent by Repsnapper to the printer, the MISO pin would turn LOW and in terms of dry powder dispensing device, it meant that the dispenser would be OFF. On the Arduino side, there was only a need to declare one pin as INPUT that would receive the OUTPUT sent by MISO and show it. Before connecting the dispensing device, the signal was tested using a simple LED connected to pin 2 of Arduino. It turned ON/OFF according to the sent g-codes. Fig. A.6 shows the powder dispenser attached to the extruder of the 3D printer.

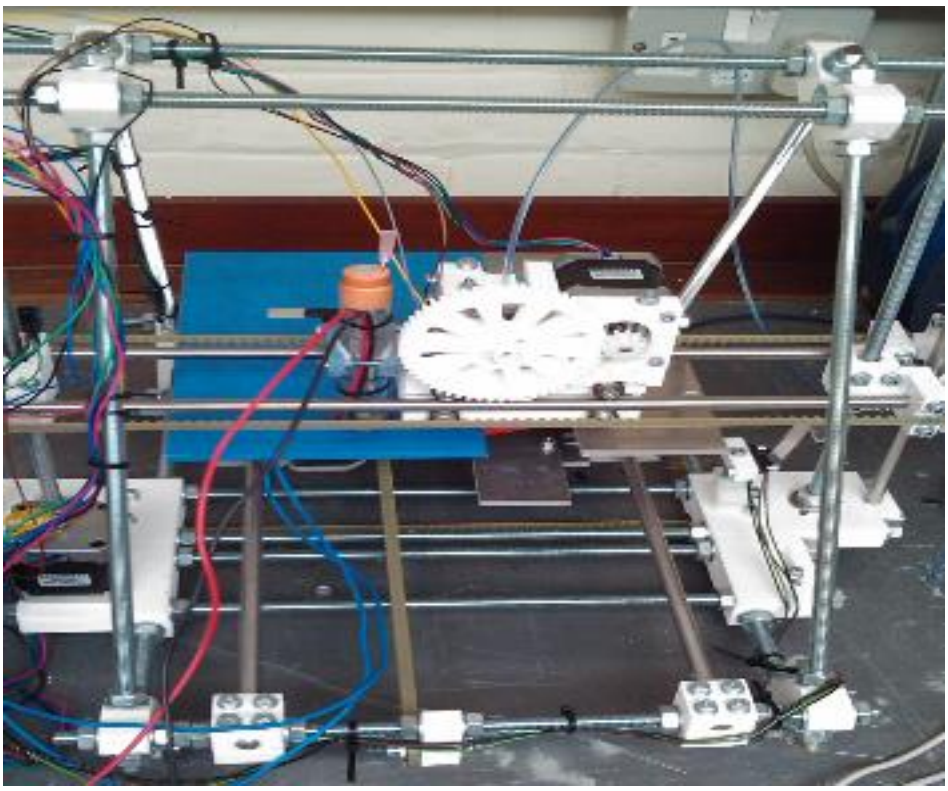

Figure A.6: Mendel with dry powder dispensing device

A.5 Electrical Connections for Powder Dispenser

The block diagram in Fig. A.7 shows the connections made for the dry powder dispensing device.

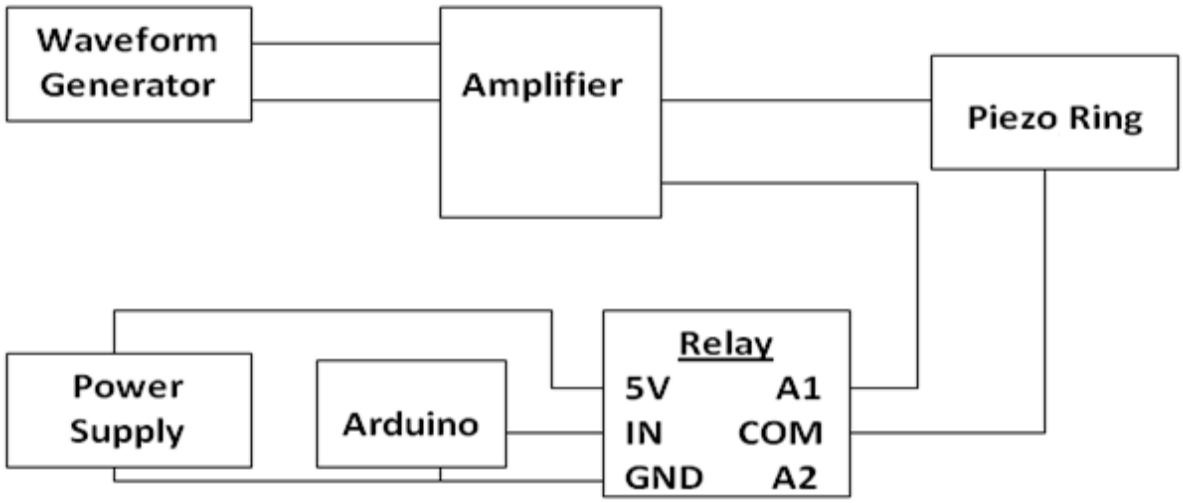

Figure A.7: Electrical Connections for the device

The signal came from the waveform generator whose period was set at 100 micro seconds and it was supplying a voltage in the range of 1-10 Volts needed to run the device. The voltage was set to 5V for the purpose of dispensing powder. A square wave was selected that could range from 0.1 Hz to 10 MHz (set at 5 MHz). The connections from the generator went into the amplifier. One wire was then connected to the piezo ring of the dispensing device and the other to a 12V relay. The relay was connected to a power supply of 12V based on its rating. The digital and analogue signals from the Arduino were connected to the relay and the circuit was completed by connecting the ground.

A.6 Experimentation & Results

Blue translucent PLA (polylactide which is a thermoplastic aliphatic polyester), 1.75mm filament was used by Mendel and 45 micron particle size solder powder was filled in the powder dispenser. Mendel was fully capable of printing plastic parts with one click but for

the sake of printing multiple materials parts, certain parameters were changed that could affect the integrity of the part. In the print options, the infill distance was reduced from the normal value of 0.8 to 0.5 and also the optimization value was reduced from 0.050 to 0.035 in order to make sure that a more dense part could be made. The production of a dense part was critical so that when powder was dispensed, it would stay in the path intended for it rather than sink into the part and cause problems. For the purpose of printing, a part was made in solid works having an electrical circuit in it. It had space to place a chip with the legs lying along the grooves made in the part as shown in Fig. A.8i. The part was a square of 35mm having grooves of 1mm so that only one layer of powder would be enough. The file containing the drawing was saved in .STL format and was then opened in Repsnapper for printing. The software converted the .STL into a G-code file (Fig. A.8ii) with one click because the 3D printer only responds to G-codes.

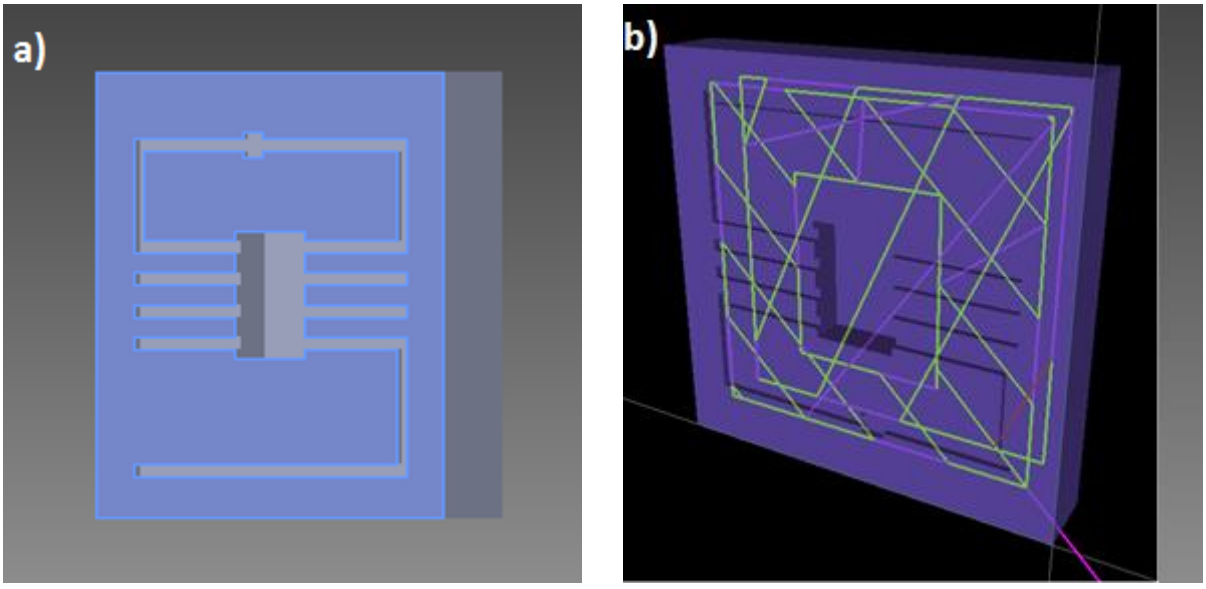

Figure A.8: 3D printing of part: i) CAD design of the part with electronic circuit inside; ii) Part after conversion from .STL to g-codes

The 35mm square part was then made by clicking the “PRINT” button on the software. As it was a small structure, it took almost 4 minutes for the part to be made. Afterwards,

customized G-codes according to the electronic circuit in the part were written and then sent to the printer via serial communication that was established for this purpose. Since the printer only responds to G-codes, the code was first tested in a G-code simulator to make sure that it was correct and then sent to the printer for the dispensing of powder in the defined circuit. The newly defined G-codes i.e., G100 (dispenser ON) and G101 (dispenser OFF) were sent along with the regular G-code format for a 3D printer so that the dispenser would know when to turn ON and when to turn OFF because the powder dispensed outside the circuit would be of no use. After dispensing of powder, a multiple materials part was ready with a base of plastic and a layer of powder dispensed into the electronic circuit defined in the part. Fig. A.9 shows the part after the dispensing of powder and also with a chip placed perfectly in the groove made for it.

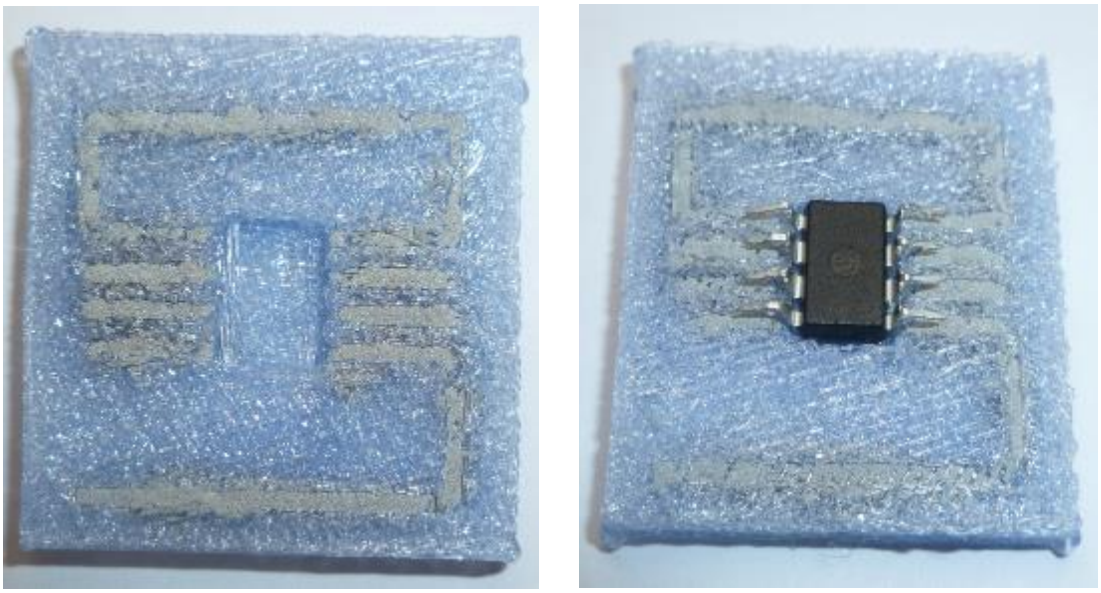

Figure A.9: Multiple materials part